CAPILLARY ELECTROPHORESIS – HIGH RESOLUTION INDUCTIVELY COUPLED PLASMA MASS SPECTROMETRY: ELEMENTAL SPECIATION AND APPLICATIONS IN PHARMACEUTICAL PROCESS RESEARCH

By

XIAODONG BU

A Dissertation submitted to the

Graduate School –New Brunswick

Rutgers, The State University of New Jersey

in Partial Fulfillment of the Requirements for

the Degree of Doctor of Philosophy

Graduate Program in Chemistry

written under the direction of

Professor Gene Hall

and Approved by

_____

_____

_____

_____

New Brunswick, New Jersey

October, 2007

ABSTRACT OF THE DISSERTATION

CAPILLARY ELECTROPHORESIS – HIGH RESOLUTION INDUCTIVELY COUPLED PLASMA MASS SPECTROMETRY: ELEMENTAL SPECIATION AND APPLICATIONS IN PHARMACEUTICAL PROCESS RESEARCH

By Xiaodong Bu

Dissertation Director: Professor Gene Hall

The high efficiency of capillary electrophoresis (CE) was combined with the element specificity and low detection limits of high resolution inductively coupled plasma mass spectrometry (HR-ICP-MS) for rapid elemental speciation. A novel sheath flow interface coupled to a PFA Teflon micro-flow concentric nebulizer was developed to provide an efficient method for interfacing capillary electrophoresis with the inductively coupled plasma. The sheath interface provides control over the nebulizer induced laminar flow in the separation capillary allowing the tradeoff between separation efficiency and analysis time to be selected.

In chapter 3, this CE-HR-ICP-MS system was used to study various hydration/hydrolysis processes of hexachloro complexes of Rh in aqueous solutions. The migration speed of various mixed aquo/chloro rhodium species through the capillary depends on the charges they carry, which is dictated by the solution pH as well as their aging period in the solution. Several Rh species were tentatively identified according to their relative mobilities and their equilibrium distributions were quantified using peak area calculation in the experiments.

In chapter 4, to meet the need of speciation analysis for applications in pharmaceutical process research, a non-aqueous CE with HR-ICP-MS detection method was developed. The novel sheath interface between the CE and ICP-MS enabled the use of CE with up to 100% organic electrolyte without organic loading in the plasma. Two unique aspects of non-aqueous CE, non-aqueous CE with wide-bore capillaries and influence of organic solvent on the CE separation selectivity were discussed.

Information on chemical speciation is much needed in mechanistic and kinetic studies on catalyst formation processes in pharmaceutical research. In chapter 5, non-aqueous CE-ICP-MS speciation analysis was applied to the identification and quantification of various rhodium species involved in a ligand exchange process leading to formation of catalyst dirhodium(II) tetrakis[methyl 2-oxopyrrolidin-5(*S*)-carboxylate]. A variety of reaction intermediates were identified and quantified along the pathway to formation of the desired product. This has provided new insights into the mechanism and kinetics of the reaction.

In chapter 6, the feasibility of the determination of sub ppm to percentage levels of halogen elements (fluorine, chlorine, bromine, and iodine) in solid organic compounds and drug substances by HR-ICP-MS was investigated. In chapter 7, the application of HR-ICP-MS for the determination of isotopic composition of enriched stable isotope calcium samples is described. The interferences from ^{40}Ar isotope at the calcium mass 40 are greatly minimized by operating the ICP-MS in the cool plasma mode. The rest polyatomic ions are overcome by high resolution mode of the ICP-MS.

DEDICATION

To my wife Shu and my son Andrew

ACKNOWLEDGMENTS

I would like to express my sincere appreciation to my research advisors, Dr. Gene Hall, for giving me the opportunity to work with him and for his guidance, encouragement and support throughout the course of my Ph. D. program. I would also like to thank my supervisor and mentor at Merck, Dr. Tiebang Wang, for his understanding and support which made much of this work possible. Thanks also to the members of my examination committee for their helpful suggestions and thought provoking questions. I thank Merck for providing me the financial support. Finally, I wish to extend my thanks to my dear wife Shu for her love and support and my lovely son Andrew for giving me much happiness and joy.

TABLE OF CONTENTS

LIST OF TABLES

LIST OF FIGURES

Chapter 1

Introduction

1.0 The need for Elemental speciation

It is increasingly realized that the distribution, mobility, removal and biological availability of chemical elements depends not simply on their total concentrations but also, critically, on their chemical species[1-3]. Changes in environmental conditions can strongly influence the behavior of toxic metals by altering the forms in which they occur. Cr(III) for example, is a trace nutrient essential for the maintenance of lipids, glucose and proteins.[4] Cr(VI), on the other hand, cannot be incorporated into the human body and is highly toxic, and carcinogenic.[5] Arsenic also has widely varying toxicities depending on speciation. Monomethylarsenate, dimethylarsenate, and arsenobetaine, are all common forms of organic arsenic. These species of arsenic are frequently present in high concentrations in shellfish and other marine animals, but are comparatively non-toxic. Inorganic arsenic, on the other hand, is both acutely toxic and carcinogenic.[6-8]. Speciation is important for the study of the transport properties of waste metals in soil samples and is important for the determination of migration rates of metals and metal-ion ligand complexes into the water table.[9] In both cases, simply knowing the total concentration of elements is not sufficient and an element speciation analysis is necessary to determine the amount of toxic substance present.

In addition to toxicological information, speciation can be a powerful tool in identification and quantitation of various metal species during the course of the synthesis of pharmaceutical candidates and commercial products. Nowadays, heavy metals (Pd, Rh, Ru, etc,) are used routinely as catalysts in pharmaceutical industries in synthesizing raw materials, intermediates and final active pharmaceutical ingredients (API's)[10-15]. The reaction ability of a metal ion and, in particular, its catalytic activity is to a great extent dependent on the forms in which the metal exists in solution. Therefore, the capability of distinguishing and identifying the presence of various species of a catalyst metal at various stages of a reaction may provide a better insight into the mechanism of a catalytic reaction. Armed with the qualitative and quantitative knowledge of the species presence in a reaction system, the optimization of reaction conditions for more efficient use of the catalyst and selectivity control would be greatly facilitated.

Furthermore, the eventual residual catalyst metal removal is also very critical since many catalyst metals in final drug compounds may pose adverse health effects to patients. Studies of metal speciation and binding mechanisms of metal-ligand complexes are necessary for a basic understanding of the important metal removal processes since simply knowing the total concentration of the metal is not sufficient.[16-17] It is reasonable to suggest that the removability of a residual catalyst metal in a drug substance is dictated by the forms it exists, these forms include free metal atoms, metal at various oxidation states, and their complexation reaction products with various ligands in the system. Only an elemental speciation analysis can provide an insight into the microenvironment of the metal in the sample matrix.

Elemental speciation involves the determination of particular species of an element, including both the qualitative (what species?) and quantification (how much) aspects. It is more challenging than the determination of the total concentration of an element due to difficulties in: (1) separating the species of interest from the many other species present, (2) maintaining species integrity by preventing changes in the equilibrium among various possible chemical species present in the system under study, (3) lacking of standards used in identifying unknown species, and (4) measuring species at ultra-trace levels (ng/mL), which requires highly sensitive analytical techniques.

Traditional trace metal detection schemes such as ICP-OES) and ICP-MS offer part-per-billion (ppb) and part-per-trillion (ppt) detection limits, but provide no speciation information.[18] After entering the plasma, any ligands associated with a metal will be atomized. Flame atomic emission and graphite furnace atomic emission analysis, suffer the same limitations. Electrochemical techniques such as cathodic and anodic stripping voltammetry also offer good detection limits and metal specificity.[19] These techniques, however, also provide no speciation information since the metal is reduced and plates onto the electrode surface prior to analysis. Some metal ions such as lead and iron can be analyzed by complexiometric methods using UV detection.[20, 21] These techniques are limited to only a few metals at a time. In addition, large concentrations of ions with similar charges and complexation behavior present in solution with the analyte ions cause large uncertainties in the measurement. Titration can also be used, but once again is limited to a few ions at a time because the broadband spectra characteristic of UV absorption makes spectral overlaps likely.[22] Titration reactions are also time consuming and cumbersome to use.

With this increasing need for a better understanding of the role of speciation in biological and environmental systems and the limitations of available techniques, there is demand for rapid, selective methods of qualitative and quantitative measurement of speciation. In this work, a new hyphenated technique to perform rapid elemental speciation in the same amount of time as currently required for conventional ICP analysis was developed and characterized.

The development of capillary electrophoresis inductively coupled plasma mass spectrometry (CE-ICPMS) for rapid elemental speciation will be described in Chapters 2-5. This technique provides a complementary extension to the types of analyses possible with the ICP. By taking advantage of the low limits of detection and element specificity of the ICP-MS and the high resolution and fast analysis times of capillary electrophoresis, the combined technique can perform analyses that neither alone is can.

1.1 Previous Approaches to the Analysis of metal speciation

To identify and quantify different elemental species in a complicated chemical system, it is typically prefer using at least two analytical techniques. The first is used to separate the species and the second analytical technique is used to identify and quantify the species.[23-27] Many different separations and detection systems have been used for elemental speciation. To reduce analysis time and improve accuracy, hybrid or coupled techniques are usually preferred.

In a hybrid technique, the separation process and elemental detection occurs on-line, which involves designing an effective and compatible interface. The favored detectors for hybrid systems are sensitive and element selective. Selective detection is

very useful in speciation studies because in this case only species of the element of interest will be detected, even in a complex mixture of substances. Examples of these hybrid speciation techniques include: ion chromatography (IC),[28,29] gas chromatography,[30,31] high-performance liquid chromatography (HPLC),[10,11,34] and capillary electrophoresis (CE)[41,42] coupled to detectors such as: ultraviolet absorbance or fluorescence detection spectrometry,[26-31] inductively coupled plasma (ICP) optical emission (OES) or, mass spectrometry (MS),[41-45] electrospray (ES) MS,[35] microwave induced plasma (MIP)[21,37] and atomic absorption spectrometry (AAS)[31,47].

Among the above separation techniques, ion chromatography (IC) is currently the most common method of metal and metal-ligand complex determination and has been demonstrated for the speciation of nearly all metal ions and many metal-ligand complexes.[48,49] Although this technique provides good speciation information, the limits of detection are not as good as those for ICP-OES and ICP-MS. In addition, this technique suffers from a number of other drawbacks. Most importantly, ion chromatography is relatively slow which can be a problem for species that undergo interconversion on a fast time scale. Typical separations take upwards of thirty minutes for complete speciation. Some separations require hour time-scales especially if gradient elution is not possible. Complex mixtures of mobile phases and mobile phase gradients must often be used to achieve separations in a reasonable amount of time. In addition, recycle time back to the beginning conditions of the gradient is time consuming. Some ions cannot be separated from one another in reasonable amounts of time so complexation chemistry is employed to bind with one metal ion specifically. This greatly facilitates the separation, but destroys the original speciation of that ion. In addition, it is

difficult to find a complexing agent that will selectively bind to only one element and not interact with other elements in the sample.

Detection is typically carried out with either indirect UV detection or electrochemically. Direct UV detection and fluorescence detection can be used with the addition of a post-column reactor to bind a chromophore or fluorophore to the ions as they elute. This can degrade resolution since the post-column reaction is chromatographic dead volume. In addition, it adds another level of complexity to the technique. Electrochemical detection, in general, offers much lower limits of detection, but has the added complexity of a suppressor column to reduce the background current of the solvent(s). The suppressor column reacts with the ionic eluent and converts the charged electrolyte solution used to elute the ions to a neutral compound. This greatly decreases the background current and the baseline noise, resulting in lower limits of detection. Suppressor columns also degrade resolution since post column dead volume is now present.

1.2 Capillary Electrophoresis for the Separation of Metal ions in Solution

Recently, CE has been increasingly used for speciation of metal ions and metal ion complexes[50-60]. This technique has a number of advantages over other separation techniques. Chief among them is the increased speed at which analysis can be performed. In addition, the amount of sample and electrolyte required is reduced to a few microliters (compared to mL to liter volumes typically used in IC) due to the small physical dimensions of the capillaries used. Capillaries are typically 50 μm i.d. or smaller and between 50 and 100 cm in length. The small capillary size is important in the

reduction of Joule heat. Joule heating, that is the resistive heating caused by placing a strong electric field through a conductive media, can be a major cause of band broadening in capillary electrophoresis. Band broadening due to Joule heat production is so great that CE in open tubes was impractical until small capillaries could be fabricated. Prior to the existence of small i.d. capillaries, the column must be spun around its central axis or a stabilizing gel must be used to reduce or eliminate the convection currents induced by Joule heating.[61-63]

Another advantage of CE over many other separation techniques, such as chromatography, is that it does not rely on any interaction between analyte and a stationary phase. Rather, separation is based solely on physical properties of analytes, such as the difference in size, charge, and electrophoretic mobility of an ion in solution[61-63]. This is important for the separation of metal ions because there is little difference in chemical functionality from one ion to another making separation using a stationary phase difficult. Typically, strong cation or anion exchange resins must be employed as a stationary phase to achieve adequate separation of metal ions. There is also less chance of a metal ion or metal-ligand complex adsorbing to a surface and undergoing a redox reaction or ligand exchange reaction that would disturb the original speciation. Because there is a difference in the size and charge between many different metal ions and metal-ligand complexes, capillary electrophoresis can be used for the efficient separations of these species.

In the CE experiments, the capillary and electrode reservoirs are filled with a background electrolyte, which conducts electric current and provides buffering capacity. The sample, consisting of a mixture of anions and cations, is introduced into the

continuous electrolyte system at one end of the capillary. As shown in Figure 1.1, the applied voltage produces an electric field gradient (with an average value of Voltage/Length). Under the influence of the electric field, the ionic species of the carrier electrolyte and the sample migrate to the corresponding electrode. Positive ions will migrate toward the negatively charged end of the capillary and negative ions will migrate toward to the positively charged end of the capillary.

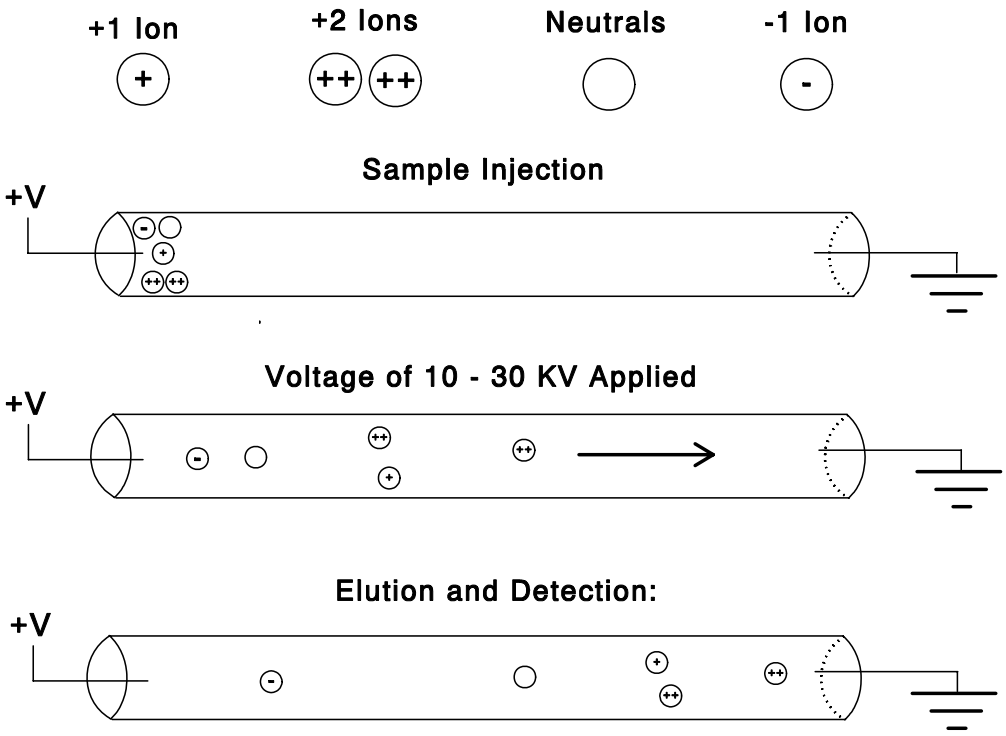

Figure 1.1 Process of capillary zone electrophoresis separations.

Due to its high concentration the electrolyte determines the physical properties such as conductance and pH throughout the capillary. The influence of the sample on conductance and pH can be generally neglected. Therefore, the sample components

migrate independently from the carrier electrolyte with their specific velocities, which depend on its charge, size and shape.

The small size of the capillary makes detection difficult in capillary electrophoresis. This is especially true for metal ions because many metal ions and metal ion ligand complexes lack chromophores or fluorophores which make direct UV and fluorescence detection impossible. The most widely used detectors for capillary electrophoresis, UV-visible absorbance and laser induced fluorescence (LIF) are not effective for direct detection because the ions of interest lack chromophores. Conductivity detection has also been used but can be complicated by low limits of detection due in part to the necessity of measuring the small change in conductivity due to the analyte ion in the presence of the large background conductivity of the electrolyte solution which is typically present in concentrations of 3 to 6 orders of magnitude greater than the analyte ions.

Detection for CE analysis of metal ions is typically performed with indirect UV absorption by placing a UV absorbing substance in the electrophoretic electrolyte.[64-65] As metal ions focus into sharp bands, they displace the UV absorbing species and a decrease in UV absorption is noted at the detector. This technique has high sensitivity, but provides no means other than migration time for species identification. Because detection is non-selective, baseline resolution between each analyte is required. This greatly increases the amount of time required to achieve the separation and is difficult for some ions because their migration times in an electric field are nearly identical. Limits of detection are also unsatisfactory for trace analysis with these types of indirect detection systems. In order to improve the limits of detection for these systems, there has been

some focus on the use of bubble cells or Z-shaped capillary cells to increase the path length which can be as short as 25 μm in normal fused silica CE capillaries. With the use of these types of detectors, limits of detection in the tens of parts per million range (ppm) have been observed.[66-68] For the purposes of trace speciation, this is still not adequate because many species of biological and environmental interest must be monitored at the parts per billion (ppb) to parts per trillion (ppt) level.[69]

Because samples containing a mixture of divalent ions or a mixture of trivalent ions, are very difficult to separate based upon their electrophoretic mobility alone, complexing electrolytes must be used in order to achieve adequate separation.[70-73] This, of course, destroys the natural speciation of the sample.

Electrochemical detection has also been employed for detection of metal ions in capillary electrophoresis. Pulsed amperometry, conductivity, and voltammametric detection systems using ultra-micro electrodes have been used with some success.[74,76] Ion selective electrodes were also employed and offer the advantage of independent species confirmation. Electrochemical detection offers vastly improved detection limits compared to indirect UV detection and can provide some degree of independent species identification. Reproducibility of detection due to the high background current present in electrophoresis and difficulty in maintaining a clean, reproducible electrode surface for detection are still problems with these techniques.

1.3 High Resolution Inductively Coupled Plasma Mass Spectrometer for Rapid Element Selective Detection for Capillary Electrophoresis

In this work, an inductively coupled plasma mass spectrometer (ICP-MS) has been used for on-line combination with CE for elemental speciation. Since its

commercial introduction in the early 1980's, ICP-MS has been widely used as a multi-element analytical technique for trace elemental determinations and isotope ratio measurements in various disciplines. It offers part-per-trillion detection limits and can be used to detect a wide range of metals[77-79]. The advantage of using a mass spectrometer as the detector versus UV for CE is not only its high sensitivity, but also its high selectivity: only different forms of a particular element of interest must be separated from each other rather than needing to separate species containing different elements from each other[79].

The ionization process of ICP-MS is demonstrated in Figure 1.2. The plasma consists of a hot partially ionized Argon gas. The sample is introduced to the plasma as an aerosol by means of a nebulizer and spray chamber combination. The pneumatic nebulizer uses high velocity Ar gas to generate an aerosol, which is then transported through the spray chamber to remove drops that are too large and to limit the total amount of solvent that enters the ICP. The analyte transport efficiency of this aerosol is determined by several parameters such as sample uptake rate, nebulizer gas flow rate, and nebulizer/spray chamber design. Because of the high temperatures (5,000-10,000 K) of the ICP, the aerosol containing the analyte is desolvated and the remaining solid particles are converted to free atoms and singly charged ions regardless of its original chemical structure. The ions are then transferred through a differentially pumped interface into a mass spectrometer. Once in the mass spectrometer, the ions are then separated based on their mass-to-charge ratio (m/z) and detected.

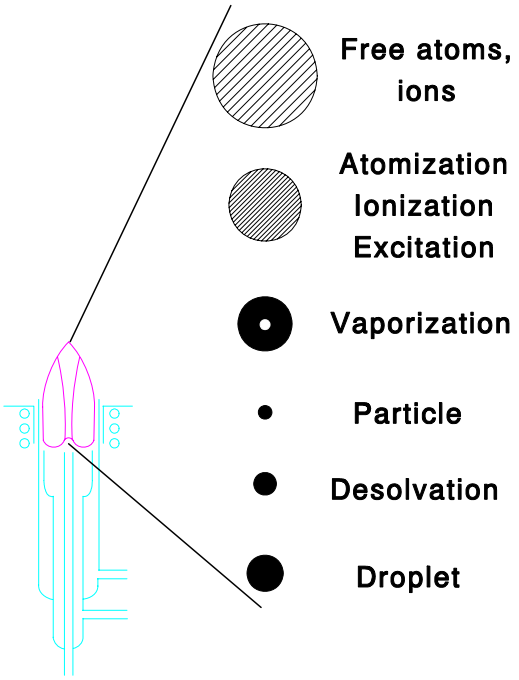

Figure 1.2 Scheme of production of sample atoms, ions in the ICP

Figure 1.3 shows the general CE-ICP-MS instrument set up. Briefly, a high voltage is applied between the ends of the capillary, which typically is a bare fused silica capillary with an inner diameter of 20 to 100 μm, an outer diameter of 200-400 μm and a length of 0.2 to 1.0 m. Metal ions move through the capillary at a speed that depends on the charge and size of the ion. A pneumatic nebulizer generates an aerosol. The aerosol is then converted mainly into singly charged elemental ions in a hot ICP. The MS signals from selected ions are detected as a function of time.

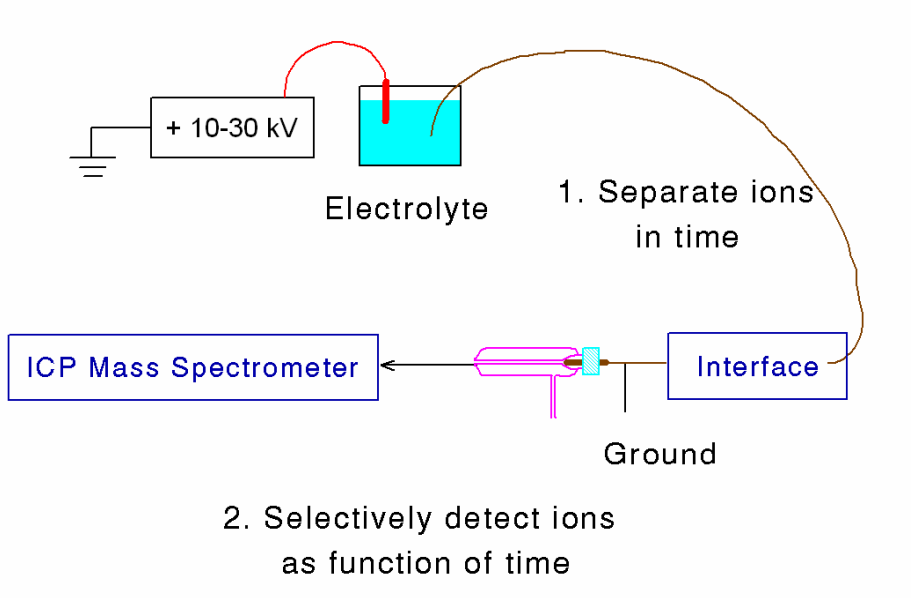

Figure 1.3 Capillary Electrophoresis-Inductively Coupled Plasma Mass Spectrometer instrument set up

Because ICP-MS is a mass selective detector, there is no need to separate electrophoretically all species in the sample because the detector can distinguish between different elements. It is not necessary to separate electrophoretically Cr^{3+} from As^{3+}, for example, because the spectrometer can distinguish between these atoms. Electrophoresis is required to distinguish Cr(III) from Cr(VI), since both species will be converted to Cr^{+} in the plasma. Using this technique, resolution can be exchanged for increased analysis speed allowing speciation to be accomplished in less time than required for conventional capillary electrophoresis using a non-selective detector.

By combining the rapid separation characteristics of CE and the low detection limits and element selective nature of the ICP-MS, the two techniques together can perform better quantitative analyses (ppb level) than the other common detection methods used in CE[54, 55,80,81].

However, the ICP-MS offers no species information because any species that enter the plasma are converted to free atoms and singly charged ions. The identification of species has to rely on the electrophoretic migration time. It may be necessary to measure the sample with known species in order to identify the molecular composition of the species.

Most commercial ICP-MS utilizes a quadrupole mass spectrometer as an analyzer. However, since only unit mass resolution is achievable for a quadrupole ICP-MS instruments, spectral interferences can make speciation analysis extremely difficult or impossible for certain elements.

Isotope	Interference	Resolution Required
^{28}Si	**$^{14}N_2$**	**960**
	$^{12}C^{16}O$	**1600**
^{31}P	$^{14}N^{16}O^{1}H$	970
^{39}K	$^{38}Ar^{1}H$	5700
^{44}Ca	**$^{12}C^{16}O_2$**	**1281**
^{52}Cr	$^{40}Ar^{12}C$	2400
	$^{35}Cl^{16}O^{1}H$	1700
^{56}Fe	**$^{40}Ar^{16}O$**	**2500**
	$^{40}Ca^{16}O$	2500
^{63}Cu	$^{40}Ar^{23}Na$	2800
^{64}Zn	$^{32}S^{16}O_2$	2000
	$^{32}S_2$	4300
^{75}As	**$^{40}Ar^{35}Cl$**	**7800**
^{80}Se	**$^{40}Ar_2$**	**9700**

Table 1.1 Lists of the examples of the major spectral interferences and the resolution required to resolve them for the interested elements.

Table 1.1 lists the examples of the major spectral interferences and the resolution required to resolve them for the interested elements. The majority of such interferences are caused by the presence of the plasma gas, water, acids used, and concomitant elements, from which a variety of molecules with overlapping nominal mass to charge ratios (m/z) are formed[82-84].

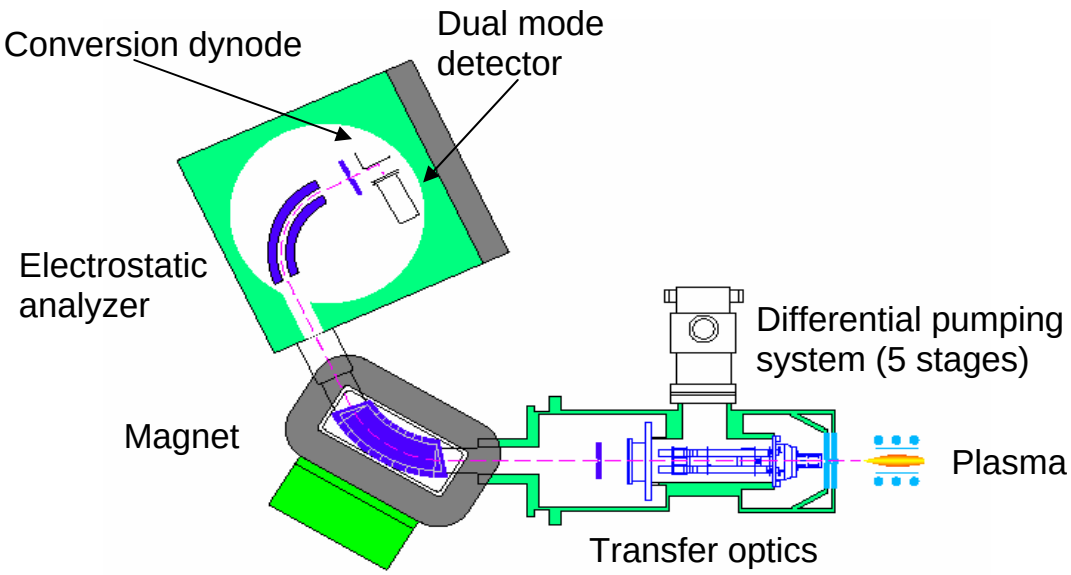

Figure 1.4 Schematic diagram of HR-ICP-MS with double focusing reverse Nier-Johnson geometry

In this work, all CE-ICP-MS experiments will be carried out with a Finnigan Element 2 (Finnigan, Bremen, Germany) high resolution inductively coupled plasma sector-field mass spectrometer (HR-ICP-MS). The instrument is equipped with a double focusing mass analyzer using reversed Nier-Johnson geometry (Figure 1.4) The system

allows three pre-defined nominal mass resolutions (m/Δm) of 300, 4,000, and 10,000 by means of selectable slits. The actual mass resolutions vary between 300-500 for low, 3,500-4,500 for medium, and 8,000-14,000 for high-mass resolution mode depending on the optimization of parameter settings.

Figure 1.4 shows the Schematic diagram of HR-ICP-MS. The Magnetic sector field focuses ions with diverging angles of motion from the entrance slit to the intermediate slit. The magnetic sector field is dispersive with respect to ion energy and mass (exactly momentum [mv]). The electric sector field (ESA) focuses ions with diverging angles of motion from the beta slit on to the exit slit. It is dispersive with respect ion energy (1/2 m.v2) only. Together, if the energy dispersion of magnet and ESA are equal in magnitude but of opposite direction, magnet and ESA focus both ion angles (first focusing) and ion energies (double focusing), while being dispersive for m/z: a mass spectrometer[85].

The high resolution capability of the HR-ICP-MS allows most of these elements to be distinguished from the interfering masses. Figure 5 shows the comparison of the mass spectra of Fe in quadrupole ICP-MS and HR-ICP-MS. Results demonstrated that under the medium resolution mode, interested Fe^{56} ion was completely separated from ArO^{56} interferences.

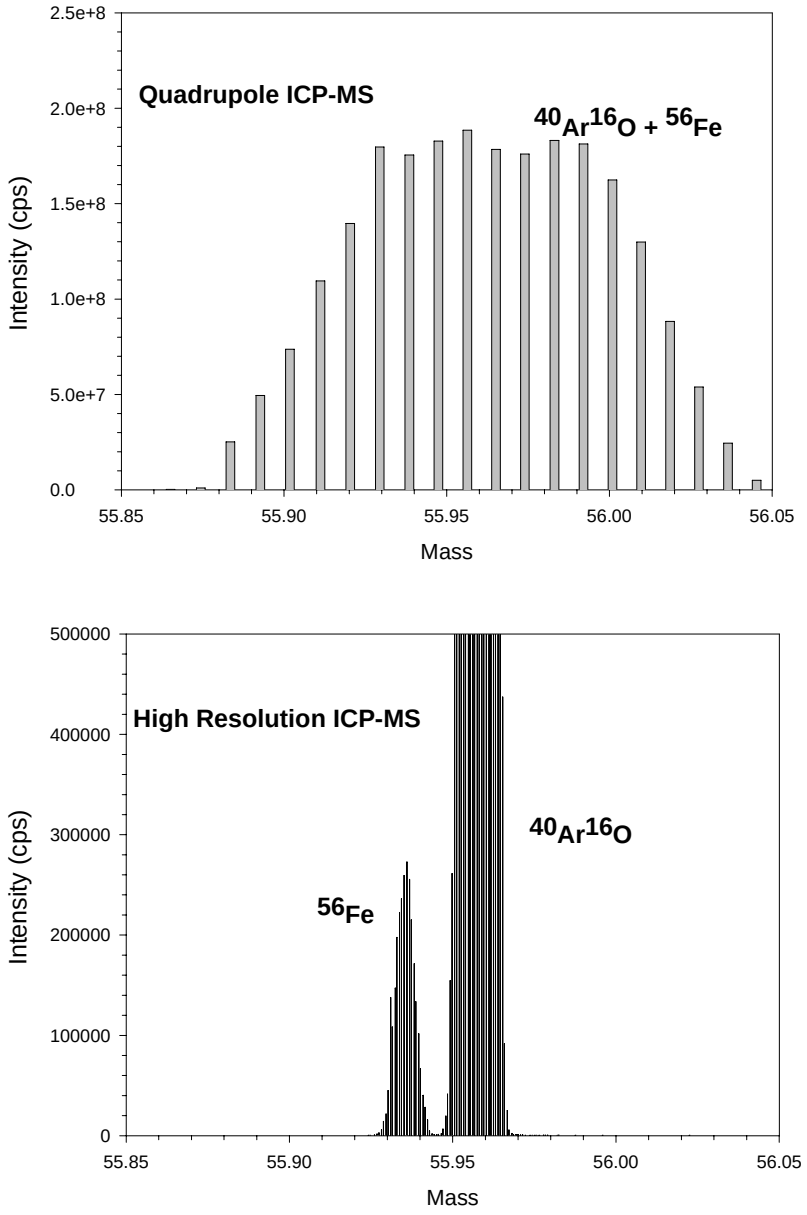

Figure 1.5 The comparison of the mass spectra of Fe in quadrupole ICP-MS and HR-ICP-MS

Besides high resolving power, another attractive feature of a magnetic sector instrument is its very high sensitivity combined with extremely low background level. High ion transmission in low resolution mode translates into sensitivity specifications of typically 100-200 million counts per second (mcps) per ppm, while background levels resulting from extremely low dark current noise are typically 0.1-0.2 cps. This compares with a typical sensitivity specification of 10-50 mcps per ppm and a typical background level of ~10 counts per second (cps) for a quadrupole instrument [4]. High ion transmission combined with extremely low background levels results in superior detection limits, typically orders of magnitude better than those achievable by a quadrupole-based instrument.

1.4 Separation of ions by capillary electrophoresis

The movement of ions towards the detector is governed by three forces that all must be considered for the optimization of any electrophoretic separation: electrophoretic migration, electroosmotic flow, and laminar flow.

Capillary electrophoresis (CE) differs from many other separation techniques, such as chromatography, in that it does not rely on any interaction between analyte and a stationary phase. Rather, separation is based solely on the difference in size, charge, and electrophoretic mobility of an ion in solution. This is important for the separation of metal ions because there is little difference in chemical functionality from one ion to another making separation using a stationary phase difficult. Typically, strong cation or anion exchange resins must be employed as a stationary phase to achieve adequate separation of metal ions. There is also less chance of a metal ion or metal-ligand complex

adsorbing to a surface and undergoing a redox reaction or ligand exchange reaction that would disturb the original speciation. Because there is a difference in the size and charge between many different metal ions and metal-ligand complexes, capillary electrophoresis can be used for the efficient separations of these species.

The mobility of the ion depends not only on the geometric size of the ion itself, but also the hydrodynamic radius (solvation sphere) of the ion. Electrophoretic mobility, refers to the rate at which an ion migrates in an electric field, and is directly proportional to the equivalent ionic conductivity (EIC) of the simple ion or charged complex.[61-62] Tables 1.2, 1.3 and 1.4 show representative EIC values for some common metal ions.[63] These tables illustrate both the strengths and weaknesses of using capillary electrophoresis for the separation of metal ions. Table 1.1 shows that monovalent cations have widely varying EIC values. Therefore the monovalent cations will migrate at very different rates and can be easily separated.

Ion	**Equivalent Ionic Conductance $\lambda_i(10^{-4}m^2Smol^{-1})$**	**Ionic Conductance (Valance x EIC) $\lambda_i(10^{-4}m^2Smol^{-1})$**
Li^+	38.66	38.66
Na^+	50.08	50.08
K^+	73.48	73.48
Rb^+	77.80	77.80

Table 1.2 Monovalent Cations

Ion	**Equivalent Ionic Conductance $\lambda_i(10^{-4}m^2Smol^{-1})$**	**Ionic Conductance (Valance x EIC) $\lambda_i(10^{-4}m^2Smol^{-1})$**
$1/2Cu^{2+}$	53.60	107.20
$1/2Fe^{2+}$	54.00	108.00
$1/2Mg^{2+}$	53.00	106.00
$1/2Mn^{2+}$	53.50	107.00
$1/2Zn^{2+}$	52.80	105.60

Table 1.3 Divalent Cations

Ion	**Equivalent Ionic Conductance $\lambda_i(10^{-4}m^2Smol^{-1})$**	**Ionic Conductance (Valance x EIC) $\lambda_i(10^{-4}m^2Smol^{-1})$**
$1/3Fe^{3+}$	68.00	204.00
$1/3Cr^{3+}$	67.00	201.00
$1/3Eu^{3+}$	67.80	203.40
$1/3Gd^{3+}$	67.30	201.90

Table 1.4 Trivalent Cations

As can be seen from Table 1.3, however, the EIC values for divalent cations are very similar. As a result, the electrophoretic mobilities of these ions and their migration

rates in an electric field will be very similar. An increase in the applied voltage across the capillary will improve the separation efficiency, but is limited by the resulting increase in Joule heating that leads to increased band broadening. In order to separate divalent ions from one another, complexing agents such as hydroxyisobutyric acid (HIBA) or crown ethers are typically employed to bind selectively to the ion and increase the difference in mobility.[86-88] The complexing electrolyte interacts with the metal ions to a differing extent which results in larger differences in migration rate since each ion will be bound to a chelate molecule for a different fraction of time. The migration rate of the metal ions will be proportional to the stoichiometry of the metal-chelate interaction and the fraction of time that the ion is free compared to the fraction of time it is bound to the chelate. The more chelated molecules an ion has, the larger the hydrodynamic radius of the complex is. This in turn results in a slower rate of migration in the electric field. In this manner, ions that have nearly identical EIC values can be separated providing that the fraction of time the chelate is bound varies from cation to cation. Any modification of the original sample due to the introduction of a complexing agent is undesirable for the measurement of the natural speciation of a sample, however, because it disturbs the original equilibrium and speciation of the sample. Therefore this method is of limited use for speciation analyses. Table 1.4 shows that the migration rates of triply charged ions are also similar; EIC values differ by only 1% between the slowest and fastest ion.

It should be noted that all of these values are adjusted for the ions valence. Hence, the true ionic conductance of a doubly charged ion would be twice the value shown and three times the value shown for a triply charged ion. For example, the true ionic conductance of Fe(II) would be 108×10^{-4} m^2 S mol^{-1} and the ionic conductance of

Fe(III) would be 204 x 10^{-4} m^2 S mol^{-1}. The migration of the ion in an electric field is proportional to the equivalent ionic conductance not the true ionic conductance. Therefore, the monovalent K^+ ion with a value EIC value of 73.48 x 10^{-4} m^2 S mol^{-1} is more mobile than the divalent Cu^{2+} ion with a value of 53.6 x 10^{-4} m^2 S mol^{-1}. The separation of inorganic ions with similar valancies by electrophoresis is difficult; however the separation of a set of divalent ions from a set of trivalent ions is easily achieved due to the large differences in equivalent ionic conductance.

The mass selective detector allows differentiation of one divalent ion from another. For example, Fe^{2+} (m/z=56) can easily be distinguished from Co^{2+} (m/z=59) in the mass spectrometer even though they cannot be effectively separated in time by capillary electrophoresis. Therefore, using a mass selective detector, it is only necessary to separate Fe^{2+} from Fe^{3+} (a divalent ion from a trivalent ion), for example, which is readily achieved using capillary electrophoresis.

When a voltage is applied to the separation capillary, the bulk electrolyte migrates toward the detector dragging all analyte species along with this bulk migration (electroosmotic flow). This process is discussed in more detail in chapter 2. Electroosmotic flow rates are typically small, on the order of 50-100 nL/min.

In addition to the electroosmotic flow of the bulk electrolyte and the electrophoretic migration of analyte ions, a third force is present in the CE-ICPMS interface and other similar systems such as electrospray mass spectrometry or condensation nucleation light scattering detection where the sample must be physically transported to the detector: nebulizer induced laminar flow. Laminar flow results in the non-selective transport of ions through the separation capillary. This force is typically

absent in traditional electrophoresis and is often considered undesirable because the resulting parabolic flow profile will lead to additional band dispersion and reduced separation efficiency.

The existence of laminar flow has positive implications for electrophoretic separations, however, such as increased analysis speed and the analysis of cations, neutral species and anions in one injection. Under conditions of high ionic strength, the laminar flow results in an increase in separation efficiency. The sheath flow interface allows the operator to change easily the magnitude and direction of laminar flow in the separation capillary to tailor separation conditions to a specific type of analysis. Another key advantage of laminar flow is the magnitude of the flow allows the user to easily control the tradeoff present between separation efficiency and analysis time. For samples where high separation efficiency is not required, such as the separation of Cr^{3+} from $Cr_2O_7^{2-}$ or Cu^{2+} from Cu-EDTA, a high laminar flow rate is advantageous because the total analysis time can be dramatically reduced. For more difficult analyses, where high resolution is required, the laminar flow can be eliminated for improved separation. The benefits of the sheath flow system will be discussed extensively in Chapter 2.

1.5 Goals of using capillary electrophoresis inductively coupled plasma mass spectrometry for speciation analyses

Currently available analytical techniques for quantitative elemental speciation often suffer from one or more of the following deficiencies: long analysis times, inadequate limits of detection, limited sample amenability, and insufficient selectivity. The goal of this research was to develop a technique that will provide rapid (1-2 minutes)

and quantitative elemental speciation of metal ions and metal ion complexes in a variety of samples with sub ppb detection limits.

To achieve this goal, capillary electrophoresis was combined with inductively coupled plasma atomic emission spectrometry and inductively coupled plasma mass spectrometry.

Capillary electrophoresis and inductively coupled plasma emission and mass spectrometry complement each other and offset the weakness of one technique with the strengths of the other. Plasma spectroscopy provides sensitive, element selective detection, but no speciation information. Capillary electrophoresis has high separation efficiencies, but detection is complicated by the extremely small size of the capillary. Typically, total column volumes are only a few microliters. This means that the detection volume will be on the order of 10 to 100 nanoliters. Coupling the high separation efficiency of capillary electrophoresis with the element selectivity and the low limits of detection of inductively coupled plasma emission and mass spectrometry provides a rapid, sensitive method for the speciation of metal ions, metal ligand complexes, and organometallic complexes.

This work will discuss in detail many aspects of interfacing capillary electrophoresis with inductively coupled plasma spectroscopy for elemental speciation. The most important consideration is physically coupling the two techniques. The interface between the two instruments must have a very small dead volume in order to preserve the high separation efficiencies inherent in capillary electrophoresis. In addition, the capillary electrophoresis effluent must be efficiently converted to aerosol for

effective transport to the plasma. The effect of the aerosol generation process on electrophoretic resolution and precision must also be considered.

A sheath flow interface was developed that allows control of the tradeoff between sample resolution and time of analysis by manipulating laminar flow in the electrophoretic separation capillary. Examples demonstrating this control will be discussed. Once the capillary electrophoresis effluent was effectively coupled to the inductively coupled plasma, a number of other parameters were investigated. The selection of electrolyte used in the electrophoretic separation plays a critical role in enhancing efficiency and achieving the goal of rapid speciation.

Factors such as electrolyte composition and concentration that have profound effects on the band broadening, influence of Joule heating, sample complexation, electrophoretic focusing, and separation efficiency will also be discussed in detail. Interaction between the electrolyte and the analyte ions was also studied in order to insure that these interactions do not alter the native speciation of the sample.

Next, applications showing the speciation of varies metal ions among others, are presented that demonstrate that this technique can be successfully used to achieve speciation in times less than short time.

Studies of formation, distribution, lability, inertness of various metal species in aquatic environment are of great importance, and CE is an effective tool for these studies. The chapter 3 is to evaluate the capability of CE-ICP-MS as a tool for speciation studies in aqueous system for different metal species. In particular, using a solution with well-defined chemistry ($RhCl_3$ aqueous solution), it is possible to separate metal fractions into its various components and more importantly, identify and quantify these species

distribution using migration time and peak area calculation. The effects of solution pH as well as solution ageing on various Rh species will also be discussed.

The majority of CE coupled with ICP-MS for metal speciation study found in the filed of applying CE for speciation study has focused on the use of aqueous buffers as background electrolytes. One of the problems in applying aqueous CE method on pharmaceutical compound analysis is poor water solubility of certain pharmaceutical drugs and drug precursors. In chapter 4, CE using non-aqueous electrolytes will be demonstrated. Other advantages of using non-aqueous electrolytes in CE include greater ability to manipulate separation selectivity due to a wide range of physicochemical properties of different organic solvents, lower separation current and joule heating, increased compatibility for coupling CE with mass spectrometry when using volatile solvents such as methanol were also be discussed.

In chapter 5, the feasibility of application of non-aqueous CE for speciation analysis for the synthesis of pharmaceutical products, particularly, for understanding of reaction mechanism and kinetics of catalyst formation by identification and quantitation of various catalyst metal species during the course of the reaction was discussed. The reaction media typically is a complex organic system consisting of different metal species which undergo constant transformation over the course of reaction. To our knowledge, this is the first application employing the resolving power of non-aqueous CE-ICP-MS in this field.

Post-reaction removal of trace metal impurities has become an increasingly important purification need in recent years, paralleling the growing use of organometallic reagents and metal catalysts in pharmaceutical synthesis. While heterogeneous metal

catalysts can often be removed by simple filtration after the reactions, the use of homogeneous catalysts frequently requires removal of residual metals from the product, a problem that can be considerably more challenging. The use of non-aqueous CE-ICP-MS to help design an effect route to remove metal impurities will be demonstrated.

1.6 Other Applications of HR-ICP-MS in Pharmaceutical Research and Development

Metal in pharmaceutical materials may be inadvertently introduced in many ways, such as from raw materials, reagents, solvents; from electrodes, reaction vessels, plumbing and other equipment used in the synthesis; exposure to the air-borne particles; or from container/closure systems, etc. Most importantly, metals may be introduced through the utilization of catalysts at various steps during the synthesis. Due to the ability of metals to catalyze decomposition and their potential for toxicity, metal content monitoring of process intermediates and final drug substances is widely employed[88-92].

The applications of HR-ICP-MS for trace element analysis including Residual catalyst analysis and quality control, contamination control and monitoring, Purification optimization and cleaning verification, process troubleshooting and optimization, molecular identification and confirmation of stoichiometries and analytical support for clinical trials. Some elements that need to be tested have potential isobaric and/or polyatomic interferences that only a high resolution ICP-MS can provide an unambiguous and reliable result. In this work, two particular applications of HR-ICP-MS were studied.

In chapter 6, an application of HR-ICP-MS for non-metals (Halogen) analysis was described. Since halogen-containing compounds are used widely as drug substances, the

knowledge of the exact halogen content would be extremely helpful in fast molecular identification and confirmation of stoichiometry of a drug compound under development. The identification and quantitation of unintended halogen impurities in drug substances has also been requested by organic chemists. A method has been developed for the determination of Fluorine (F), Chlorine (Cl), Bromine (Br), and Iodine (I) using high resolution ICP-MS from sub ppm to major levels in various organic compounds. This method has proven to be very useful and reliable in support of ever-increasing demands from organic chemists to efficiently support new drug discovery and development programs at Merck.

The most important and innovative aspect of ICP-MS is the possibility to greatly extend the use of stable isotopes as tracers in biomedicine, which originates from its ability to determine isotope ratios in biological samples using much simpler and faster procedures than before yet maintaining a precision sufficient enough for most biomedical applications. In chapter 7, a method for the determination of all six Ca isotopes was developed. The determination of calcium isotopic composition using a quadrupole-based ICP-MS is subject to numerous polyatomic interferences, which affect all calcium isotopes to various degrees. The high resolution ICP-MS was the only choice for accurate determination of all six natural isotopes of calcium. With the resolution set at medium to high, most of the polyatomic interferences can be overcome or minimized with the high resolution ICP-MS such that satisfactory precision can be achieved. Calcium composition of ^{40}Ca (using cold plasma conditions), ^{42}Ca, ^{43}Ca, ^{44}Ca, ^{46}Ca, and ^{48}Ca were determined with the high resolution ICP-MS, and excellent agreements were obtained with the COA's.

These applications have demonstrated that high resolution ICP-MS has become an important tool in pharmaceutical research, and will become an essential tool in the near future, as the drive to shorten the development time for new pharmaceutical entities is getting stronger and stronger and the detection limit requirements for pharmaceutical impurities and metabolites are getting lower and lower. The fast, reliable and unambiguous results high resolution ICP-MS provides will be used to meet regulatory requirements, contamination monitoring, process troubleshooting and optimization as well as support of clinical trials.

References

1 Salbu, B.; Steinnes, E., Trace Elements in Natural Water; CRC Press: Boca Raton, FL, 1995

2 Caroli, S., Element Speciation in Bioinorganic Chemistry; John Weiley & Sons, Inc: New York, 1996

3 Natusch, D. F. S.; Hopke, P. K., Analytical Aspects of Environmental Chemistry; John Wiley & Sons, Inc: New York, 1983

4 Beceiro-Gonzalez, E.; Bermejo-Barrera, P.; Bermejo-Barrera, A.; Garci-Barciela, J.; and Barciela-Alonso, C. J. Anal. At. Spectrom., 1993, 8, 649.

5 Merian, E., Carcinogenic and Mutagenic Metal Compounds: Environmental andAnalytical Chemistry and Biological Effects; Gordon and Breach Science Press,New York 1985.

6 Demesmany, C.; Olle, M.; Porthault, M., Fresenius J. Anal. Chem. 1993, 348, 250.

7 Beceiro-Gonzalez, E.; Bermejo-Barrera, P., J. Anal. At. Spectrom. 1993, 8, 348

8 Buffer, J., Complexation reactions in aquatic systems: an analytical approach; Horwood: Chichester, 1988.

9 Hobbs, S. E.; Olesik, J. W., Spectrochim. Acta, 1993, 48B, 817.

10 Qiang Tu, Tiebang Wang, Christopher J. Welch, Peng Wang, Xiujuan Jia, Conrad Raab, Xiaodong Bu, and Michael P. Doyle, Anal. Chem., 78 (4), 1282 -1289, 2006

11 Christopher J. Welch, Qiang Tu, Tiebang Wang, Conrad Raab, Peng Wang, Xiujuan Jia, Xiaodong Bu, Darren Bykowski, Benjamin Hohenstaufen, Michael P. Doyle, Adv. Synth. Catal. 2006, 348, 821 – 825

12 I. Ojima (Ed.), Catalytic Asymmetric Synthesis,2nd edn., Wiley, New York, 2000;

13 J. M. Hawkins, T. J. N. Watson, Angew. Chem. Int. Ed. 2004, 43, 3224–3228;

14 Y. Hsiao, N. R. Rivera, T. Rosner, S. W. Krska, E. Njolito, F. Wang, Y. Sun, J. D. Armstrong III, E. J. J. Grabowski, R. D. Tillyer, F. Spindler, C. Malan, J. Am. Chem. Soc. 2004, 126, 9918–9919; d) J. G. De Vries,

15 H. M. De Vries, C. E. Tucker, J. A. Miller, Innov. in Pharm. Tech. 2001, 01, 125–126, 128, 130.

16 Svelana, S.; Anatoly, P.; Gumenyuk, S.; Lubov, F.; Andrei, R.; Talanta 61 (2003) 195-202

17 C. J. Welch, J. Albaneze-Walker, W. R. Leonard, M. Biba, J. DaSilva, D. Henderson, B. Laing, D. J. Mathre, S. Spencer, X. Bu, Xiadong, T. Wang, Org. Proc. Res. Dev. 2005, 9, 198 – 205;

18 Montaser, Akbar and Golightly, D. W. (editors) Inductively Coupled Plasmas in Analytical Atomic Spectrometry 3nd Edition. 2005 VCH Publishers, New York.

19 Copeland, T. R. and R. K Skogerboe, Anal. Chem. 1981, 46, 1257A.

20 Sandell, E. B. and Onishi, H. Photometric Determination of Traces ofMetals, 4th ed., Wiley-Interscience, New York, 1978.

21 Snell, F. D. Photometric and Fluorometic Methods of Analysis: Metals,Wiley-Interscience, New York, 1978.

22 Skoog, D. A.; West, D. M.; and Holler, F. J. Fundamentals of AnalyticalChemistry. 1988 Saunders Publishing, New York, New York.

23 V. Gómez and M.P. Callao TrAC Trends in Analytical Chemistry, Volume 25, Issue 10, November 2006, Pages 1006-1015

24 Biyang Deng, Jinrong Feng and Jun Meng Analytica Chimica Acta, In Press, Corrected Proof, Available online 26 September 2006,

25 Michalke, B.; P, S., Fresenius J. Anal. Chem. 1997, 357, 594-599.

26 Michalke, B.; Lustig, S.; Schramel, P., Eelectrophoresis 1997, 18, 196-201

27 Olesik, J. W.; Kinzer, J. A.; Olesik, S. V., Anal. Chem 1995, 67, 1-12.

28 Frankenberger, W. T.; Mehra, H. C.; Gjerde, D. T., J. Chromotogr. 1990, 504, 211

29 Dasgupta, P. K., J. Chromatogr. Sci. 1989, 27, 422.

30 Estes, S. A.; Uden, P. C.; Barnes, R. M., Anal. Chem. 1981, 1829-1837.

31 Ebdon, L.; Ward, R. W.; Leathard, D. A., Analyst 1982, 107, 129-143.

32 Sutton, K. L.; Caruso, J. A., J. Chromatogrphy A. 1999, 856, 243-258.

33 Cai, J.; Henion, J., J. Chromatography A 1995, 603, 667-692.

34 Dabek-Zlotorynaska, E.; Lai, E. P. C.; Timebaev, A. R., Analytica Chimica Acta 1998, 359, 1-26.

35 Buchberger, W.; Semenova, O. P.; Timerabev, A. R., J. High Resoulution Chromatography 1993, 16, 153.

36 Westen, A.; Brown, P. R.; Jandik, P.; Jones, W. J.; Heckenberg, A. L., J. Chromatogr. 1992, 593, 289.

37 Timerbaev, A.; Semenova, O.; Bonn, G., Chematographia 1993, 37, 497.

38 Gross, L.; Yeung, E., Anal. Chem. 1990, 62, 247.

39 Swaile, D. F.; Sepammiak, M. J., Anal. Chem. 1991, 66, 1.

40 Lu, W.; Cassidy, R. M., Anal. Chem. 1993, 65, 1649.

41 Sutton, K.; Sutton, R. M. C.; Caruso, J. A., J. Chromatography A 1997, 789, 85-126.

42 Arar, E. J.; Long, S. E.; Martin, T. D.; Gold, S., Environ. Sci. Technol. 1992, 26, 1944.

43 Tomlinson, M. J.; Wang, J.; Caruso, J. A., J. Anal. At. Spectrom. 1994, 9, 957.

44 Stewart, I. I.; Olesik, J. W., J. Chromatography A 2000, 872, 227-246.

45 Olesik, J. W., Anal. Chem. 1991, 63, 12A.

46 Estes, S. A.; Uden, P. C.; Barnes, R. M., Anal. Chem. 1981, 53.

47 De Jonghe, W.; Chakraborti, D.; Adams, F., Anal. Chim. Acta. 1980, 115, 89-105.

48 Haddad, P. R. and Jackson, P. E. Ion Chromatography: Principles andApplications Elsevier Press, Amsterdam, 1990.

49 Walton, H. F. and Rocklin, R. D. Ion Exchange in Analytical Chemistry,CRC Press, Boca Raton, FL, 1990.

50 Dong-Dong Wang, Feng Li and Xiu-Ping Yan Journal of Chromatography A, Volume 1117, Issue 2, 9 June 2006, Pages 246-249

51 Karine Faure, Michael Loughran and Jeremy D. Glennon Analytica Chimica Acta, Volume 557, Issues 1-2, 31 January 2006, Pages 130-136

52 Talanta, Volume 66, Issue 1, 31 March 2005, Pages 153-159
Sasi S. Kannamkumarath, Katarzyna Wrobel and Rodolfo G. Wuilloud

53 Gloria Álvarez-Llamas, María del Rosario Fernández de laCampa and Alfredo Sanz-Medel, TrAC Trends in Analytical Chemistry, Volume 24, Issue 1, January 2005, Pages 28-36

54 Bu, X., Wang, T., Hall, G. Journal of Analytical Atomic Spectrometry, *in press*

55 Stewart, I. I.; Olesik, J. W., J. Chromatography A 2000, 872, 227.

56 Chen, M.; Casidy, R., J. Chromatorgr. A 1993, 640, 425.

57 Guevremont, R.; Nerman, S., J. Am. Soc. Mass Spectrom 1992, 3, 216.

58 Rivello, J. M.; Harrold, M. P., J. Chromatogr. A 1993, 652, 385.

59 Shi, Y.; Fritz, J. S., J. Chromatogr. 1993, 640, 473.

60 Romano, J. P.; Krol, J., J. Chromatogr. 1993, 640, 403.

61 Landers, J. P., Hand Book of Capillary Electrophoresis; CRC Press: New York, 1997.

62 Guzman, N. A., Capillary Electrophoresis Technology; Marcel Dekker, INC: New York, 1993.

63 Righetti, P. G., Capillary Electrophoresis in Analytical Biotechnology; CRC Press: New York, 1996.

64 Lu, W.; Cassidy, R. M., Anal. Chem. 1993, 65, 1649.

65 Sutton, K.; Sutton, R. M. C.; Caruso, J. A., J. Chromatography A 1997, 789, 85-126.

66 Tsuda, T.; Sweedler, J. V.; Zare, R. N. Anal. Chem. 1990, 62, 2149.

67 Chervet, J. P.; van Soest, R. E. J.; Ursem, M. J. Chromatogr. 1991, 543, 439.

68 Gordon, G. B.; Tella, R. P.; Martins, H. A. S. Hewlett-Packard Journal 1995, 62.

69 Meek, M. E.; Hughes, K. Regulatory Toxicology and Pharmacology,1995, 22, 206.

70 Nobuhiko Iki, Hitoshi Hoshino, and Takao Yotsuyanagi, J. Chromatogr. A., 1993, 652, 539.

71 Swartz, M. E. J. Chromatogr. A, 1993, 640, 441.

72 Shi, Y and Fritz, J. S. J. Chromatogr. A., 1993, 640, 473.

73 Jones, W. R. and Jandik, P. J. Chromatogr. 1993, 608, 385.

74 Lu, W. and Cassidy, R. M. Anal. Chem. 1993, 65, 1649.

75 Lu, W. and Cassidy, R. M. Anal. Chem. 1993, 65, 2878.

76 Ye, J. and Baldwin, R. P. Anal. Chem. 1993, 65, 3525.

77 Hill, S., Inductively coupled plasma mass spectrometry and its applications; Sheffield Academic: Sheffield, 1999.

78 Montase, A., Inductively coupled plasma mass spectrometry; Wiley VCH: New York, 1998.

79 Houk, R. S., Spetrochimica Acta Part B 1998, 53, 267-271.

80 Olesik, J. W.; Kinzer, J. A.; Olesik, S. V., Anal. Chem. 1995, 34, 1.

81 Kinzer, J. A.; Olesik, J. W.; Olesik, S. V., Anal. Chem. 1996, 68, 3250-3257.

82 Field M.P. and R.M. Sherrell, 2003, Journal of Analytical Atomic Spectrometry, 18, 254

83 Bu X., Wang T. and Gene Hall, J. Anal. At. Spectrom., 2003, 18,

84 Zheng J. and H. Hintelmann, J. Anal.At. Spectrom., 19, 2004,

85 Training documents from Thermo Finigan

86 Shi, Y and Fritz J. S. J. Chromatogr. A, 1993, 640, 473.

87 Jones, W. R. and Jandik, P. J. Chromatogr., 1993, 608, 385.

88 R. Nageswara Rao, M.V.N. Kumar Talluri, Journal of Pharmaceutical and Biomedical Analysis 43 (2007) 1–13

89 Xiujuan Jia, Tiebang Wang, Xiaodong Bu, Qiang Tu , Journal of Pharmaceutical and Biomedical Analysis, Volume 41, Issue 1, 11 April 2006, Pages 43-47

90 Xiujuan Jia, Tiebang Wang, Xiaodong Bu and Jane Wu Microchemical Journal, Volume 75, Issue 2, September 2003, Pages 103-107

91 J.G. Hardman, L.E. Limbird, P.B. Molinoff, R.W. Ruddon and A.G. Gilman, Good and Gilman's The pharmaceutical Basics of Therapeutics (9th ed.), McGraw-Hill, New York (1999) p. 3–63.

92 In: S. Gorog, Editor, Identification and determination of Impurities in Drugs, Elsevier Science, Amsterdam (2000), p. 748.

Chapter 2

Coupling Capillary electrophoresis (CE) with Inductively Coupled Plasma Mass Spectrometry (ICP-MS): Design, Optimize and Characterize a Sheath Flow Interface

2.0 Introduction

Capillary electrophoresis (CE) has been used extensively for the separation of organic ions, biological molecules and proteins but less frequently to the separation of metal ions in solution[1-5]. Although capillary electrophoresis has excellent resolution in the realm of biological molecules where there are large differences in both the size and number of charges present on an ion, its effectiveness is more limited for high resolution analysis of metal ions[6-8]. This is due to the small, element dependent difference in hydrodynamic radii and electrophoretic mobility for divalent and trivalent ions. The electrophoretic mobility of an ion in solution is proportional to the equivalent ionic conductance of that ion. Many divalent metal cations, such as Cu^{2+}, Fe^{2+}, Mg^{2+} are very difficult to separate from one another using capillary electrophoresis because their equivalent ionic conductances (107.2×10^{-4}, 108×10^{-4}, and 106×10^{-4} m^2 S mol^{-1} at 25^{o}C, respectively)[9-12], are similar. For the same reasons, many trivalent ions such as

Fe^{3+} and Cr^{3+}, are difficult to separate by capillary electrophoresis because their equivalent ionic conductances (156×10^{-4} and 154×10^{-4} m^2 S mol^{-1} at 25 ^oC, respectively)[10] are similar.

This chapter describes the development of a novel sheath flow interface with PFA micro flow nebulizer for CE-ICPMS that provides the ability to control the tradeoff between resolution and sample analysis time by manipulating laminar flow rates in the separation capillary. This chapter will explore the effect of the nebulizer induced laminar flow profile on peak widths, peak asymmetry, separation efficiency and analysis time. The sheath flow interface will be used to manipulate both the velocity and direction of laminar flow in the separation capillary. Surprisingly, it will be shown that despite the fact that laminar flow results in increased band dispersion, the addition of laminar flow can be used to great advantage in not only reducing analysis time but to also increase separation efficiency under some conditions.

2.1 Interfacing Consideration for Combining CE with ICP-MS and Previously Developed Interfaces

ICP-MS is inherently off-line detector that requires the sample to be physically transported from the separation capillary to the detector unlike UV-Visible and LIF detection which can be used on-column. Care must be taken in the design of the interface so that the aerosol generation and transport of the analyte to the detector does not degrade the high separation efficiency of capillary electrophoresis.

Because sample sizes in capillary electrophoresis are typically less than 100 nL, care must be taken to transport the sample to the ICP with high efficiency in order to maintain the low detection limit potential offered by ICP-MS detection. Optimization of

the interface must consider both the need to transport sample efficiently to the plasma while maintaining an effective electrophoretic separation.

As with any interface to a separation technique, the interface must be designed to minimize the amount of unswept dead volume that may result in increased band dispersion and loss of resolution.

Because capillary electrophoresis relies on a high potential field gradient, typically 20 - 40 kV/m, the CE-ICP-MS interface must provide a location for the stable connection of the terminal end of the separation capillary to ground in order to complete the electrophoretic circuit. For on-line detection this is accomplished by simply inserting the terminal end of the capillary into a terminating electrolyte vial that is held at ground potential. Because the sample must be physically transported to the ICP, another means of insuring a stable ground connection is required.

Most commonly, sample uptake rates for ICP-OES and ICP-MS analyses are on the order of 1 mL/min. At these sample flow rates, conventional nebulizer/spray chamber configurations result in only 1 to 2% of the aerosol being transported to the plasma.[13] Because injection volumes in capillary electrophoresis are on the order of a few nanoliters, the interface should transport the sample to the plasma with as close to 100% efficiency as possible because one cannot afford to lose 99% of the sample to the drain as is typical with conventional nebulizer/spray chamber configuration operating with 1 mL/min uptake rates. Even with 100% transport efficiency, the amount of material entering the plasma per unit time will be less for the CE sample introduction system. Assume, for example, that 5 nL of solution containing 1 ng/mL of arsenic is injected into the CE with an aerosol transport efficiency of 100%. For a 10 s wide electrophoresis

peak, an average of 0.5 fg of arsenic would enter the plasma per second. In contrast, for a sample introduction rate of 1 mL/min and an aerosol transport efficiency of 1%, 167 fg of arsenic would enter the plasma per second. Approximately 300 times less sample enters the plasma per unit time for the CE-ICPMS compared to conventional sample introduction.

The signal in ICP-MS is dependent on the amount of sample introduced to the plasma per unit time, the fraction of that sample that is converted to ions, the fraction of those ions that traverse the ion optics and the mass filter to reach the detector. Typically, approximately one in 105 to 106 ions generated in the ICP reach the detector.[14,15] Because the ion transport could not be easily changed, optimization of signal was accomplished primarily by improving the fraction of sample that reached the plasma. Because the ICP-MS signal is dependent on the total amount of material introduced to the plasma at a given time not the concentration of the analyte, dilution of the sample by the interface is unimportant. Changes in aerosol transport, however, are very important.

In order to be useful as a research and analytical tool, the interface needs to allow for precise, reproducible positioning of the separation capillary with the nebulizer because the connection between the separation capillary and the capillary of the nebulizer determines in large part the magnitude of laminar flow. In addition, the interface should be easy for the user to assemble and maintain for routine, trouble-free performance.

2.2 Transport of Sample to The ICP-MS

The conversion of liquid sample to aerosol has been accomplished in conventional ICP spectroscopy in a variety of ways. The most common methods are either pneumatic nebulization or ultrasonic nebulization, with pneumatic nebulization by

far being dominant in frequency of use. The most common nebulizer is the concentric pneumatic nebulizer that is amenable to a variety of sample uptake rates ranging from a few microliters per minute to 1 mL/min. Reviews of many of these nebulizers and other variations can be found elsewhere.[16,17]

Pneumatic nebulizers all produce aerosol in a similar manner by using a high velocity gas flow, typically argon, to break the liquid stream into small droplets for transport to the ICP and have shorter washout times and less sample carryover than other types of nebulizers.

Pneumatic nebulization was selected over ultrasonic nebulization because an argon gas flow is used to fracture the liquid stream into many fine droplets with little sample carry over. In ultrasonic nebulization, liquid is allowed to flow across a piezoelectric substrate and mechanical vibration is used to produce the aerosol. This type of nebulization allows for the potential of sample carryover because the substrate can adsorb analyte ions. In addition, washout times of the substrate can be on the order of several seconds resulting in the introduction of extra column dead volume. For this work, PFA (Perfluoroalkoxy) micro-flow concentric nebulizers were used for CE-ICP-MS experiments.

Compare to traditiontial Meinhard® glass concentric nebulizers, the micro-flow PFA nebulizers provide low sample uptake rates (20-100µL /min), thus more suitable to use with CE. A schematic diagram showing an end-on and side-on view of the nebulizer tip is shown in Figure 2.1. The PFA MicroFlow Nebulizers used for this research compared to Meinhard® SB-30-A3 and Meinhard® high efficiency (HEN) glass concentric nebulizers differ from one another mainly in the size and spacing of the

concentric glass channels as shown in Table 2.1.

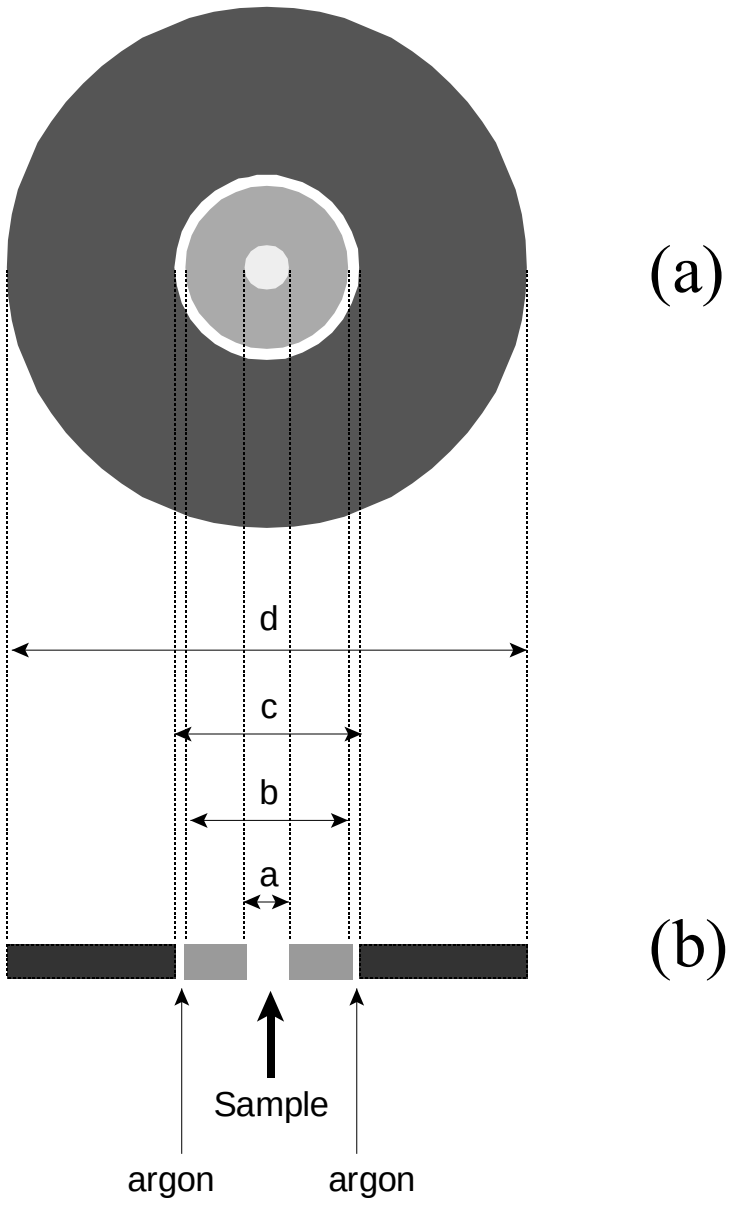

Figure 2.1 Diagram of the Meinhard® glass, pneumatic nebulizer a) End on view of the nebulizer b) Side on view of the nebulizer tip

	a	b	c	d
Meinhard® SB-30-A3	280 µm	440 µm	480 µm	2065 µm
Meinhard® HEN	90 µm	140 µm	167 µm	1075 µm
PFA MicroFlow Nebulizers (50uL/min)	66 µm	120 µm	137 µm	768 µm

Table 2.1: Nebulizer dimensions for the two Meinhard® nebulizers and PFA MicroFlow Nebulizers used for these experiments

Previously, a direct insertion interface consisting of a silver-plated fused silica capillary that was inserted into a concentric pneumatic nebulizer was described.[18,19] This interface show in Figure 2.2 allows for very precise positioning of the capillary in the nebulizer to minimize dead volume in the interface and generate aerosol directly from the tip of the separation capillary.

The silver plating on the separation capillary serves two purposes. First, because the effluent from the separation capillary is in intimate contact with the silver coating, the coating provides a favorable location for the electrical ground connection. Second, the thickness of the silver coating can be adjusted to completely fill the tapering inner channel of the Meinhard® SB-30-A3 nebulizer holding the separation capillary in place and eliminating unswept dead volume in the interface. The separation capillary was inserted into the nebulizer to within approximately 0.5 mm of the nebulizer tip. The sample effluent from the separation capillary enters the nebulizer and is converted to a fine aerosol assisted by a rapid jet of argon gas.

One key side effect of this type of interface is the generation of a laminar flow profile in the separation capillary that is normally absent in capillary electrophoresis.

Laminar flow is induced in the separation capillary by the pressure drop that results from the rapid expansion of argon escaping from the end of the glass concentric, pneumatic nebulizer. This results in aspiration of liquid from the separation capillary. The magnitude of laminar flow in the separation capillary is on the order of 2 μL/min which is over an order of magnitude greater than the electroosmotic flow rate of 51 nL/min measured earlier for a 100 μm i.d. capillary.[20]

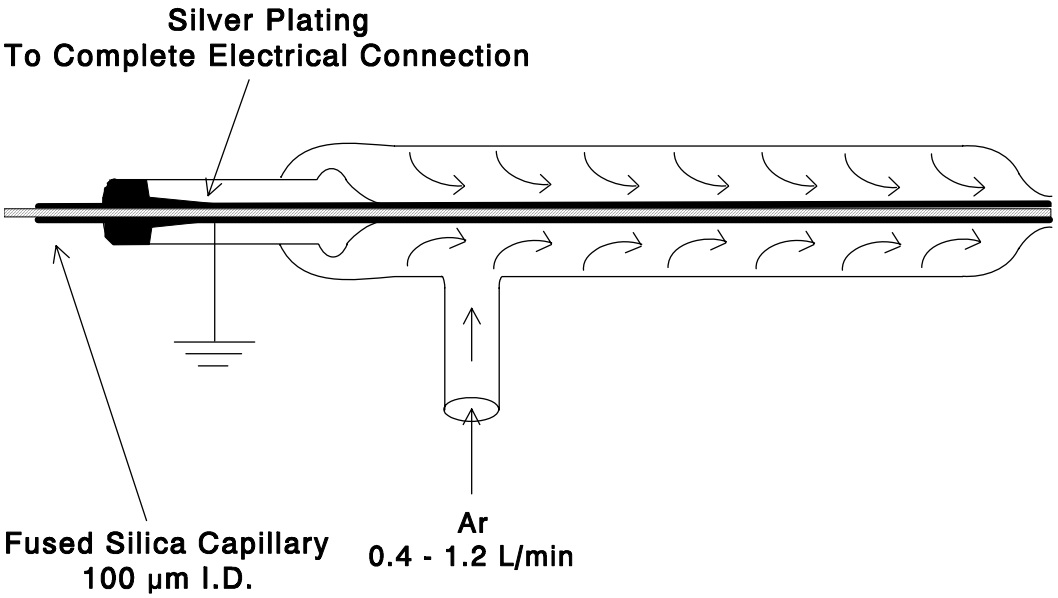

Figure 2.2 Diagram of the direct insertion interface between the separation capillary and the concentric, pneumatic nebulizer

The existence of laminar flow can be undesirable because it introduces band dispersion in the electrophoretic zones and results in the non-selective movement of ions in the separation capillary, and this type of direct insertion interface provide no contronl

of the laminar flow.

As will be shown in this chapter, a novel sheath flow CE-HR-ICP-MS interface coupled to a PFA Teflon micro-flow concentric nebulizer will be developed and characterized. The effects of sheath flow, induced laminar flow, electroosmatic flow, and the separation electrolytes on sensitivity and separation efficiency will be discussed**.** The laminar flow profile can be used to achieve rapid separation of positive, neutral and negative ions all in one electrophoretic run that would not always be possible in the absence of laminar flow. In addition, the existence of laminar flow allows one to rapidly and conveniently exchange resolution for significantly decreased analysis time. Under conditions of high sample conductivity, the laminar flow introduced by the nebulizer also results in an enhancement in separation efficiency.

2.4 Electroosmotic and Laminar Flow Profiles in Capillary Electrophoresis

Unlike most other separation techniques, capillary electrophoresis exhibits a flat flow profile that minimizes sample zone dispersion and leads to high efficiency separations. Laminar flow while common in many separation techniques such as liquid chromatography and ion chromatography that use a pump to force solvent through the capillary is normally absent in capillary zone electrophoresis.

Bulk flow of electrolyte in capillary electrophoresis is driven by the net migration of ions sliding across a stagnant double layer at the inner wall surface of the separation capillary called the Debye layer. This bulk flow of ions is termed electroosmotic flow (EOF). Figure 2.3 illustrates a schematic representation of the ions at the fused silica-electrolyte interface. Fused silica consists predominately as of a number of negatively charged, exposed $Si\text{-}O^-$ groups at the pH typically used for analysis. The number of these

anionic groups is strongly dependent on the pH of the electrolyte solution. The pK_a of fused silica is nominally 5.3 although this varies somewhat from manufacturer to manufacturer.[21,22] At high pH, most of the surface is covered with negatively charged silica groups. At low pH, many of these sites are in the protonated silanol form. The number of negatively charged silica groups in part controls the velocity of the electroosmotic flow. Changing the pH from pH = 3 to pH = 9 results in an increase of the electroosmotic flow rate from 30 nL/min to 240 nL/min.[23,24]

Because the capillary surface has a net excess of negative charge, cationic counter-ions from the electrolyte solution form a stagnant double layer on the anionic surface of the fused silica. Successive alternating positively and negatively charged layers build up gradually becoming more diffuse towards the radial center of the capillary. This layer ranges in thickness from a few nanometers to around 300 nm depending on the number of negatively charged sites, the voltage applied across the capillary and the concentration of the electrolyte.[25] The potential across this double layer is termed the zeta potential (ζ) and is defined in equation 1. [10]

$$\zeta = \frac{4\pi\eta\mu_{eo}}{\varepsilon} \qquad \textbf{(1)}$$

Where: η is the viscosity of the solution
μ_{eo} is the coefficient for electroosmosis
ε is the dielectric constant of the electrolyte solution

The velocity of the electroosmotic flow (μ_{eof}) is proportional to the zeta potential across the stagnant double layer as shown in equation 2. [10]

$$\mu_{eof} = \frac{\varepsilon}{4\pi\eta} E\zeta \qquad (2)$$

Where: μ_{eof} is defined as the electroosmotic velocity
ε is the dielectric constant
ζ is the zeta potential
η is the solution viscosity
E is the potential applied across the capillary

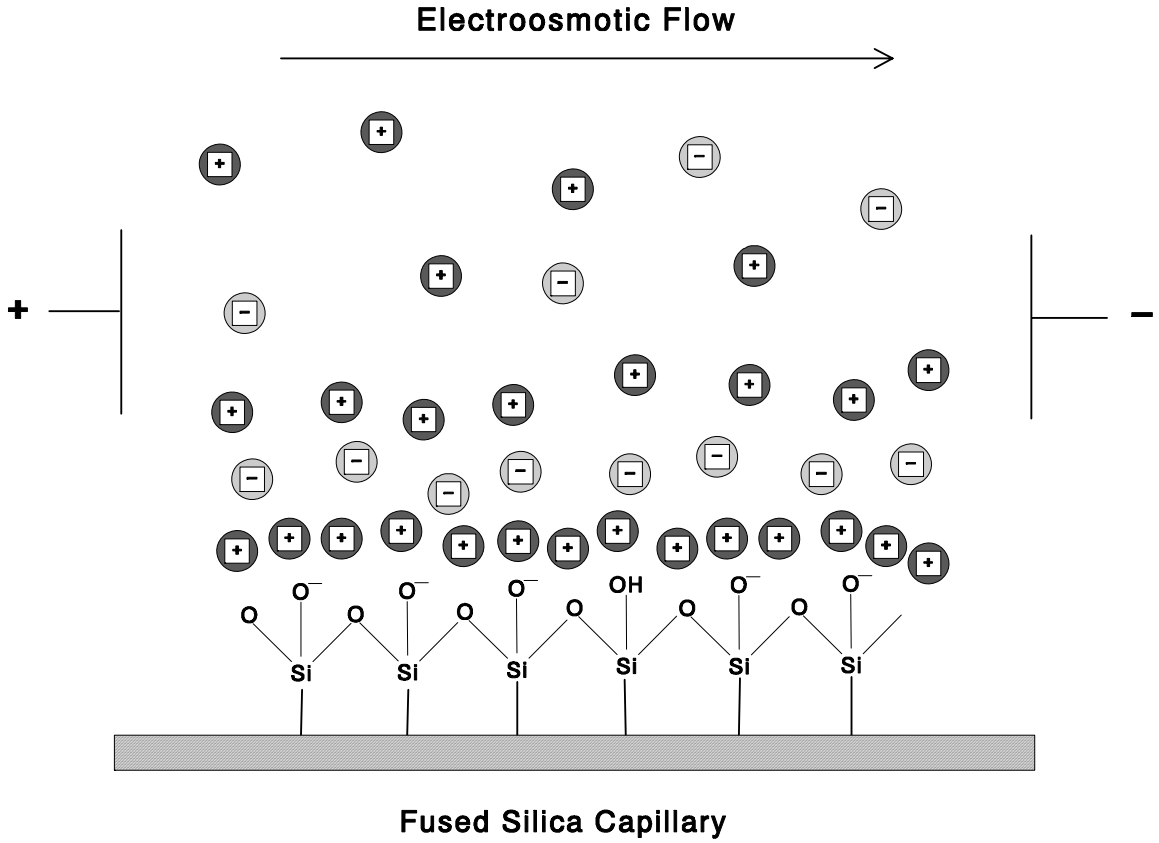

Figure 2.3 Schematic representation of the fused silica surface showing the stacking of ion layers which lead to electroosmotic flow.

Figure 2.4 shows the potential distribution as a function of radial position in a capillary after the voltage is applied.[10] This potential field distribution gives rise to electroosmotic flow in the direction of the detector.

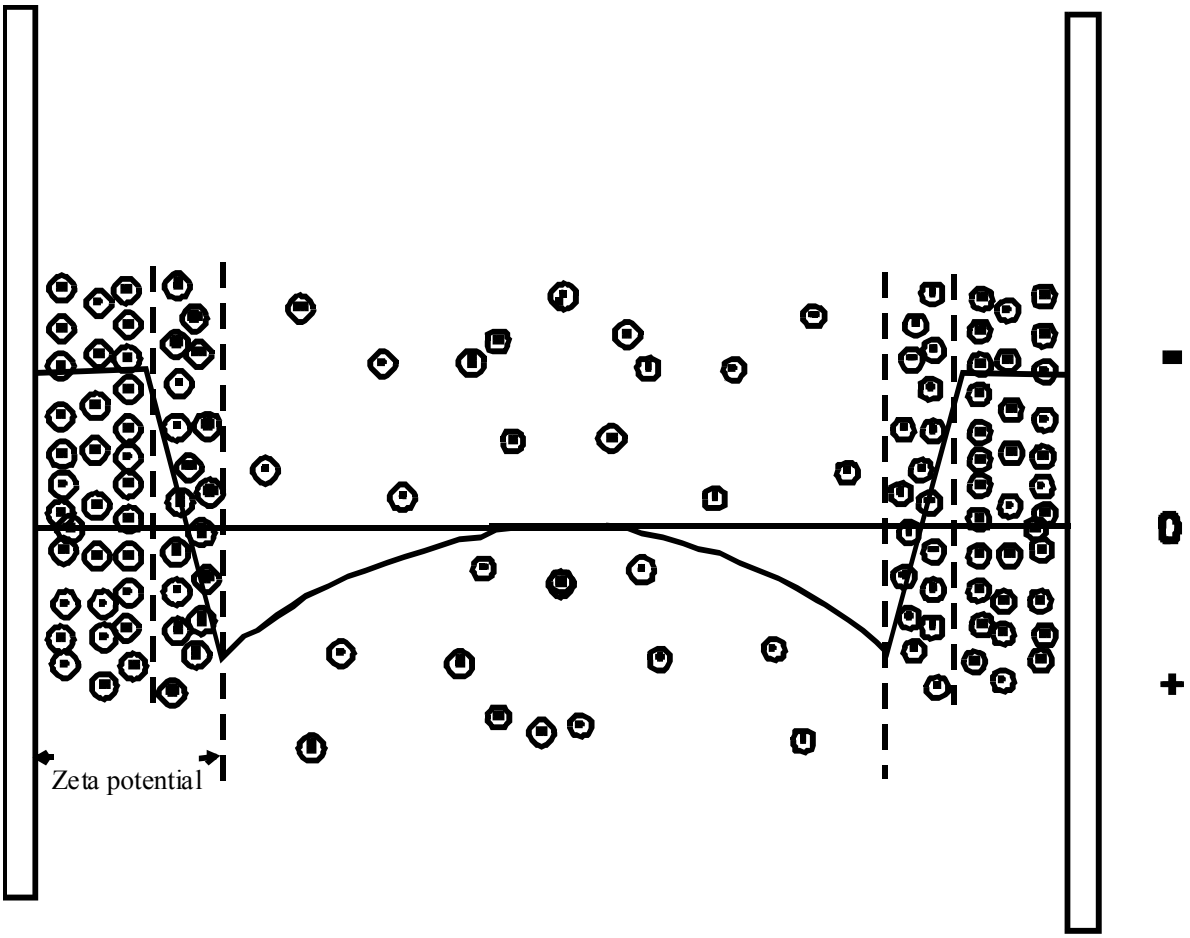

Figure2.4 Schematic of interior of a fused silica capillalry showing the potential across the capillary as a function of radial position. Note: The thickness of the stagnat double layer is greatly exaggerated for clarity. Parabolic potential distribution gives rise to electroosmotic flow in the direction of the detector.

Although the double layer is stagnant, the cationic attraction to the negatively charged fused silica surface rapidly becomes more diffuse in the center of the capillary. These weakly attracted cations are mobile and will migrate away from the high potential end of the capillary towards the detector. There is a net excess of cations in the vicinity of the double layer. These ions will begin to migrate towards the ground electrode. Because these cations are solvated by water molecules, they drag bulk solution along with them resulting in flow towards the detector. Because the thickness of the double layer is very small with respect to the diameter of the capillary, the flow profile is essentially flat. The double layer of ions acts as a slip plane with one layer of ions sliding across the other. The flat EOF flow profile is highly desirable for improved separation efficiency because there is no band dispersion on the injected zone induced by the flow profile.

Because ions will be carried by the bulk flow of the solution due to electroosmotic flow in addition to migration, control of electroosmotic flow is important for the optimization of an electrophoretic separation. Figure 2.5 shows the effect that the electroosmotic flow has on the migration of cations, anions, and neutral compounds.

The net result is that positive ions will migrate at the sum of the rate of their migration in the electric field plus the magnitude of the electroosmotic flow rate. Negative ions, that migrate in the opposite direction as the positive ions, will also be carried towards the detector as long as the magnitude of the electroosmotic flow is greater than the rate of migration in the opposite direction. Neutral species, which are not influenced by the electric field gradient, will travel at the same rate as the magnitude of the electroosmotic flow.

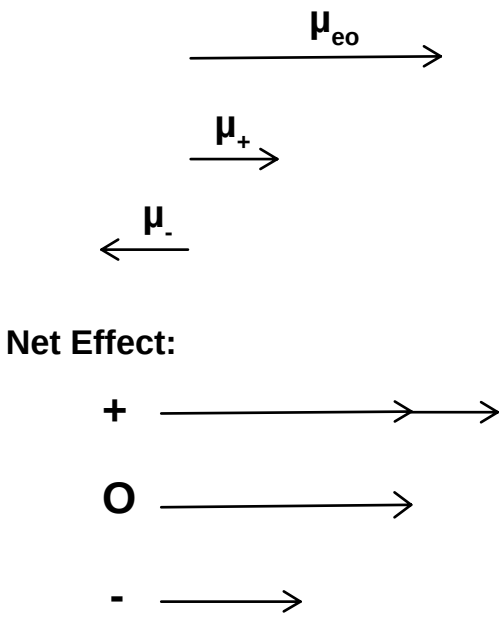

Figure 2.5 Effect of electrophoretic migration and electroosmotic flow on cationic, anionic and neutral species.

Where: **μ_+ is the electrophoretic mobility of a cation**
μ_- is the electrophoretic mobility of an anion
μ_{eo} is the magnitude of electroosmotic flow

Figure 2.6 shows the contribution of the flow profile to band broadening for both the laminar flow and electroosmotic flow models.

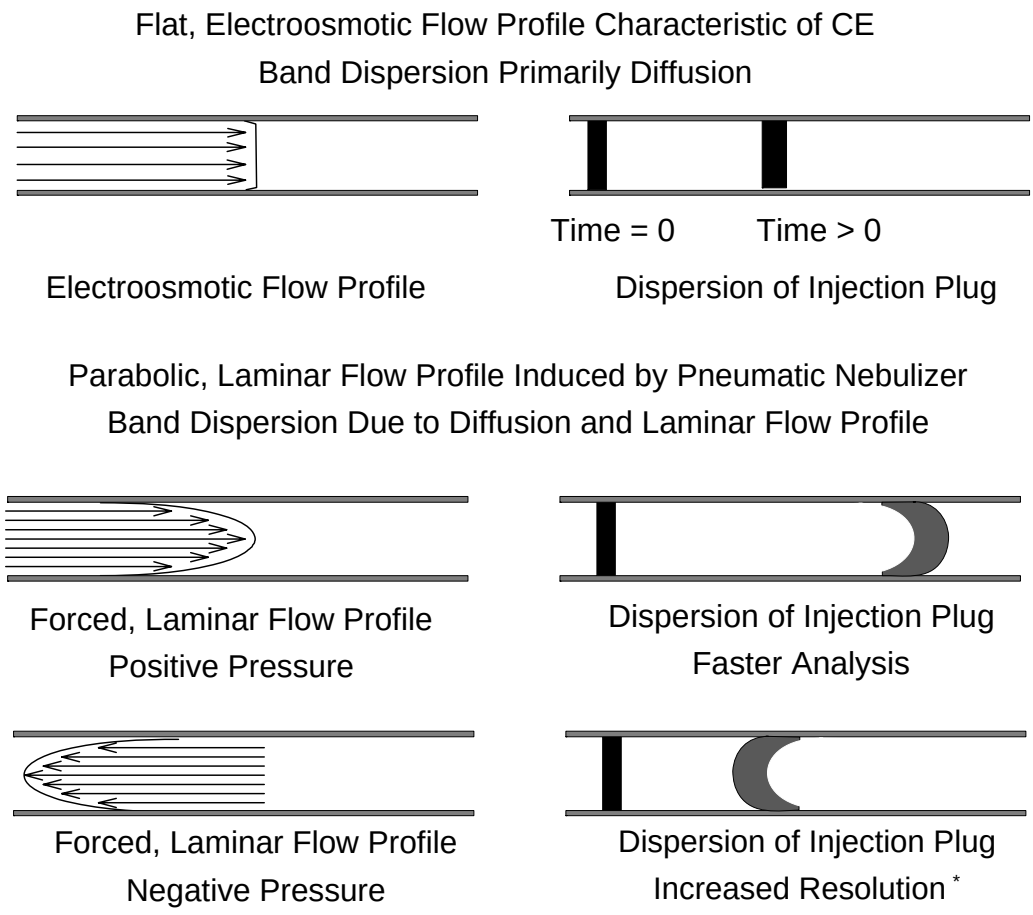

Figure 2.6 Effect of electroosmotic flow and pressure induced laminar flow on band dispersion in capillary electrophoresis. (* under conditions of concentration overload)

Because the electroosmotic flow profile in capillary electrophoresis is flat, no flow induced band dispersion is observed when a narrow sample plug is introduced into the capillary (Figure 2.6 Top). In the presence of positive laminar flow (in the direction towards the detector) the sample zone can be significantly distorted because analyte in the center of the capillary is traveling faster than analyte near the walls of the capillary (Figure 2.6 Middle). However, the overall time that analyte remains in the capillary

decreases. This results in less band dispersion due to the effects of diffusion. In addition, the analysis time is decreased. With the generation of a negative laminar flow profile in the separation capillary (in the direction away from the detector) band dispersion is introduced and analysis time increases (Figure 2.6 Bottom). As will be illustrated later, each of these regimes: no laminar flow, positive laminar flow and negative laminar flow can have advantages for CE-ICP-MS analysis of metal ions in different circumstances. For this reason, it is desirable to design an interface that allows the user to change from one regime to another quickly and conveniently. This was accomplished by building an external sheath flow interface that has some characteristics of those utilized in electrospray and LC-MS interfaces.[26-32] These interfaces, however were used to transport the sample to the mass spectrometer. No attempt was made to use the sheath flow rate to control the magnitude and direction of laminar flow. As shown in this work, this control of laminar flow has many advantages in capillary electrophoresis and could be applied to other separation techniques.

2.5 Design of a Sheath Flow Interface for the Control of Nebulizer induced Laminar Flow

Although the direct insertion interface provides excellent transport efficiency, low limits of detection, good reproducibility, and relative ease of construction, the nebulizer induced laminar flow degrades electrophoretic resolution for some applications. In order to overcome this problem, in this work a novel sheath flow interface and a PFA (Perfluoroalkoxy) micro-flow concentric nebulizer were used for CE-ICP-MS experiments. The design and characteristics of this interface is similar to the one described by Kinzer and Olesik.[33,34] This interface, illustrated schematically in Figure

2.7, combines the attributes of the previous interface such as good transport of the sample to the plasma and ease of use, with the added advantage of allowing for convenient user control over both the magnitude and direction of laminar flow in the separation capillary.

Like the direct insertion interface, the sheath flow interface uses a concentric pneumatic nebulizer to generate an aerosol from the sample. Unlike the direct insertion interface, the separation capillary is not sealed tightly into the nebulizer, but rather is held with the nebulizer tube via a Teflon chromatographic union with space between the separation capillary and the inner capillary of the nebulizer to allow passage of a coaxial sheath electrolyte. Although this may appear to introduce a significant amount of dead volume to the interface, the addition of the external sheath insures that this extra volume is efficiently swept. At typical sheath flow rates ranging from 10 to 100 μL/min for the high efficiency PFA MicroFlow nebulizer using a 50μm i.d. fused silica capillary, this extra column dead volume is swept out in only 0.1 to 1 sec depending on the sheath flow rate.

The sheath electrolyte which had the same composition as the electrolyte used in the separation capillary (although this is not a requirement) was introduced via a liquid chromatographic syringe pump. The flow rate is user controllable from 1 to 2000 μL/min.

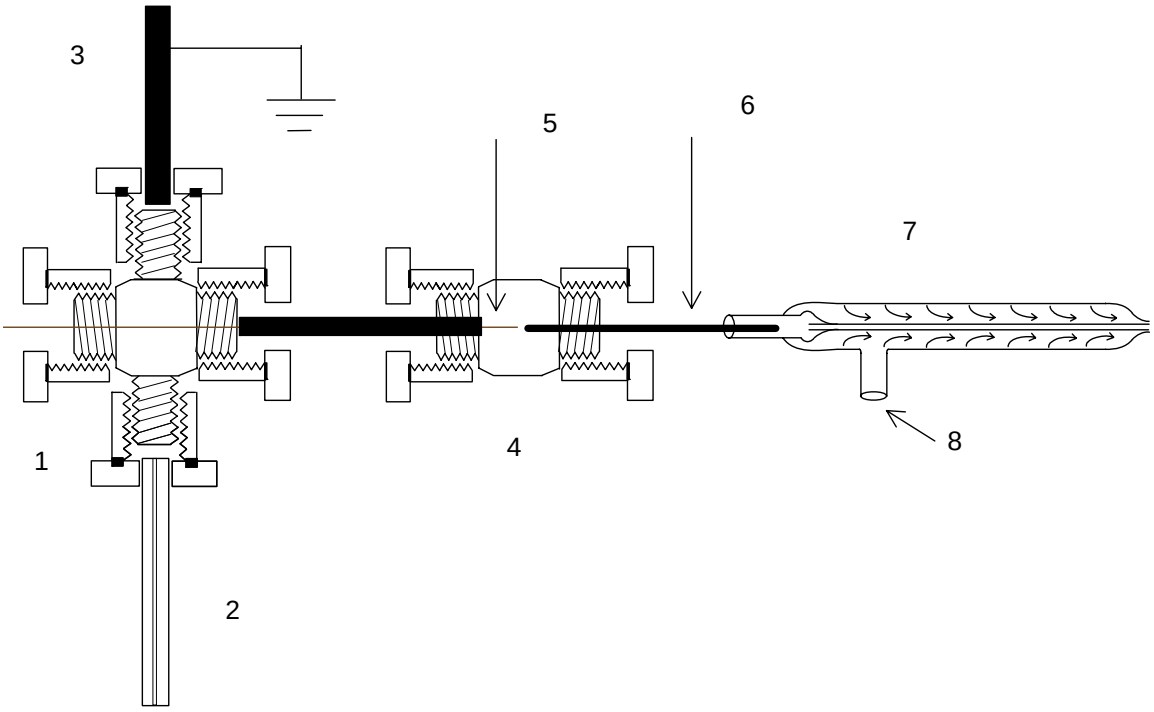

Figure 2.7 Schematic diagram of the sheath-flow interface for CE-ICP-MS. 1) Teflon cross 2) Sheath flow electrolyte PEEK tubing from syringe pump 3) Platinum tubing with ground 4) Teflon union 5) Fused silica CE separation capillary 6) Inlet tubing of Nebulizer 7) PFA microflow nebulizer 8) Argon nebulizer gas inlet

As shown in Figure 2.7, the inlet end of the separation capillary begins in a vial of electrolyte solution and the capillary proceeds through a Cheminert Teflon Cross (Valco instrument, Houston, TX; 1/16" o.d, 0.5 mm i.d). The capillary exits the Cross and passes through a sealed peek sleeve (Valco, 5 cm length, 1.57 mm o.d, 1.32 mm i.d). Since the Mircoflow nebulizer has its own capillary (400 μm o.d × 100 μm i.d), a zero dead volume PTFE union (Valco instrument, 16" o.d, 0.5 mm i.d) was used to connect the CE capillary to the nebulizer capillary. A platinum wire was connected to one site of the cross to

provide ground which shares the common ground with the CE instrument. A syringe pump (KD Scientific, Holliston, MA) was used to deliver the sheath electrolyte from a 10 ml glass syringe (14.57 mm ID) (Hamilton, Reno, Nevada). Sample together with the electrolyte from both the capillary and the sheath flow were introduced into the plasma as aerosols through the PFA micro-concentric nebulizer and a PFA spray chamber (Elemental Scientific, Omaha, NE). The choice of a platinum wire (instead of stainless one) and the use of the Cheminert cross were to reduce the metal background counts in the mass spectrometer. Because the electrolyte solution is flowing throughout the system and is in intimate contact with the effluent from the separation capillary, a stable ground connection to the solution at the end of the separation capillary is achieved.

The key advantage of this interface over the direct insertion interface discussed previously is the ability of the user to control the magnitude and direction of laminar flow in the separation capillary. This has implications on both separation efficiency and time of analysis. Control over the laminar flow is realized by controlling the flow rate of the external sheath electrolyte. Laminar flow in the separation capillary results from the rapid expansion of argon generating a suction force or Venturi effect that draws liquid through the separation capillary. By offsetting this suction force the degree of laminar flow can be mitigated.

By increasing the sheath flow rate and consequently increasing the back pressure in the nebulizer, the laminar flow induced in the separation capillary by the Venturi effect decreases. At some sheath flow rate, the back pressure generated in the nebulizer exactly offsets the suction induced by the escaping argon and laminar flow is eliminated. The sheath flow rate required to balance the back-pressure and nebulizer induced suction is

dependent on the size of the nebulizer used, the o.d. of the separation capillary, the argon flow rate supplied to the nebulizer, and the position of the separation capillary in the nebulizer. This point, which will be called the blance point, is determined experimentally and remains constant for any given set of nebulizer conditions. Increasing the sheath flow rate beyond the balance point results in a back-pressure that is greater than the nebulizer-induced suction resulting in the net flow of liquid backwards into the separation capillary, away from the detector. The relative advantages and disadvantages of positive laminar flow, towards the detector, no laminar flow, and negative laminar flow in the separation capillary will be discussed in detail in next section.

2.6 Control of the Laminar Flow Rate using the Sheath Flow Interface

The relationship between sheath flow and the laminar flow through the electrophoresis capillary can be studied by measuring the time required for a sample plug to travel the entire length of capillary with no voltage applied versus the sheath flow rates. At the balance point where laminar flow is eliminated, the elution time will approach infinity since laminar flow becomes the only drawing force of the sample with no voltage applied to the capillary. The determination of the balance point is made experimentally by introducing a small 8-14 nL plug of sample into the separation capillary in the absence of a separation voltage. The only force that can cause the transport of sample to the detector is laminar flow. As the sheath flow increases, resulting in a decrease in the positive laminar flow rate in the nebulizer, the observed elution times will increase. At the balance point, the elution time will approach infinity. Figure 2.8 shows a plot of the observed elution time as a function of sheath flow rate.

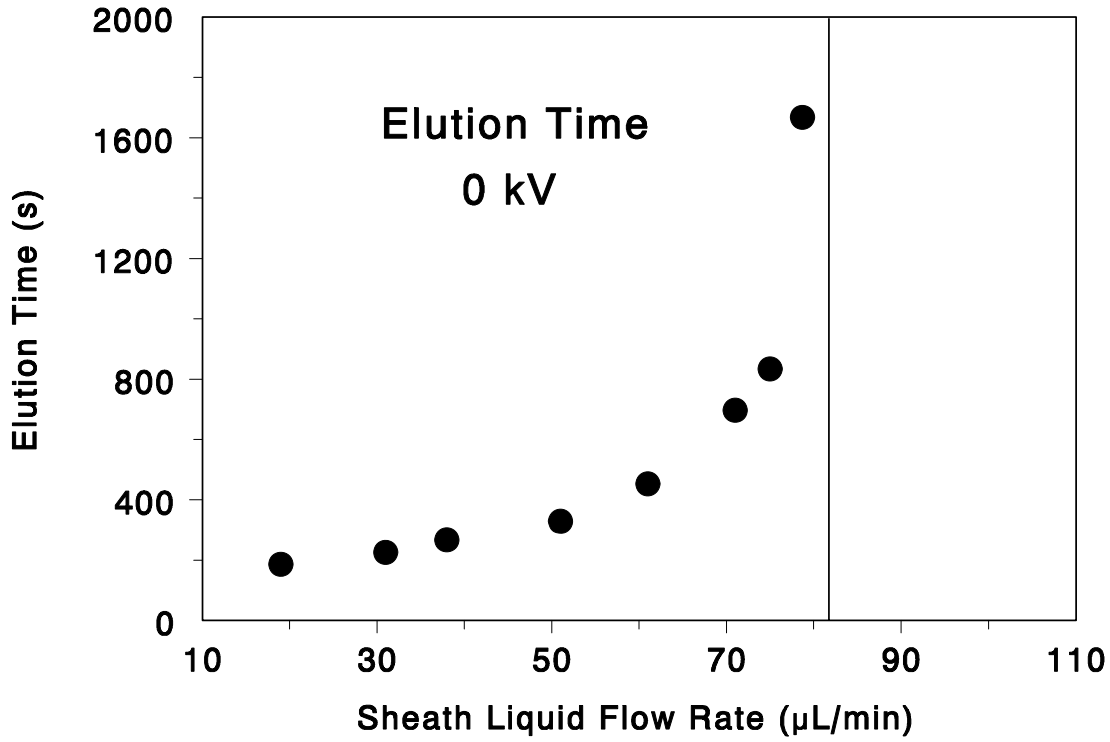

Figure 2.8 Determination of the balance point in the absence of applied voltage. As the sheath flow rate is increased, the elution time increases indicating a reduction in laminar flow. At 83µL/min, marked by the vertical line, the laminar flow in the separation capillary is eliminated. (Error bars are on the order of the size of the data points)

The laminar flow rate through the capillary can be calculated in two ways. The first was by performing the experiment in the absence of separation voltage (V). Under this condition, only laminar flow will result in the transport of the analyte to the detector. Because the volume of the capillary can easily be measured, the volumetric flow rate of the laminar flow can be calculated by monitoring the arrival time of analyte at the detector. Laminar flow was also estimated assuming constant values for the

electroosmotic coefficient (v_{eof}) and analyte mobilities (v_{em}) and measuring the migration times of an analyte ion in the presence of voltage.

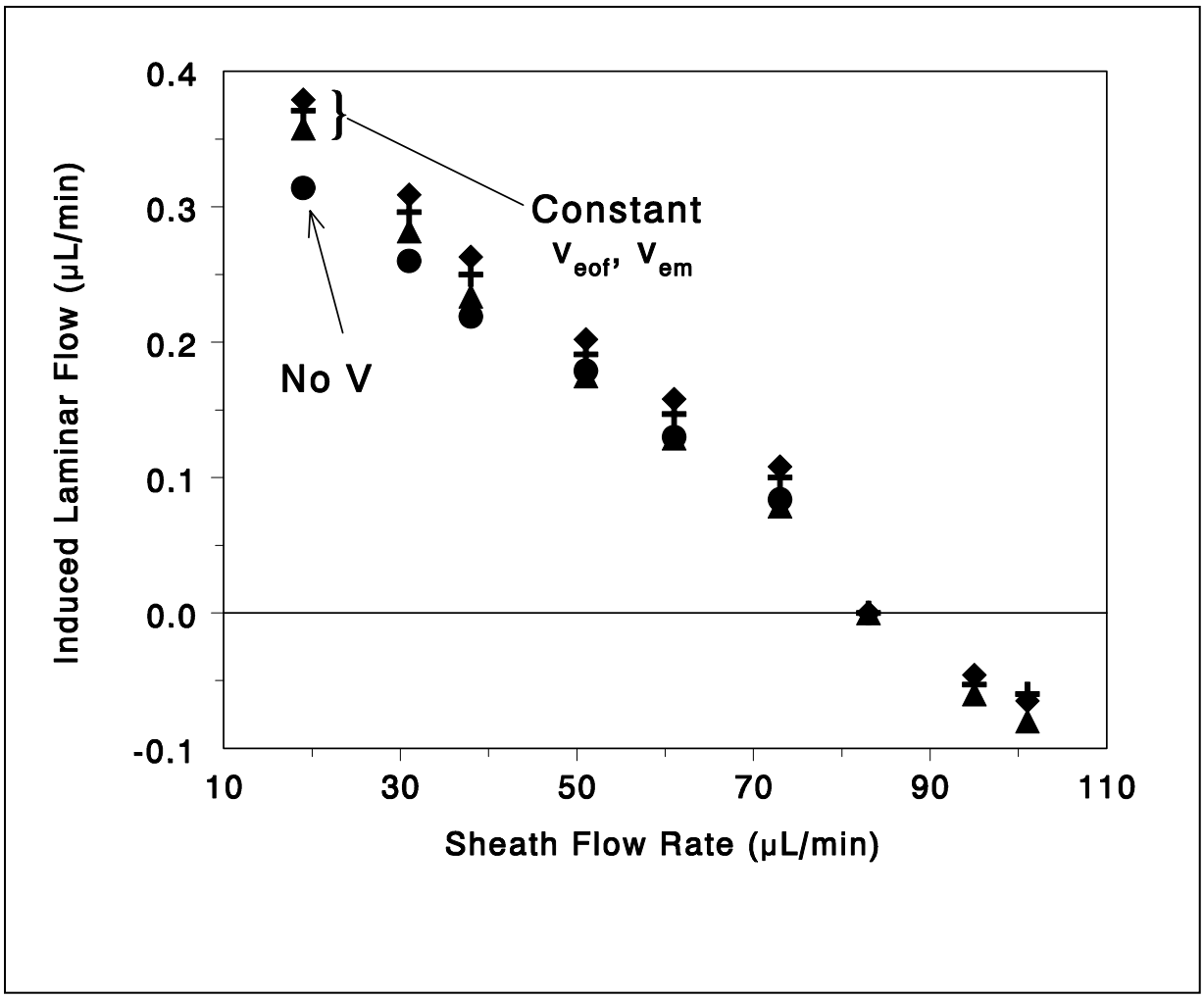

Figure 2.9 Effect of sheath flow rate on the laminar flow rate in the separation capillary; PFA micro-Flow nebulizer (50 µL/min), Separation capillary: 50 cm x 50µm i.d. x 360 µm i.d. fused silica. using measured Cs^+ migration times. Balance point is the calculated sheath flow rate where laminar flow rate is zero;

Calculated from measurement made with no applied voltage●,
Calculated assuming constant values of v_{eof} and v_{em} and measured migration times for K^+ (+), Co^{2+} (♦), and Y^{3+} (▲)

The sum of the ion velocity in the capillary due to electroosmotic flow and electrophoretic migration is independent of the laminar flow rate. Therefore, they can be subtracted from the overall migration velocity of ions when laminar flow is present. In this manner, the laminar flow velocity can be calculated as shown in equation (3).

$$V_{la\,\min ar} = \frac{L_d}{t_{mlf}} - (V_{eof} + V_{em}) = \frac{L_d}{t_{mlf}} - \frac{L_d}{t_{mnolf}} \qquad \textbf{(3)}$$

Where: L_d is the length of the separation capillary, $t_{m\ lf}$ is the migration time in the presence of laminar flow and $t_{m\ no\ lf}$ is the migration time in the absence of laminar flow. The ions, K^+ (+), Co^{2+} (♦), and Y^{3+} (▲) were used for these calculations and are shown in Figure 2.9.

Figure 2.9 shows a plot of the velocity and direction of laminar flow as a function of the external sheath flow rate. There are some small differences, of unknown origin, in the calculated laminar flow rates using the two methods and some differences between the laminar flow rates calculated using a monovalent, divalent, or trivalent ion. These differences may be due to small variations in the sheath flow rate from day to day or uncertainty in the electrophoretic velocities of the ions used. .

For the high efficiency micro-flow PFA nebulizer used at a fixed nebulizer gas flow rate of 0.8 L/min and a separation capillary of 50 μm i.d., a sheath flow rate of 49 μL/min resulted in the elimination of the laminar flow. This is lower than those of Meinhard high efficiency nebulizer (HEN) and SB-30-A3 nebulizer, which have much

higher sheath flow rates of 100-1000 μL/min needed to eliminate laminar flow in the separation capillary as reported in the literature.

It has also been proven in the experiments that at a relatively high, positive laminar flow rate (sheath flow 20 uL/min, laminar flow +0.14 μL/min) it is possible to separate positive and negative ions rapidly in the same electrophoretic run because the positive laminar flow results in the bulk flow of solution carrying all the analyte ions towards the detector at a greater rate than the rate at which the negative ions are migrating away from the detector due to electro-osmotic flow. By increasing the sheath flow rate from 20 μL/min to 49 μL/min, the laminar flow rate is reduced from +0.14 μL/min to 0 μL/min. Under this condition, the anions can no longer be measured because they migrate away from the detector unlike their cations counterparts that are moving towards the detector. This also leads to a better separation for the positive ions at the expense of almost doubling the analysis time. Increasing the sheath flow rate further to 70 μL/min results in a laminar flow rate of -0.17 μL/min (the sign represents direction of laminar flow relative to the detector). This laminar flow in the opposite direction results in an increase in the resolution of the positive ions by a factor of about 2-3 because the analyte ions are forced to remain in the electric field for a longer period of time.

The PFA micro-concentric nebulizer has two advantages over the SB-30-A3 for CE-ICPMS: a lower internal liquid dead volume (about 0.2 μL versus 2.5 μL) and a lower sheath flow requirement needed to eliminate laminar flow. As shown previously, a lower liquid flow rate to the nebulizer results in an increased aerosol transport efficiency.[34] Aerosol transport efficiencies improve from <2% to approximately 20% when the liquid flow rate delivered to the nebulizer is reduced from 1000 to 80 □L/min

resulting in improvements in limits of detection by over a factor of 10. Because ICP-MS signals depend on the total amount of material transported to the plasma per second and not concentration of the sample, dilution of the analyte by the sheath is unimportant. Changes in the aerosol transport efficiency to the system, however, are critical because increased aerosol transport results in higher ion signals at the detector.

The use of a sheath flow interface in a capillary electrophoresis system coupled to an inductively coupled plasma mass spectrometer allows for a greater deal of control over both separation efficiency and analysis times.

2.7 Effect of Nebulizer Gas Flow rate on Laminar Flow and Peak Parameters

As discussed in previous section, the coupling of the capillary electrophoresis separation capillary to a concentric pneumatic nebulizer results in the introduction of laminar flow if the Venturi effect is not offset by some other process. This is a potential problem not only in CE-ICPMS interfacing, but also in many interfaces which transport liquid sample to an ion source such as LC-MS or ionspray-MS.[26-32] This section will explore the effect of the nebulizer induced laminar flow profile on peak widths, peak asymmetry, separation efficiency and analysis time. The sheath flow interface will be used to manipulate both the velocity and direction of laminar flow in the separation capillary. Surprisingly, it will be shown that despite the fact that laminar flow results in increased band dispersion, the addition of laminar flow can be used to great advantage in not only reducing analysis time but to also increase separation efficiency under some conditions.

The velocity of the laminar flow in the separation capillary increases with the velocity and volumetric flow rate of the escaping argon gas. As can be seen in Figure

2.10, the laminar flow rate increases steadily with an increase in argon flow rate from 0.5 L/min to about 0.8 L/min. However, the rate of rise decreases dramatically from 0.8 L/min to 1.1 L/min. Because the nebulizer induced laminar flow is related to the argon gas flow rate, this effect can be explained by looking at the measured aerosol velocities.

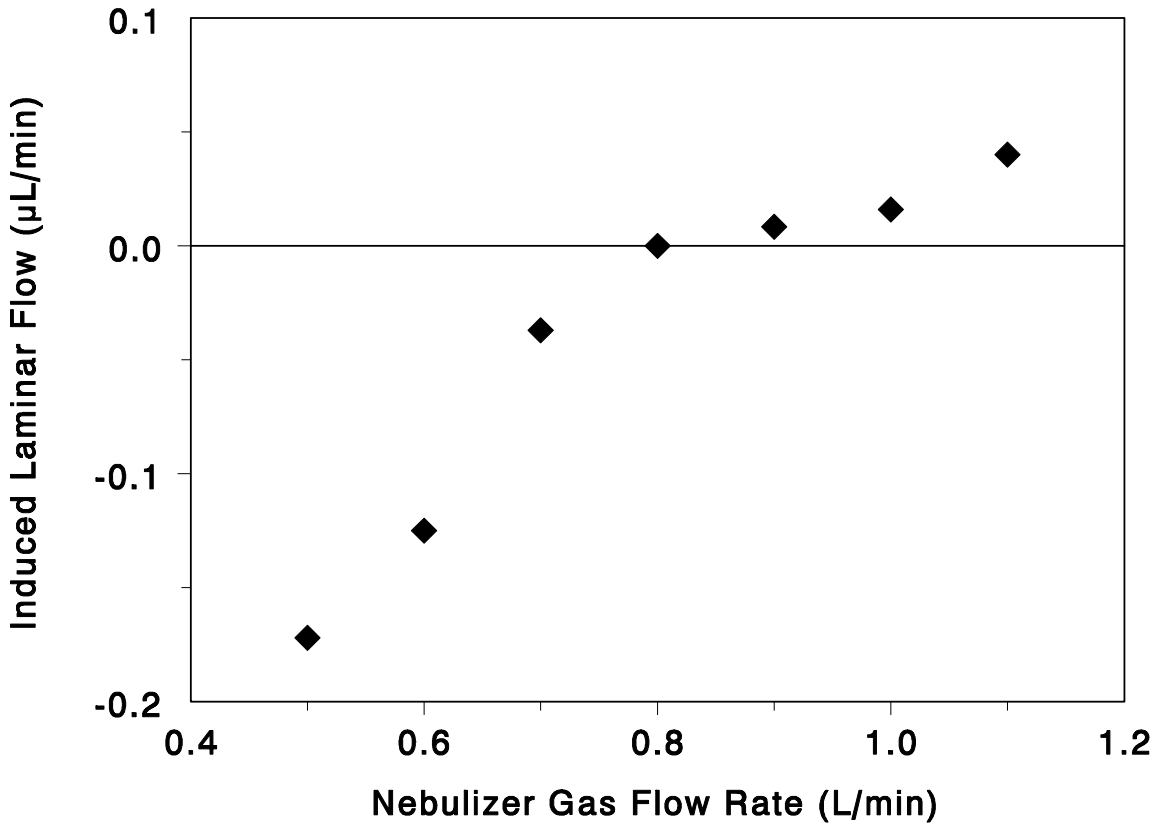

Figure 2.10 Effect of nebulizer gas flow rate on the induced laminar flow in the CE separation capillary. PFA micro-Flow nebulizer (50 µL/min), Separation capillary: 50 cm x 50µm i.d. x 360 µm i.d. fused silica. Sheath flow rate 83 µL/min.

As laminar flow increases in the separation capillary the peak width variance also increases as shown in equation 4.[11]

$$\sigma^2_{la\,\min ar} = \frac{2D_i^2 . v^2_{la\,\min ar} . t_m}{96D} \qquad \textbf{(4)}$$

Where:

	σ	is the peak width variance
	D_i	is the inner diameter of the separation capillary (m)
	$V_{laminar}$	is the laminar flow rate (m s^{-1})
	t_m	is the migration time of the analyte zone (s)
	D	is the diffusion coefficient (m^2 s^{-1})

As a consequence of increased band dispersion, the separation efficiency (Figure 2.11) decreases as the argon gas flow rate to the pneumatic nebulizer increases resulting in an increase in laminar flow.

As shown in Figure 2.11, the separation efficiency decreases by approximately a factor of three from 30000 plates/meter to about 11000 plates/meter as the nebulizer gas flow rate is increased from 0.5 to 0.8 L/min. Beyond 0.8 L/min argon flow rate however, the separation efficiency remains essentially constant because beyond this point an increase in nebulizer gas flow rate does not result in any further increase in the laminar flow. Although the nebulizer gas flow rate does influence the laminar flow and the resulting separation efficiency, these effects can be offset by changing the flow rate of the externally introduced sheath electrolyte. As the nebulizer gas flow rate is increased (resulting in an increase in laminar flow) the external sheath flow rate can be correspondingly increased to balance the forces in the nebulizer to reduce the nebulizer induced laminar flow. In this manner, it is possible to optimize the laminar flow for any

nebulizer gas flow simply by changing the pump flow rate of the external sheath electrolyte. In practice, the nebulizer gas flow rate is adjusted for optimum signal response of the ICP-MS. The sheath flow rate is then independently optimized to control the nebulizer induced laminar flow rate as required for the analysis.

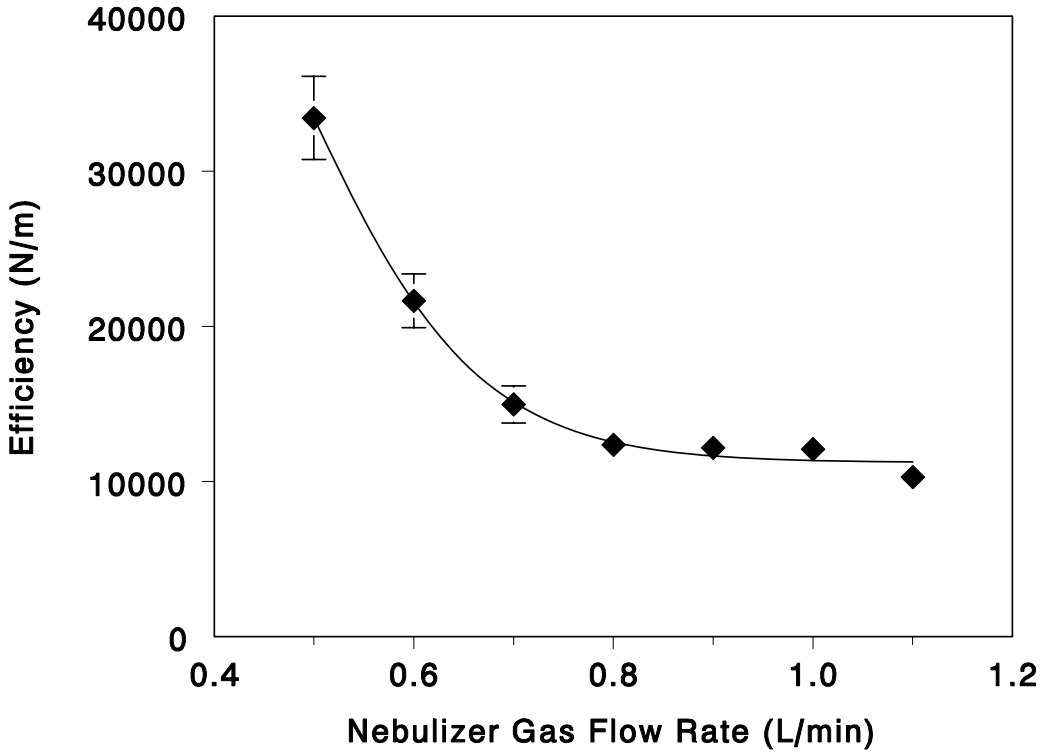

Figure 2.11 Effect of nebulizer gas flow rate on CE separation efficiency; PFA micro-Flow nebulizer (50 µL/min), Separation capillary: 50 cm x 50µm i.d. x 360 µm i.d. fused silica. Data shown is for 1 ppm Co^{2+} at 30kV. (Line is a spline fit to the data)

2.8 Effect of Laminar Flow Rate on Electrophoretic Peak Parameters

The velocity and direction of laminar flow in the separation capillary has a significant effect on separation efficiency, peak width, peak shape and analysis time.

Introduction of laminar flow into a separation system is typically detrimental to separation efficiency.[35] Under conditions of a pressure driven flow profile, the center of the zone will travel at a higher velocity than the outer edges of the zone. This leads to additional band dispersion that is proportional to the magnitude of the forced flow profile (Equation 4).

Figure 2.12 illustrates the effect of the pressure induced laminar flow profile on the full width at half maximum (FWHM) for 1 ppm K^+. As the sheath flow rate is increased, the back-pressure in the nebulizer increases resulting in a decrease in the laminar flow velocity. As expected, the peak widths are broader under conditions where the sheath flow rate is low and the velocity of the pressure induced laminar flow is large. The peak width steadily decreases as the sheath flow rate increases resulting in a decrease in the laminar flow magnitude. At the balance point of approximately 83 μL/min, the peak width reaches a minimum of 5.8 seconds. As the sheath flow rate increases beyond the balance-point of 83 μL/min, the peak widths for the potassium ion begin to increase once again because laminar flow is now being generated in the opposite direction (away from the detector).

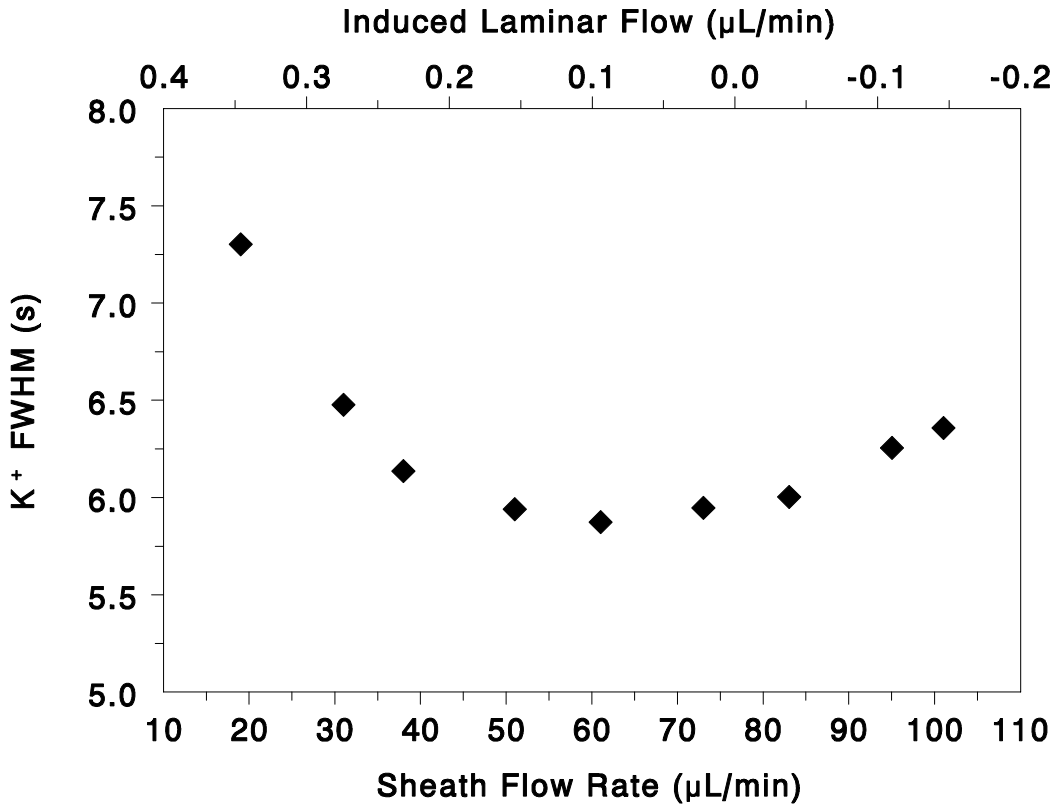

Figure 2.12 Effect of the external sheath electrolyte flow rate on the observed peak width for 1 ppm potassium ion. (Error bars are on the order of the size of the data points)

In addition to affecting the peak width, peak asymmetry, is also influenced. For this discussion, peak asymmetry is defined as the ratio between the centerline of the zone and the left (B_{12}) and right (B_{21}) inflection points as illustrated in Figure 2.13.[21]

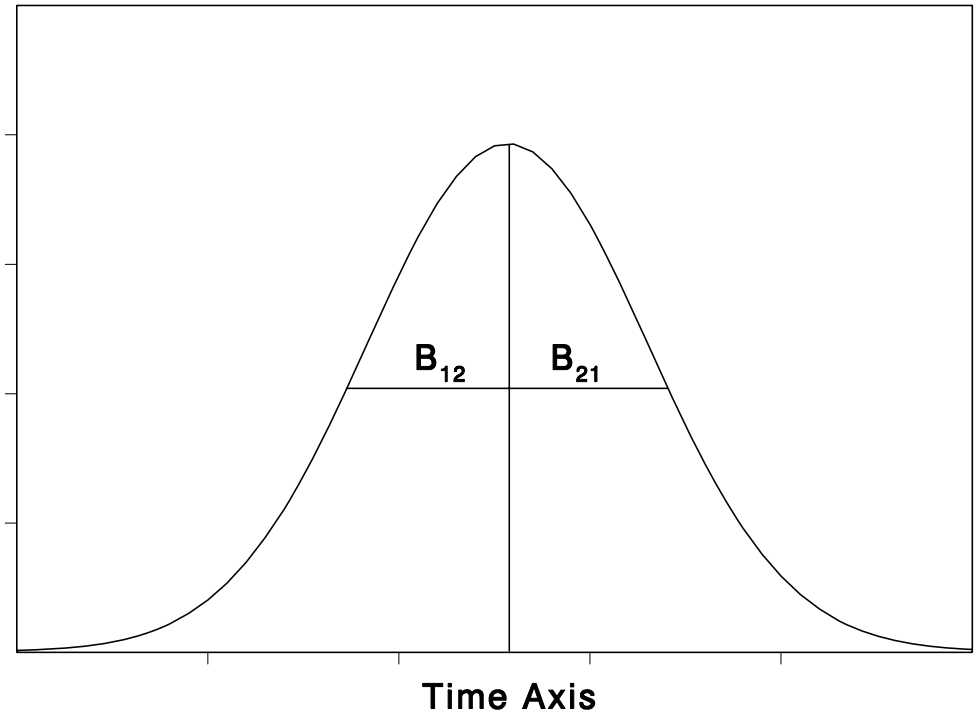

Figure 2.13. Peak asymmetry

Asymmetry Factor = B_{12}/B_{21}

B_{12}/B_{21} < 1 Fronting Peak
B_{12}/B_{21} = 1 Gaussian Peak
B_{12}/B_{21} > 1 Tailing Peak

Figure 2.14 illustrates the effect of the nebulizer induced laminar flow rate on K^{+} (highest mobility, μ_{eff} = 73 x 10^{-9} kg^{-1} sec coul), Co^{2+} (μ_{eff} = 55 x 10^{-9} kg^{-1} sec coul) whose mobility is most similar to that of the Ca^{2+} electrolyte cation (μ_{eff} = 59 x 10^{-9} kg^{-1} sec coul), and Li^{+} (lowest mobility, μ_{eff} = 38 x 10^{-9} kg^{-1} sec coul) on peak asymmetries. Unlike other separation techniques, such as liquid chromatography or gas chromatography, where zones are nearly always Gaussian, asymmetric zones are typical in electrophoretic separations of highly mobile metal ions. Symmetric zones are usually

only observed when the mobility of the analyte ion closely matches the mobility of the background electrolyte.[36-38] Analytes with a higher mobility than the background exhibit peak fronting while analytes with lower mobilities will have tailing peaks. This asymmetry is exaggerated in the presence of laminar flow. The analyte in the radial center of the capillary travels faster than the analyte at the capillary walls. This results in tailing peaks, evidenced by asymmetry values greater than 1. The asymmetry factors for Co^{+} and K^{+} are approximately 1 at the balance point where laminar flow is eliminated yielding symmetric, Gaussian zones. When laminar flow is generated in the negative direction (away from the detector) slightly fronting zones are observed for K^{+} and Co^{2+} because the laminar flow profile is inverted. Li^{+} ($\mu_{eff} = 38 \times 10^{-9}$ kg^{-1} sec coul) which has a lower mobility than the electrolyte cation (Ca^{2+}, $\mu_{eff} = 59 \times 10^{-9}$ kg^{-1} sec coul), shows tailing that becomes progressively worse as the laminar flow rate is decreased.

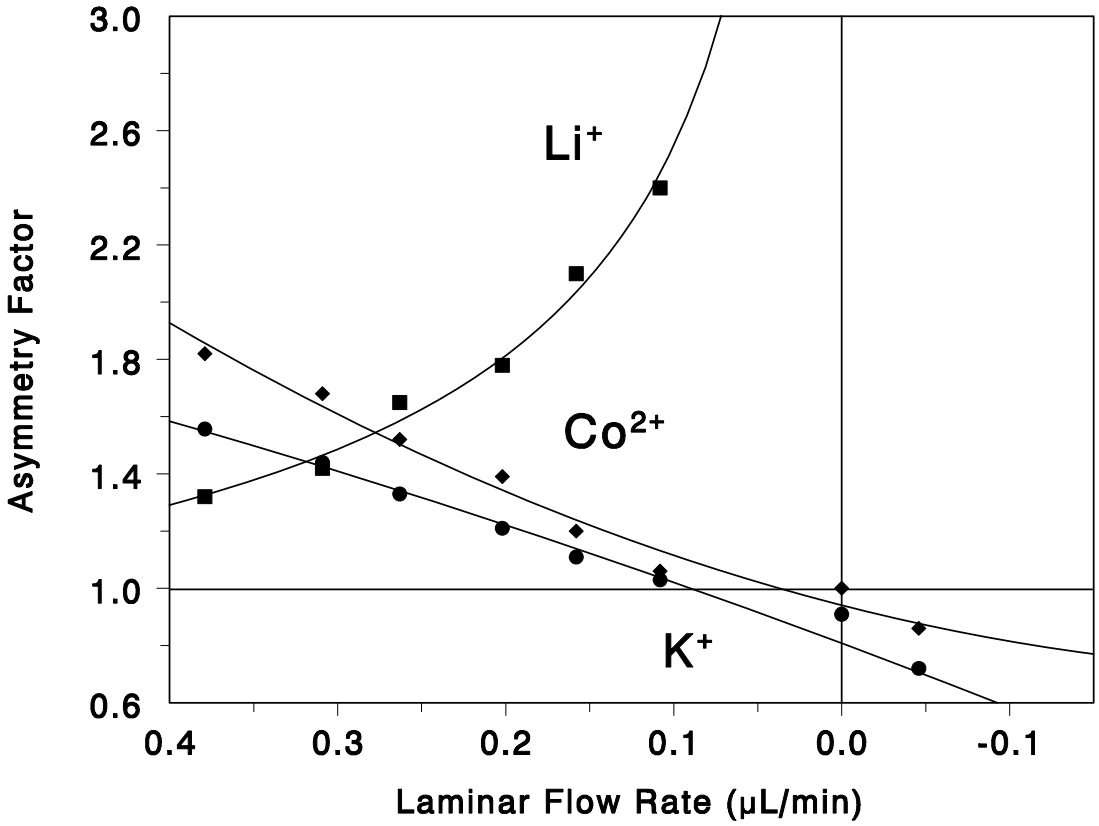

Figure 2.14. Effect of laminar flow on the observed peak asymmetries. Asymmetry is defined by measuring the distance from the center line of a peak maximum to the left and right edges of the peak at the inflection point. The ratio of the right chord B_{21} to the left chord B_{12} is the asymmetry factor.

● K^{+} $\mu_{eff} = 73 \times 10^{-9}$ kg^{-1} sec coul

■ Li^{+} $\mu_{eff} = 38 \times 10^{-9}$ kg^{-1} sec coul

♦ Co^{2+} $\mu_{eff} = 55 \times 10^{-9}$ kg^{-1} sec coul

(All lines are a spline fit to the data)

2.9 Manipulating Laminar Flow in the Separation Capillary by use of an External Sheath Electrolyte to Control the Tradeoff Between Separation Efficiency and Time of Analysis

Laminar flow can be effectively used in capillary electrophoresis to control the tradeoff between separation efficiency and analysis time. The external sheath electrolyte controls both the magnitude and direction of laminar flow in the separation capillary, dramatically influencing analyte residence time, peak widths, peak asymmetries and separation efficiency, as shown previously.

In order to compare quantitatively the effects of laminar flow on separation parameters such as analysis time and separation efficiency, a solution containing 1 ppm each of Ce^{+}, Y^{3+}, Co^{2+}, and Li^{+} representing trivalent, divalent and monovalent ions was used. Recall that the equivalent ionic conductances and hence the electrophoretic mobility of most divalent ions are similar to one another. Similarly, most trivalent ions have similar electrophoretic mobilities. For this reason, Co2+ exhibits similar migration times as all divalent ions and Y^{3+} will be representative of the trivalent ions. Because all of the ions in this mixture have a different masses, they can be easily distinguished from one another in the mass spectrometer. In this manner, the effect of laminar flow can be assessed even under conditions where resolution is poor. For real samples analyzed by CEICPMS, there would be no need to separate electrophoretically Ce^{+}, Y^{3+}, Co^{2+}, and Li^{+} from one another because the mass spectrometer would be capable of that task.

At a high, positive laminar flow rate of 0.38 μL/min it is possible to separate positive and negative ions rapidly in the same electrophoretic run because the laminar flow results in the bulk flow of solution carrying all of the analyte ions towards the detector at a greater rate than the negative ions migrate away from the detector (Figure

2.15).

By increasing the sheath flow rate from 20 μL/min to 83 μL/min, the laminar flow rate is reduced from +0.38 μL/min to 0 μL/min. Under this condition, the system is comparable to conventional capillary electrophoresis where only electrophoretic mobility and electroosmotic flow are present. Under this condition (Figure 2.16) the dichromate anion can no longer be measured because it migrates away from the detector at a velocity faster than the bulk electroosmotic flow towards the detector. Resolution of the positive ions increased substantially at the expense of a factor of 2 in analysis time.

Increasing the sheath flow rate further to 100 μL/min results in a laminar flow rate of -0.07 μL/min (the sign represents direction of laminar flow relative to the detector). Although laminar flow is present, resulting in an increase in band dispersion, the resolution of the positive ions increased by a factor of 2-3 because the analyte ions are forced to remain in the electric field for a longer period of time (Figure 2.17). This is surprising because laminar flow is almost universally thought to degrade resolution Laminar flow was used previously by Jorgenson *et al.* to improve resolution by allowing analyte to migrate to the end of the capillary and then forcing it back to the beginning using a pump. This increased the effective length of the capillary by the number of times that this process was repeated.[39] It was found that this worked well because the i.d. of the capillary used was only 5 to 10 μm inner diameter. With capillaries of this size, calculations show that the amount of band dispersion due to laminar flow is on the order of that due to diffusion alone.[40] For the conditions shown in Figure 2.17, the capillary i.d. was comparatively large (50 μm) and still resolution improvement was clearly observed.

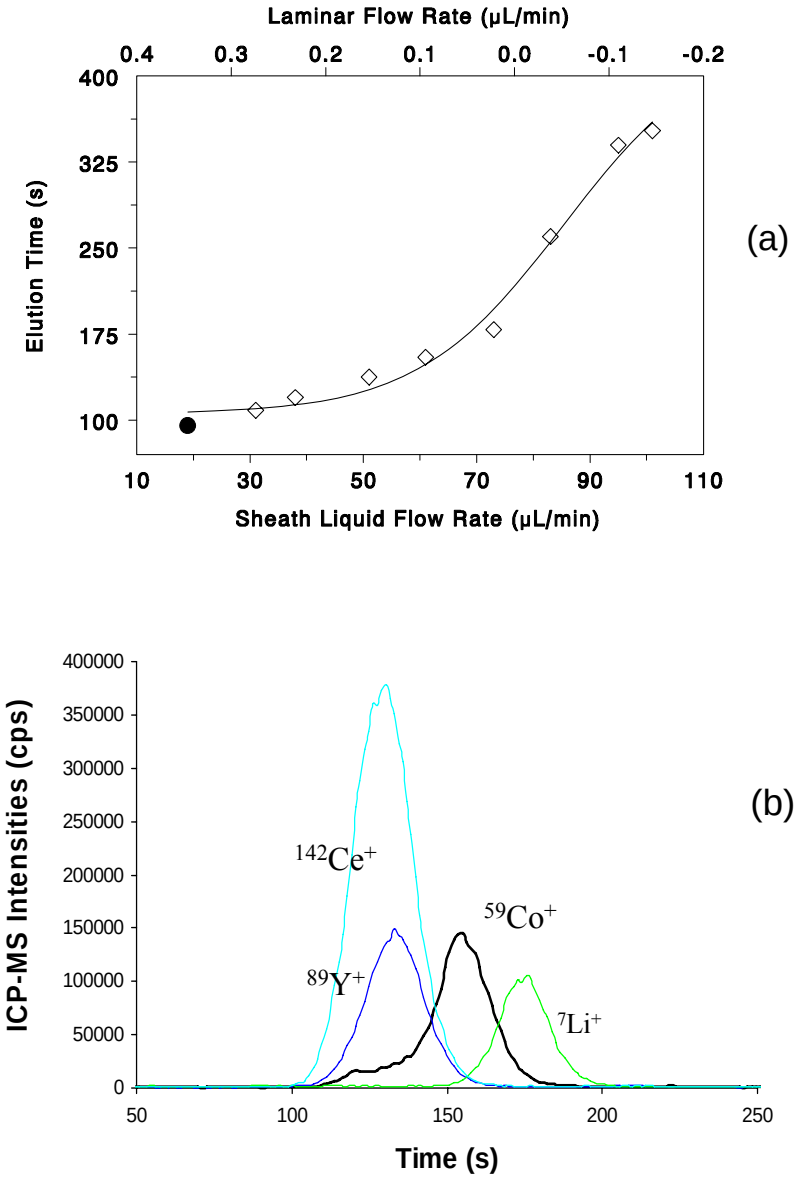

Figure 2.15 (a)Plot of elution time vs. both sheath flow rate and laminar flow rate. The electropherogram in (b) was measured at the point denoted by (●).(b)Electropherogram each of 1 µg/mL Ce^{+}, Y^{3+}, Co^{2+}, and Li^{+}. Laminar flow rate of 0.38 µL/min, (sheath flow rate 20 µL/min) Applied separation voltage of 30 kV. Separation capillary: 50 cm x 50 µm i.d. fused silica.

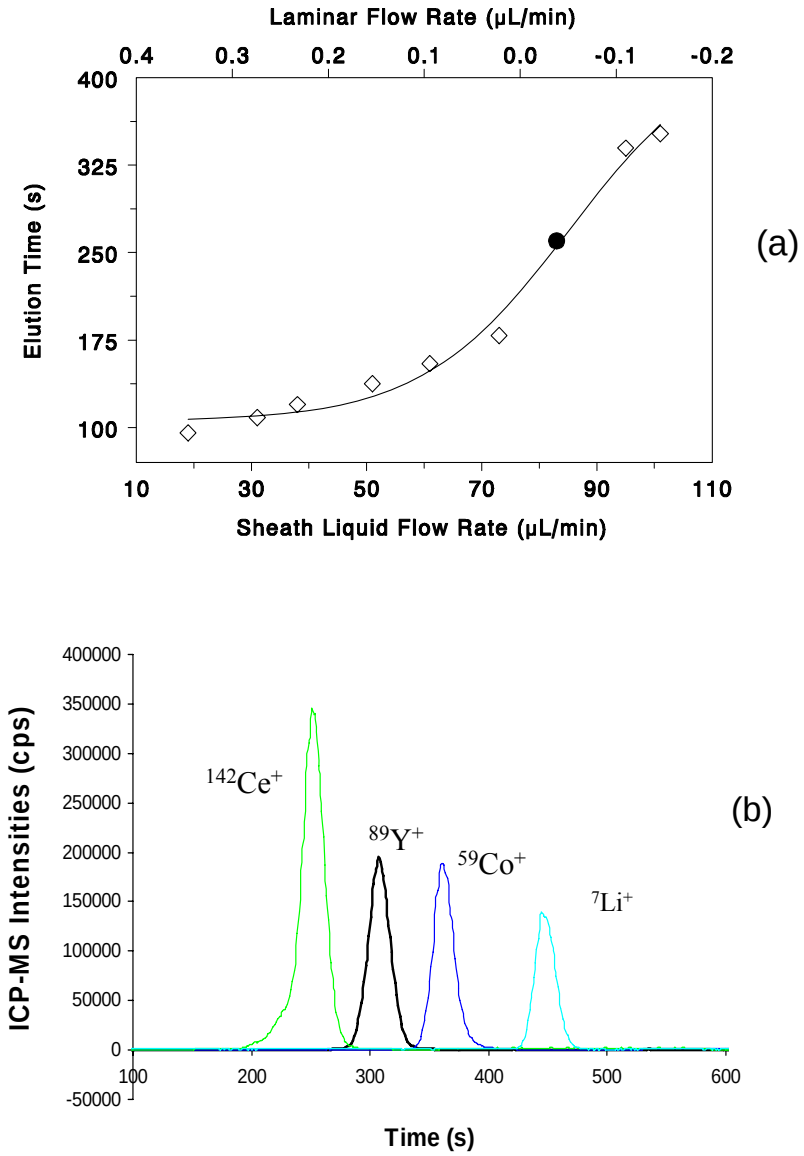

Figure 2.16 (a) Plot of elution time vs. both sheath flow rate and laminar flow rate. The electropherogram in (b) was measured at the point denoted by (●). (b) Electropherogram of 1 µg/mL each of Ce^{+}, Y^{3+}, Co^{2+}, and Li^{+}. Laminar flow rate of 0 µL/min (sheath flow rate 83 µL/min). Applied separation voltage of 30 kV. Separation capillary: 50 cm x 50 µm i.d. fused silica.

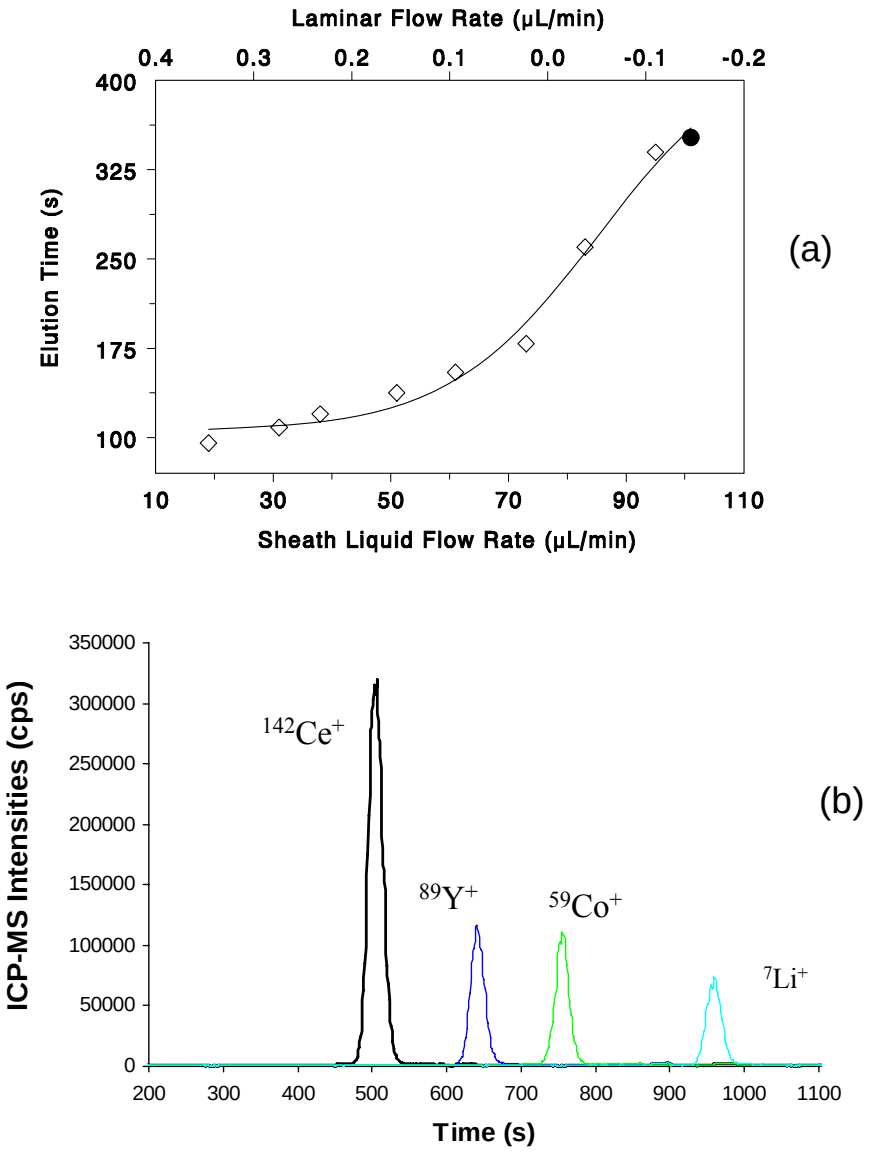

Figure 2.17 (a) Plot of elution time vs. both sheath flow rate and laminar flow rate. The electropherogram in (b) was measured at the point denoted by (●). (b) Electropherogram of 1 µg/mL each of Ce^{+}, Y^{3+}, Co^{2+}, and Li^{+}. Laminar flow rate of -0.065 µL/min in the direction away from the detector, (sheath flow rate 101 µL/min). Applied separation voltage of 30 kV. Separation capillary: 50 cm x 50 µm i.d. fused silica.

2.10 Effect of Sheath Flow Rate on Aerosol Transport and Limits of Detection

Because the size of the capillaries used for this work was small (50 μμm i.d. x 50 cm long) injection volumes were only a few nanoliters. This small injection volume makes limits of detection a concern. Because injection volumes in capillary electrophoresis are on the order of a few nanoliters, the interface should transport the sample to the plasma with as close to 100% efficiency as possible because one cannot afford to lose 99% of the sample to the drain as is typical with conventional nebulizer/spray chamber configuration operating with 1 mL/min uptake rates. Even with 100% of the aerosol transport efficiency, the amount of material entering the plasma per unit time will be less for the CE sample introduction system. Assume for example that 5 nL of solution containing 1 ng/mL of arsenic is injected into the CE with an aerosol transport efficiency of 100%. For a 10 s wide electrophoresis peak, an average of 0.5 fg of arsenic would enter the plasma per second. In contrast, for a sample introduction rate of 1 mL/min and an aerosol transport efficiency of 1%, 167 fg of arsenic would enter the plasma per second. Approximately 300 times less sample enters the plasma per unit time for the CE-ICPMS compared to conventional sample introduction.

Because injection volumes for this work were ~ 11 nL, a higher aerosol transport efficiency was desirable in order to achieve the low limits of detection characteristic of ICP-MS. With this transport efficiency, limits of detection on the order of a few ppb were obtained even though the quantity of sample supplied to the nebulizer was five orders of magnitude smaller than what is typical for conventional ICP-MS analysis due to the enhanced aerosol transport efficiency.

The effects of sheath flow rates on ICP-MS performance are shown in Figure 2.18. With all other experimental conditions held constant, the Cs^+ signal intensity was improved by nearly a factor of 20 when the sheath flow rate was reduced from 50 µL/min to 20 µL/min while the migration time was reduced by only ~ 8%. This can be explained by increased aerosol transport efficiency with decreased sheath flow rate. Since the signals produced by the ICP-MS depends on the total amount of materials transported to the plasma per unit time and not the concentration of the sample, dilution of the analyte by the sheath solution is irrelevant. This is similar to the findings by Scott and Smith et al[40,42] that for Meinhard HEN nebulizer, transport efficiency decreased from 20 % to 8 % with liquid uptake rate increased from 50 µL/min to 200 µL/min.

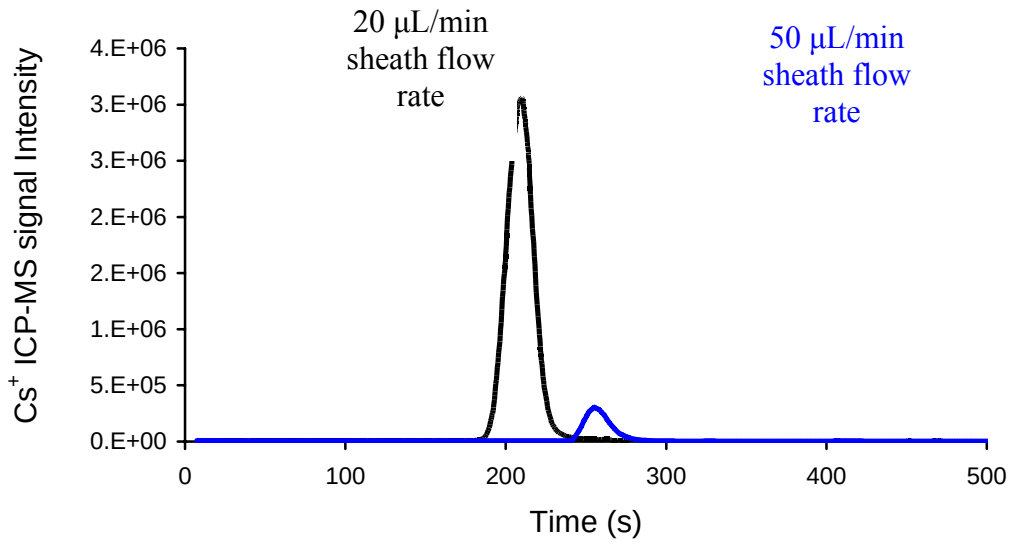

Figure 2.18 The effect of sheath flow on CE-ICP-MS signal. Cs signal recorded from 1 ppm Cs sample solution with 20 mM $NaNO_3$ electrolyte solution and dilute HNO_3 sheath flow solution. The conductivity electrolyte is ~ 2200 µS, injection volume: 47 nL, CE voltage: 30 kV, CE current: 15 µA. (-)50 µL/min sheath flow rate (--) 20 µL/min sheath flow rates

Because the sheath flow rate impacts the aerosol transport efficiency, the limits of detection will surely be affected. Listed in Table 2.2 are the concentration limits of detection (ppb) and absolute limits of detection (fg) based upon the amount injected (fg) measured on a Finnigan Element-2 HR-ICP-MS with the sheath flow interface and a PFA microflow nebulizer at liquid uptake rates of 20 μL/min, 48 μL/min and 70 μL/min corresponding to the conditions that yield positive laminar flow, no laminar flow and negative laminar flow in the separation capillary, respectively.

Limits of detection were assessed by injecting a blank solution and measuring the intensities of all the data points across a peak width. There are between 25 and 32 data points across the width of the base of the peak depending on the species. Limit of detection for one species is calculated based upon 3 times the standard deviation of these baseline data points across the peak width of this species.

As shown in Table 2.2, decreasing the sheath flow rate from 70 μL/min to 20 μL/min results in an improvement in limit of detection by a factor of 5.2 for Cs^+ while improvement in limits of detection for Rh^{3+} and Pd^{2+} were slightly smaller (by a factor of 3.3 to 4.4, respectively).

Compared to the same Finnigan Element 2 HR-ICP-MS without the CE interface at a nebulizer gas flow rate of 1.0 L/min and a liquid uptake rate of 100 μL/min, the limits of detection are only about 10 to 100 times better than those measured by CE-ICPMS with the sheath flow interface. This is quite good considering that only 4.7 nL sample is injected into the CE versus the 100 μL/min flow in the conventional ICP-MS analysis. Since the aerosol transport efficiency decreases as the liquid flow rate increases, it is desirable to keep the external sheath flow rate as low as possible to achieve the best

possible limits of detection. One of the advantages the microflow PFA nebulizer over Meinhard HEN and the SB-30-A3 nebulizers normally used for CE-ICPMS research is that a very low sheath flow is enough to eliminate laminar flow and maintain good separation efficiency while achieving superior limits of detection.

Because the aerosol transport rate decreases as the liquid flow rate increases, it is desirable to keep the external sheath flow rate as low as possible to maximize limits of detection. In cases where resolution is not critical, the direct insertion interface can be used because it yields limits of detection approximately a factor of 10 better than the sheath flow interface with a sheath supply of 20 μL/min as shown in Table 2.2. Negative pressure on the inlet end of the capillary could also be used to counteract the laminar flow and reduce the required sheath flow rate.

A / B	CE-ICP-MS Sheath Flow Rate			Conventional ICP/MS (Element 2)
	20 μL/min	48 μL/min	70 μL/min	100 uL/min
Y	1.5	0.5	0.35	~100
	2.5 ppb/8 fg	5.2 ppb/23 fg	6.3 ppb/26 fg	0.001 - 0.01 ppb
Co	1.1	0.52	0.31	~65
	2.9 ppb/10 fg	5.4 ppb/21fg	7.1 ppb/29 fg	0.01 - 0.1 ppb
Cs	4.1	1.2	0.8	~100
	0.6 ppb/2.4 fg	2.3 ppb/9.2 fg	3.1 ppb/10.4 fg	0.001 - 0.01 ppb
Rh	1.3	0.4	0.35	~95
	2.5 ppb/10 fg	8.2 ppb/33 fg	8.3 ppb/33 fg	0.001 - 0.01 ppb
Pd	0.8	0.32	0.28	~50
	3.6 ppb/14 fg	11 ppb/45 fg	16 ppb/62 fg	0.01 - 0.1 ppb

Table 2.2. Effects of Sheath Flow Rate on (A) Singal intensity (1 ppm solution, peak high, million counts/s) (B) CE-ICP-MS Limits of Detection (ppb and fg) with conventional ICP-MS data attached for comparison

2.11 Conclusions

The development of a capillary electrophoresis (CE) system coupled to a high resolution inductively coupled plasma mass spectrometer (HR-ICP-MS) for elemental speciation is described. A novel sheath flow CE-HR-ICP-MS interface coupled to a PFA Teflon micro-flow concentric nebulizer was developed and characterized.

This interface design allows the user to control the extent of nebulizer induced laminar flow in the separation capillary. The sheath-flow interface uses an external electrolyte sheath to generate back-pressure in the nebulizer. As the liquid flow rate supplied by the sheath exceeds the natural aspiration rate of the nebulizer, the pressure within the nebulizer will increase. At low sheath-flow rates, the natural aspiration of the nebulizer is greater than the back-pressure in the nebulizer resulting in positive laminar flow. In this mode, rapid separation of positive, neutral and negative species can be analyzed in one electrophoretic run.

At the balance point, where the sheath-flow rate has been increased such that the back-pressure generated in the nebulizer exactly offsets the natural aspiration rate of the nebulizer, laminar flow is eliminated. In this mode, separation efficiency is improved at the expense of increased analysis times.

Increasing the sheath-flow rate further, beyond the balance-point produces laminar flow in the opposite direction (away from the detector). This results in the increased residence time of analyte ions in the electric field further improving separation efficiency.

The ability to control the nebulizer induced laminar flow rate in the separation capillary allows easy tailoring of the separation conditions to the analysis desired. At

high positive laminar flow rates, both positive and negative ions can be separated and detected in the same electrophoretic analysis. Because the detector is mass selective, this mode can also be used if there is only one form of each cation to be determined. By eliminating laminar flow using a higher sheath flow rate, resolution can be increased for samples where it becomes important to separate multiple cationic forms of the same element (such as Fe2+ from Fe3+). Generating a small negative laminar flow allows a further increase in the resolution of the analysis for samples where the mobilities of different cationic forms of the same element are very similar. Control of the sheath flow and therefore control of the laminar flow allows easy control over the tradeoff between separation efficiency and time of analysis.

Peak area based limits of detection were within a factor of 10 to 100 of conventional ICP-MS and sub ppb limits of detection were illustrated even though the amount of sample is five orders of magnitude smaller for the CE-ICPMS analysis compared to conventional ICPMS analyses. Further optimization of the nebulizer spray chamber interface was show only modest improvements in limits of detection. Limits of detection can be further improved using electro-stacking methods which can focus relatively large volumes of dilute sample into a small plug of more concentrated[43-47] This method has been used with good success in biological capillary electrophoresis to improve limits of detection by as much as three orders of magnitude which would make the limits of detection for CE-ICPMS as good or better than conventional ICP-MS analyses.

REFERENCES

1. Melissa M. Harwood, Elisabeth S. Christians, Md. Abul Fazal and Norman J. Dovichi Journal of Chromatography A, Volume 1130, Issue 2, 20 October 2006, Pages 190-194

2. Shaorong Liu, Qiaosheng Pu, Lin Gao and Joann Lu Talanta, Volume 70, Issue 3, 15 October 2006, Pages 644-650

3. Sheila Mohabbati and Douglas Westerlund Journal of Chromatography A, Volume 1121, Issue 1, 14 July 2006, Pages 32-39

4. Kuhr, W. G.; Monnig, C. A. Anal. Chem. 1992, 64, 389R.

5. Righetti, P. G. J. Chromatogr. Libr. 1992, 52, A481.

6. Chen, M.; Cassidy, R. M. J. Chromatogr. 1993, 640, 425.

7. Timerbaev, A. R.; Buchberger, W.; Semenova, O. P.; Bonn, G. K. J. Chromatogr. 1993, 630, 379.

8. Rivello, J. M.; Harrold, M. P. J. Chromatogr. 1993, 652, 385.

9. Robert C. Weast (Editor), CRC Handbook of Chemistry and Physics 68th Edition, pp. D267-269. 1987-1988.

10. Landers, J. P., Hand Book of Capillary Electrophoresis; CRC Press: New York, 1997.

11. Guzman, N. A., Capillary Electrophoresis Technology; Marcel Dekker, INC: New York, 1993.

12. Righetti, P. G., Capillary Electrophoresis in Analytical Biotechnology; CRC Press: New York, 1996.

13. Sharp, B. L. J. Anal. At. Spectrom, 1988, 3, 939.

14. Training documents from Thmo Finigan

15. Hieftje, G. M., J. Anal. At. Spectrom., 1992, 7, 783.

16. Greenfield, S.; Montaser, A. in Inductively Coupled Plasmas in Analytical Atomic Spectrometry, 3nd edition. Montaser, A.; Golightly, D. W. eds. 2005.

17. Sharp, B. L. J. Anal. At. Spectrom. 2005 3, 613.

18. Kinzer, J. A.; Olesik, J. W.; Olesik, S. V. Anal. Chem. 1996, 68, 3250.

19. Liu, Y.; Lopez-Avila, V.; Zhu, J. J.; Weiderin, D. R.; Becket, W. F. Anal. Chem. 1995, 67, 2020.

20. Olesik, J. W.; Kinzer, J. A.; Olesik, S. V. Anal. Chem., 1995, 34, 1.

21. Poole, C. F.; Poole, S. K. Chromatography Today Chpt 4. pp.322-323, Elsevier Press, New York, 1993.

22. Schwer, C.; Kenndler, E. Anal. Chem. 1991, 63, 1801.

23. Tsuda, T.; Nomura, K.; Nakagawa, G. J. Chromatogr., 1983, 264, 385.

24. Fujiwara, S.; Honda, S. Anal. Chem., 1996, 58, 1811.

25. Wallingford, R. A. and Ewing, A. G. in Advances in Chromatography: Biotechnological Applications and Methods. Giddings, J. C.; Grushka, E.; and Brown, P. R. eds. Marcel Dekker Press, New York, New York 1989.

26. Smith, R. D.; Wahl, J. H.; Goodlett, D. R.; Hofstadler, S. A. Anal. Chem., 1993, 65, 574A.

27. B. Santos, B.M. Simonet, B. Lendl, A. Ríos and M. Valcárcel Journal of Chromatography A, Volume 1127, Issues 1-2, 15 September 2006, Pages 278-285

28. Pleasance, S.; Thibault, P.; Kelly, J. J. Chromatogr. 1992, 591, 325.

29. Kostiainen, R.; Franssen, E. J. F.; Bruins, A. P. J. Chromatogr. 1993, 647, 361.

30. Anne-Catherine Servais, Marianne Fillet, Roelof Mol, Govert W. Somsen, P. Chiap, Gerhardus J. de Jong and Jacques Crommen Journal of Pharmaceutical and Biomedical Analysis, Volume 40, Issue 3, 24 February 2006, Pages 752-757

31. Huggins, T. G.; Henion, J. D. Electrophoresis 1993, 14, 531.

32. Liu, Y.; Lopez-Avila, V.; Zhu, J. J.; Weiderin, D. R.; Becket, W. F. Anal. Chem. 1995, 67, 2020.

33. Stewart, I. I.; Olesik, J. W., J. Chromatography A 2000, 872, 227.

34. Kinzer, J. A.; Olesik, J. W.; Olesik, S. V., Anal. Chem. 1996, 68, 3250-3257.

35. Giddings, J .C.; Unified Separation Science, Wiley Interscience, New York, New York, 1991.

36. Jones, W. R.; Jandik, P.; J. Chromatogr. 2002, 608, 385.

37. Romano, J. P.; Krol, J.; J. Chromatogr., 2003, 640, 403.

38. Barger, W. R.; Mowery, R. L.; Wyatt, J. R., J. Chromatogr. A., 2004, 680, 659.

39. Culbertson, C. T.; Jorgenson, J. W. Anal. Chem. 1994, 66, 955.

40. Lu, Q.; Bird, S. M.;Barnes, R. M. Anal. Chem. 1995, 67, 2949.

41. Scott, R. H.; Fassel, V. A.; Kniseley, R. N.; Nixon, D. E. Anal. Chem. 1974, 46, 75.

42. Smith, D. D.; Browner, R. F.; Anal. Chem., 1982, 54, 533.

43. 29. Hjert, S.; Elenbring, K.; Kilar, F. Liao, J. L.; Chen, J. C..; Sibert, C. J.; Zhu, M. D., J. Chromatogr., 1987, 403, 47.

44. Albin, M.; Gross, P. D.; Moring, S. E., Anal. Chem., 1993, 65, 489A.

45. Vinther, A.; Sberg, H. J. Chromatogr., 1991, 559, 3.

46. Smyth, W. F.; Heiland, G .D.; McClean, S.; McGrath, G. Oxspring, D. J. Chromatogr. A. 1997, 772, 161.

47. Yanfang Shi, Ying Huang, Jianping Duan, Hongqing Chen and Guonan Chen Journal of Chromatography A, Volume 1125, Issue 1, 25 August 2006, Pages 124-128

Chapter 3

Investigation of Elemental Speciation of Rhodium (III) in Aqueous System by Capillary Electrophoresis-High Resolution Inductively Coupled Plasma Mass Spectrometry

3.0. Introduction

Considerable work in the fields of biological and environmental science has focused on the subject of element speciation. It is increasingly realized that the distribution, mobility, removal and biological availability of chemical elements depend not simply on their total concentrations but, critically, on the chemical species in the systems.[1-3] Studies of formation, distribution, lability, inertness of various metal species in aquatic environment are of great importance. The hydration/hydrolysis of Rhodium(III) is a fundamental process that occurs in most aqueous solutions and is often a natural precursor to the formation of more complex polynuclear (polymeric) species or oligomers.[4] The importance of these species is becoming increasingly recognised in a variety of systems and matrices. For example, the formation of polymeric species in natural waters[5] can have a significant impact on the mobilisation, transport and fate of Rh(III) in the environment. As such there is now a growing need for the development of methods capable of the accurate determination of these polymeric species.

Another needs for Rh speciation study is in pharmaceutical process research. Nowadays, Rh complexeses are used routinely as catalysts in pharmaceutical industries in synthesizing raw materials, intermediates and final active pharmaceutical ingredients (API's).[6-10] The reaction ability of a metal ion and, in particular, its catalytic activity is to a great extent dependent on the forms in which the metal exists in solution.[6-12] Therefore, the capability of distinguishing and identifying the presence of various species of an catalyst metal at various stages of an reaction may provide a better insight into the mechanism of a catalytic reaction. In addition, both more efficient use of metal catalysts and eventual faster residual catalyst removal from the drug substances would be facilitated with the speciation knowledge, thus contributing to the shortening of the drug discovery processes as a whole.

Since the bioavailability and toxicity of an element also depend on its species, the information obtained from speciation studies might potentially lead to a decision not to spend time, money and efforts to remove certain residual catalyst metals, since the residual catalyst species remained after the reaction may pose no harmful effects to humans or animals.

To identify and quantify different elemental species in a complicated chemical system, at least two analytical techniques have to be applied. The first is used to separate the species and the second analytical technique is used to identify and quantify the species.[14-16] Many different separation and detection systems have been used for elemental speciation. To reduce analysis time and improve accuracy, hybrid or coupled techniques are usually preferred. However, various obstacles and difficulties are frequently encountered with speciation work such as low species concentrations, complex

chemical matrices, and potential pitfall associated with inter-conversions among various species during the sample preparation and the measurement processes. In this work, a new hyphenated technique-capillary electrophoresis inductively coupled plasma mass spectrometry (CE-ICPMS) to perform rapid elemental speciation was applied for Rh speciation study. This technique provides a complementary extension to the types of analyses possible with the ICP. By taking advantage of the low limits of detection and element specificity of the ICP-MS and the high resolution and fast analysis times of capillary electrophoresis, the combined technique can perform analyses that neither alone is can.

3.1 Rhodium Aqueous Speciation

The chemistry of hydration/hydrolysis Rh(III) species has been discussed in the literature. The distribution of species is typically dependent on the metal ion concentration, solution pH, solution matrix and the solution history or "ageing" period. Often, however, the absence of information on a sample's history and thermodynamic data make accurate speciation modeling a difficult and perhaps impractical task. An assessment of chemical speciation is therefore critical before any true understanding of an element's reactivity, transport or interaction within a particular environment can be achieved.

The prevalent oxidation states of rhodium are +3 and +1, with +3 complexes usually dominating in chloride-containing solutions. Rhodium (III) forms octahedral complexes with anions such as halides and other oxygen-containing ligands. The presence of a variety of Rh aquo/chloro complexes in chloride-containing solutions was revealed in early studies.[17-21]

Starting with hexachlororhodate ($RhCl_6^{3-}$) in aqueous solution, the following substituting reaction will occur:

$$RhCl_6^{3-} + nH_2O \leftrightarrow [RhCl_{6-n}(H_2O)_n]^{(3-n)-} + nCl^-$$

The resulting species, therefore, can range from the completely aquated hexaaquo-rhodate, $[Rh(H_2O)_6]^{3+}$, to hexachloro-rhodate, $RhCl_6^{3-}$, with various mixed aquo/chloro complexes, $[RhCl_{6-n}(H2O)_n]^{3-n-}$, in between. The formation and distribution of each of the species depends on the chloride concentration, pH of the solution, aging period of the solution, and the ambient temperature.

When pH is higher than 3, the aquo/chloro complexes are known to undergo hydrolysis as follows:

$$[RhCl_{6-n}(H_2O)_n]^{(3-n)-} + H_2O \leftrightarrow [RhCl_{6-n}(H_2O)_{n-1}OH]^{(4-n)-} + H_3O^+$$

Therefore it will not be surprising to see a wide variety of species of Rh in aqueous solutions in the electrochromgraph of the CE-ICP-MS, which makes Rh speciation a challenging and complicated task.

In the laboratory, solution based hydration/hydrolysis Rh(III) speciation can be monitored as a function of pH and time by potentiometric methods[22-29]. Further characterisation of test solutions is typically performed using open column cation-exchange chromatography (e.g., Sephadex) incorporating off-line UV–Vis detecti[22-29]. Although these methods above are effective for research purposes, they do suffer from limitations. In particular, poor sensitivity and non-element specific detection associated with UV–Vis techniques can significantly limit the analytical performance. Additional off-line element specific detection is possible, however, it can further increase already long total analysis times. For example, Collins et al.[30] report analysis times for on-line

separation and detection in excess of 50 min. In addition, specific interactions within the separation column can potentially modify semi-labile speciation and degrade the analytical accuracy of the measurement.

High performance capillary electrophoresis (CE) is receiving considerable attention as a highly efficient separation tool for speciation research.[31-42] Capillary electrophoresis has a number of advantages over other separation techniques.[16, 43-45] Chief among them is high resolving power with the increased speed at which analysis can be performed. In addition, the amount of sample and electrolyte required is reduced to a few nanoliters (compared to μL to liter volumes typically used in HPLC and IC) due to the small physical dimensions of the capillaries used. Another advantage of CE over gas chromatography and liquid chromatography is that CE separates analytes on basis of physical properties of the analytes (size, shape and charge), rather than a chemical interaction and partitioning between a stationary phase and a mobile phase. As a result, electrophoretic separations may disturb the elemental speciation less than chromatographic separation techniques. Last, due to its high concentration, the electrolyte used determines the conductance and pH throughout the capillary. The influence of the sample on conductance and pH can be generally neglected. Therefore, the sample components migrate independently from the carrier electrolyte with their specific velocities, which depend on its charge, size and shape. Capillary zone electrophoresis has also proven to be an attractive method to study free and complexed metal ions. When changes in the electrophoretic mobility of an analyte are induced by its complex formation, electrophoresis can be used to quantify binding properties.

Detection of the separated species is often achieved using ultraviolet absorbance or fluorescence detection.[46-52] However, these detection systems are limited to a small number of metals, due to the fact that most metal ions in solution lack the chromophores or fluorophores that make UV and fluorescence detection possible. In this work, inductively coupled plasma mass spectrometer (ICP-MS) has been interfaced with the CE system for elemental speciation. The advantage of using a mass spectrometer as the detector for CE is not only its high sensitivity (ppt), but also its high selectivity: only different forms of a particular element of interest must be separated from each other rather than needing to separate species containing different elements from each other.[53-61]For example, there is no need to electrophoretically separate different elements with the same charge (such as Fe^{3+} from Rh^{3+}). The high separation efficiencies afforded in CE allow species of the same element with different charge and/or size to be separated before reaching the ICP. By combining the rapid and efficient separation characteristics of CE with the low detection limit, species-independent sensitivity, and element-selective nature of the ICP-MS, the marriage of these two techniques creates a much more powerful analytical tool than CE with conventional detection methods (UV or fluorescence).

Theoretically, capillary electrophoresis–inductively coupled plasma mass spectrometry (CE–ICP-MS) should provide an effective means to separate and detect Rh(III) species in solution. Although the Rh aqueous species are considered thermodynamically unstable, research using ion-exchange chromatography indicates that they can be separated and stored for short periods of time and therefore should be stable over the course of a CE–ICP-MS separation (5 min).

In contrast with other CE methods, CE–ICP-MS does not require the use of complexing agents or specific interactions to separate intra-element species in a single run.[53] This is beneficial for maintaining accurate speciation information. A number of simple, non-complexing electrolyte salt solutions such as alkali, alkaline earth and lanthanide halides and nitrates have been used successfully by Olesik et al.[54-55] as separation electrolytes. Although, CE–ICP-MS has been used for the rapid, sensitive determination chromium fractions, there have been no reports in the literature on the separation and detection of Rh(III) hydration/hydrolysis species.

The purpose of this study is to evaluate the capability of CE-ICP-MS as a tool for speciation studies and determine the detection limit and the migration characteristics of different metal species. In particular, using a solution with well-defined chemistry ($RhCl_3$ aqueous solution), it is possible to separate metal fractions into its various components and more importantly, identify and quantify these species distribution using migration time and peak area calculation. In the study, the choice of separation electrolyte, including type, pH and concentration, will be discussed in terms of optimum performance of the separation of metal species. As well, the importance of other experimental parameters such as sheath flow rate and induced laminar flow rate will be discussed in relation to separation, resolution, and sensitivity. The effects of solution pH as well as solution ageing on various Rh species will also be discussed.

3.2 Experimental

3.2.1 Chemical reagents and preparation

All the chemical reagents were of analytical grade. Standard stock solutions (100 mM) for each metal ion were prepared by dissolving the appropriate amount of analytical grade solid reagents in ultra pure water (18MΩ cm^{-1}), which was made in-house with a Milli-Q water purification system (Millipore, Milford, MA, USA). Analytes include, $LaCl_3$ (Fisher Scientific, Pittsburgh, PA), CsCl (Fisher Scientific, Pittsburgh, PA), RbCl (Fisher Scientific). $FeCl_2$ (Fisher Scientific), $FeCl_3$ (Fisher Scientific), $RhCl_3$ (Sigma, St. Louis, MO). Dilute solutions for analysis were prepared daily.

The sheath flow solution used was dilute nitric acid in which the conductivity matched that of the separation electrolyte (e. g. 2200 μS). The separation electrolyte solution contained 20 mM $NaNO_3$ (Fisher). If necessary, the solution pH was adjusted through addition of small aliquots of 2 % (v/v) HNO_3 or 10 % (v/v) NaOH solution. A Fisher Scientific Accumet Portable AP63 pH/mV/Ion meter calibrated with pH 4, 7 and 10 buffer standard solutions was used for all pH measurements; the same meter calibrated with 1403 μS KCl standard was used for all conductivity measurements.

3.2.2 Inductively Coupled Plasma Mass Spectrometry

All the measurements were carried out with a Finnigan Element 2 (Finnigan, Bremen, Germany) high resolution inductively coupled plasma sector-field mass spectrometer. The instrument is equipped with a double focusing mass analyzer using reversed Nier-Johnson geometry. The system allows three pre-defined nominal mass resolutions ($m/\Delta m$) of 300, 4,000, and 10,000 by means of selectable slits. The actual mass resolutions vary between 300-500 for low, 3,500-4,500 for medium, and 8,000-14,000 for high-mass resolution mode depending on the optimization of parameter settings.

Plasma gas flow-rate	17 L/min
Auxiliary	0.7 L/min
Nebulizer (variable)*	0.8-1.2 L/min*
Plasma Power	1050-1300 W
Sample	Pt
Skimmer	Pt
Injector	Sapphire
Replicate time (ms)	1500
Dwell time (ms)	100
Scanning mode	E-scan
Sweeps/reading	1
Readings/replicate	1
Number of data points	800-1200

Table 3.1 CE-ICP-MS with sheath flow interface operating conditions

The ICP-MS operating conditions and data acquisition parameters are given in Table 3.1. Optimization of the ICP-MS operating parameters, including the position of the plasma torch, ion lens voltages, RF power, and nebulizer gas flow rate, was performed daily using a 100 ppb solution containing elements of interest. Normally one end of the electrophoresis capillary is placed in the sample that is drawn through the capillary. Nebulizer gas flow and the sheath flow rate are set to provide a fixed laminar flow rate (e.g. ~0.1 μL/min) and therefore a constant uptake of the analyte. The optimized

nebulizer gas flow rate typically was ~0.90 L/min. The dwell time was 100 ms per peak and the number of replicates was chosen such that the total experiment time was slightly longer than the time required for a given separation. Depending on the number of masses measured, the total analysis time was between 10-30 minutes.

An accurate mass calibration at the beginning of the measurement session was routinely performed for low resolution (LR), medium resolution (MR), and high resolution (HR) modes by using a 1.0 ng/ml multi-element standard tuning solution containing Li, B, Na, Al, Sc, Fe, Co, Ga, Y, In, Rh, Ba, Lu, Tl and U.

3.2.3 Capillary electrophoresis

CE measurements were carried out using Agilent HPCE system (Palo Alto, CA, USA) with untreated fused-silica capillary with a total length of 95 cm and an effective length 75cm x 50 μm i.d. The reversed polarity mode of the CE system (cathodic injection and anodic detection) was applied. All experiments were conducted at 25°C (capillary cassette).

Prior to use, capillary was preconditioned for 10 minutes with 0.1 N NaOH at 25°C followed by 10 minutes rinse in deionized water before the final rinse with the background electrolyte for 10 more minutes. Before each run the capillary was flushed with 0.2 mM HCl for 2 minutes followed by a 2-minute deionized water wash before the final 3-minute background electrolyte (BGE) rinse. Applying the above procedures has proven to be essential in achieving reproducible migration time.

Hydrodynamic injections were used for all measurements. Typically a hydrodynamic pressure of 50 mBAR for 4 seconds resulted in an injection volume of 47 nL (~ 4 % of the total capillary volume) for fused silica. The injection end of the capillary

was held at +30 kV positive, which produced about an average of 400 V/cm potential gradient and a current of 10-15 μA measured by the ammeter on the CE instrument simultaneously.

3.2.4 CE-ICP-MS interface

In this work, a novel sheath flow interface and a PFA (Perfluoroalkoxy) micro-flow concentric nebulizer were used for CE-ICP-MS experiments. The design and characteristics of this interface was discussed at previous chapter and its schematic is shown in Figure 2.7.

The sheath flow used in this study served three purposes: (1) Since CE flow rates are commonly too low to make the nebulizer work properly in the ICP-MS, which requires a minimum liquid flow rate of about 20 μL/min, the special sheath flow is needed to make up the low CE electroosmotic flow (< 1 μL/min) so that the nebulizer in the ICP-MS sample can produce usable aerosols. Since the sheath flow solution constitutes the majority of the solution that reaches the plasma, the sheath flow interface together with the syringe pump can be used to control both the composition and the flow rate of the solution that reaches the plasma, which is desirable under certain conditions. (2) Since the sheath solution is flowing around the capillary that merges with the eluent flow from the capillary at the interface, a stable electrical ground for CE through the platinum wire is established. (3) Another purpose of utilizing sheath flow is to control the laminar flow in the capillary, which is generated when the rapid gas flow goes through the annular tip of the pneumatic nebulizer used in this study. The details of the effect of the laminar flow on the performance of the CE system will be discussed later. For a regular CE experiment, better peak shape and greater separation efficiency can be

obtained by eliminating the laminar flow. However, the selection of the sheath flow rate may also be a compromise between analyte resolution and analysis time. Whenever separation is of no concern, it is often possible to work with a significant laminar flow rate towards the detector in order to shorten the analysis time. Most CE experiments in this work were performed under a sheath flow rate that introduces positive laminar flow.

The stability of the CE-ICP-MS set up can be monitored by checking the electrical current, the electro-osmatic flow (EOF), and the nebulization during CE separation. It has been demonstrated that with 30 KV applied to the separation capillary, a stable electrical current can be achieved, which indicates that the interface used in this study provides a stable and continuous electrical contact. This is essential for reproducible CE separations. With the ICP-MS system, it is also possible to observe the stable EOF by adding 100 ppb Rb to the CE electrolyte and monitoring Rb85 signal. The nebulization can be monitored by adding 10 ppb Y89 into make up flow solution, which is independent of the CE performance. Replicate injections of the same sample were performed to assess the precision of the method. Better than 1% RSD on migration time can be obtained routinely with the current method.

For data acquisition and evaluation, raw data were acquired by the Element 2 software (Finnigan, Bremen, Germany) and then exported as ASCII files to EXCEL program for further processing calculations to generate electropherograms.

3.3 Experimental considerations

3.3.1 Sheath flow rate

As discussed in previous chapter, in CE-ICP-MS interface, argon gas exiting the nebuliser will induce a natural aspiration through its central solution uptake capillary. As a consequence, liquid will flow from the separation electrolyte reservoir through the electrophoresis capillary to the nebuliser tip (induced laminar flow) at a rate proportional to the natural aspiration rate. When the sheath electrolyte is pumped around the capillary tip towards the nebuliser tip it reduces the effect of natural aspiration through the electrophoresis capillary and, therefore, the accompanying degradation in separation efficiency due to induced laminar flow. When the sheath electrolyte flow-rate approaches the natural aspiration rate induced by the argon gas flow-rate, an approximate "balance point" will be reached and the induced laminar flow will approach zero at the electrophoresis capillary tip. In such cases, the pressure differential between the liquid in the sheath flow and the liquid in the capillary approaches zero. Higher sheath flow-rates generate a reverse laminar flow-rate through the electrophoresis capillary.

For a fixed nebuliser gas flow-rate, the sheath flow-rate required to eliminate the laminar flow through the electrophoresis capillary was estimated in the following manner. A sample plug (47 nl) from a Cs sample solution (100 ppb) is introduced to the electrophoresis capillary and the time required for the plug to migrate the length of capillary can be measured with no voltage applied. Knowing the volume of the capillary (1.2 μl) and the migration time at a given sheath flow-rate, the laminar flow-rate through the capillary can be calculated. In this manner, a plot of sheath flow-rate vs. laminar flow-rate was recorded and the sheath flow-rate necessary to eliminate the laminar flow can be estimated by extrapolating to zero. As showed in Figure 3.1, for the high efficiency micro-flow PFA nebulizer used at a fixed nebulizer gas flow rate of 0.8 L/min

and a separation capillary of 50 μm i.d., a sheath flow rate of 49 μL/min resulted in the elimination of the laminar flow. This is lower than those of Meinhard high efficiency nebulizer (HEN) and SB-30-A3 nebulizer, which have much higher sheath flow rates of 100-1000 μL/min needed to eliminate laminar flow in the separation capillary as reported in the literature[36,37]. Normally the selection of sheath flow-rate is a compromise between analyte resolution and analysis time. For simple systems it is often possible to work with a significant laminar flow-rate towards the detector to minimise the analysis time.

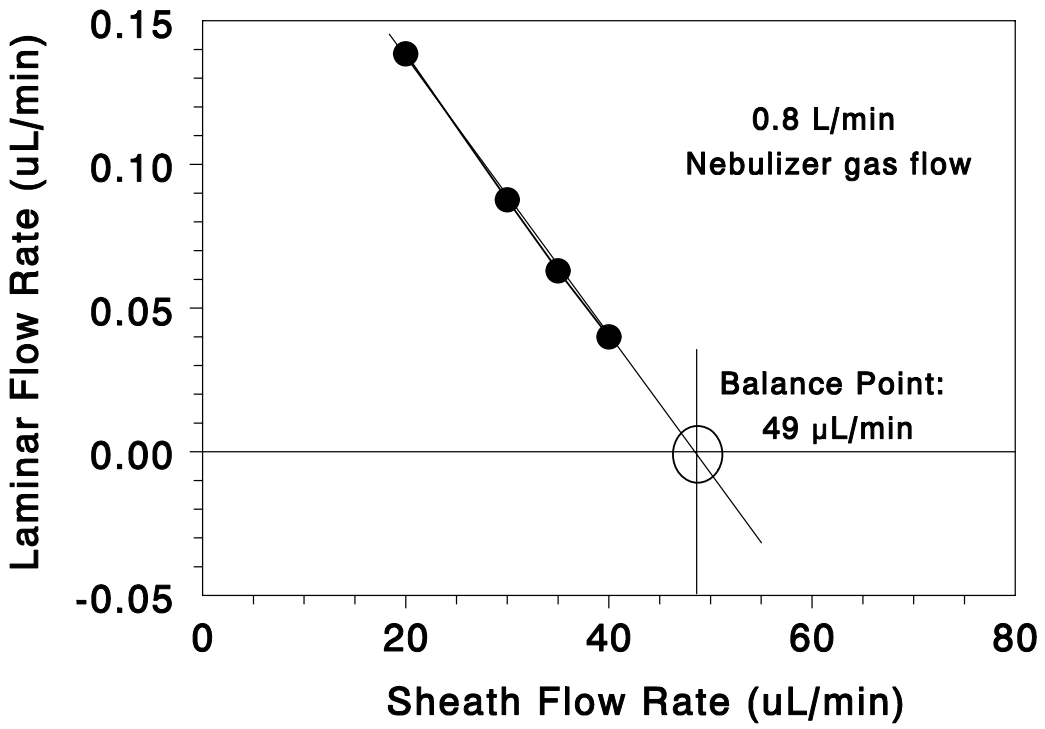

Figure 3.1 The effect of sheath flow rate on laminar flow rate. Nebulizer gas flow rate 0.8 L/min. Calculated from measurement made with no CE voltage applied and using measured Cs^+ migration times. Balance point is the calculated sheath flow rate where laminar flow rate is zero.

3.3.2 Electrolyte selection

The physical properties of the separation electrolyte are important, as they will ultimately affect the quality of the separation. The composition, concentration, and pH of the separation electrolyte are important parameters that effect migration, selectivity, and peak shape in CE. In particular, the concentration of the electrolyte chosen should be high enough to provide an electrolyte conductivity that is large compared to the sample solution containing injection volume (plug), but not so large as to cause Joule heating upon application of the external field. The large conductivity difference between sample plug and separation electrolyte ensures a high-voltage gradient across the sample plug and an additional focussing of analyte bands due to electrostacking .

The type of electrolyte chosen can be equally as important as its concentration. Typically considerations in selecting a suitable buffer for CE-ICP-MS coupling includes: (1) the electrolyte should have a low enough dissolved solid so that the deposition of salt on the sampler and skimmer cones can be avoided to prevent clogging (2) the electrolyte species should not have serious space charge effects to lower the sensitivity of analyte; and (3) the electrolyte should not form adduct ions with the analytes to decrease the sensitivity of the target analyte and complicate mass spectra by spreading the ion abundances among several masses. (4) In order to maintain accurate solution speciation, it is essential that the separation electrolyte does not react or complex significantly with the analyte. Thus, for CE-ICP-MS, the separation electrolyte is typically restricted to a few volatile buffers such as ammonium acetate and Tris. Ideally, the cations and anions of the electrolyte components should not survive the hot plasma after serving their purpose in the capillary.

As discussed above, one of the advantages of using sheath flow interface is that the sheath flow can be delivered independently of the CE effluent. Since the electro-osmotic flow is only a small portion of total flow that reaches the nebulizer, a nonvolatile CE buffer could be used for better separation and sensitivity as long as a volatile sheath flow solution is used. In our experiments, dilute nitric acid is used as the sheath flow solution. This nitric acid sheath flow solution was always adjusted before use so that it was conductivity matched with the CE buffer electrolyte. As shown in Figure 3.2, results using the dilute HNO_3 solution as the sheath flow and 20 mM $NaNO_3$ as the CE electrolyte are compared to those using 20 mM ammonium acetate as both the sheath flow solution and the CE electrolyte based on a 47 nL injection of a 1.0 μg/mL CsCl solution. In addition to a much better peak shape, the ICP-MS Cs^+ signal intensity was improved approximately by an order of magnitude simply by using $NaNO_3$ rather than the volatile ammonium acetate as the separation electrolyte. Column efficiencies for Cs, with peak widths at half peak height, were also improved from 20×10^3 to 15×10^4 by simply switching to $NaNO_3$ from ammonium acetate. The formation of analyte and Na clusters such as $M.Na^+$ and $M.Na(NaNO_3)^+$ that have been reported elsewhere were not observed in the experiment. Using the dilute HNO_3 sheath flow solution, it was observed that sampler and skimmer cones on the ICP-MS remained very clean after days of continued operation with no sign of clogging.

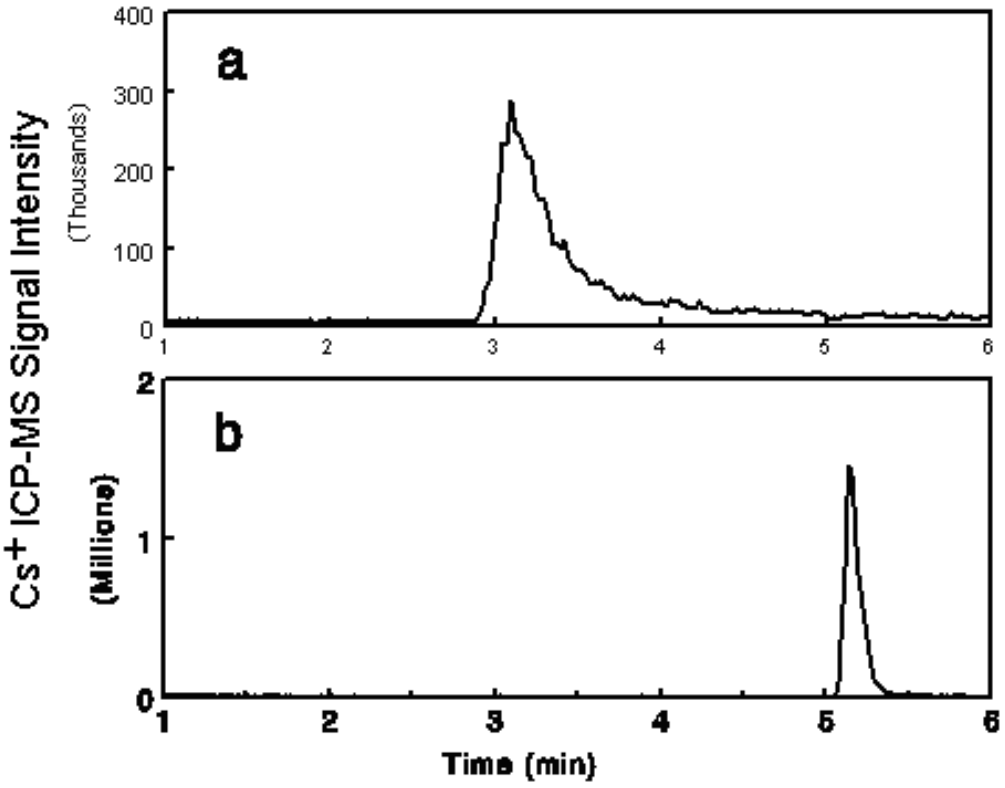

Figure 3.2 The effect of separation electrolyte composition on CE-ICP-MS signals. CE-ICP-MS electropherograms for 1 ppm Cs^+ using an electrolyte containing a) 20 mM NH_4CH_2COOH, conductivity 2246μS b) 20 mM $NaNO_3$, conductivity 2108 μS.

In addition, the electrolyte chosen should have a greater(or as large as possible) affinity for any active surface sites along the inner-wall of the capillary than the analyte. This is necessary to minimise analyte–wall interactions and consequently sample loss due to trapping. In parallel with the above discussion, $NaNO_3$ separation electrolyte solution was chosen. The electrolyte concentrations used were 20mM $NaNO_3$ and were pH modified to between 3 and 6 with HCl (where specified) resulting in electrolyte conductivities between 1100 and 1800 μS. At 30 kV, currents between 10 and 15 μA were observed. The electrolyte conductivity was typically 5× greater than the analyte sample solutions studied. Although, $La(NO_3)_3$ or $La(ClO_4)_3$ electrolyte solutions would

probably have made better choices due to the non-complexing nature of the anions[54-57], as discussed in next section, $LaCl_3$ separation electrolyte–sheath flow electrolyte are not suitable for this application due to the space charge effects.

3.3.3 Sheath flow solution selection

Even though the $LaCl_3$ separation electrolyte–sheath flow electrolyte has demonstrated its utility for the separation of the metal species, it also appears to limit the analytical performance of the ICP-MS. In particular, the potential degradation in signal sensitivity due to space-charge effects can be significant. La^+ (*m/z* 139) is larger in mass and is delivered to the plasma per unit mass at rates much greater than the analyte (Rh^+, *m/z* 103). For example, consider a 5×10^{-4} *M* sample plug (47 nL) that travels through the capillary under the influence of laminar flow alone (i.e. no external voltage applied). For simplicity, if the peak is assumed to elute with a perfect rectangle or 'plug' like profile with a peak width of 30 s at the base, then during this time 1 pmol/s analyte is delivered to the nebuliser tip. Over the same time period, the $LaCl_3$ separation electrolyte/sheath flow (4 m*M*) is delivered to the nebuliser tip at a rate of 50 µl/min or 3000 pmol/s. Assuming a transport rate efficiency of 30% [55]this corresponds to 1000 pmol/s $LaCl_3$ and 0.3 pmol/s Rh^{3+} delivered to the plasma on average. For comparison, the typical transport efficiency through a double pass spray chamber with a sample uptake rate of 1 mL/min (typical sample introduction) is only 1–2%. For a 4m*M* $LaCl_3$ solution, this would correspond to transport rates between 700 and 1400 pmol/s respectively. Therefore, a large amount of lanthanum is introduced into the plasma that may result in significant space charge induced loss of analyte sensitivity. The use of higher sheath flow rates

normally associated with inceeased resolution (decreased induced laminar flow rate) will exacerbate this effect.

An additional consequence of the use of high concentration electrolyte solutions is the gradual accumulation of electrolyte salt deposits on the sampling orifice, skimmer cone and the cylinder ion optic lens. Significant accumulation could degrade the sampling efficiency and hence, analytical performance of the ICP-MS. For $LaCl_3$, significant cloudy white enamel-like deposits become noticeable on the tip of the skimmer after several hours of operation.

Although the separation electrolyte is required in the electrophoresis capillary, is not essential in the sheath flow. As discussed above, one of the purposes of the sheath flow electrolyte is to provide sufficient conductivity such that a good electrical contact can be made with the grounded stainless steel tubing. Large differences in conductivity between the solution exiting the electrophoresis capillary and the sheath flow electrolyte can lead to additional field gradients that might affect the quality of the separation. With this in mind a dilute nitric acid solution was prepared for use as a sheath electrolyte. The nitric acid sheath flow electrolyte was conductivity matched with the sheath flow electrolyte (e.g., 1200 μS). Results using the dilute HNO_3 sheath flow electrolyte were compared to the standard $LaCl_3$ sheath electrolyte based upon a 47-nl injection of $5 \cdot 10^{-4}$ *M* $RhCl_3$ (pH 2.85). Experimental runs with and without applied voltage were conducted, in both cases the analytical area of the Rh^+ MS signal increased approximately one order of magnitude without any significant change in the migration time or peak shape. The experimental results for the injections where voltage was applied as in a normal analytical run is given in Fig. 3.3a. Comparison of peak areas with a multi-element

solution using the same experimental conditions is given in Fig. 3.3b. For a sheath flow-rate of 50 μl/min this improvement is presumably due to the fact that now only 0.03 μl/min (1/1700) $LaCl_3$ is delivered to the nebuliser due to induced laminar flow. Although the improvements in sensitivity are consistent with that expected based upon space-charge phenomenon, it should be noted that the ICP-MS ion-optic was optimised only for Rh^+. Using the dilute HNO_3 sheath flow it was also found that the sampler and skimmer cones remained relatively clean and that there was little or no discernible salt accumulation over periods of 8–10 h of operation.

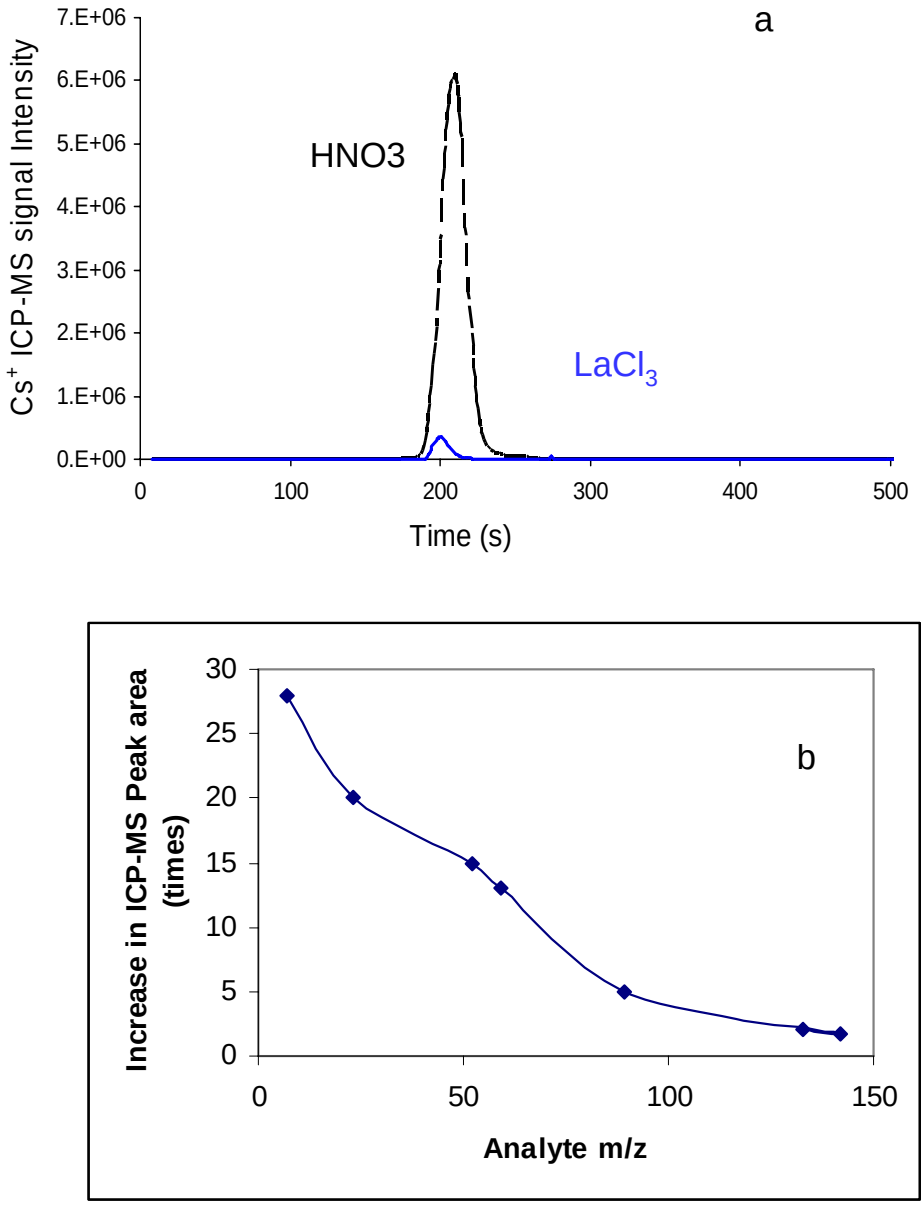

Figure 3.3. Effect of sheath flow electrolyte on CE–ICP-MS signal. (a)Cs^+ signal traces recorded with dilute HNO_3 and $LaCl_3$ (4 m*M*, pH 3) sheath flow electrolyte solutions. The conductivity of both electrolyte solutions is 1800 µS. Solution pH: 2.85, injection volume: 47 nl, laminar flow-rate: 0.034 µl/min., CE voltage: 30kV, CE current: 10 µA (b) Change in the peak area recorded for a series of analytes with increasing mass when a dilute HNO_3 sheath flow electrolyte is used compared with an $LaCl_3$ sheath electrolyte.

Under the conditions used, a slight positive laminar flow was present in addition to the positive electroosmotic flow. As such, there was a net flow of liquid from the capillary tip into the sheath flow. Although there was little or no significant change in the migration time or peak shapes recorded using simple chemical systems, it is unknown whether there are any deleterious effects due to the pH modification or mixing of the different electrolyte solutions at the electrophoresis capillary tip. It would seem reasonable, however, that matching the counter ion in the separation electrolyte with that of the sheath flow electrolyte would be desirable to minimize any mixing due to the counter-migration of anions with the applied electric field.

A further consideration when using a dilute HNO_3 sheath flow electrolyte for CE–ICP-MS, is that all metal in contact with the charged electrolyte solution should be inert. In particular, to avoid electrochemical contamination of the sheath electrolyte, a platinum tube should replace the stainless steel ground tubing. In addition, non-conducting materials (plastic based) should be used in place of any metal (brass) connections at the syringe pump. When this precaution is not taken, contamination from the stainless steel or brass fittings can give rise to significant Rh, Fe and Cu contamination. Matrix dependent molecular ion overlaps such as $^{40}Ar^{12}C^{+}$ (*m/z* 52) or $^{37}Cl^{16}O^{+}$ (*m/z* 53) that have been reported in other Rh ICP-MS literature [62] were not observed here.

3.3.4 Electroosmotic flow rate

In order to estimate the migration time of the neutral species, it is necessary to calculate the electro-osmotic flow.

In the absence of laminar flow, there are only two forces that are responsible for the motion of ions in the separation capillary: the electroosmotic flow described by μ_{eof} and the electrophoretic mobility μ_{eff} of the ion. The migration time t_m(s) can be expressed by the following equation [44-45]

$$t_m = \frac{L_0}{\mu_{eff}.E + \mu_{eof}.E} \qquad (1)$$

Where L_0 is the length of the capillary, E is the potential gradient. For small metal cations, μ_{eff} is approximately equal to the ion's equivalent ionic conductance (EIC). With the t_m determined experimentally, the electroosmotic flow can be accurately predicted by equation 2.

$$\mu_{eof} = \frac{L_0 - t_m E \mu_{eff}}{t_m E} \qquad (2)$$

Using the same capillary applied with the same potential gradient filled with the same electrolyte in the CE system, the electroosmotic flow rate is a constant as predicted in Equation (2) above regardless of the sheath flow rates. An electroosmotic flow of 32×10^{-9} $m^2V^{-1}s^{-1}$ was obtained in our study when experimentally obtained migration times of Cs^+ ion under different sheath flow rates were plugged in equation 2. With the obtained $\boldsymbol{\mu}_{eof}$ plugged back into equation (1) and with the sheath flow induced laminar flow taken into account, the migration time $\mathbf{t}_m$ for neutral species can be calculated easily since $\boldsymbol{\mu}_{eff}$ is now zero for neutral species. Calculated migration times under various sheath flow rate are listed in Table 3.2. At a fixed nebulizer gas flow rate with the sheath flow rate set to eliminate the laminar flow through the electrophoresis capillary, neutral species should have a migration time of about 840 s.

Cs^+ EIC (10^{-9} $m^2V^{-1}s^{-1}$)	77.2		
Sheath Flow Rate (μL/min)	20	49	70
Cs^+ CE migration Time (s)	228	250	275
Calculated Electroosmotic flow (10^{-9} $m^2V^{-1}s^{-1}$)	32.1		
Laminar flow (μL/min)	0.14	0	-0.17
Neutral species CE migration time (s)	760	840	1240

Table 3.2 Experimentally determined electroomotic flows, laminar flow, and calculated migration time for neutral species under different sheath flow rate; Solution pH: ~4, ion: Cs^+, injection volume: 47 nL, CE voltage: 30 kV, CE current: 10 μA.

3.4. Results and discussion

3.4.1. Freshly prepared solutions

A freshly prepared stock solution of 100 □g/mL $RhCl_3$ were diluted immediately to 1.0 μg/mL with deionized water and divided into three portions, with the pH of each portion adjusted to 1, 2, 4 through the addition of small aliquots of 2 % (v/v) HNO_3 and/or 10 % (v/v) NaOH solution, respectively. The formation of at least seven Rh complexes should be considered: $Rh(H_2O)_6^{3+}$, $RhCl(H_2O)_5^{2+}$, $RhCl_2(H_2O)_4^{+}$, $RhCl_3(H_2O)_3$, $RhCl_4(H_2O)_2^{-}$, $RhCl_5(H_2O)^{2-}$, $RhCl_6^{3-}$. The species, such as $[RhCl_3(H_2O)_2OH]^{-}$, as a result of hydrolysis when pH is higher than 3 should be also be considered.

The electropherogram of the Rh solution at pH 4 obtained using the CE-HR-ICP-MS system is shown in Figure 3.4A. To identify the four major peaks with a migration time of 600s, 785s, 1050s, and 1205s, it is important first to verify the charges of these species. As discussed previously, one of the purposes of using the sheath flow is to control the laminar flow inside the capillary. When the sheath flow rate was set at 50 μL/min used in our experiment, the laminar was eliminated. Under this zero-laminar flow condition, only positive and neutral species would migrate toward the nebulizer and thus be detected in the CE-HR-ICP-MS while the negatively charged species were moving in the opposite direction. In order to detect negatively charged species (anions), the sheath flow rate was adjusted such that a positive laminar flow was also introduced in addition to the electroosmotic flow. Under these experiment conditions, there would be a net flow of liquid inside the capillary toward the nebulizer even with the absence of the electroosmotic flow. If the bulk solution flow (electroosmotic flow and laminar flow) rate toward the detector is greater than the migration rate of the anions in the opposite direction in the capillary, the detection and analysis of positively charged, neutral, and negatively charged species can be realized from one single injection. The normal side-effect of introducing laminar flow is the loss of separation efficiency, luckily, the mobilities of the Rh species involved in our studies are far apart, and thus the loss of resolution is of no great concern and all the Rh species peaks could still be resolved.

The mobilities of the species depend first of all on the overall charges the species carries. Since a negative voltage was applied to the detector end of the capillary, the higher the positive charge, the faster the species migrates toward the detector and thus the shorter the migration time. It was predicted from Table 3.2 that the neutral species under

these experimental conditions with a sheath flow rate set at 20 μL/min should elute at about 760s. The migration time of the fourth species in Figure 3.4A coincides with that of a neutral species, which points to the most probable Rh neural complex, $RhCl_3(H_2O)_3$. It is now also not difficult to assign the first minor peak as $Rh(H_2O)_6^{3+}$, the second minor one as $RhCl(H_2O)_5^{2+}$, and the third major one as $RhCl_2(H_2O)_4^{+}$. The first peak after the neutral species should be that of $RhCl_3(H_2O)_2OH^-$, the result of hydrolysis when pH is higher than 3. The last peak is assigned to $[RhCl_4(H_2O)_2]^-$ not to $[RhCl_3(H_2O)_2OH]^-$, since it remains to be present when the pH was adjusted to lower than 3 while the other peak that was assigned to $[RhCl_3(H_2O)_2OH]^-$ simply disappeared under this condition.

Migration times in CE may be affected by various factors such as changes in electroosmotic flow, the presence of charged ligands from the electrophoresis buffer, and temperature variations. All these changes can lead to variations in conductivity and viscosity of the electrolyte used and variations in capillary wall adsorption of different species. Therefore, the interpretation of any changes in migration time must be made with great care. At least one non-interacting marker metal ion should be present in the sample in order to monitor the electroosmotic flow or other non-specific effects. Cs^+ was used in this study since it only has one peak in CE under diverse conditions with reliable and constant migration time under fixed experimental conditions.

The electropherogram of the Rh solution at pH 2 obtained using the CE-HR-ICP-MS system is shown in Figure 3.4B. In contrast to the electropherogram at pH 4, only two major Rh peaks were observed. Compared to Figure 3.4A, the first peak obviously belongs to $[RhCl_2(H_2O)_4]^+$, and the second to the $[RhCl_4(H_2O)_2]^-$ complexes. The

disappearance of the $[RhCl_3(H_2O)_2OH]^-$ peak is consistent with the assumption that formation of hydrolysis species only occurs at pH above 3.

The electropherogram of the Rh solution at pH <1 is shown in Figure 5C. Unlike the electropherogram obtained at pH 2, three major peaks were detected. In comparison to Figure 5A, the first two can be easily assigned to $[RhCl_2(H_2O)_4]^+$ and $[RhCl_4(H_2O)_2]^-$. The third one has noticeably longer migration time than all the previously observed peaks. There are only two negatively charged species can be possibly assigned to this peak, $[RhCl_5(H_2O)]^{2-}$ and $[RhCl_6]^{3-}$. Since the probability of forming $[RhCl_6]^{3-}$ in an aqueous system is small, this peak very likely belongs to $[RhCl_5(H_2O)]^{2-}$.

Integration time of as long as one hour was used to try to "catch" all rhodium species peaks and no other peaks were ever detected after the $[RhCl_5(H_2O)]^{2-}$ peak.

In order to quantify the equilibrium distribution, peak integration was performed using PeakFitTM (Systat Software, Point Richmond, CA) with peaks fit to the Haarhoff-Van der Linde (HVL) equation. Both fronting and tailing peaks are allowed in this equation. The sum of all peak areas in each of the three electropherograms in Figure 5A, 5B, and 5C are very similar as shown in Table 4, indicating that all rhodium species are probably accounted for and migrated out of the capillary.

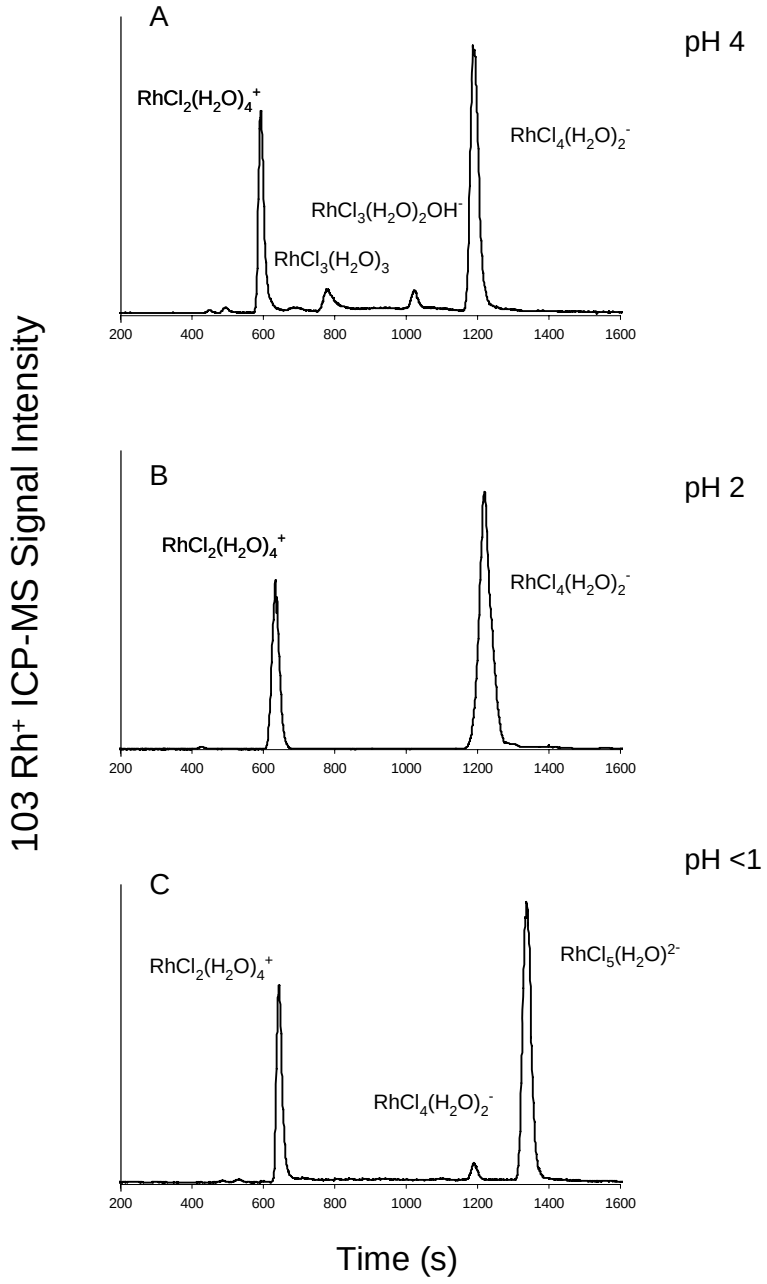

Figure 3.4 CE-ICP-MS electropherogram of freshly prepared 1 ppm $RhCl_3$ solution (a) pH 4 (b) pH 2 (c) pH <1. Electrolyte: 20 mM $NaNO_3$, hydrodynamic injection (5mbar, 4s) injection volume: 47 nL, CE voltage: 30 kV, CE current: 10 µA. 0.8 L/min nebulizer gas flow and 20 µL/min sheath flow rate, 0.14 µL/min laminar flow ; All Y-axis scales are the same with minimum =0 and maximum = 2×10^6 count/s.

For comparison, the relative peak areas for electropherograms shown in Figure 3.4 were determined and expressed as % fractions of the total Rh peak area calculated in each electropherogram. The results are listed in Table 4. It is obvious that at all three pH's, the relative peak area of $RhCl_2(H_2O)_4^+$ basically remain unchanged (~28%), whereas the relative peak areas of other species differ greatly from one pH to anther. The results clearly illustrated the trend of reduced chloro complexation and increased aquo complexation with increased pH. For example, when pH was adjusted to 1 , $RhCl_5(H_2O)^{2-}$ accounted for about 64 % of total Rh present in the sample; at pH 2, there was no $RhCl_5(H_2O)^{2-}$ detected and 71% of Rh was present as $RhCl_4(H_2O)_2^-$.

	pH	Peak #1* $RhCl_2(H_2O)_4^+$	Peak #2* $RhCl_3(H_2O)_3$	Peak #3* $RhCl_3(H_2O)_2OH^-$	Peak #4* $RhCl_4(H_2O)_2^-$	Peak #5* $RhCl_5(H_2O)^{2-}$
Figure 5 A	4	28	9.2	8.6	54	0
Figure 5 B	2	29	0	0	71	0
Figure 5 C	<1	28	0	0	7.8	64

Table 3.3 A comparison of the relative peak areas of the Rh(III) species detected in Figure 3.4
*Expressed as a percentage of the total of all $^{103}Rh^+$ CE-ICP-MS peak areas in each electropherogram.

3.4.2 Aged samples

In addition to pH, the age of the sample after it was freshly made also plays an essential part in dictating the distribution of the species in the solution. Since water molecules need time to displace Cl^- and reach equilibrium, the distribution of species in aqueous solutions is mostly dependent on pH when fresh. As time passes, water molecules have more time to compete with Cl^- for binding sites of the rhodium ions such that a new distribution of species is continuously taking place until reaching equilibrium. CE-ICP-MS is an ideal tool in monitoring the changes in the distribution of rhodium species with time through different electropherograms. Quantitatively, it is also possible to follow the changes in species distribution by determining the relative peak area of each species with time.

In order to determine the effect of solution aging on the changes in the allocation of various rhodium species, a freshly prepared stock solution of $RhCl_3$ was diluted immediately to 1.0 μL/mL and adjusted to a pH of 4 before it was analyzed immediately and after one day by CE-ICP-MS and the resulting electropherograms are shown in Figure 6. Three major species are present in the freshly made solution at pH <1 and they elute at about 615, 1195, 1385 seconds, respectively, corresponding to $RhCl_2(H_2O)_4^+$, $RhCl_4(H_2O)_2^-$, and $RhCl_5(H_2O)^{2-}$. The first specie $RhCl_2(H_2O)_4^+$, eluded at 615 seconds in the freshly made solution, however, disappeared after one day, and the new specie $RhCl_3(H_2O)_3$ emerged as shown in Figure 3.5. In addition, the relative intensity of the $RhCl_4(H_2O)_2^-$ species increased considerably in the aged solution compared to that in the freshly made solution.

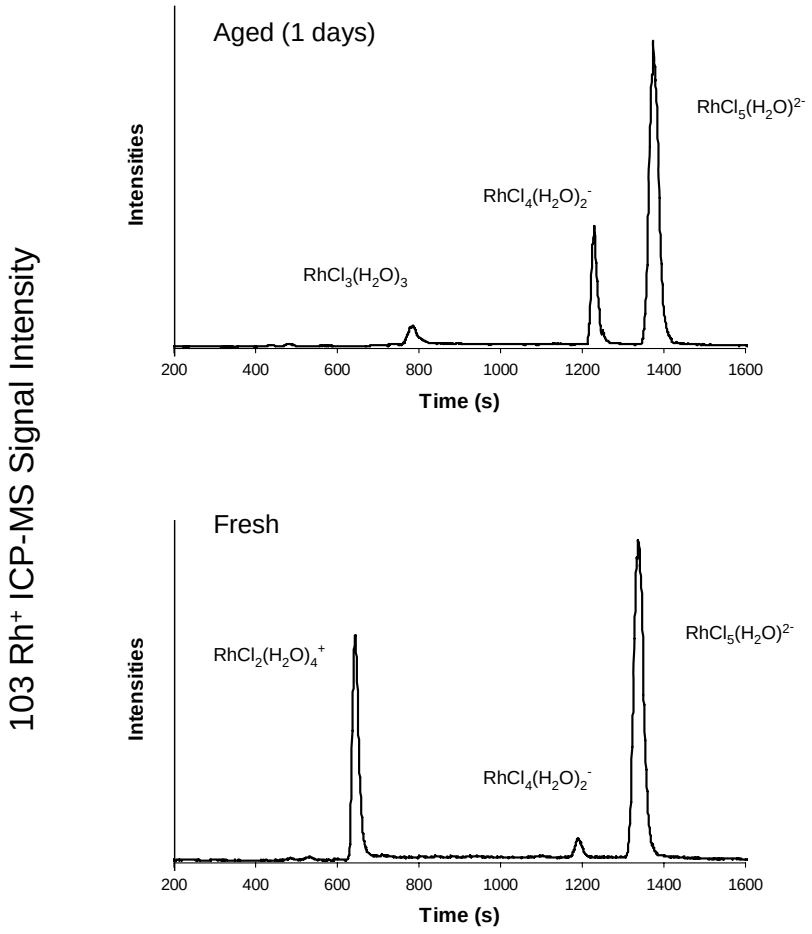

Figure 3.5 CE-ICP-MS electropherogram of 1 ppm $RhCl_3$ solution at pH <1 (a) Fresh (b) aged 1 day. Electrolyte: 20 mM $NaNO_3$, hydrodynamic injection (5mbar, 4s) injection volume: 47 nL, CE voltage: 30 kV, CE current: 10 µA. 0.8 L/min nebulizer gas flow and 20 µL/min sheath flow rate, 0.14 µL/min laminar flow ; All Y-axis scales are the same with minimum =0 and maximum = 2×10^6 count/s.

Another freshly prepared stock solution of $RhCl_3$ was also diluted immediately to 1.0 μL/mL and adjusted to a pH of 2 before it was analyzed after 20 minutes, 3 hours, and ten days by CE-ICP-MS and the resulting electropherograms are shown in Figure 3.6. There are two major Rh species in all three time points which elute after about 595, and 898 seconds corresponding to $RhCl_2(H_2O)_4^+$ and $RhCl_4(H_2O)_2^-$, respectively. Although there are no species changes in all three time points, the distribution of the two Rh species is certainly altered with time. With only about half the intensity of $RhCl_4(H_2O)_2^-$ peak at 20 minute time point, the peak height of $RhCl_2(H_2O)_4^+$ is already slightly larger than $RhCl_4(H_2O)_2^-$ after 3 hours, and turned twice the peak height of $RhCl_4(H_2O)_2^-$ in 10 day as illustrated in Figure 3.6.

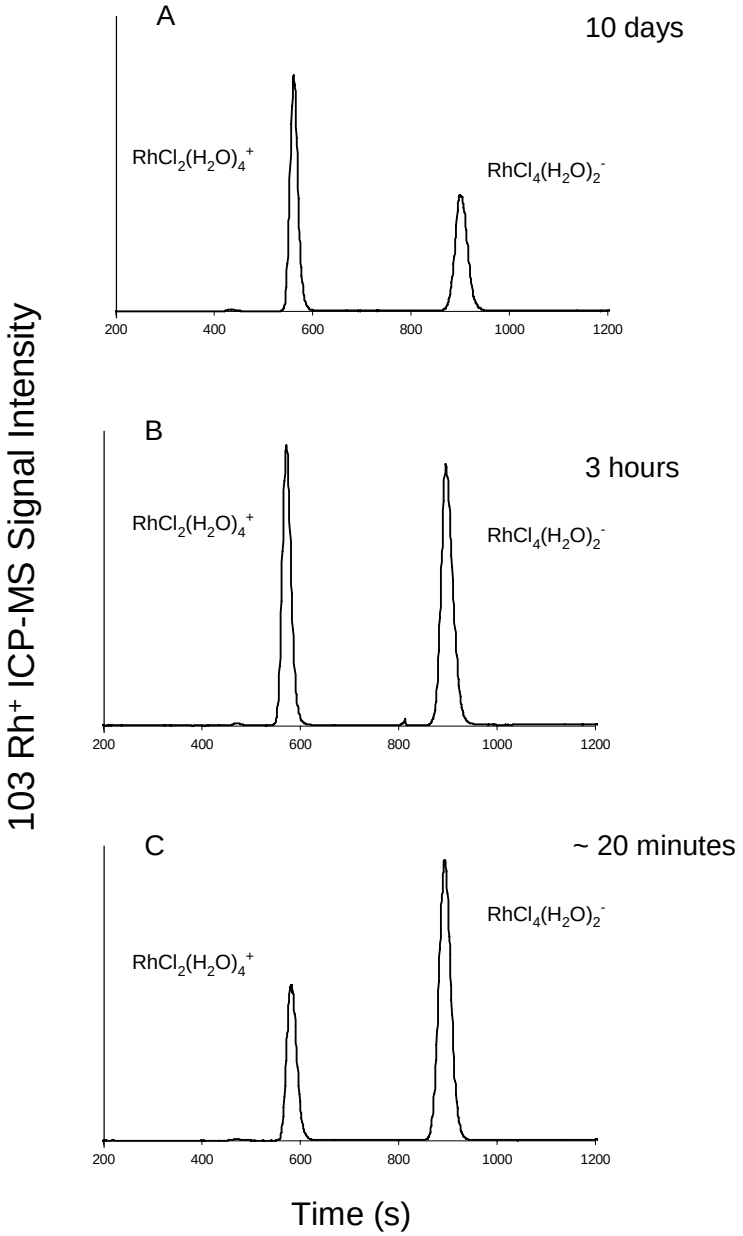

Figure 3.6 CE-ICP-MS electropherogram of 1 ppm $RhCl_3$ solution at pH 2 (a) Fresh (b) aged 3 hours (c) aged 10 days. Electrolyte: 20 mM $NaNO_3$, hydrodynamic injection (5mbar, 4s) injection volume: 47 nL, CE voltage: 30 kV, CE current: 10 μA. 0.8 L/min nebulizer gas flow and 20 μL/min sheath flow rate, 0.14 μL/min laminar flow; All Y-axis scales are the same with minimum =0 and maximum = 2×10^6 count/s.

In order to quantify the changes in these peaks, the peak areas expressed as % fractions of the total Rh peak area for each species in each of the electropherograms and their changes with time are plotted in Figure 3.7. With the aging time increasing, the data clearly showed an inter-exchange of two species. There are about 56% of total Rh present as $RhCl_2(H_2O)_4^+$ and 42 % as $RhCl_4(H_2O)_2^-$ in solution after 3 hours, whereas, after 30 days, the percentage of $RhCl_2(H_2O)_4^+$ increases to 85% and the percentage of $RhCl_4(H_2O)_2^-$ decreases to 15% of total Rh. The gradual displacement of Cl^{-1} by H_2O in the rhodium complex with time is obvious.

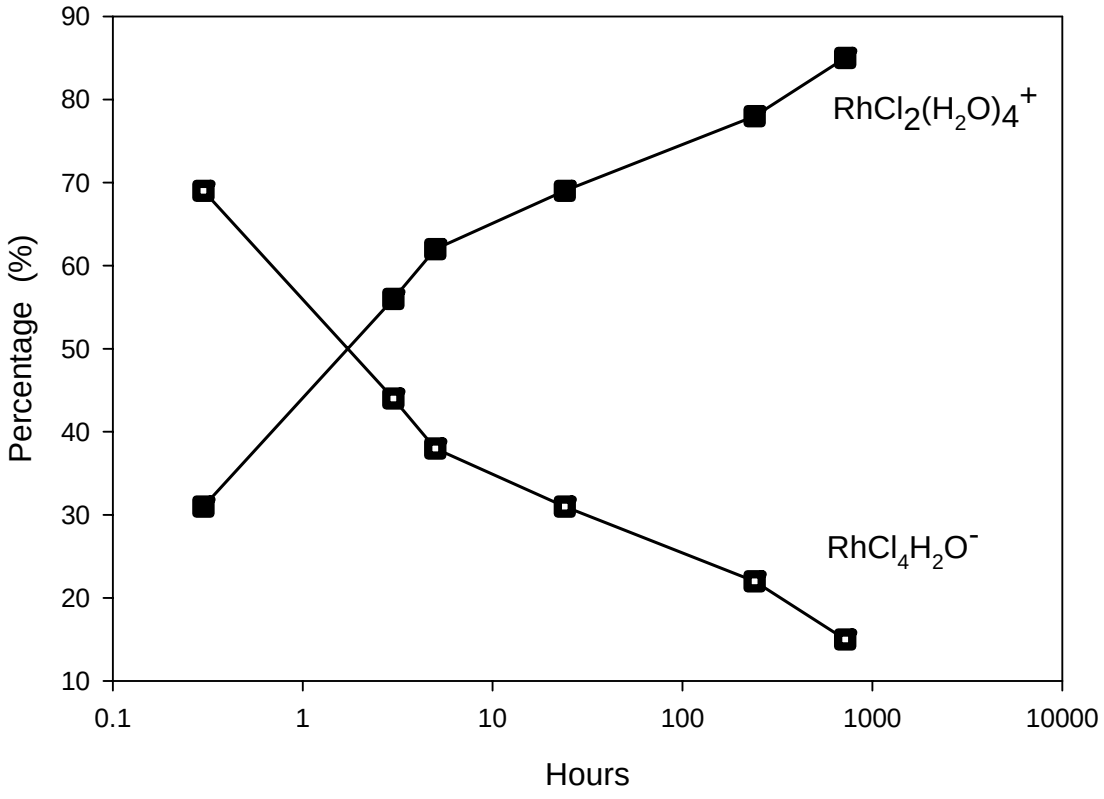

Figure 3.7 A comparison of the peak areas* of the Rh species detected by CE-ICP-MS as function of aging period.

3.4.3. Relative electrophoretic mobility

Using the above method, the relative mobility of Rh(III) species was investigated in more detail. To a freshly prepared multi-element solution (Table 3.4), containing $RhCl_3$ (1.0 µL/mL and 5 µL/mL), HCl was added to provide a final concentration of 1 m*M* and a pH of 2.01. The mixture was separated using a 20 m*M* $NaNO_3$ electrolyte that was pH modified to 2. According the previous study, the that the dominant species present should be $RhCl_2(H_2O)_4^+$ and $RhCl_4(H_2O)_2^-$.

The CE–ICP-MS electropherogram of this mixture is shown in Fig. 3.8a. The figure clearly indicates that the dominant species present is $RhCl_2(H_2O)_4^+$, and $RhCl_4(H_2O)_2^-$ did not show here due to long migration time. Also shown in Fig. 3.8a are a number of "marker" species used to gauge the relative mobility of the Rh(III) species. The equivalent ionic conductance of each ion is listed in Table 2. As a bench mark for this pH and concentration, the $RhCl_2(H_2O)_4^+$ elutes before a typical 2+ solution ion (Co^{2+}).

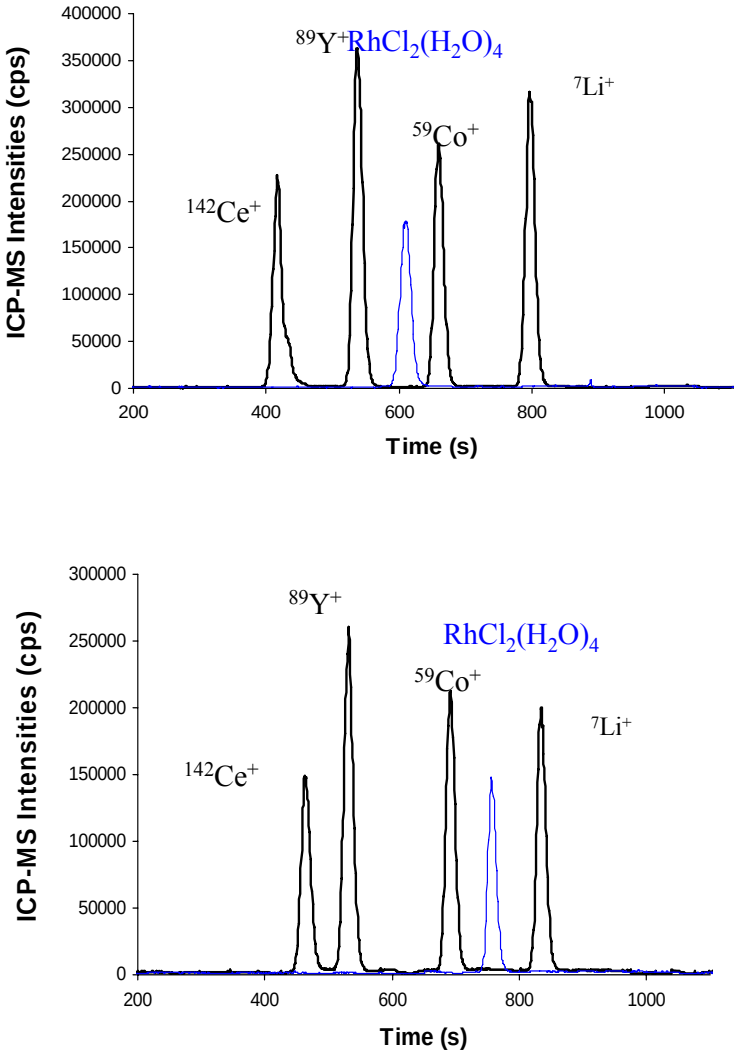

Fig. 3.8. CE–ICP-MS electropherograms of (a) $RhCl_3$ -1.0 µL/mL (b) $RhCl_3$ – 5 µL/mL, both solutions were freshly prepared aged and giving a final pH of 2.0. Each solution contains various electrophoretic mobility markers for reference (Table 2). The separation electrolyte in each case was pH matched ($NaNO_3$, 20 m*M*). The sheath electrolyte was dilute HNO_3 (conductivity matched) generating an induced laminar flow-rate of 0.03 µl/min.

Element	m/z monitored	Equivalent ionic conductance $\lambda_i(1.10^{-4}\ m^2\ S\ mol^{-1})$
Li	7	38.7 (Li^+)
Co	59	55.0 ($1/2Co^{2+}$)
Y	1.1	62.0 ($1/3Y^{3+}$)
Ce	142	69.4 ($1/3Ce^{3+}$)
Cs	133	77.2 (Cs^+)

Table 3.4. A list of the test analytes used and relevant physical parameters

In Fig. 3.8b, a similar multi-element solution mixture was freshly prepared with RhCl3 concentration increased to 5μL/mL. The separation electrolyte was pH matched to that of the sample solution prior to analysis. In this electropherogram, The relative separation between the Ce^{3+}, Y^{3+} and Co^{2+} marker ions, however, changes little as a function of concentration, whereas the mobility of the Rh(III) species changes significantly relative to these markers. At concentration of 5μL/mL, the monomer equilibrium distribution will shift from primarily the Rh^{3+} aquo-ion to more $RhCl_2(H_2O)_4^+$, thus reducing the overall mobility of this fraction resulting in migration times longer than the Co^{2+} ion. Because the overall migration time is based upon the relative contribution of the equilibrium species it can probably be assumed that the $RhCl_2(H_2O)_4^+$ species has a mobility less than that of Co^{2+} (λ_i=55, Table 2).The data in Fig. 3.8 illustrates one important points that the relative migration time of Rh species is

dependent on the equilibrium distribution, which in turn is dictated by concentration and the solution pH.

3.4.5 Speciation of metal ions in different oxidation states

The chemical and physical properties of a metal species depend very much on its oxidation state. Pre-capillary reactions using chelating reagents are normally being needed to carry out such metal speciation.[38-40] However, this kind of approach has the risk of changing the original form of metal ions. In our experiments, a simultaneous determination of iron(II) and iron(III) without employing a complexing ligand using CE-HR-ICP-MS was developed.

Figure 3.9A shows CE-HR-ICP-MS electropherograms for the separation of a mixture of Fe^{2+} and Fe^{3+} ions. The mixture solution was made by mixing 1ppm $FeCl_2$ and 1ppm $FeCl_3$. The pH of the solution was adjusted to 2 with drop wise additions of concentrated HCl to retard the formation of insoluble $Fe(OH)_3$ and to preserve the oxidation of Fe. The equilibrium distribution of iron in solution was also calculated using the Phreeqc 1.03 program distributed by the United States Geological Society. Equilibrium calculations predict that $FeCl_2$ in solution is present as Fe^{2+}, and the $FeCl_3$ in solution is present as Fe^{3+}. By comparing the CE electropherograms of standard solutions of iron(II) and iron(III), the assignment of the first peak to the Fe^{3+} and second peak to the Fe^{2+} can be made.

With the Finnigan Element2, high mass resolution is used to separate interferences from target isotopes by their small difference in mass. This high resolution

technique is particularly useful for this application because of $^{40}Ar^{16}O^{+}$ interferences for ^{56}Fe, which is impossible to separate by a quadrupole ICP-MS.

In the experiments, the interpretation of a change in peak appearance time must be carefully evaluated. At least one non-interacting marker metal ion (Cs^{+}, in this case) should be present in the sample to monitor the electro-osmotic flow rate or other non-specific effects.

Figure 3.9B shows the CE-HR-ICP-MS electropherograms results of the Di-Ca phosphate excipient sample submitted by Pharmaceutical Analysis & Control, which contains a total of ~ 250 ppm Fe. The determination of Fe oxidation state in this sample is important for the evaluation of the stability of API in the final formulation. By comparing the migration time of the Fe peak of figure A with B, the single Fe peak in figure B can be assigned to Fe^{3+} ions. So the Fe species in this excipient sample was determined to be +3 state. In this case, the successful speciation of Fe oxidation state in a real world sample has been demonstrated.

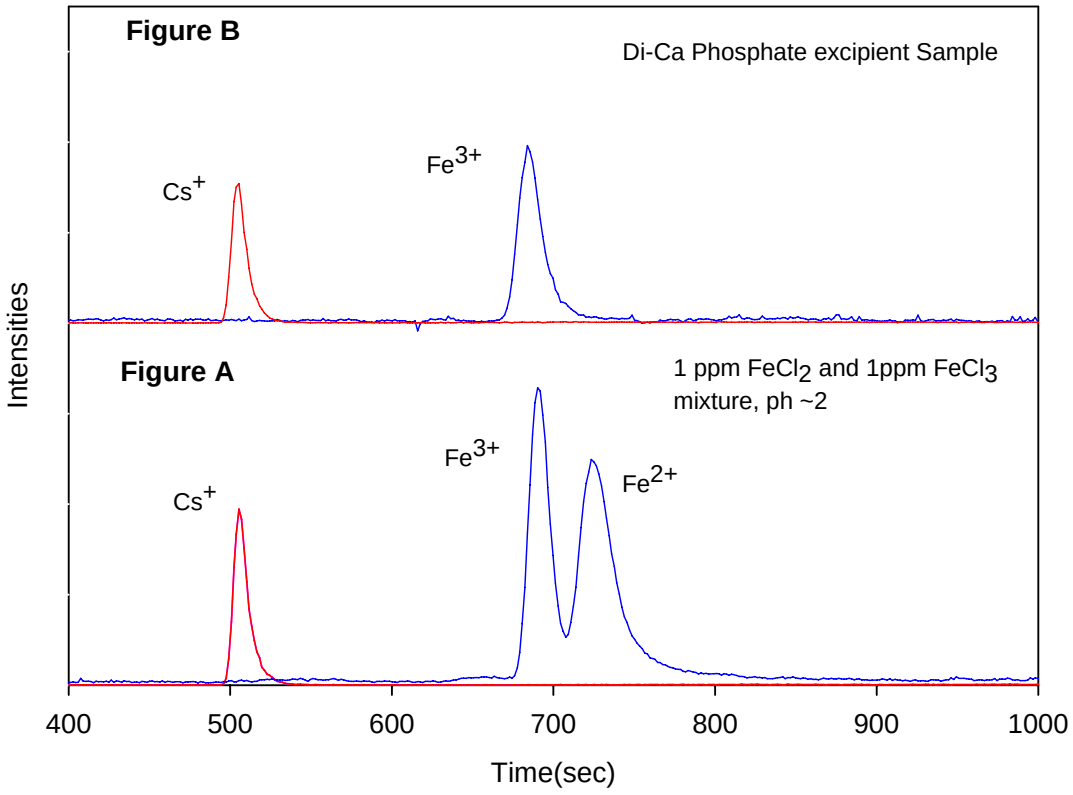

Figure 3.9 (A) CE-ICP-MS electropherogram of 1 ppm FeCl2 and 1 ppm FeCL3 mixture (B) CE-ICP-MS electropherogram of DI-Ca phosphate excipient sample; Using a separation electrolyte contains 20 mM $NaNO_3$ Solution pH: ~6, hydrodynamic injection (60 s), injection volume: 47 nL, CE voltage: 30 kV, CE current: 15 µA. 0.8 L/min nebublizer gas flow and 20 µL/min sheath flow rate, All Y-axis scales are same with minimum = 0 and maximum = 1×10^6 count/s.

3.5. Conclusions

The novel sheath flow interface described in this study coupled with a PFA micro flow nebulizer provides a stable and versatile connection between the capillary electrophoresis system and the high resolution ICP-MS. By combining the powerful separation capabilities of the CE with the element-specific ICP-MS with superior detection limit as detector, rapid elemental speciation can be performed on the time scale of a normal CE separation.

The interface sheath flow rate, induced laminar flow rate and electroosmatic flow and the choice of separation electrolyte can affect CE-ICP-MS resolution and signal sensitivity extensively. With a proper adjustment of the interface sheath flow rate and careful selection of electrolyte, it is possible to separate cations, anions and neutral species in a single injection. Seven to eight major aquo-chloro and hydroxo-chloro species are formed in $RhCl_3$. The formation and distribution of these species, which are both identifiable and quantifiable with the experimental conditions and setups described in this article, are dependent on both the pH and aging period of the solution.

From the work presented above, a number of important conclusions can be drawn on the use of CE–ICP-MS as a tool for polymeric Rh(III) speciation. (1) CE–ICP-MS can be used to separate and detect various Rh(III) species; (2) the species distribution is similar, qualitatively to that predicted in aged and ageing solutions of Rh(III); (3) the various species migrate through the capillary at a rate proportional to their equilibrium distribution in that a single peak may have a migration time that is the concentration weighted average of more than one species (such as Rh^{3+} and $RhCl_2(H_2O)_4^+$) if the kinetics of inter-conversion are rapid enough. Further, the relative Rh(III) speciation as a function of time, pH and concentration are consistent (qualitatively) with that determined in the analogous CE–ICP-MS experiments. A final, significant outcome from this work is the development of methodology capable of separating and detecting hydrolytic polymeric species. In particular, the use of element selective detection, allows the use of simple electrolyte systems which do not contribute to a significant change in speciation, sample loss or MS signal suppression. Recognition of this fact, promotes the further development of even more efficient systems.

REFERENCES

1. Salbu, B.; Steinnes, E., Trace Elements in Natural Water; CRC Press: Boca Raton, FL, 1995.

2. Caroli, S., Element Speciation in Bioinorganic Chemistry; John Weiley & Sons, Inc: New York, 1996.

3. Natusch, D. F. S.; Hopke, P. K., Analytical Aspects of Environmental Chemistry; John Wiley & Sons, Inc: New York, 1983.

4. C.F. Baes and R.E. Mesmer. The Hydrolysis of Cations Wiley, New York (1976).

5. F.Y. Saleh, G.E. Mbamalu, Q.H. Jaradat and C.E. Brungardt. Anal. Chem. **68** (1996), p. 740.

6. Qiang Tu, Tiebang Wang, Christopher J. Welch, Peng Wang, Xiujuan Jia, Conrad Raab, Xiaodong Bu, and Michael P. Doyle, Anal. Chem., 78 (4), 1282 -1289, 2006

7. Christopher J. Welch, Qiang Tu, Tiebang Wang, Conrad Raab, Peng Wang, Xiujuan Jia, Xiaodong Bu, Darren Bykowski, Benjamin Hohenstaufen, Michael P. Doyle, Adv. Synth. Catal. 2006, 348, 821 – 825

8. I. Ojima (Ed.), Catalytic Asymmetric Synthesis,2nd edn., Wiley, New York, 2000;

9. J. M. Hawkins, T. J. N. Watson, Angew. Chem. Int. Ed. 2004, 43, 3224–3228;

10. Y. Hsiao, N. R. Rivera, T. Rosner, S. W. Krska, E. Njolito, F. Wang, Y. Sun, J. D. Armstrong III, E. J. J. Grabowski, R. D. Tillyer, F. Spindler, C. Malan, J. Am. Chem. Soc. 2004, 126, 9918–9919; d) J. G. De Vries,

11. H. M. De Vries, C. E. Tucker, J. A. Miller, Innov. in Pharm. Tech. 2001, 01, 125–126, 128, 130.

12. Svelana, S.; Anatoly, P.; Gumenyuk, S.; Lubov, F.; Andrei, R.; Talanta 61 (2003) 195-202

13. C. J. Welch, J. Albaneze-Walker, W. R. Leonard, M. Biba, J. DaSilva, D. Henderson, B. Laing, D. J. Mathre, S. Spencer, X. Bu, Xiadong, T. Wang, Org.

Proc. Res. Dev. 2005, 9, 198 – 205;

14. Michalke, B.; P, S., Fresenius J. Anal. Chem. **1997,** 357, 594-599.

15. Michalke, B.; Lustig, S.; Schramel, P., Eelectrophoresis **1997,** 18, 196-201.

16. Olesik, J. W.; Kinzer, J. A.; Olesik, S. V., Anal. Chem **1995,** 67, 1-12.

17. Benguerel, E; Demopoulos, G. P.; Harris, G. B., Hydrometallurgy 40 (1996) 135-152

18. Bastien Léger, Audrey Nowicki, Alain Roucoux and Jean-Paul Rolland Journal of Molecular Catalysis A: Chemical, November 2006,

19. Palmer, D. A.; Harris, G. M., Inorganic Chemistry 14, 1975, 1316

20. Robb, W.; Steyn, M. M. Inorganic Chemistry 6, 1967, 617

21. Bernd Sures and Sonja Zimmermann Environmental Pollution, October 2006,

22. L. Spiccia and W. Marty. Polyhedron **10** (1991), p. 619.

23. L. Spiccia. Polyhedron **10** (1991), p. 1865.

24. M.R. Grace and L. Spiccia. Polyhedron **10** (1991), p. 2389.

25. S.J. Crimp, L. Spiccia, H.R. Krouse and T.W. Swaddle. Inorg. Chem. **33** (1994), p. 465.

26. A. Drljaca and L. Spiccia. Polyhedron **12** (1995), p. 1653.

27. A. Drljaca and L. Spiccia. Polyhedron **15** (1996), p. 2875.

28. A. Drljaca and L. Spiccia. Polyhedron **15** (1996), p. 4373.

29. L. Spiccia and M. Marty. Inorg. Chem. **25** (1986),

30. S.H. Collins, S.H. Pezzin, J.F.L. Rivera, P.S. Bonato, C.C. Windmoller, C. Archundia and K.E. Collins. J. Chromatogr. A **789** (1997), p. 469.

31. Jackson, P.; Haddad, P., Trends Anal Chem **1993,** 12, 23.

32. Chen, M.; Casidy, R., J. Chromatorgr. A **1993,** 640, 425.

33. Guevremont, R.; Nerman, S., J. Am. Soc. Mass Spectrom **1992,** 3, 216.

34. Rivello, J. M.; Harrold, M. P., J. Chromatogr. A **1993,** 652, 385.

35. Shi, Y.; Fritz, J. S., J. Chromatogr. **1993,** 640, 473.

36. Romano, J. P.; Krol, J., J. Chromatogr. **1993,** 640, 403.

37. Chen, M.; Cassidy, R. M., J. Chromatogr. **1992,** 602, 227.

38. Jones, W. R., J. Chromatogr. **1993,** 640, 387.

39. Koberda, M.; Konkowski, M.; Youngberg, P.; Jones, W.; Weston, A., J. Chromatogr. **1992,** 602, 235.

40. Sanchez, J.; Salvado, V.; Havel, J., J. Chromatogr. A **1999,** 834, 329-340

41. Sanchez, J.; Salvado, V.; Hidalgo, M.; Havel, J., Talanta **2002,** 56, 1061

42. Alekenko, S. S; Gumenyuk, A. P.; Mushtakova, S. P, Fresenius J. Anal. Chem. 2001**,** 370, 865-871

43. Landers, J. P., Hand Book of Capillary Electrophoresis; CRC Press: New York, 1997.

44. Guzman, N. A., Capillary Electrophoresis Technology; Marcel Dekker, INC: New York, 1993.

45. Righetti, P. G., Capillary Electrophoresis in Analytical Biotechnology; CRC Press: New York, 1996.

46. Buchberger, W.; Semenova, O. P.; Timerabev, A. R., J. High Resoulution Chromatography **1993,** 16, 153.

47. Westen, A.; Brown, P. R.; Jandik, P.; Jones, W. J.; Heckenberg, A. L., J. Chromatogr. **1992,** 593, 289.

48. Timerbaev, A.; Semenova, O.; Bonn, G., Chematographia **1993,** 37, 497.

49. Gross, L.; Yeung, E., Anal. Chem. **1990,** 62, 247.

50. Swaile, D. F.; Sepammiak, M. J., Anal. Chem. **1991,** 66, 1.

51. Lu, W.; Cassidy, R. M., Anal. Chem. **1993,** 65, 1649.

52. Sutton, K.; Sutton, R. M. C.; Caruso, J. A., J. Chromatography A **1997,** 789, 85-126.

53. Stewart, I. I.; Olesik, J. W., J. Chromatography A **2000,** 872, 227.

54. Olesik, J. W.; Kinzer, J. A.; Olesik, S. V., Anal. Chem. **1995,** 34, 1.

55. Kinzer, J. A.; Olesik, J. W.; Olesik, S. V., Anal. Chem. **1996,** 68, 3250-3257.

56. Maria Montes-Bayon, Daniel Pröfrock, Alfredo Sanz-Medel and Andreas Prange Journal of Chromatography A, Volume 1114, Issue 1, 5 May 2006, Pages 138-144

57. G. Álvarez-Llamas, M.R. Fernández de la Campa and A. Sanz-Medel Analytica Chimica Acta, Volume 546, Issue 2, 8 August 2005, Pages 236-243

58. Gloria Álvarez-Llamas, María del Rosario Fernández de laCampa and Alfredo Sanz-Medel TrAC Trends in Analytical Chemistry, Volume 24, Issue 1, January 2005, Pages 28-36

59. R. Nageswara Rao and M.V.N. Kumar Talluri Journal of Pharmaceutical and Biomedical Analysis, Volume 43, Issue 1, 4 January 2007, Pages 1-13

60. Hill, S., Inductively coupled plasma mass spectrometry and its applications; Sheffield Academic: Sheffield, 1999.

61. Montaser, A., Inductively coupled plasma mass spectrometry; Wiley VCH: New York, 1998.

62. M. Pantsar-Kallio and P.K.G. Manninen. J. Chromatogr. A **170** (1996), p. 89

Chapter 4

The Development of Non-Aqueous Capillary Electrophoresis-High Resolution Inductively Coupled Plasma Mass Spectrometry

4.0 Introduction

Previous chapters has demonstrated that CE-ICP-MS has rapidly become an important analytical tool with attractive features such as short analysis time, high separation efficiency, small sample size, low solvent consumption, and selective detection. CE-ICP-MS has been successfully applied to the separation and quantitation of metal ions in chapter 4. The majority of works found in literature has focused on the use of aqueous buffers as background electrolytes[1-5]. One of the problems in applying aqueous CE method on pharmaceutical compound analysis is poor water solubility of certain pharmaceutical drugs and drug precursors. Recently, CE using non-aqueous electrolytes has been reported [6,7] for the separation of a range of cations including ammonium, alkali and other metal ions, which offers potential for being compatible with water-insoluble drug substances.

Even though for many years organic solvents have provided an alternative to aqueous media in conventional electrophoresis and isotachophoresis, and although they have commonly been employed as modifiers in capillary electrophoresis (CE), the potential of applying them in CE as background electrolyte solutions has only recently

begun to attract close attention[8]. The low currents present in non-aqueous capillary electrophoresis not only allow the use of higher electrolyte salt concentrations and higher electric field strengths, but also the sample load can be scaled-up by employing capillaries with wider inside diameter. CE under non-aqueous media holds great promise, especially for easy manipulation of separation selectivity by changing the solvent and for semipreparative applications. In addition, an effective sample introduction to the mass spectrometer, in terms of volatility, surface tension, flow-rate and ionization, can be expected to further extend the use of non-aqueous CE.

Organic solvents also offer the potential for separation mechanisms based on interactions that cannot take place or are too weak to be measured in aqueous media. Furthermore, the solubilities of many promising additives for analyte–additive interactions are substantially greater in some organic solvents than in aqueous solutions[9,10].

Most applications of non-aqueous CE today are using indirect UV detection. In developing an indirect CE method with UV detection, the probe used as the visualizing chromophore should have an electrophoretic mobility that closely matches the mobilities of the analytes. Consequently, if the mobility of the analyte differs from that of the background electrolyte, there will be differences in the conductivity, and hence the electric field strength, across the sample zone. The resultant electrodispersion results in peak fronting if the mobility of the analyte is greater than that of the probe, and tailing if the analyte mobility is less than the probe[11-14]. Thus, electrodispersion can severely degrade peak shape, and consequently lower both the resolution and sensitivity of the

method. One advantage using ICP-MS as the detector of CE is no need of adding chromophore additive to the electrolyte, thus, eliminated above experiment consideration.

The aim of this report is to develop an analytical method specifically for applications in pharmaceutical process research using non-aqueous CE with HR-ICP-MS detection. Two unique aspects of non-aqueous CE compared to aqueous CE, non-aqueous CE with wide-bore capillaries and influence of organic solvent on the CE separation selectivity, will be discussed. Quantitation analysis by using internal standard was also demonstrated. To our knowledge, this is the first application employing the resolving power of non-aqueous CE-ICP-MS in this field.

4.1 Physical chemical properties of solvents used for non-aqueous capillary electrophoresis

The physical chemical properties of the organic solvents (Table 4.1) have a major impact on the choice of solvent or solvent mixture for a given electrophoretic separation. Some of the more practical considerations are the chemical resistance of parts in the CE towards the solvent, the volatility of the solvent, the solvating power of the solvent towards electrolytes, the UV transparency and the viscosity of the solvent. The more polar solvents like MeOH, DMSO, FA, NMF and DMF possess a good solvation power towards the electrolytes commonly used in non-aqueous CE.

Non-aqueous CE exploits the vastly different physicochemical properties of organic solvents to control electroosmotic flow (EOF) and analyte migration. The ability of organic solvents to accept protons from the silanol groups of the capillary wall appears to play a crucial role in the development of EOF. Although EOF may not be required or even may be completely undesired in a few electromigration capillary techniques, it plays

a significant role in separations in free solution CE.

Organic solvents differ widely in their autoprotolytic behaviour and the right choice of solvent may yield separations that are not possible in aqueous systems. Because viscosity has an inverse effect on electroosmotic and electrophoretic mobilities, it should be low, to allow the separations in a reasonable time frame. Stable solvents with low vapor pressures and present as liquids at room temperature are the most convenient for practical purposes. Toxic solvents should be avoided. Unlike water, organic solvents may exhibit strong absorbance of ultraviolet light, so that indirect ultraviolet (UV) or other alternative detection methods are required. These may, in fact, provide better sensitivity than is achievable in water; for example, the sensitivity in fluorescence detection can be enhanced[13], and the low heat of vaporisation and low surface tension of organic solvents can be exploited in coupling of CE with electrospray ionization mass spectrometry.

The viscosity of the electrophoresis medium affects the time needed to flush the capillary as well as the time to inject a certain volume into the capillary. Generally, a flushing time corresponding to four to five capillary volumes are recommended in order to ensure complete renewal of the electrophoresis medium in the capillary. Separations performed in a medium with a high viscosity such as FA may be time consuming especially if the capillary inner diameter is low. The viscosity also have an impact on the diffusion coefficient of the species in the electrophoresis buffer and thereby also an influence of the separation efficiency. For separation of tetracyclines, amides and DMSO have been used to decrease EOF by increasing the viscosity[15].

Solvent	t_{boil} (^oC)	η (mPa s)	ε	pK_{auto}	γ (10^2 N m^{-1})
Methanol (MeOH)	**64.7**	**0.545**	**32.70**	**17.20**	**2.212**
Ethanol (EtOH)	78.3	1.078	24.55	18.88	2.190
1-Propanol (1-PrOH)	97.2	1.956	20.33	19.43	2.330
2-Propanol (2-PrOH)	82.3	2.073	19.92	20.80	2.124
1-Butanol (1-BuOH)	117.7	2.593	17.51	21.56	2.416
Acetonitrile (ACN)	**81.6**	**0.341**	**b37.5**	**$33.3**	**2.760**
Propylene carbonate (PC)	242	2.513	66.1	–	4.14
Formamide (FA)	210.5	3.30	111.0	b16.8	5.791
N-Methylformamide (NMF)	180	1.65	182.4	10.74	3.87
N,*N*- Dimethylformamide (DMF)	153.0	0.802	36.71	29.4	3.52
Dimethyl sulphoxide (DMSO)	189.0	1.996	46.68	33.3	4.286
Tetrahydrofuran (THF)	66.0	0.460	7.58	–	2.64
Water	**100.0**	**0.890**	**78.39**	**14.00**	**7.181**

t_{boil}, boiling point; η, coefficient of viscosity; ε, dielectric constant (relative permittivity); pK_{auto}, autoprotolysis constant; and γ, coefficient of surface tension.

Table 4.1 Properties of selected organic solvents at 25 ^oC

4.2 Analysis of organic solvents by ICP-MS

Direct analysis of organic solvents by Inductively Coupled Plasma–Mass Spectrometry (ICP-MS) can be problematic[16,17]. The viscosity and volatility of organic solvents have a significant effect on the efficiency of sample introduction and ICP stability. A higher viscosity solvent causes inefficient nebulization, which requires

dilution with water, if it is water miscible or with some other organic solvent. On the other hand, volatile organic solvents have a higher vapor pressure and most probably would result in the plasma being extinguished. A cooled spray chamber might help to reduce the vapor pressure, and also to use an optimized sample introduction system, with smaller sample uptake rate, smaller injector ID. The other issue with run organic solvent directly to the plasma, carbon will be deposited on the tip of the interface cones resulting Decreased sensitivity and clogged interface. This can be avoided by adding a small amount of oxygen into the injector gas flow between the spray chamber and the torch. The amount of oxygen is very critical, because an insufficient amount can cause deposition of carbon at the cones, while too much can cause erosion and result in shorter cone lifetime.

One approach is to produce a desolvated aerosol for sample introduction, as long as the element species are not removed with the solvent. The use of desolvation apparatus such as a Nafion membrane drier with a cryogenic condenser[18] and ultrasonic nebulizer with built-in desolvation system[19] has been reported. However, these can lead to very complex and not robust, and flexible interface for non-aqueous CE-ICP-MS applications.

In order to minimize the amount organic solvent into ICP system, the sheath flow CE-HR-ICP-MS interface coupled to a PFA Teflon micro-flow concentric nebulizer was applied in this study. Since the sheath flow rate is much higher than the electroomotic flow rate and the sheath flow solution constitutes majority of the solution that reaches the plasma, the sheath flow interface can also function as an on-line diluter to dilute the non-aqueous CE elute to aqueous system before it reaches the plasma. The sheath flow solution used in this case is much diluted HNO_3 acid. Because mixing occurs after CE

separation and the ICP-MS is an element selective instrument, the CE electropherogram will remain the same even metal specie changed after CE elution.

Another problem of intruding organic solvent into ICP-MS is polyatomic interferences. The addition of oxygen to the carbon rich plasma may cause the formation of polyatomic interferences from Ar, C and O. A partial listing of possible polyatomic interferences is given in Table 2.

Potential Interfering Species	m/z	Affected Element
12C2	24	Mg
12C13C	25	Mg
40Ar16O	56	Fe
12C16O	28	Si
12C16O2	44	Ca
40Ar12C	52	Cr
40Ar12C16O	68	Zn
46Ti16O	63	Cu
143Nd16O	159	Tb

Table 4.1 Potential interferences in a carbon and oxygen rich plasma

The high resolution capability of the HR-ICP-MS allows most of these elements to be distinguished from the interfering masses. Figure 4.1 shows the HR-ICP-MS mass spectra of Zn in pure IPA. Results demonstrated that under the high resolution mode,

interested Zn^{64} ion was completely separated from organic molecular ions interferences. This result clearly show that in order to perform an accurate and low detection metal speciation in organic solvent, high resolution ICP-MS is desired and quadrupole based ICP-MS system is not suitable.

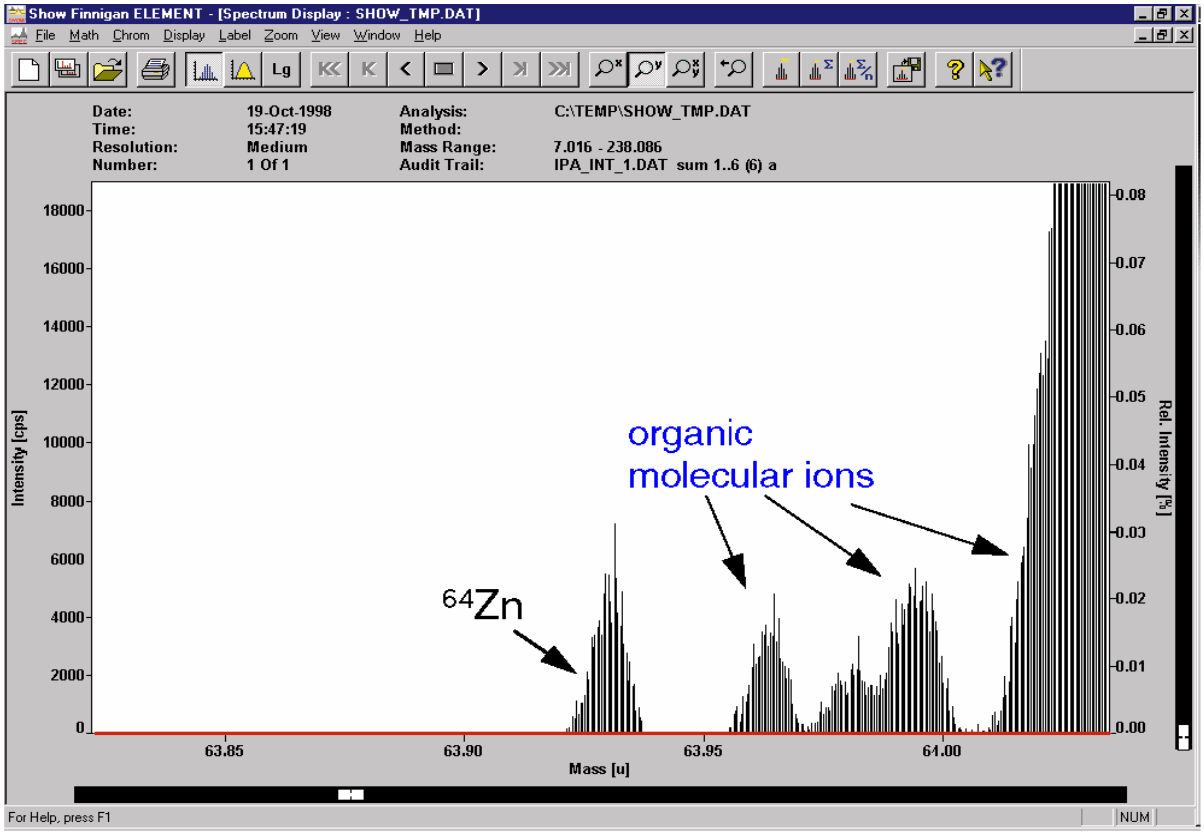

Figure 4.1 The high resolution ICP-MS mass spectra of Zn in 100% IPA

4.3 Experimental

Chemical reagents and preparation

All chemicals were of analytical grade unless otherwise stated. HPLC-grade very organic solvents were from Sigma products (St. Louis, MO, USA). Standard stock solutions (100 mM) for each metal ion were prepared by dissolving the appropriate amount of analytical grade solid reagents in ultra pure water (18MΩ cm^{-1}), which was made in-house with a Milli-Q water purification system (Millipore, Milford, MA, USA). Analytes include, CsCl (Fisher), RbCl (Fisher). $FeCl_2$ (Fisher), $FeCl_3$(Fisher), $RhCl_3$ (Sigma). Dilute solutions for analysis were prepared daily.

The sheath flow solution used was dilute nitric acid in which the conductivity matched the separation electrolyte (e. g. 2200 μS). The separation electrolyte solution contained 20 mM $NaNO_3$ (Fisher). If necessary, the solution pH was adjusted through addition of small aliquots of 2 % (v/v) HNO_3 or 10 % (v/v) NaOH solution. A Fisher Scientific Ω 31 pH meter calibrated using pH 4, 7 and 10 buffer standard solutions was used for pH measurements and a Fisher Scientific Accumet Portable AP63 pH/mV/Ion meter calibrated with 1403 μS KCl standard was used for all conductivity measurements.

Inductively Coupled Plasma Mass Spectrometry

All the measurements were carried out with a Finnigan Element 2 (Finnigan, Bremen, Germany) high resolution inductively coupled plasma sector-field mass spectrometer. Details please see previous chapters.

Capillary electrophoresis

CE measurements were carried out using Agilent HPCE system (Palo Alto, CA, USA). The reversed polarity mode of the CE system (cathodic injection and anodic detection) was applied. All experiments were conducted at 25^C (capillary cassette).

Fused-silica capillaries with different internal diameters were used: 50 μm I.D.×375 μm O.D, 100 μm I.D.×375 μm O.D., 150 μm I.D.×375 μm O.D. and 200 μm I.D.×350 μm O.D. from Agilent (Palo Alto, CA, USA). The effective capillary length was 65 cm. The background electrolyte was Methanol–acetonitrile–formic acid (50:49:1, v/v). For comparison, an aqueous background electrolyte of water containing 20 m*M* $NaNO_3$ was used as well. The injection conditions as well as the applied voltage were changed in accordance with the capillary I.D. and are described in the text. The capillary temperature was kept constant at 25°C. The levels of the electrolyte in the inlet and outlet vials were kept the same except when siphoning was studied.

Prior to use capillary was preconditioned for 10 min with 0.1 N NaOH at 25^{C}, 10 min with water and finally the capillary was rinsed for 10 min with background electrolyte. Before each run the capillary was flushed with 0.2 mM HCl for 2 min, followed by washing with water for 2 min and the background electrolyte (BGE) solution for 3 min. Applying this procedure the values of migration time were reproducible.

CE-ICP-MS interface

In this work, a novel sheath flow interface and a PFA micro-flow concentric nebulizer are used for CE-ICP-MS experiments. The interface also serve as an on-line diluter to convert organic solvent to inorganic solution to minimize the organic effect on ICP plasma. The design and characteristics of this interface is described in chapter 2. A schematic of the CE-ICP-MS sheath flow interface used for all measurements is shown in Figure 2.1.

The stability of the CE-ICP-MS set up can be monitored by checking the electrical current, the electroosmatic flow (EOF) and the nebulization during the CE separation. Experiments show that at 30 KV, a stable electrical current can be achieved, which indicates that the interface used in this study provides a stable and continuous electrical contact. This is necessary for reproducible CE separation. With the ICP-MS system, it is also possible to observe the stable EOF by adding 100 ppb Rb to the CE electrolyte and monitoring Rb^{85} signal. The nebulization can be monitored by adding 10 ppb Y^{89} into make up flow solution, which is independent of the electrophoresis. Three-repeated injections of the same sample were performed to assess the precision of the method. Better than 1% RSD of migration time can be obtained for sample ions.

For the data acquisition and evaluation, the transient signals are acquired by the Element 2 software (Finnigan, MAT) and exported as ASCII files. The values were exported to EXCEL program for further calculations.

4.4 Non-aqueous wide bore capillary electrophoresis

The dimensions of the capillary in capillary electrophoresis (CE) have a considerable influence on the separation. While the capillary length typically varies widely, between 25 and 100 cm, most of the CE applications use capillaries with 50 μm internal diameter (I.D.). This internal diameter is a compromise between the need for acceptable sensitivity, resolution, and low electric currents. For many practical purposes this compromise works well, but sometimes the I.D. of the capillary has to be determined by other requirements and narrower or wider capillaries are used.

With aqueous electrolyte solutions, very small internal diameter (I.D.) capillaries have to be used to ensure effective dissipation of Joule heat. Less heat is produced in non-aqueous CE because of the low electrical conductivities of the non-aqueous electrolyte solutions. Organic electrolyte solutions have somewhat lower thermal conductivities than water, which slightly increases the resistance to heat transfer but has only a minor effect on the performance. Low heat production leads to enhanced separation efficiency owing to lowered longitudinal diffusion and more uniform temperature distribution inside the capillary. With non-aqueous CE the capillary diameter can be increased without excessive rise in the electrolyte solution temperature. The heating power can be further be reduced by appropriate choice of CE solvent, for example, by using longer chain alcohols.

The maximum sample load in conventional CE usually is limited by the length of the sample plug. However, since the sample load ability increases with the cross-sectional area of the capillary, even semi-preparative fractionations can be performed with a wide bore capillary. Special arrangements (such as restrictors) may be needed to minimize siphoning during the vial change in semi-preparative work. Owing to the larger sample load, wide bore capillaries also serve to increase the overall detection sensitivity. The sensitivity of ICP-MS detection is enhanced by the amount of sample transferred to detector.

One of the drawbacks of CE as compared to high-performance liquid chromatography is that, because of the limited capillary diameter, it is not suitable for preparative purposes. The ratio of injected volume to effective volume determines the limiting efficiency of the separation. Because of the limited possibility of increasing the

capillary volume, the sample load in CE is usually very low. With pressure injection the injected volume (V_{inj}) can be calculated as:

$$V_{inj} = \frac{ptr^3\pi}{8L\eta} \qquad (2)$$

where p is the injection pressure, t is the injection time and η is the dynamic viscosity of the background electrolyte[20].

One step towards wide bore CE may be to use low conductivity background electrolytes, which allow increase in the capillary diameter without excessive generation of electric current. Since the electric current is usually weaker in non-aqueous media than in conventional aqueous buffers[22], we studied the utility of organic solvents for separations in wide bore capillaries. In this section, we investigated the usefulness of a non-aqueous background electrolyte in capillaries from 50 μm to 200 μm I.D. Our results and theoretical calculations clearly show that organic solvents may better suit for semi-preparative purposes in CE than water does.

The electric current (I) determines the maximum capillary I.D. and maximum electric field strength (E) that can be used with a certain buffer in particular CE equipment. The electric current in a circular cross-section capillary is determined by the applied voltage (U), the specific conductance of the electrolyte (κ), and the capillary dimensions; the capillary radius (r) and the capillary length (L), as follows:

$$I = r^2\pi \cdot \frac{U\kappa}{L} = AE\kappa \qquad (1)$$

where A is the cross-section area. Since the current is proportional to r^2, the capillary radius has a decisive effect on the Joule heat production. The Joule heat production results in a radial gradient of temperature, viscosity and, as a result, velocity in the capillary, which can deteriorate the efficiency of the separation. Controlling the temperature of the entire capillary is difficult and, in addition to the radial temperature gradients, several zones at different temperatures may develop along the capillary. CE equipment usually has an upper electric current and/or power limit at which the run is automatically terminated, or the voltage is kept below the preset value so that the upper current or power limit cannot be exceeded. For the above reasons, the capillary diameter cannot be increased as much as desired.

The electric current was measured as a function of the applied voltage in a non-aqueous buffer of methanol-acetonitrile mixture 50:50 (v/v) with 0.5 v% formic acid and in a corresponding aqueous buffer of 20 mM $NaNO_3$. The voltage was raised from zero to 30 kV in 5 min. The Ohm plots are shown in Figure 4.2.

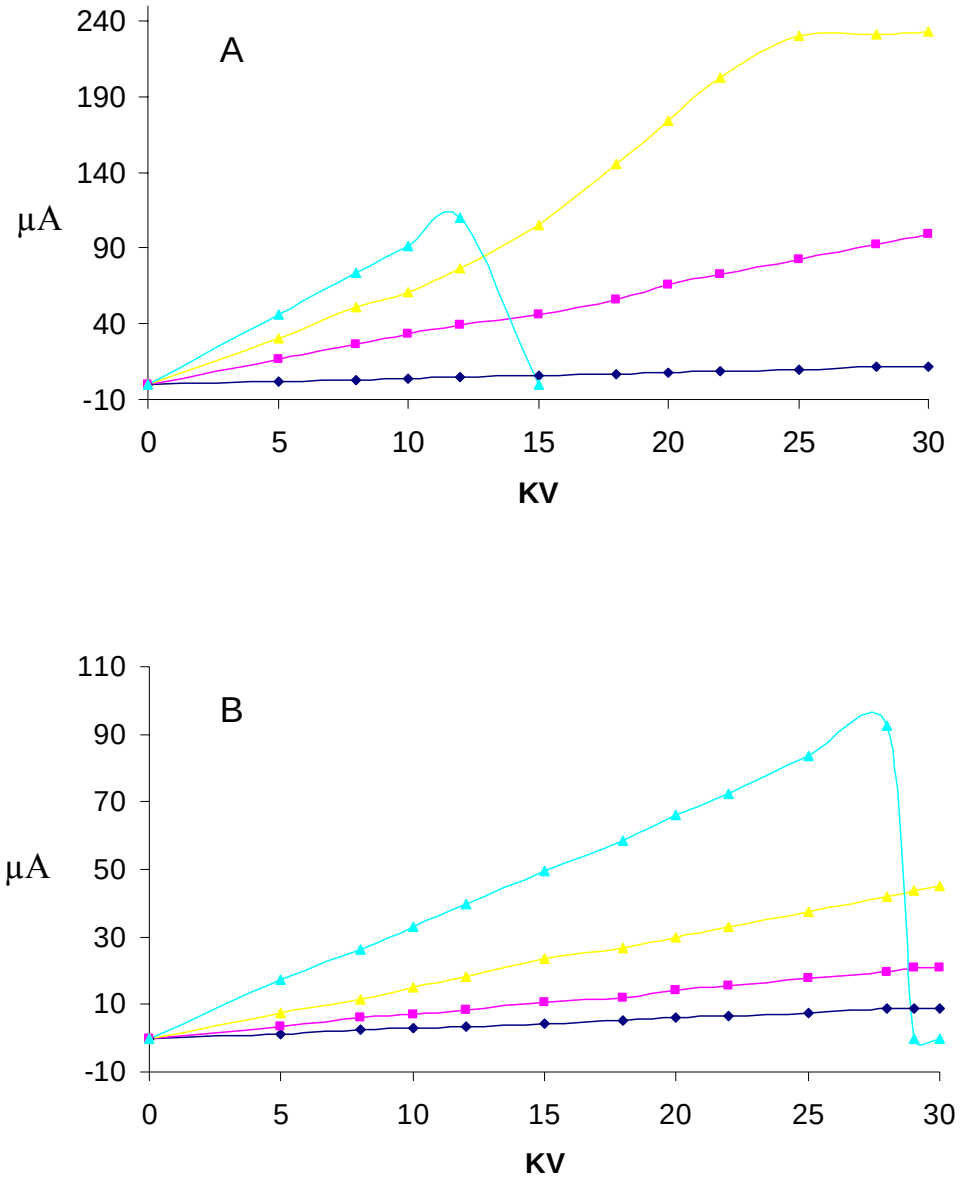

Figure 4.2 Ohm plots in 58.5 cm long fused-silica capillaries. The capillaries were filled with (A) 20 mM $NaNO_3$ and (B) methanol-acetonitrile mixture 50:50 (v/v) with 0.5 v% formic acid. The voltage was increased linearly from 0 to 30 kV and the capillary was thermostatted at 20°C.

With the aqueous buffer (Fig. 4.2A) the currents were high and the Ohm plots seriously deviated from linearity as the I.D. increased. In the 150 μm I.D. capillary the voltage could not be increased to more than about 25 kV because the built-in upper power limit of the CE equipment (6 W) was reached at 240 μA. Increasing the I.D. of the capillary to 200 μm resulted in even higher currents. At about 12 kV the current broke down, most probably because the solvent started to boil and the bubbles disrupted the current.

With the non-aqueous buffer (Fig. 4.2B) the current was a linear function of the voltage at all capillary diameters. The currents were only one-fourth to one-third as high as in the aqueous buffer. In the 200 μm I.D. capillary the voltage could be increased to about 28 kV, at which point the current was just 100 μA. No further increase was possible because the current broke down, probably as a result of bubble formation in the buffer due to boiling.

The results show that non-aqueous buffers allow the use of wider capillaries and higher voltages. While the electric current is generally lower in organic solvents than in water, the boiling point of many of the organic solvents used in CE is below 100°C. The boiling points of ethanol and acetonitrile, the organic solvents used in this study, are 78 and 82°C, respectively. Apparently, the advantages of lower currents compensate for the disadvantages arising from the lower boiling point of the non-aqueous buffer.

Recently, Wright et al. [23]showed that electroosmotic flow develops in many solvents even without the addition of ionic species. Although CE in pure solvents may be impractical because of the lack of buffering, use of organic solvents with low ionic strength would reduce the electric current below the level of conventional CE buffers.

The low specific conductance of non-aqueous buffers may reduce buffer depletion due to coulombic titration, which occurs in CE as a result of the ion transport between the inlet and the outlet vials and can be very serious in wide-bore capillaries.

To assess the potential of organic solvents for metal speciation purposes in CE, we investigated the effect of increased capillary diameter on the separation of four metal ions. Fig. 4.3 shows electropherograms run under identical experimental conditions where capillaries were of different I.D. To keep the ratio of injected volume to total volume (V_{tot}) constant (0.3%) we varied the injection conditions, as shown in the legend. When the capillary diameter is increased four-fold (from 50 to 200 μm) with V_{inj}/V_{tot} kept constant, the injected mass then increased 16-fold. The efficiency of the separation was slightly lower when the 200 μm I.D. capillary was used, but the loss was well compensated by the increased sample load. The selectivity of the separation is changing when wider capillaries are used as one can clearly notice in panel C. The reason for this may be that the temperature has a strong effect on the apparent pH of the background electrolyte, which in turn, may selectively influence the ionization and therefore the electrophoretic mobility of the analytes. The results also clearly demonstrate that ICP-MS signal intensities are greatly improved by using wider bore capillary.

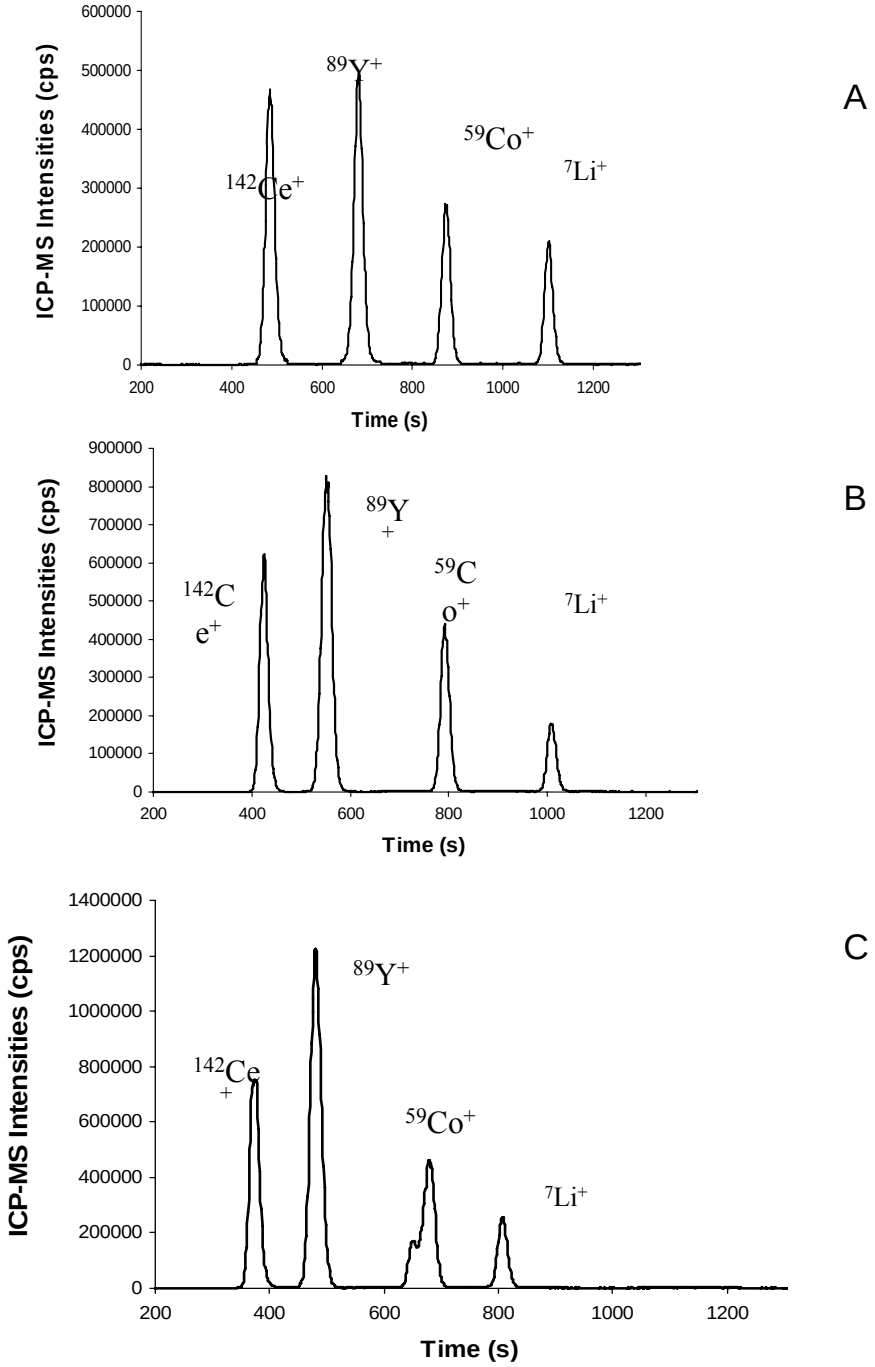

Figure 4.3 Effect of the internal capillary diameter on the separation of 1 ppm each of Ce^+, Y^+, Co^+ and Li^+ Effective capillary length 75 cm, internal diameter: 50 µm (A), 100 µm (B) and 200 µm (C). Applied voltage 25 kV, detection, capillary temperature 20°C. The ratio of injected volume to total volume was kept constant at 0.3%. Injection: 41 mbar for 3 s (A), 15 mbar for 2 s (B) and 4 mbar for 2 s (C).

If the buffer level at the inlet and outlet ends of the capillary is different, a hydrodynamic flow is generated[24]. Since this flow is pressure driven, it has a parabolic profile, which decreases the efficiency of the separation. Wide bore capillaries provide much less friction to suppress Poiseuille flow induced by hydrostatic pressure (i.e. siphoning flow) than do conventional 50-mm capillaries. Usually siphoning can be avoided by exact levelling of the CE electrolyte vials, but with wide bore capillaries the volume of solution carried by electroosmosis from inlet vial to outlet vial during the run is great enough to change the liquid levels in the vials and establish siphoning flow. Valko et al.[25] have shown how, with 200-mm capillaries, siphoning can ruin the separation with a difference in level of just 2 or 3 mm. They filled buffer vials so that initial liquid levels differed by a few millimeters. With just a 3-mm difference in initial level the peaks were about five times as broad and the migration time of the last migrating peak was almost double that in a run with balanced solution levels. Their results also showed that forward directed flow may have a less detrimental effect on the separation efficiency than backward flow, probably because the migration accelerates with increasing forward driving flow.

The siphoning flow velocity at distance x from the centre axis of the capillary (v_x) can be calculated as

$$v_x = \frac{pr^2}{8L\eta} \cdot (1 - 2r_x^2) \qquad (3)$$

where p is the pressure, r is the internal capillary radius, and r_x is the normalized radius variable (x/r) at distance x from the central axis of the capillary [18]. Across the cross-section of the capillary, r_x averages zero, and so the overall linear velocity of the siphoning flow ( ) can be calculated by neglecting the term in parenthesis in Eq. 3.

Since the linear flow velocity is proportional to the square of the capillary diameter, the effect of siphoning can be very significant when wide bore capillaries are used. When the inlet level is higher than the outlet (Figure 4.4) the hydrodynamic and electroosmotic flows are in the same direction, which results in faster migration and overlapping peaks.

When the inlet level was kept lower than the outlet buffer level, the electropherograms recorded in a 200 μm I.D. capillary became highly distorted. The apparent electroosmotic velocity, which can be calculated from the migration time of the negative peak produced by the sample solvent, is the sum of the flows generated by electroosmosis and by siphoning. In this case the electroosmotic and hydrodynamic flows are in opposite directions, which reduces the efficiency dramatically. Furthermore, the electroosmotic flow carries electrolyte from the inlet to the outlet vial, which further raises the outlet level. In our experiments the apparent electroosmotic flow velocity was 1.49 μl/min, and if we assume a constant flow-rate, then in a 20 min run about 30 μl buffer is transported from the inlet to the outlet vial resulting in a 60 μl difference.

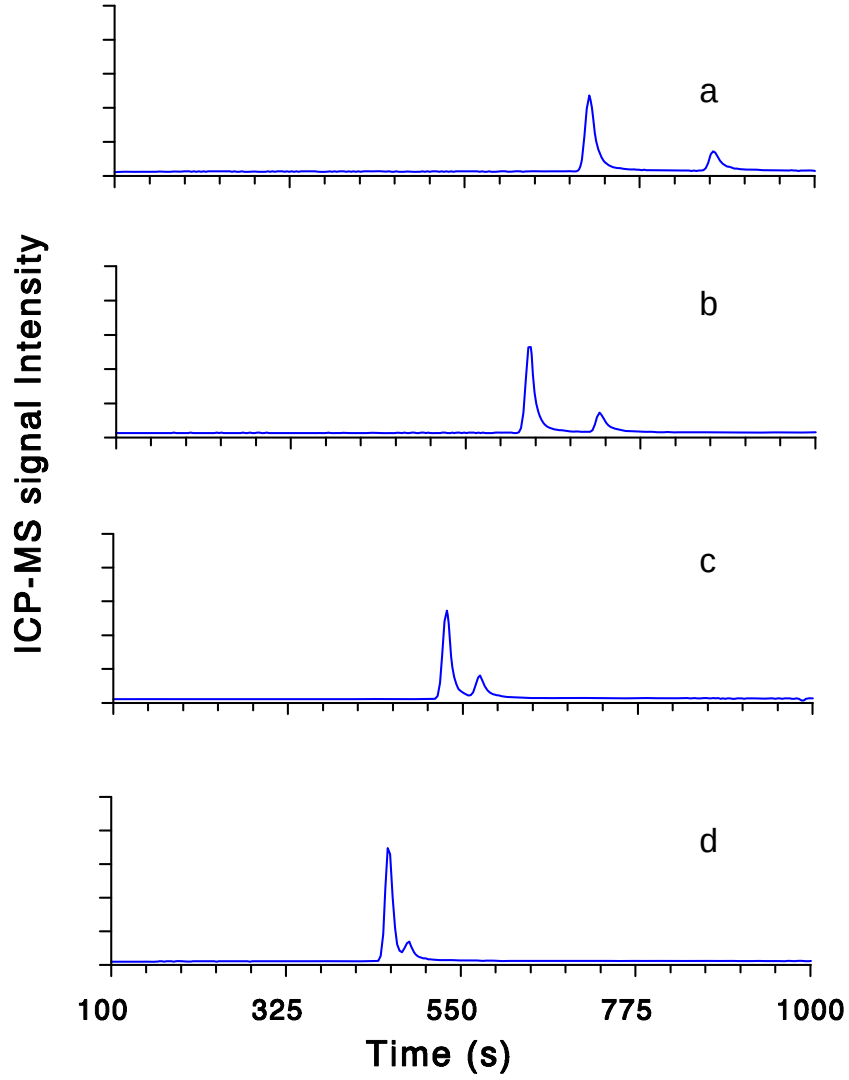

Figure 4.4 Siphoning effect on the separation of 1 ppm Ce and Li. Capillary: fused-silica, 33.5 cm total length, 200 μm I.D. Background electrolyte: ethanol–acetonitrile–formic acid (50:49:1, v/v). Inlet buffer level 0 mm (A), 2 mm (B), 4 mm (C) and 6 mm (D) higher than outlet buffer level. Applied voltage 15 kV, injection 3 mbar for 5 s, capillary temperature 20°C.

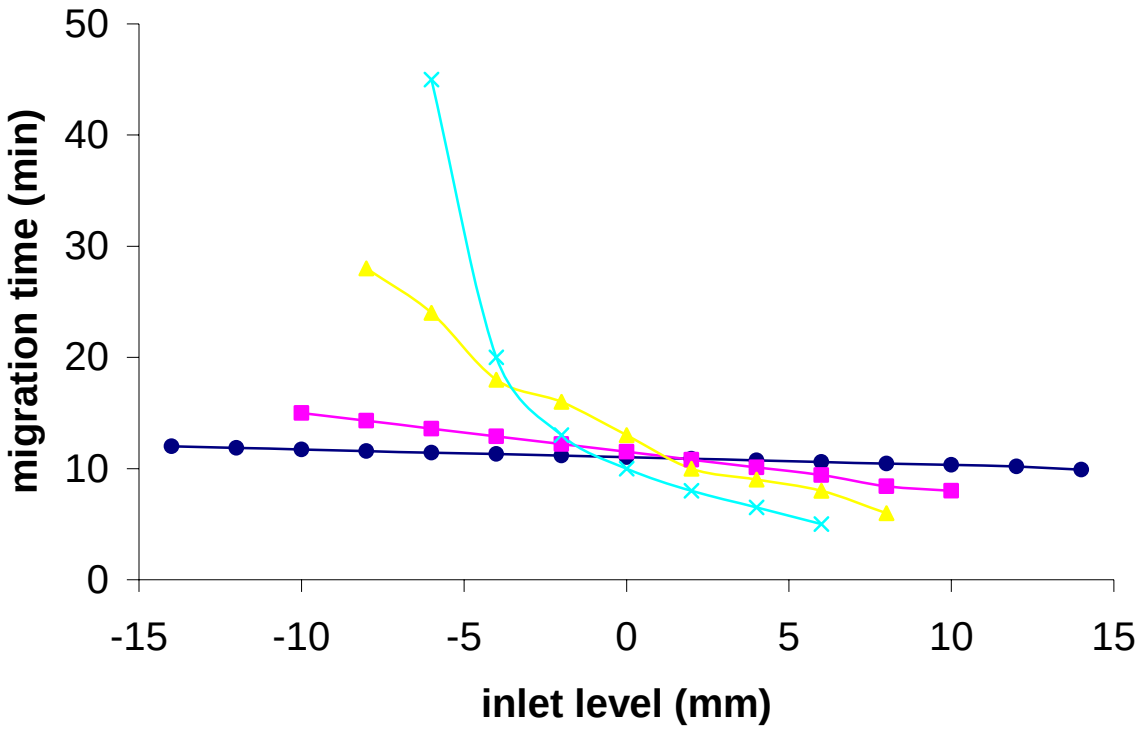

Figure 4.5 Effect of siphoning on the migration time of Cs+. Background electrolyte: Methanol–acetonitrile–formic acid (50:49:1, v/v) Capillary length 33.5 cm, internal diameter: (•) 50 µm; (□) 100 µm; (▲) 150 µm; (×) 200 µm.

The effects of siphoning on the Cs+ ion in capillaries of different internal diameter are depicted in Fig. 4.5. In a 50 µm I.D. capillary, the siphoning effect is very weak: it is hardly noticeable if neither the inlet nor the outlet buffer level is lower than 5 mm below the other. At 100 µm I.D. the siphoning effect becomes noticeable and is always more pronounced if the inlet level is lower than the outlet. +4 mm buffer level at the outlet end of a 200 µm I.D. capillary resulted in a four-fold increase in the migration time of ethacrynic acid. The efficiency of the Cs^+ peak is plotted as a function of the

difference in the buffer levels in Figure 4.6. In general, the efficiency decreases with the increasing capillary diameter. Siphoning has a more pronounced effect on the efficiency than on the migration time. The wider the capillary the more sensitive is the efficiency to the difference between the inlet and outlet levels.

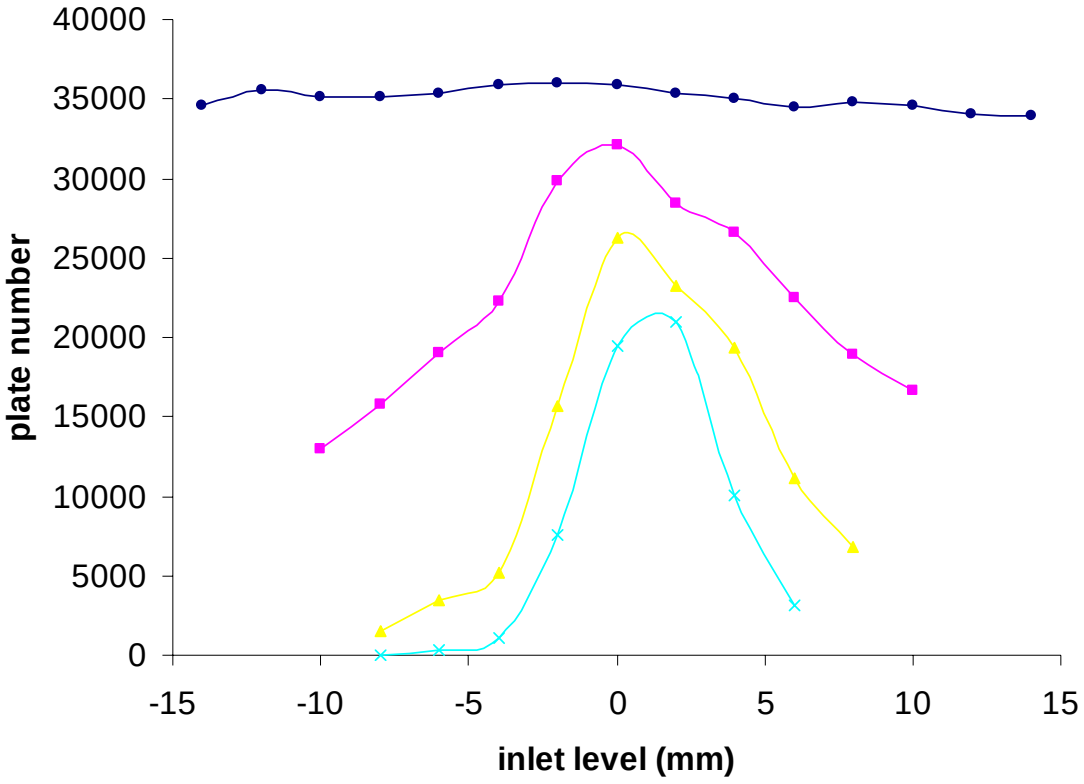

Figure 4.6 Effect of siphoning on the plate number of the Cs+. Background electrolyte: Methanol–acetonitrile–formic acid (50:49:1, v/v). Capillary length 33.5 cm, internal diameter: (•) 50 µm; (□) 100 µm; (▲) 150 µm; (×) 200 µm.

During method development one should consider both the need for selective separation and minimization of siphoning. The relative importance of these requirements depends on the particular solvents, capillary diameter and analytes to be separated. Siphoning can be reduced in various ways, such as buffer replenishment and the use of restrictors and wide buffer vials. In even wider capillaries, suppression of the electroosmosis may be necessary because the electroosmotic flow may transport so much buffer in a single run that efficient separation becomes impossible even if the buffer levels are the same at the beginning of the run. There are two effective ways to suppress siphoning: by adding small I.D. restrictors to the ends of the separation capillary and by increasing the cross-sectional area of the vials. Alteration of the vial height during the run can also be used to equalize the liquid levels. The inlet vial can be lifted with a special computer controlled instrument, and if the lifting speed is carefully optimized the siphoning will be completely eliminated. The approximate lift rate can be calculated [11], but the final optimization must be carried out experimentally. With this technique, 320-or even 530-mm I.D. capillaries can produce acceptable separation efficiency.

In summary, there are several advantages of using non-aqueous media for speciation purposes in CE. Because the currents are generally lower, higher electric field strength and wider capillaries can be used without reaching the current or power limit of the equipment, and boiling of the buffer may be avoided. The low currents in non-aqueous buffers also reduce the buffer depletion due to coulombic titration. Siphoning has serious undesired effects in wide-bore capillaries, which can be reduced by using organic solvents with low ratio of density to dynamic viscosity.

4.5. Selectivity

One of the most attractive features of organic solvents is that their physical and chemical properties differ widely, both from each other and from water (Table 4.1). Accordingly, selectivity manipulation in non-aqueous CE can be achieved simply by changing the organic solvent or varying the proportions of two solvents.

The electrophoretic migration of the solutes is influenced by the solvent or solvent mixture used for the electrophoresis medium in mainly three ways. The mobility can be changed due to changes in the size of the solvated ion. Secondly, the dielectric constant may influence the equilibrium of the protolytic reaction. The higher the value of the dielectric constant, the less influence will the solvent have on the ionization of acids and bases. Third, the acid–base property of the solute expressed by its pK_a value may change due to the differentiating effect of many organic solvent. The latter effect being the most significant as the dissociation constant, K_a, may change many orders of magnitude for different solvents[10]. Furthermore, solvation of the solutes in the electrophoresis medium and in some cases hetero conjugation of buffer electrolytes with the analytes are known to play a role[26].

The pK values in organic solvents can be significantly different from those in water allowing separations which are difficult to achieve in aqueous media. It has been shown that all solvents in which a measurable zeta potential is developed around the uncoated fused-silica capillary wall are either amphiprotic or aprotic solvents [4]. In addition to self-dissociation, amphiprotic solvents act as proton donors or acceptors if there are other proton donors or acceptors in the separation system. However, there are differences in their proton donor and acceptor capabilities. Methanol, like water, has an

equal tendency to donate and accept protons, but basic amide-type solvents are worse proton donors than proton acceptors. Aprotic solvents, such as acetonitrile, which have very weak autoprotolysis constant, can only accept protons. Inert solvents are capable of neither autoprotolysis nor donation–acceptance of protons to a considerable extent, which makes them less suitable for non-aqueous CE.

Organic solvents are favorably applied to enhance the separation selectivity of CE by influencing the effective mobility of the separands and the mobility of the electroosmotic flow, the EOF. The selectivity can be expressed for a certain pair of separands, *i* and *j*, by the selectivity coefficient, r_{ji}, given by

$$r_{ji} = \frac{\mu_i^{tot}}{\mu_j^{tot}}$$

where μ_i^{tot} is the total (or apparent) mobility of separand, *i*; it is the sum of the effective mobility, μ_i^{eff}, and the mobility of the EOF, μ^{eo}: $\mu_i^{tot}=\mu_i^{eff}+\mu^{eo}$. Note that the mobilities are signed quantities, in contrast to the usual theory of conductance. The sign is positive for cation separands, and negative for anions. The mobility of the EOF has positive sign when it is directed towards the cathode.

Organic solvents may affect the electrophoretic properties of the separands two-fold: on the one hand by changing the actual mobility (that of the fully charged ion, which depends obviously on the viscosity of the solution); on the other hand by influencing the pK_a value of weak electrolytes specifically. Both effects are the result of solvation processes that take place in different solvents.

Addition of organic solvents to the background electrolyte will affect the mobility of both EOF and the analytes. Thus, it is important to assess the mobility of EOF relative to the mobility of the analytes in the mixed organic-aqueous solvent systems to ensure optimal efficiency and sensitivity. The change of the EOF in a series of mixed aqueous–organic solvents consisting of up to 100% MeOH and ACN was systematically investigated in fused-silica capillaries (Figure 4.7). The migration time of the water peak was used to calculate the electrophoretic mobility of EOF. It was found that organic solvents reduce the mobility of the EOF in nearly all cases, even under conditions of full dissociation of the chargeable groups of the wall, namely at high pH. In addition, the pK_a values of the dissociable groups on the capillary surface are found to be shifted to higher values, which is in accordance to expectations based on the concept of the transfer activity coefficient.

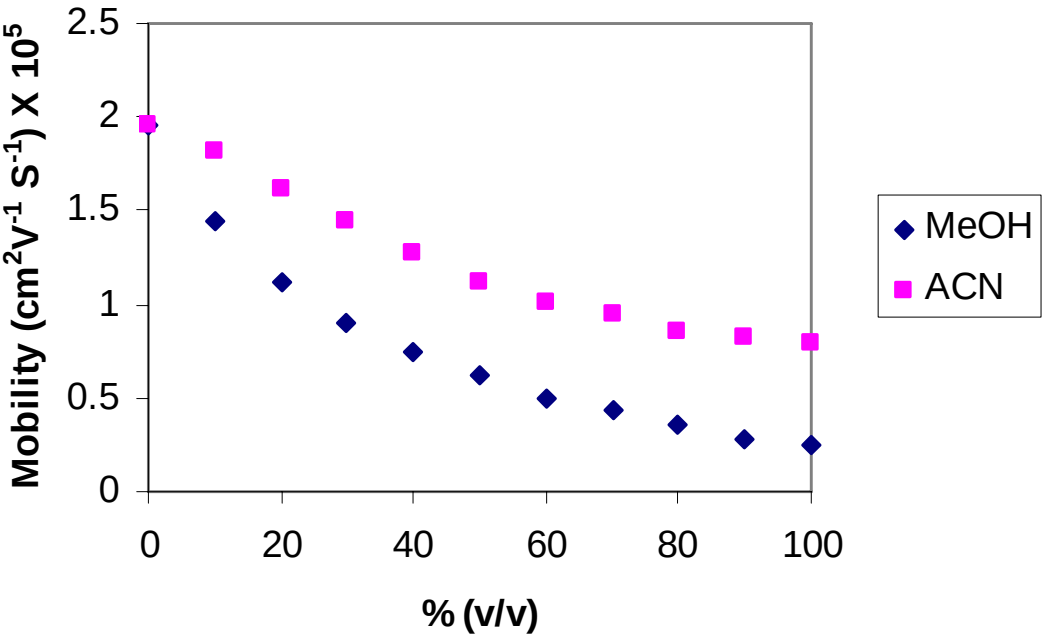

Figure 4.7 Change of the velocity, v_{eo}, of the EOF in fused-silica capillaries in dependence on the percentage of the organic modifier in aqueous–organic buffer solutions (field strength 208 V/cm, temperature 25°C, ionic strength about 10 mmol/l, apparent pH between 9 and 12

The change in selectivity for the separation of metal ions was investigated in non-aqueous and mixed aqueous–organic solvents with MeOH, ACN as constituents. Furthermore, the addition of organic solvents had not only a major influence on the EOF in comparison to a pure aqueous solution, but also a significant increase on the separation selectivity was observed, with many ions showing reversed separation order.

The effect of methanol on mobility of various metal ions was examined under ICP-MS detection conditions using methanol with 0.5 v% formic acid. Figure 4.8 shows the electrophoretic mobilities of the metals studied at different concentrations of

methanol. In the presence of organic solvents, all ions exhibit lower mobility than in aqueous solutions. This is due to the increase in viscosity and the decrease in dielectric constant of the running buffer upon addition of methanol. The viscosity of methanol–water mixtures change from 0.89 cP in pure aqueous solution to 0.55 cP in 100% MeOH reaching a maximum value of 1.60 cP at about 45% MeOH[27]. The dielectric constant deceases almost linearly as the amount of organic solvent increases[27]. Hence, the ratio of the dielectric constant to the viscosity is an important parameter determining the mobility of an ion in different solvent systems. For methanol/water mixture this value first decreases and reaches a minimum at about 45% MeOH and there after increases slightly.

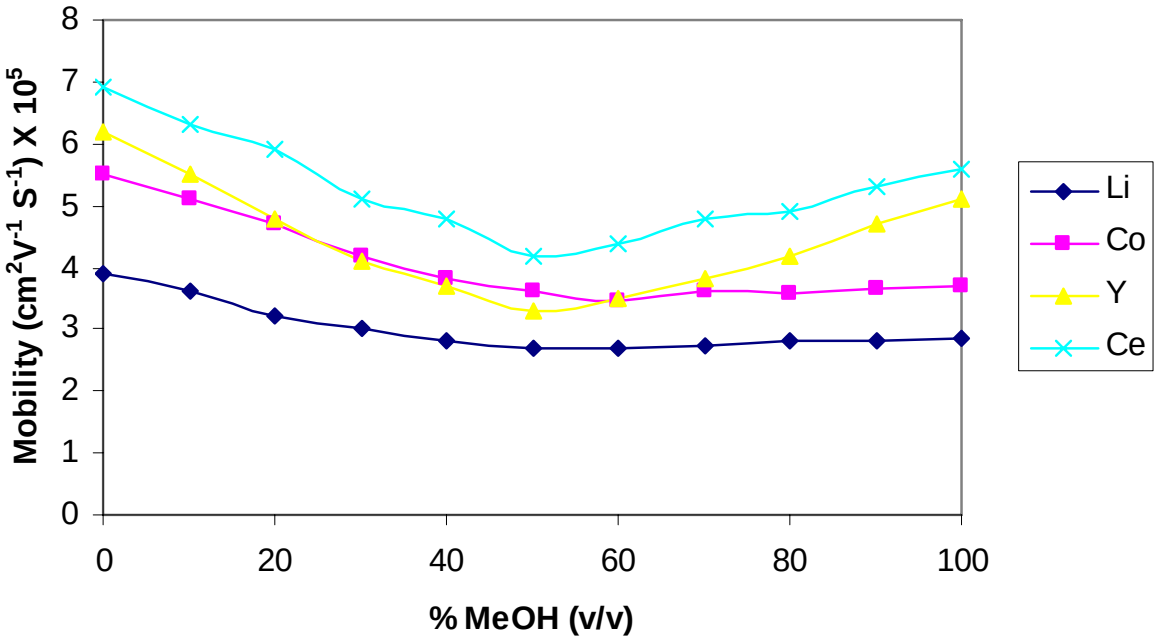

Figure 4.8 Selectivity changes of metal ions with percent methanol. Li^{+}(♦), Co^{2+} (■), Ce^{3+} (×), Y^{3+}(▼)

In Figure 4.8, Y shows significant decrease in mobility when the buffer is changed from pure aqueous to 40% MeOH buffer. Y is the faster migrating ion in aqueous solution but the slower migrating in 40% MeOH than Co. Y and Ce have the highest mobility and co-migrate in aqueous solution but are well separated in 40% MeOH. Y and Co are well resolved in aqueous solutions but their separation is compromised in 40% MeOH. Here also significant selectivity changes are observed. The migration order in 100% aqueous is Ce > Y > Co > Li, while in 40% MeOH the order is Ce > Co > Y > Li.

The electropherograms in Figure 4.9 show the comparison of separation of four different metal ions using aqueous and non-aqueous CE with ICP-MS detection. Significant changes in mobilities among the ions are observed with various amount of methanol used.

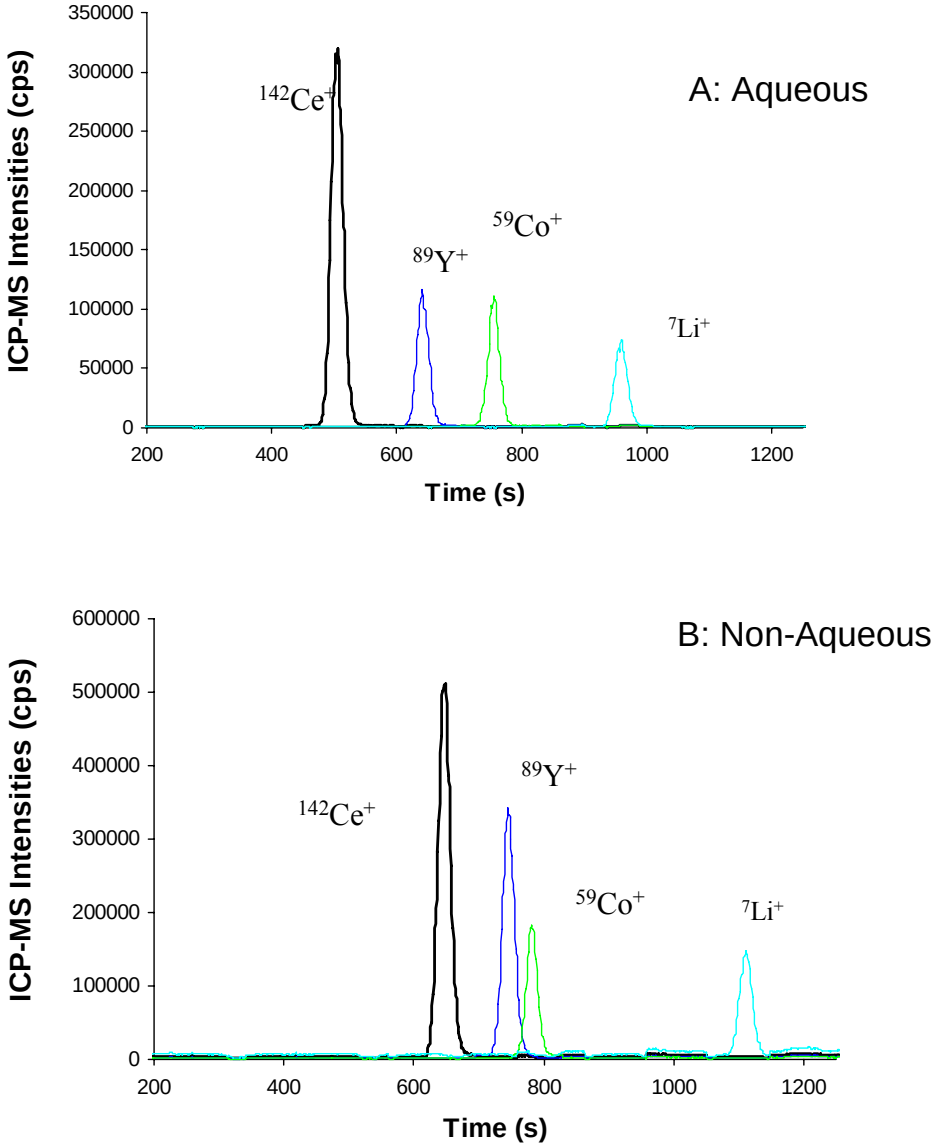

Figure 4.9. Effect of methanol on the separation selectivity of four metal ions. (a) Pure aqueous, 20mM $NaNO_3$; (b) methanol with 0.5 v% formic acid

As shown in Figure 4.8 and 4.9, the metal ions show significantly different mobility behaviors in mixed methanol/water buffer than in aqueous solutions. In addition to the viscosity and dielectric constant of the solvent system, the solvated radius of ions will be affected in mixed organic/aqueous solvents due to changes in the solvation behavior of the medium. In a different but related model, the solvation phenomena have been explained in terms of changes in the frictional forces acting on the ions[28]. Roy and Lucy have shown that dielectric friction can be an important factor affecting the mobility of ions particularly in nonaqueous solvents in addition to the hydrodynamic friction. They found that the Hubbard-Onsager (HO) dielectric friction model is successful at predicting solvent-induced selectivity changes in alcohol–water and acetonitrile–water media[29-31]. The HO model treats ion-solvent interactions as a dynamic perturbation of the solvent orientation caused by the ion's charge and size. Thus, dielectric friction can be considered as a charge-induced friction resulting from the finite relaxation time of the solvent dipoles surrounding the ion. The viscosity, dielectric constant, and relaxation time for methanol, respectively, are 0.55 cP, 32.7, and 53 ps. For water these values are 0.89 cP, 78.4, and 10 ps, respectively. Hence, the dielectric friction in solvent systems with lower dielectric constant and higher relaxation time becomes more important as the charge density on the ion increases. This indicates that the contribution of the dielectric friction will be much stronger in methanol than in water.

As shown from the results herein the mobility of doubly and triplely charged Y3+ and Co2+ decreased more significantly than the singly charged anions as the amount of MeOH increased from 0 to 40% (v/v). This is consistent with the predictions[30]. The

contribution of dielectric friction for the Li+ would be smaller, as these ions possess only a single charge. For similarly charged ions, the HO model predicts a direct dependence of dielectric friction on ion size and solvent composition. Smaller ions will experience higher frictional forces.

Properties of a solvent are important for understanding and control of EOF and uep of ions; these include dielectric constant (e), viscosity (η), donor number and solvating ability[32,33]. The solvation of ions can influence ion-interaction; the term of ion-interaction is used to represent any ion-association, ion-pairing, or ion-cluster formation that may occur in non-aqueous systems. Solvation depends on the physico-chemical properties of the solvent, and a general classification often used is protic/aprotic. In a portic solvent, hydrogen bonding is strongest for the smallest anions and those with localized charge such as chloride and acetate. It becomes progressively weaker as the size of the anions increases. For examples, in methanol (protic solvent), the solvation of chloride and acetate is favored due to formation of hydrogen bonds. However, perchlorate ion, which is larger than chloride and acetate, is more polarizable and is preferentially solvated by acetonitrile (aprotic solvent) by a combination of dispersion and ion-dipole interactions. For a protic solvent, such as methanol, changes in ion association for a series of teraethylammoniym salts follow trends similar to that found in water, but in an aprotic solvent such as acetonitrile, significantly different trends are expected.

Control and characterization of EOF is important in the evaluation of reproducibility and for peak identification. Ion mobility and EOF in some non-aqueous media have been reported recently and appreciable EOF was observed in methanol and

dimethylformamide. Electrophoretic mobilities of anlytes ions, μ_{ep} were two to three times higher than electro-osmotic mobility and the magnitude of μ_{ep} and μ_{eo} depended on the electrolyte system. In methanol and dimethylformamide the direction of EOF is cathodic in basic conditions. But no studies have been reported for non-aqueous acidic electrolytes. Since it was preferable to separate metal cations in acidic conditions to prevent possible hydrolysis of alkaline earth cation with small amounts of water (0.1% v/v) in the non-aqueous solvent, the EOF behavior for acidic methanol and methnol-acetonitrile mixtures was examined.

Figure 4.10 shows electroosmotic flow rates patterns observed as a function of solvent composition (mixtures of a protic and aprotic solvent) in three different acidic electrolytes: in curve A the electrolyte anion is chloride (10 mM HCl in methanol); in curve B the electrolyte anion is acetate (10 mM acetic acid in methanol); and in curve C the electrolyte anion is formate (10 mM formic acid in methanol). With the chloride electrolyte, the observed anodic EOF (towards positive electrode) decreased with concentration of acetonitrile and, after passing through a minimum, it increased until eventually at ~75% v/v acetonitrile the direction of the EOF changed to cathodic. With the acetic and formic acid electrolyte, however, the EOF was always cathodic and increased with the concentration of acetonitrile. The different patterns shown in Fig appear to be related to a combination of effects arising from adsorption of cation and anions onto to capillary wall and from differences in ion-interaction. The anodic EOF for HCl in methanol implies the presence of a net positive charge at the surface of the capillary.

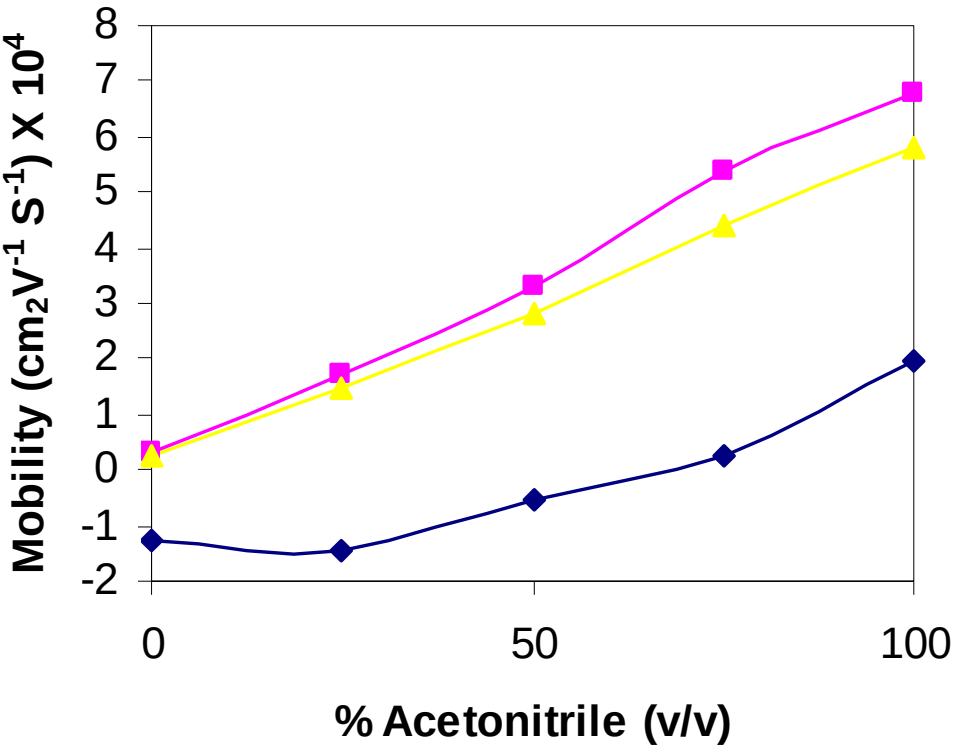

Figure 4.10 Effect of the addition of acetonitrile to methanol electrolytes on electroosmotic flow. Electrolyte: A: 10 mM HCl; B: 10 mM acetic acid; C: 10 mM formic acid

To explain the patterns observed in fig. as function of acetonitrile concentration, it is necessary to postulate a combination of anion adsorption and ion-interaction effects. Although some of the trends in EOF in fig, such as the small changes in EOF for lower acetonitrile concentrations might be attributed to changes in the ration of dielectric constant to viscosity as a function of acetonitrile content, this is not sufficient for explanation of the patterns seen as larger acetonitrile concentrations. If cation adsorption is significant, increases in acid association constants with acetonitrile concentration will result in reduced cation adsorption and thus smaller EOF values. However, increases in

acid association constants can not explain the eventual change from anodic to cathodic EOF for HCl, nor the significant increase of EOF for formic and acetate. These patterns can be explained if anions are also absorbed onto the silica surface. Solvation of chloride and acetate should decrease relative to perchlorate upon the addition of acetonitrile and this should increase any tendency f or their adsorption onto silica surfaces. Thus, combined shifts in the equilibrium for cation and anion adsorption, and for acid-association could explain the main features of the patterns seen in fig.

4.6. Application and Quantitative analysis

Previous sections have shown that aqueous CE-ICP-MS are successful in qualitatively and quantitative identifying aqueous Rh complex species. In the following section, preliminary studies of quantitative analysis using non-aqueous CE-IS-MS on-line measurement will be discussed.

The first experiment conduced was to compare aqueous CE and non-aqueous CE for the same RhCl3 standard dissolved in electrolyte. Both aqueous CE and non aqueous CE experiments were carried out (Figure 6.8). The aqueous CE results shows multiple Rh species peaks, due to that after dissolved $RhCl_3$ standard mixed with the aqueous CE buffer, the Rh has undergone hydration/hydrolysis processes as described in previous section. This is demonstrated that the aqueous CE method is not suitable for preserve Rh species in non-aqueous samples for detection of Rh species. The bottom electropherogram showed the non-aqueous results, and only one Rh peak was observed. Since in non-aqueous environment 100% methanol in this case, there is non water to affect Rh species, there should be only one Rh species in the dissolved standard. Rh

species was preserved under non-aqueous CE conditions. All the experiments in next chapter are conducted under non-aqueous CE conditions.

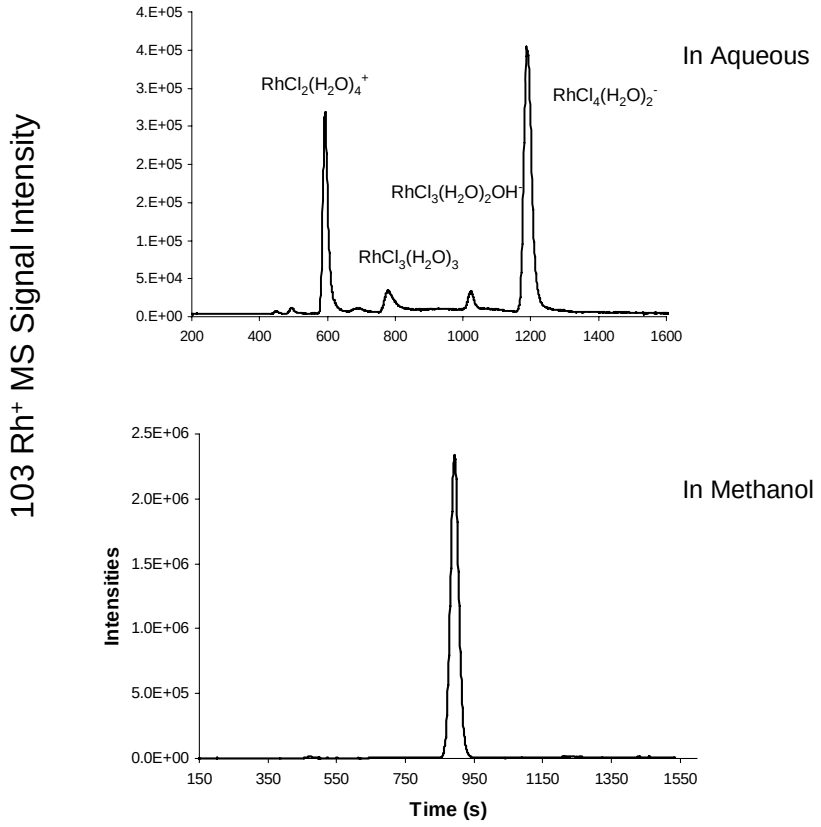

Figure 4.11 CE-HR-ICP-MS Electropherograms of 1 ppm $RhCl_3$ **Upper: result of aqueous CE-ICP-MS analysis,** Electrolyte: 20 mM $NaNO_3$, hydrodynamic injection (5mbar, 4s) injection volume: 47 nL, CE voltage: 30 kV, CE current: 10 μA**. Bottom: result of non-aqueous CE-ICP-MS analysis**, Electrolyte: methanol with 0.5 v% formic acid and 3mM imidazole (apparent pH*=4.3); hydrodynamic injection (5mbar, 4s) injection volume: 47 nL, CE voltage: 30 kV, CE current: ~15 μA

Quantification of various metal ions was examined using the optimal conditions of non-aqueous CE-ICP-MS. Using the experimental conditions described in previous Section, all the quantitative analyses were performed using calibration curves generated for each ion. In this work, the CE-IS-MS detection limits of the studied inorganic ion based on peak area were determined. Peak area detection limits were calculated by summing the points across the peak. Then, several sets of points (equal in number to the points across the peak) along the baseline were then summed. Three times the standard deviation of these summed sets (~15) of baseline points was used to calculate the detection limit. This approach determines the minimum amount of sample that can be reported to be greater than the background noise (blank run) with 99% confidence Low pg range of minimum detectable amount for each metal cations could be obtained, as shown in the table 4.3, which also compared to the available results of previously determined aqueous CE-ICP-MS detect limits.

	Non-aqueous CE-ICP-MS (ppb)			Aqueous CE-ICP-MS (ppb)
	50 μm ID	100 μm ID	200 μm ID	50 um
Y^{3+}	4.5	3.9	2.3	5.2
Co^{2+}	4.9	4.4	3.1	5.4
Ce^{3+}	1.6	1.3	0.7	2.3
Rh^{3+}	5.5	3.2	2.3	8.2
Li^{+}	9.6	7.2	5.1	11

Table 4.3 Non-aqueous CE-ICP-MS peak area based detection limits

Detection limits range low ppb level, which are better or comparable to chapter 2 values in aqueous buffers. Rh especially has the most improvement since there is no hydration/hydrolysis processes with the non-aqueous CE and all the Rh ions are eluted in one peak. The results also show that by using wide-bore capillary method, the detection limits for all metal ions are improved. As mentioned before, these due to that under the same conditions, with wide-bore capillary more samples are transferred to ICP plasma, thus lead to improved sensitivity. To examine the run-to-run reproducibility, eight replicate measurements of a standard solution of 1 μg/mL of each ion were performed. The percent relative standard deviations (% R.S.D.) for peak areas are presented in and

range from 1.3 to 2.0%. Good reproducibility of migration times is also obtained (0.2–0.6%).

When performing quantitative analysis of metals species in organic solvents, an internal standard was necessary to produce a linear calibration curve. The internal standard was most successful when it was the same charge as the analyte and it should undergo the same processes if possible. For the case of metal-ligand complexes, the internal standard should also not compete with analyte metal ions for ligands to disturb the original complexation. In this work, Y^{3+} was chosen as internal standard for Rh^{3+} analysis. Y and Rh have the same charge and oxidation state in solution (+3).

The calibration for non aqueous CE Rh ion with ICP-MS detection without an internal standard is depicted in Figure 4.12a. The $RhCl_3$ concentrations were from 0.2 ppm to 1 ppm. Ten replicates were taken of each solution. The calibration signals were calculated by calculating the peak area. Poor linearity clearly indicted the need of internal standard for the analysis.

In Figure 4.12 b calibration curve for Rh ions non-aqueous solution using Y internal standard was constructed. A 1 ppm Y standard was used with various Rh concentrations. The results clearly indicate that by using Y^{3+} internal standard linearity is much improved.

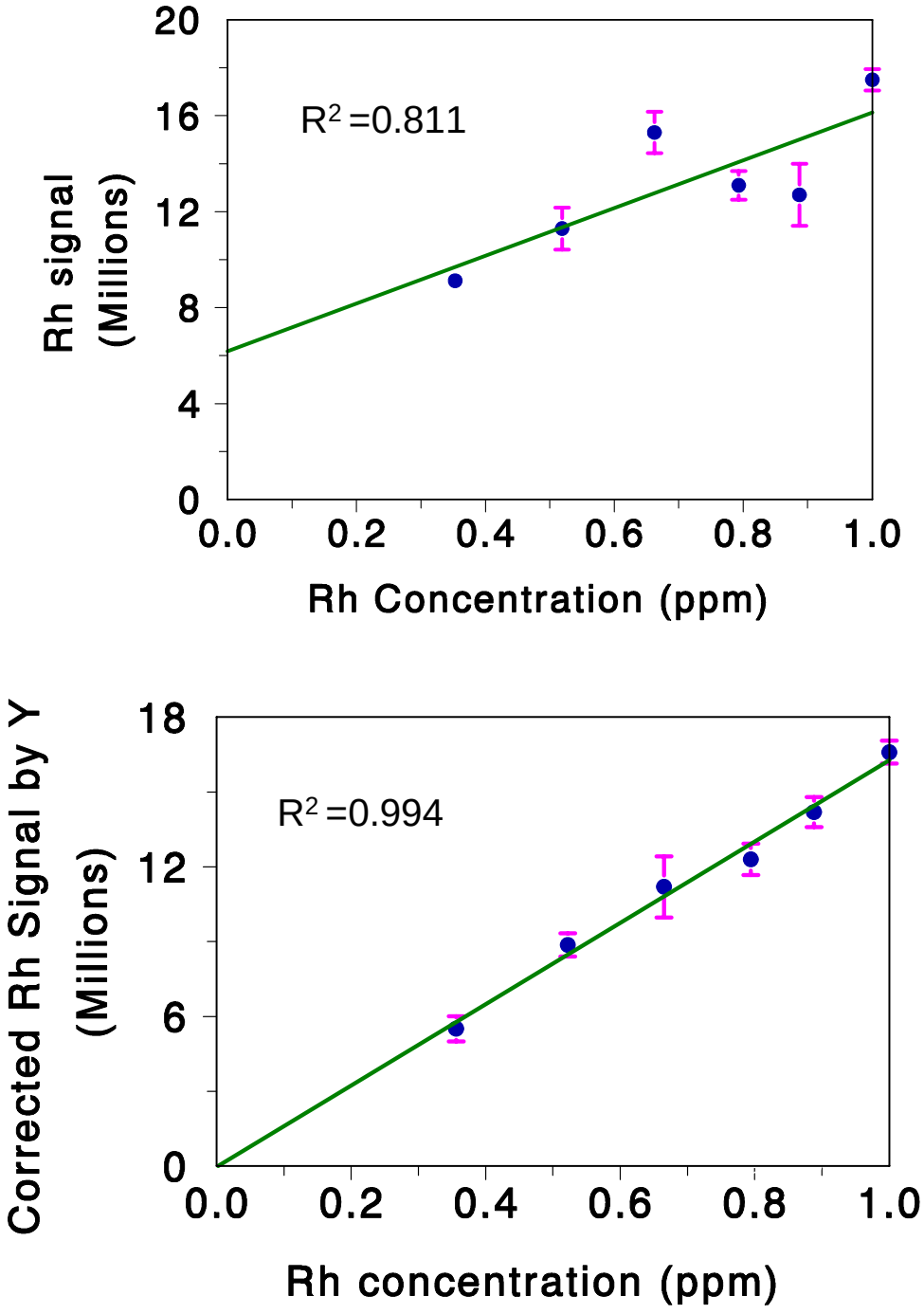

Figure 4.12 Calibration curve for Rh ion using the signal of Rh+ (m/z 103) (a) with no Y internal standard (b) with Y internal standard

4.7 Conclusions

In this work, non-aqueous CE-ICP-MS has been established as an efficient and reliable technique for the elemental speciation study with potential applications for pharmaceutical compound analysis. The newly designed sheath flow with PFA micro flow nebulizer interface provided stale and versatile connection between non-aqueous CE and ICP-MS, and functions as an on-line diluter to dilute the non-aqueous CE elute to aqueous system before it reaches the plasma.

The benefits of non-aqueous capillary electrophoresis have been discussed in two aspects. The wide selection of organic solvents, with their very different physicochemical properties, broadens our scope to manipulate separation selectivity. The lower currents present in non-aqueous solvents allow the use of high electric field strengths and wide bore capillaries, the latter in turn allowing larger sample load. In many cases detection sensitivity can also be enhanced.

Organic solvents offer the ability to alter the electrophoretic mobility of the ions and control of the EOF are essential to improve resolution and separation speed. Significant changes in selectivity among anions are observed by using up to 100% methanol in the running buffer. The ability to move peaks selectively using different percent of methanol demonstrates the flexibility of this technique. Overall highly charged show the largest decrease in mobility upon addition of methanol due to experience stronger dielectric friction and ionic strength effects than the lower charged ions.

The comparison of non-aqueous CE and aqueous CE for Rh speciation analysis is demonstrated. No hydration/hydrolysis processes were observed by using non-aqueous CE electrolyte. Peak area based limits of detection were either better or comparable with

aqueous CE, and sub ppb limits of detection were illustrated. Limits of detection can be further improved using wide-bore capillary methods which can transfer relatively large volumes of dilute sample into plasma. This method can improve limits of detection by as much as three orders of magnitude which would make the limits of detection for CE-ICPMS as good as conventional ICP-MS analyses. The results also show that when performing quantitative analysis of metals species in non-aqueous CE, an internal standard was necessary to produce a linear calibration curve.

REFERENCES

1 Stewart, I. I.; Olesik, J. W., J. Chromatography A 2000, 872, 227.

2 Bu, X., Wang, T., Hall, G. Journal of Analytical Atomic Spectrometry, *in press*

3 Dong-Dong Wang, Feng Li and Xiu-Ping Yan Journal of Chromatography A, Volume 1117, Issue 2, 9 June 2006, Pages 246-249

4 Karine Faure, Michael Loughran and Jeremy D. Glennon Analytica Chimica Acta, Volume 557, Issues 1-2, 31 January 2006, Pages 130-136

5 Sasi S. Kannamkumarath, Katarzyna Wrobel and Rodolfo G. Wuilloud Talanta, Volume 66, Issue 1, 31 March 2005, Pages 153-159

6 Altria, K.D.; Wallberg, M.; Westerlund, D. J. Chromatogr. B **1998**, 714, 99-104.

7 Salimi-Moosavi, H.; Cassdy, R.M. J. Chromatogr. A **1996**, 749, 279.

8 Marja-Liisa Riekkola , Matti Jussila, Simo P. Porras, Istvan E. Valko, Journal of Chromatography A, 892 (2000) 155–170

9 Jette Tjørnelund* , Steen Honore Hansen J. Biochem. Biophys. Methods 38 (1999) 139–153

10 Karim Sarmini and Ernst Kenndler, Journal of Chromatography A Volume 792, Issues 1-2 , 19 December 1997, Pages 3-11

11 C. Johns, M. Macka and P.R. Haddad, Electrophoresis 24 (2003), p. 2150.

12 D. Kaniansky, M. Masar, J. Marak and R. Bodor, J. Chromatogr. A 834 (1999), p. 133.

13 Wang, T.; Hartwick, R.A.; J. Chromatogr. 1992, 607, 119-125.

14 Doble, P.; Macka, M.; Haddad, P. R. Trends in Analytical Chemistry 2000, 19, 1 0l.

15 J. Tjørnelund and S.H. Hansen, J Chromatogr A **737** (1996), pp. 219–300.

16 Hill, S., Inductively coupled plasma mass spectrometry and its applications; Sheffield Academic: Sheffield, 1999.

17 Montase, A., Inductively coupled plasma mass spectrometry; Wiley VCH: New York, 1998

18 Axelsson, B.-O.; Jornten-Karlsson, M.; Michelsen, P.; Abou-Shakra, F. Rapid Comm. Mass Spectrom. 2001, 15, 375-385.

19 Cairns, W. R. L.; Ebdon, L.; Hill, S. J. Fresenius J. Anal. Chem. 1996, 355, 202-208.

20 S.F.L. Li, Capillary Electrophoresis – Principles, Practice and Applications, Elsevier, Amsterdam, 1992.

21 Istvan E. Valko, Simo P. Porras, Marja-Liisa Riekkola, Journal of Chromatography A, 813 (1998) 179–186

22 R.S. Sahota and M.G. Khaledi. *Anal. Chem.* **66** (1994), pp. 1141–1146.

23 P.B. Wright, A.S. Lister and J.G. Dorsey. *Anal. Chem.* **69** (1997), pp. 3251–3259

24 17. H. Yin, C. Keely-Templin and D. McManagill. J. Chromatogr. A **744** (1996), pp. 45–54

25 I.E. Valkó, H. Sirén and M.-L. Riekkola. J. Chromatogr. A **737** (1996), pp. 263–272

26 Adebaw Diress, Charles Lucy, J. Chromatogr. A 1085 (2005) 155-163

27 C. Schwer and E. Kenndler, Anal. Chem. 63 (1991), p. 1801

28 J. Hubbard and L. Onsager, J. Chem. Phys. 67 (1977), p. 4850.

29 K.I. Roy and C.A. Lucy, Electrophoresis 23 (2002), p. 383.

30 K.I. Roy and C.A. Lucy, Electrophoresis 24 (2003), p. 370.

31 K.I. Roy and C.A. Lucy, J. Chromatogr. A 964 (2002), p. 213.

32 Grob, M.; Steiner, F. Electrophoresis **2002**, 23, 1853-1861.

33 Doble, P.; Macka, M.; Trends in Analytical Chemistry **2000**, 19, 10l.

Chapter 5

Applications of non-aqueous CE-ICP-MS in pharmaceutical process research - Rhodium speciation analysis in a Catalyst Formation Reaction and Impurity Removal in the Reaction of Asymmetric Hydrogenation of Enamine Amide

5.0 Introduction

Metals play an increasingly important role in the synthesis of pharmaceuticals. Consequently, detailed studies of metal-containing catalysts and/or intermediates, by-products and impurities are becoming increasingly important. The reaction ability of a metal ion and, in particular, its catalytic activity is to a great extent dependent on the forms in which the metal exists in solution.[1-6] Therefore, the capability of distinguishing and identifying the presence of various species of an catalyst metal at various stages of an reaction may provide a better insight into the mechanism of a catalytic reaction. Armed with the qualitative and quantitative knowledge of the species presence in a reaction system, the optimization of reaction conditions for more efficient use of the catalyst and selectivity control would be greatly facilitated.

Understanding the mechanism and kinetics of reactions leading to the catalyst formation makes a significant impact on the development of novel synthetic routes for pharmaceutical products. Although the reaction media are normally complex systems consisting of different metal species, studies in this field generally employ conventional

tools for organic analysis, such as nuclear magnetic resonance (NMR), ultraviolet/visible (UV), infrared spectroscopy, molecular mass spectrometry (MS), etc. These techniques are responsive to many other compounds beyond a particular metal species because none of them is a metal-specific detector. Even where detection and identification of the species is possible, quantification is more challenging as the response from detectors such as UV or MS may differ with different species and suffers from matrix effects. This has to a large extent hampered the investigation of the fine details of reaction chemistry that are crucial for understanding and characterization of the catalyst formation process. Therefore, it can be assumed that a species-specific detection technique will become an invaluable tool for fundamental research in this field.

Among many different separation-detection capillary electrophoresis (CE)[7-14] has rapidly become an important analytical tool with attractive features such as short analysis time, high separation efficiency, small sample size, and low solvent consumption. Coupled with robust element (or isotope)-specific detection from ICPMS, the combination allows unambiguous identification and accurate quantitation of the amount of specific metals within each resolved species. Speciation analysis is undergoing continuous development in many fields, with the majority of applications in environmental and life sciences.[16,17] However, to our knowledge, no literature can be found employing this powerful analytical tool to look into individual metal species in metal-containing organic reactions in pharmaceutical process research or other related fields.

As demonstrated previous discussion, the majority of works found in the filed of applying CE for speciation study has focused on the use of aqueous buffers as

background electrolytes. One of the problems in applying aqueous CE method on pharmaceutical compound analysis is poor water solubility of certain pharmaceutical drugs and drug precursors. Recently, CE using non-aqueous electrolytes has been reported[68] for the separation of a range of cations including ammonium, alkali and other metal ions, which offers potential for being compatible with water-insoluble drug substances. Other advantages of using non-aqueous electrolytes in CE include greater ability to manipulate separation selectivity due to a wide range of physicochemical properties of different organic solvents, lower separation current and joule heating, increased compatibility for coupling CE with mass spectrometry when using volatile solvents such as methanol [10,11].

Since the liquid flow rates used in most CE techniques are much smaller than suitable liquid flow rates for direct aspiration of solutions into the ICP, a special design interface is needed for successful CE –ICP-MS analysis. Especially for non-aqueous CE, the direct coupling of the two techniques is problematic when large amounts of organic solvents are present in the CE buffer. Organic solvents have higher vapor pressures than aqueous solutions, which leads to increased solvent loading in the ICP and in turn results in an unstable or even extinguished plasma. Decreased sensitivity, carbide polyatomic ion interferences, carbon deposit on the ICP sampler and skimmer cones, and the resulting signal drift are some of the other problems related to the use of mobile phases with large organic content. As discussed at previous chapter, with a sheath flow interface, it is possible couple the non-aqueous CE with ICP-MS.

As the ICPMS only provides elemental information, speciation by CE-ICPMS is generally achieved by matching the retention times of the samples with those of the

standards. When peaks are observed that do not correspond to a standard, however, complimentary information is needed for the identification of unknown species or the confirmation of the actual presence of species in a given sample. This is often attempted by the use of molecular mass spectrometry techniques such as electrospray or atmospheric pressure chemical ionization mass spectrometry (ESI-MS or APCI-MS) in an off-line mode or on-line coupling with LC or CE.[8,9] However, this effort has so far been used only to a much lesser extent for speciation analysis in environmental and life science research. Insufficient sensitivity, complex spectra, and instability of the species are some of the constraints that need to be carefully addressed in using the technique for practical speciation studies.[8-10]

The aim of this research is to bring the resolving power of speciation analysis to pharmaceutical process research. Studies were arranged to develop and optimize a non-aqueous CE-ICP-MS system, and explore the feasibility of its application for speciation analysis for the synthesis of pharmaceutical products, particularly, for understanding of reaction mechanism and kinetics of catalyst formation by identification and quantitation of various catalyst metal species during the course of the reaction. The reaction media typically is a complex organic system consisting of different metal species which undergo constant transformation over the course of reaction. This approach can lead to a deeper understanding of mechanistic and kinetic aspects of the reaction under study. To our knowledge, this is the first application employing the resolving power of non-aqueous CE-ICP-MS in this field.

Furthermore, the eventual residual catalyst metal removal is critically important task in pharmaceutical process research, where final products must meet stringent purity

requirements. Removal of trace metal impurities has become increasingly in recent years, paralleling the growing use of organometallic reagents and catalysts in pharmaceutical synthesis.[25,26] While heterogeneous metal catalysts can often be removed by simple filtration, the use of homogeneous catalysts frequently requires removal of residual rhodium, ruthenium, or other metals from the product, a problem that can be considerably more challenging. Especially, metal speciation (i.e., the existence of the metal as two or more different species) can further complicate removal of metal impurities. Devolvement of a time and cost effective route for removing catalyst metal impurity for each reaction become a critically part of process research.

Studies of metal speciation and binding mechanisms of metal-ligand complexes are necessary for a basic understanding of the important metal removal processes since simply knowing the total concentration of the metal is not sufficient. It is reasonable to suggest that the ease of removal of a residual catalyst metal in a drug substance is dictated by the forms it exists, these forms include free metal atoms, metal at various oxidation states, and their complexation reaction products with various ligands in the system. Only an elemental speciation analysis can provide an insight into the microenvironment of the metal in the sample matrix. In the latter part of this chapter, CE application of metal removal will be demonstrated.

5.1 Catalyst Formation Reaction.

The dirhodium(II) tetrakis[methyl 2-oxopyrrolidin-5(*S*)-carboxylate, or Rh2(MEPY)4 catalyst is one of a series of enantioselective catalysts developed by Doyle and co-work-[23-26] and is based on amide ligand substitution around a dirhodium core.

These catalysts have proven useful in a number of enantioselective transformations, especially enantioselective cyclopropanation and CH insertion processes involving the formation of transient met-al-carbene intermediates. The structure of the reported catalyst (Figure 6.1), based on X-ray crystallographic evidence,[23] has two oxygens and two nitrogens bound to each rhodium, with the two nitrogens (or two oxygens) oriented cis to one another: the (cis-2,2) configuration.

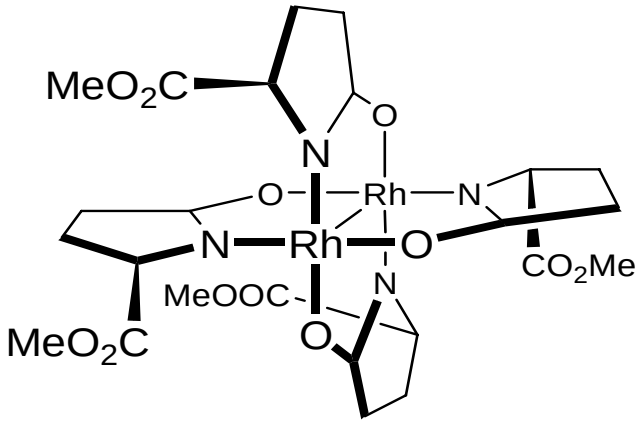

Figur 5.1. (cis-2,2)-Rh2(4S-MEPY)4.

The formation of dirhodium(II) carboxamidate compounds from rhodium acetate has been well studied [29-33] and is believed with the Rh2(MEPY)4 catalyst to involve the successive displacement of acetate ligands from the rhodium acetate precursor by methyl pyroglutamate (MEPY), as illustrated below. Catalyst formation is complicated by the potential presence of numerous isomeric species resulting from different geometries in the addition of enantiopure MEPY ligands to the dirhodium core. For example, five

isomeric species are possible for the Rh2(OAc)2(MEPY)2 intermediate, while the tri-MEPY and tetra-MEPY species can each exist in as many as four isomeric forms. Interestingly, despite the possibility of four different isomers for the Rh2(MEPY)4 product, the cis-2,2 isomer is the only species that has been reported to date. More detailed information about the reaction can be found elsewhere.[23-30]

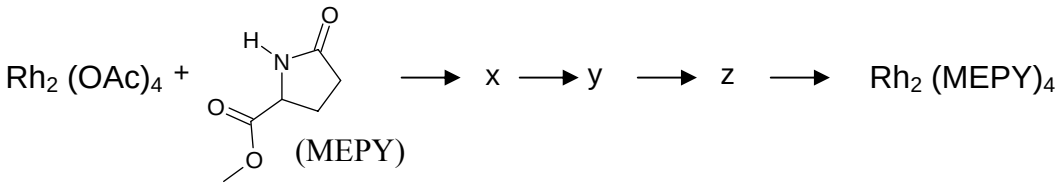

5.2 Sample Collection and Preparation.

Heat was applied to start the reaction, and the samples were collected by removing aliquots from the reaction mixture every 6 min within the first hour, every 10 min within the second hour, and every 20 min until the fifth hour. The samples were immediately cooled to room temperature, evaporated to near dryness at or below 40 °C to avoid further ligand exchange, and then transferred to the analytical laboratory over a period of a few days. Before analysis, the samples were dissolved in 2 mL of acetonitrile. To ensure the stability of the species, semi-real-time samples were collected by carrying out the synthesis reaction within the research facility where the analysis was performed. The samples were collected every 40 min within 5 h, immediately diluted with methanol, and subjected to analysis. The results from these samples were compared to those obtained from using the more "aged" samples prepared elsewhere.

For the CE-ICPMS test, preliminary determination of the total Rh concentrations of the samples was made by ICPMS determination. The samples were further diluted with methanol to a total rhodium concentration of ~50 ng mL^{-1} before being injected into the CE. Recoveries of the species were determined by comparing the total Rh concentrations of the samples with the summation of individual species after separation. For the ESI-MS test, the sample was diluted two times with methanol and had a total Rh concentration of 150 μg mL^{-1}.

5.3 Experimental

Chemical reagents

A standard of dirhodium tetraacetate (99.99+%) was obtained from Sigma-Aldrich (Milwaukee, WI). Dirhodium(II) tetrakis[methyl 2-oxopyrrolidin-5(*S*)-carboxylate] was acquired from Fisher Scientific (Pittsburgh, PA). Methanol and acetonitrile, LC-MS Chromasolv grade, were also supplied by Sigma-Aldrich (Seelze, Germany). TFA, p.a. grade, was obtained from Fluka (Steinheim, Germany). A 1000 μg mL^{-1} Rh stock standard solution used for total Rh determinations was purchased from High-Purity Standards (Charleston, SC). The water used in the experiments was prepared by passing distilled water through a Hydro Ultrapure water system (Hydro Service and Supplies, Garfield, NJ).

Instrumentation

All electrophoresis exprienments were conducted using an Agilent HPCE system (Palo Alto, CA, USA). Fused-silica capillaries with pre-made windows were purchased from Agilent with 50 μm I.D., 350 μm O.D., and 40 cm total length. All separations were

run at a constant temperature of 25°C. Injections were performed using a hydrodynamic pressure of 20 mBAR for 4 sec. The applied voltage was +30kV. Between injections, the capillary was rinsed with methanol for 120 seconds and then with run buffer for 120 seconds. The run buffer was 3 mM imidazole in methanol with the apparent pH* adjusted with formic acid (for apparent pH* 4.3), unless stated otherwise. Apparent pH*s of methanol-based electrolytes were measure by a Corning (Corning, NY, USA) pH meter calibrated using aqueous pH standards. Capillaries were rinsed with methanol for 0.5 hour and then with deionized water for 0.5 hour before long-term storage.

All the measurements were carried out with a Finnigan Element 2 (Finnigan, Bremen, Germany) high resolution inductively coupled plasma sector-field mass spectrometer. The instrument is equipped with a double focusing mass analyzer using reversed Nier-Johnson geometry. The system allows three pre-defined nominal mass resolutions ($m/\Delta m$) of 300, 4,000, and 10,000 by means of selectable slits. The actual mass resolutions vary between 300-500 for low, 3,500-4,500 for medium, and 8,000-14,000 for high-mass resolution mode depending on the optimization of parameter settings.

The CE system was coupled to the Finnigan Element 2 high resolution ICPMS through a custom-built interface. The ICPMS provided element-selective detection of rhodium (m/z 103). The CE ICP interface was the same as previous described. The instrument settings were checked daily and optimized when necessary.

For ESI-MS, an Agilent 1100 series HPLC system equipped with a photodiode array UV-visible detector was coupled to a Finnigan LCQ (San Jose, CA) mass spectrometer with an ESI source for LC-MS analysis. ESI positive mode was used for

MS detection with full scan from *m*/*z* 100 to 2000. Helium was used as damping gas in the ion trap and as sheath and auxiliary gas. The spray voltage was tuned to 5 kV with sheath and auxiliary gas at 80 and 60 units, respectively. The heated capillary temperature was set at 250 °C. Xcalibur software was used for instrumental control, data acquisition, and data analysis. The injection volume for the analysis was set at 10 μL.

Optimization of the ICP-MS operating parameters, including the position of the plasma torch, ion lens voltages, RF power, and nebulizer gas flow rate, was performed daily using a 100 ppb solution containing elements of interest. Normally one end of the electrophoresis capillary is placed in the sample that is drawn through the capillary. Nebulizer gas flow and the sheath flow rate are set to provide a fixed laminar flow rate (e.g. ~0.1 μL/min) and therefore a constant uptake of the analyte. The optimized nebulizer gas flow rate typically was ~0.90 L/min. The dwell time was 100 ms per peak and the number of replicates was chosen such that the total experiment time was slightly longer than the time required for a given separation. Depending on the number of masses measured, the total analysis time was between 10-30 minutes. The developed interface enabled the handling of organic solvents without the addition of oxygen, thanks to the use of a splitter by which the organic loading in the plasma was minimized. No visible carbon buildup was observed after prolonged use of the system. Running without oxygen addition was advantageous because problems such as the increase of the oxygen-containing polyatomic ion interferences and accelerated degradation of the sampler and skimmer cones could be avoided.

An accurate mass calibration at the beginning of the measurement session was routinely performed for low resolution (LR), medium resolution (MR), and high

resolution (HR) modes by using a 1.0 ng/ml multi-element standard tuning solution containing Li, B, Na, Al, Sc, Fe, Co, Ga, Y, In, Rh, Ba, Lu, Tl and U.

Detailed information about the reaction conditions leading to the formation of Rh_2(5*S*-MEPY)$_4$ can be found elsewhere.[26-33]

5.4 Results and Discussion

5.4.1 Optimization of Separation Conditions

Methanol was first selected as the background electrolyte solvent because it offers good dissolving properties for a great variety of analytes. Imidazole was chosen as the additive. As a weak base (pKa=6.95), at a certain condition, the mobility of imidazole is a function of the mobility of its fully protonated form and the equilibrium between the fully protonated form and its neutral form. By adjusting the apparent pH* of the background electrolytes, we can manipulate the mobility of imidazole to achieve mobility match with certain analytes. Figure 6.2a showed the electrophoregrams of the sample collected at 80 min after the start of the reaction with 100% Methanol as electrolyte. Although all 5 Rh species were separated, but the resolution need to be improved.

Consequently, mixtures of methanol-acetonitrile with various ratios were tested as the organic component of the mobile phase for separation. The best separation was achieved when the methanol-acetonitrile mixture had a ratio of 50:50 (v/v) and was used as background electrolyte solvent. As shown in figure 5.2b, with the addition of acetonitrile into methanol-based background electrolytes, the migrations of some Rh species were significantly slowed down and the resolution was much improved

The separation was also influenced by the sample preparation method. Peak fronting was observed when the samples were diluted in acetonitrile. In comparison, sharp and symmetric peaks were obtained for samples diluted in methanol. Therefore, all the samples were diluted in methanol before the CE separation. A slight change of the organic component in the mobile phase resulted in a significant variation of the peak resolution. After careful optimization of CE conditions, all 5 possible Rh species were separated and then detected by ICPMS (Figure 5.2b). The peak identification will be discussed in the later section.

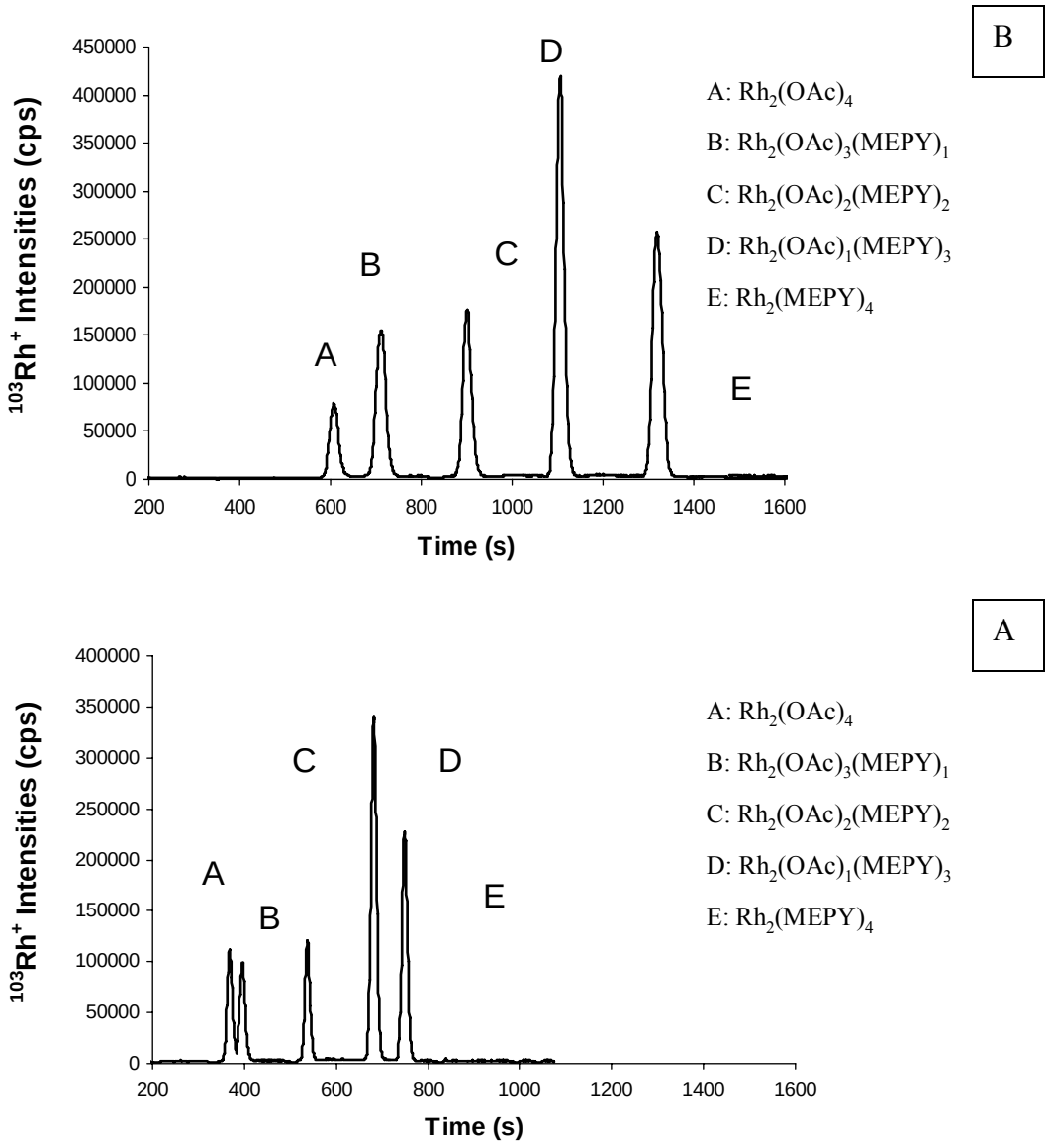

Figure 5.2 CE-HR-ICP-MS Electropherograms Of sample collected at 80 min reaction time **(A)** Electrolyte: methanol with 0.5 v% formic acid and 3mM imidazole (apparent pH*=4.3) **(b)**, Electrolyte: methanol-acetonitrile mixture 50:50 (v/v) with 0.5 v% formic acid and 3mM imidazole (apparent pH*=4.3); hydrodynamic injection (5mbar, 4s) injection volume: 47 nL, CE voltage: 30 kV, CE current: ~15 μA

5.4.2 Species Identification/Confirmation.

Unlike speciation analysis in environmental research where many standards of the species of interest are available, standards of the intermediates and different structural isomers of the same metal species in the catalyst formation reactions rarely exist. Therefore, the common approach of comparing CE retention times of unknown peaks with those of the standards is often not feasible. In this case, the only commercially available standards are the starting material $Rh_2(OAc)_4$ and the desired product $Rh_2(5S\text{-}MEPY)_4$ in the (*cis*-2,2) configuration. Comparing peak retention times in the CE-ICPMS chromatograms in Figure 6.3 with those of the two standards, first peaks and last peak can be identified as $Rh_2(OAc)_4$ and $Rh_2(5S\text{-}MEPY)_4$. As mentioned previously, it is believed that $Rh_2(5S\text{-}MEPY)_4$ is formed through successive displacement of the acetate ligand from $Rh_2(OAc)_4$.[20-22] As a result, three reaction intermediates with various degrees of substitutions could be present. Once the starting and product species have been identified, the middle three peaks can be easy identified as $Rh_2(OAc)_3(MEPY)$, $Rh_2(OAc)_2(MEPY)_2$, and $Rh_2(OAc)(MEPY)_3$, respectively, based on their relative mobility.

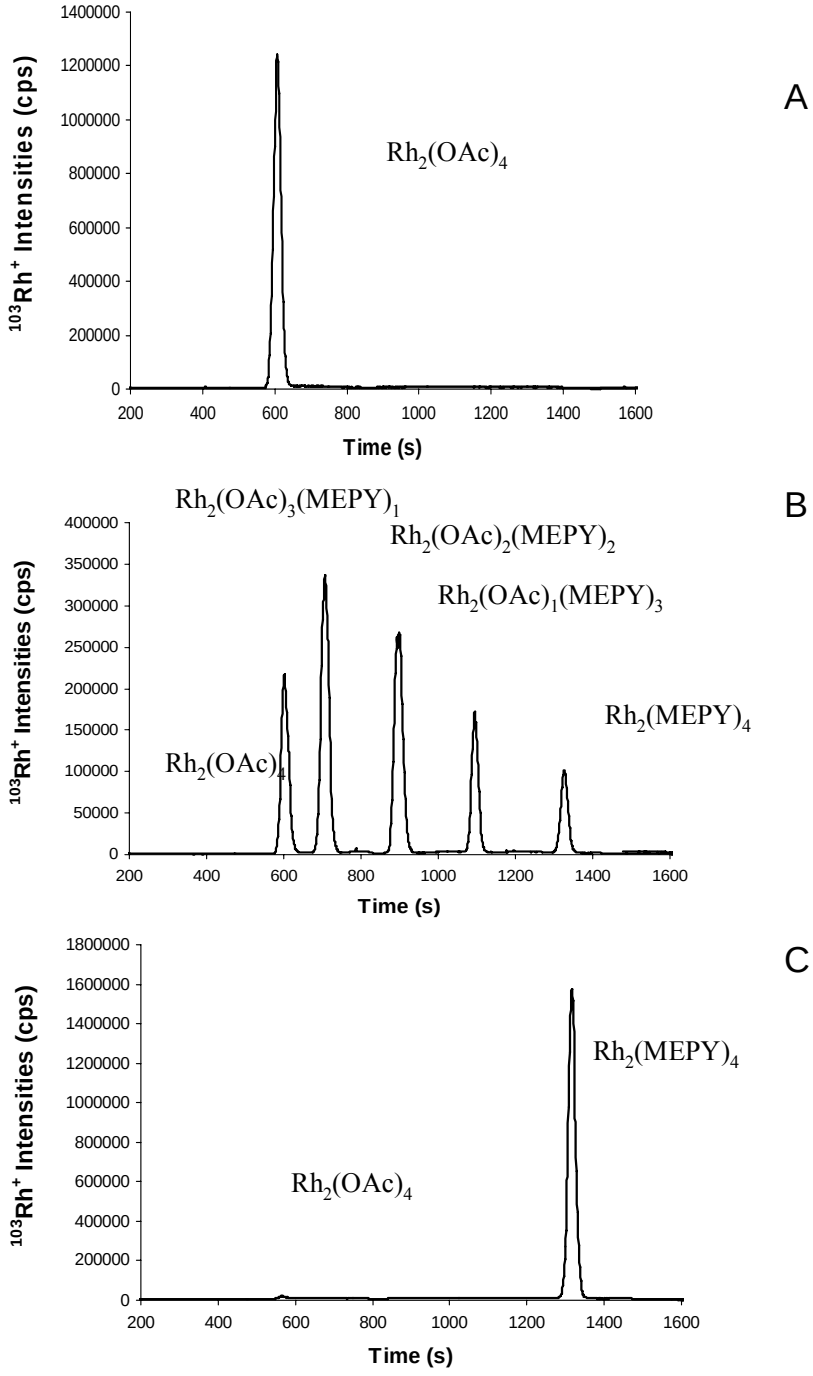

Figure 5.3 CE-HR-ICP-MS Electropherograms Of **(A)** Starting material $Rh_2(OAc)_4$ (B) intermidate (C) product $Rh_2(5S\text{-}MEPY)_4$; Electrolyte: methanol-acetonitrile mixture 50:50 (v/v) with 0.5 v% formic acid and 3mM imidazole (apparent pH*=4.3); hydrodynamic injection (5mbar, 4s) injection volume: 47 nL, CE voltage: 30 kV, CE current: ~15 μA

For the positive identification or confirmation of other species, ESI-MS became a compulsory part of the entire analysis scheme in providing molecular mass information of the species.

Initial feasibility analysis involved the preparation of Rh2(MEPY)4 on a 200-mg scale, using an established procedure,[14] with removal of aliquots over time. Aliquots were evaporated, then dissolved in acetonitrile and injected within a single chromatographic run, using the technique of flow injection analysis (FIA) HPLC-ESI-MS. In the resulting chromatogram (Figure 5.4) diagnostic masses for starting material, product, and each of the intermediates have been identified, and are expressed as separate channels for convenient assessment of relative abundance. The set-up of a method of this sort is rapid, and analysis of the collection of 30 reaction aliquots takes less than 15 min. Interestingly, the various intermediates in the formation of MEPY can be seen to change over the course of the reaction, giving some indication of reaction kinetics, and bringing to light unexpected findings

Although the TIC from ESI-MS analysis showed limited capability of providing species identification for this application, extracted ion chromatograms (EICs) could be used as an easy and explicit way to map out the distributions of all Rh-containing species detected by CE-ICPMS. The M + 1 ions for each sought-for species [*m*/*z* 526 for $Rh_2(OAc)_3(MEPY)$, *m*/*z* 609 for $Rh_2(OAc)_2(MEPY)_2$, *m*/*z* 692 for $Rh_2(OAc)(MEPY)_3$, and *m*/*z* 775 for $Rh_2(MEPY)_4$ were monitored. For $Rh_2(OAc)_4$, however, the M + 1 ion had a very weak signal, and the dominating ion with a *m*/*z* of 428 (M-O) was therefore used to monitor $Rh_2(OAc)_4$ in the EIC. As shown in Figure 6.4, the EICs clearly

demonstrate the distribution of each species and their corresponding isomers in a single chromatographic run.

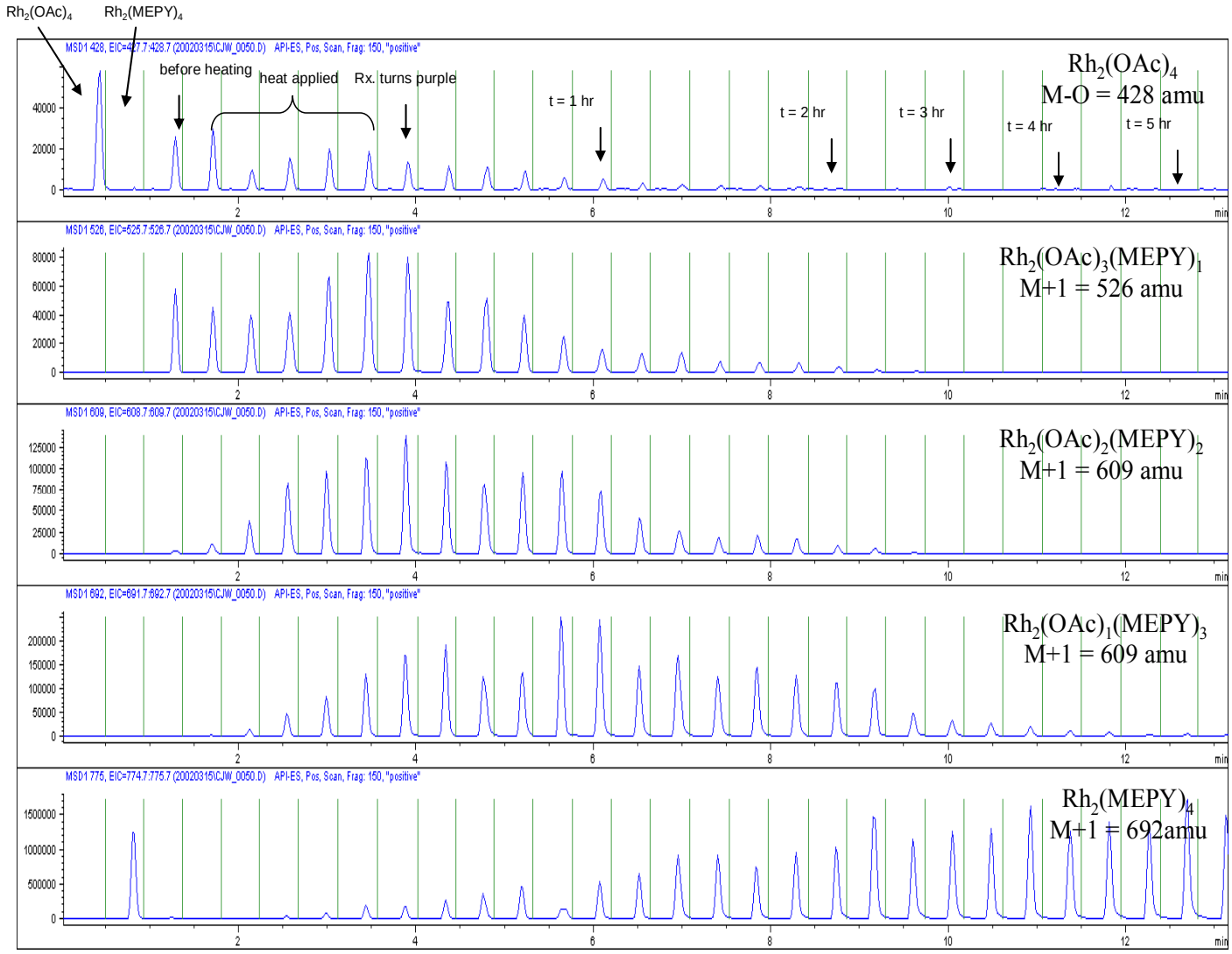

Figure 5.4. Monitoring the formation of Rh2(MEPY)4 using LC-MS with flow injection analysis. Results presented as extracted ion chromatograms at characteristic ions for each species. Analysis conditions: Agilent 1100 LC-ESI-MS FIA; Extend C18 (4.650 mm) column, flow rate 1.5 mL/min; 50% ACN/water with 2 mM ammonium formate, pH 3.5; Vfrag 150.

Compare to ESI-MS, ICPMS detection enabled accurate quantitation of individual species, while quantitation by ESI-MS was very difficult, especially without a standard of each species. Some possible effects that may have impact on ESI-MS detection include matrix-related ion suppression or enhancement, generation of new species in the ionization-extraction process, and sample carryover.

5.4.3 Reaction Mechanism and Kinetics.

Selected CE-ICP-MS chromatograms obtained for various time-course aliquots are illustrated in Figure 6.5, which vividly depict the species evolution during the course of the reaction. For the first time, the starting material, the mono-, di-, and trisubstituted intermediates as well as the tetrasubstituted product along with their isomers can not only be identified but also be quantified. This has made it possible to study the fine details of reaction mechanism as well as kinetics of ligand exchange.

Thanks to the excellent quantitation capability of the ICPMS detector, the change in concentration for each species over time can be easily determined and is illustrated in Figure 5.6. The established presence of mono, di-, tri-, and tetrasubstituted products confirms the mechanism of this reaction as ligand exchange as proposed in the literature.[15-21] Whereas, previous work suggested that the third and fourth ligand substitution would be much slower than the first two,[18-21] the current evidence from this study suggests that there is no significant rate differences in proceeding from the first through the fourth ligand exchange.

The decay of rhodium acetate is seen to be quite rapid and, as in the previous study, we observe the mono-MEPY species to rapidly grow in, then begin to decline at

about 20 min. The various di-MEPY never substantially accumulate in the reaction mixture, whereas the tri-MEPY species, grows to a maximum of about 40% area at t 3/4 h, before beginning to decline. Of greatest interest to us was the change of the tet-ra-MEPY species over time. This observation is helpful in reconciling empirical observations concerning the relationship between reaction time and yield of crystallized (cis-2,2)-Rh2(MEPY)4[14] and suggests an avenue for reaction monitoring so as to optimize yield. The capability of being able to monitor the changes of various product isomers over time is of great value in catalyst forming reactions, since the reaction conditions for maximum yield of the desired product can thus be easily achieved and optimized.

The stability of the species over time was also evaluated by comparing the CE-ICPMS electropherograms obtained from analyzing freshly prepared samples and samples aged for up to one month. No significant differences were observed for samples from the two experiments. The ligand exchange reaction was shown to have been "stopped" or extremely slowed when heat was removed. Being able to "freeze" these reactions in a certain time frame makes it easier to study the species evolution and reaction mechanism. This also confirmed the stability of these species when exposed to oxygen as reported previously,[15-18] and the interconversion of the species over the period of the study was negligible.

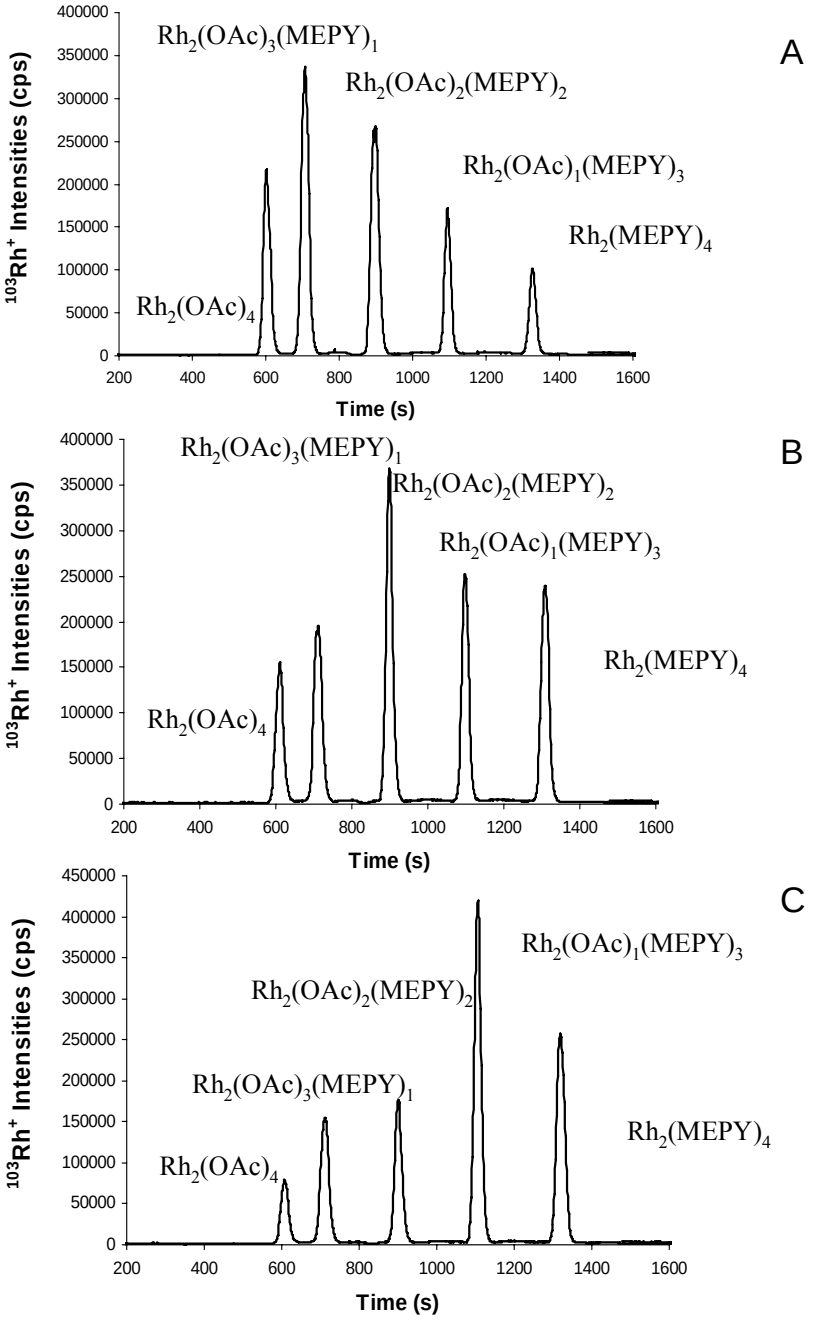

Figure 5.5 CE-HR-ICP-MS Electropherograms for selected samples collected at different time frames, showing the evolution of species during the course of the reaction. Electrolyte: methanol-acetonitrile mixture 50:50 (v/v) with 0.5 v% formic acid and 3mM imidazole (apparent pH*=4.3); hydrodynamic injection (5mbar, 4s) injection volume: 47 nL, CE voltage: 30 kV, CE current: ~15 μA

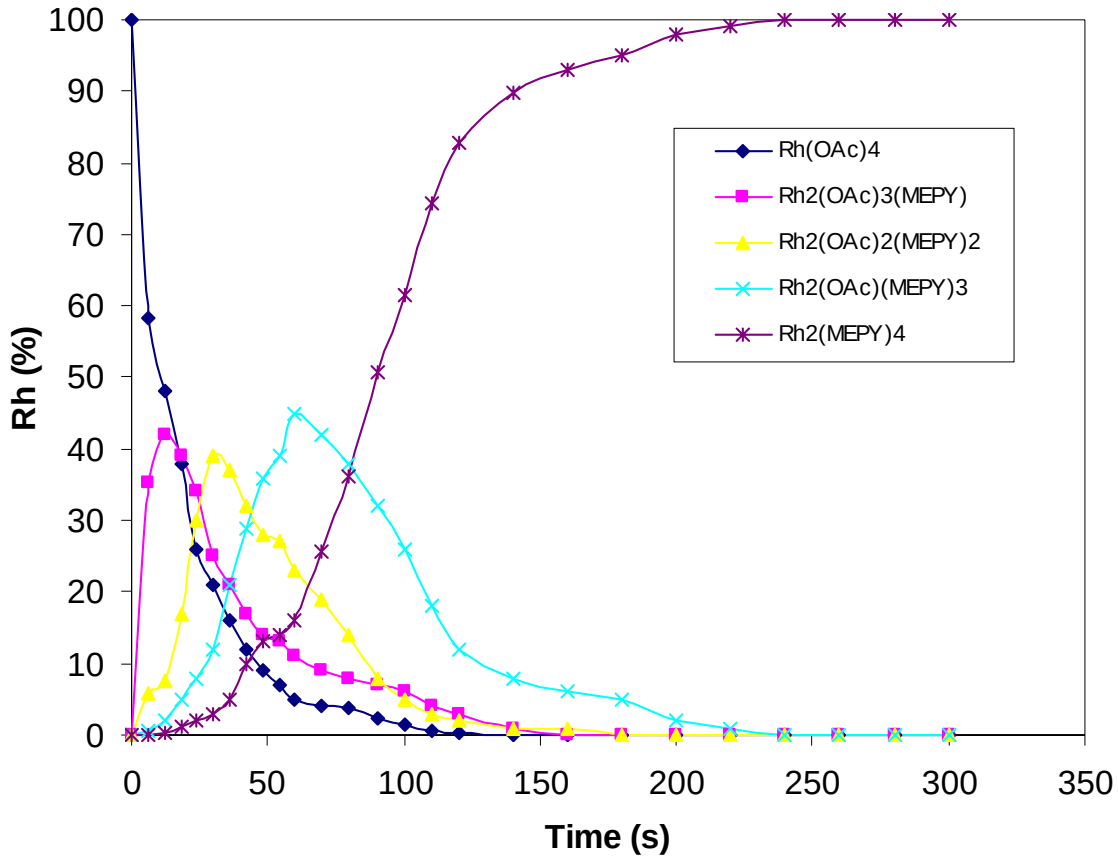

Figure 5.6 Change of species as percentage of the total Rh content over the course of reaction leading to formation of Rh_2(5*S*-MEPY)$_4$.

Having an analytical method that distinguishes the component species in the formation of the Rh2(MEPY)4 catalyst affords us an excellent tool for monitoring the progress of the reaction over time. In addition, this analytical capability may prove helpful for understanding enantiocontrol in the use of these catalysts, since each isomer has its own reactivity and selectivity profile. As has been recently emphasized by Black-[15] careful reaction monitoring can be useful for de-convoluting the reaction system or for more exacting evaluation of reaction mechanisms. The ability to perform these studies using ICP-MS detection offers a distinct advantage over more conventional ESI-MS detection, in that ICP-MS detection is not subject to the matrix-related ion suppression/ion enhancement problems that make quantitation by ESI-MS notoriously difficult.

5.5 Rhodium Catalyst Species Detection and Impurity Removal in the Reaction of Asymmetric Hydrogenation of Enamine Amide

Impurity removal is a critically important task in pharmaceutical process research, where final products must meet stringent purity requirements. Removal of trace metal impurities has become increasingly in recent years, paralleling the growing use of organometallic reagents and catalysts in pharmaceutical synthesis. While heterogeneous metal catalysts can often be removed by simple filtration, the use of homogeneous catalysts frequently requires removal of residual rhodium, ruthenium, or other metals from the product, a problem that can be considerably more challenging. Especially, metal speciation (i.e., the existence of the metal as two or more different species) can further complicate removal of metal impurities. Devolvement of a time and cost effective route

for removing catalyst metal impurity for each reaction become a critically part of process research.

Studies of catalyst metal speciation during the reaction are necessary for a basic understanding of this important metal removal processes since simply knowing the total concentration of the metal is not sufficient. It is reasonable to suggest that the removability of a residual catalyst metal in a drug substance is dictated by the forms it exists. Only an elemental speciation analysis can provide an insight into the microenvironment of the metal in the sample matrix.

In this section, CE-ICP-MS speciation technique will be applied to asymmetric hydrogenation of Enamine Amide reaction catalyst detection and removal study. Asymmetric homogeneous catalytic hydrogenation was a major innovation by Merck process chemists, and has proven to be an excellent procedure for preparing enantiopure intermediates on a large scale owing to the high enantioselectivity, high throughput and cost effective. The traditional drug synthesis to make chiral drugs, is to make 50/50 mixture and throw away half. With asymmetric catalysis, only one mirror image of catalyst can be make many single mirror-image drug “copies”. Of many concerns are the simplicity of product isolation and homogeneous catalyst impurity removal. Below show Asymmetric Hydrogenation of Enamine Amide reaction and in-situ catalyst formation:

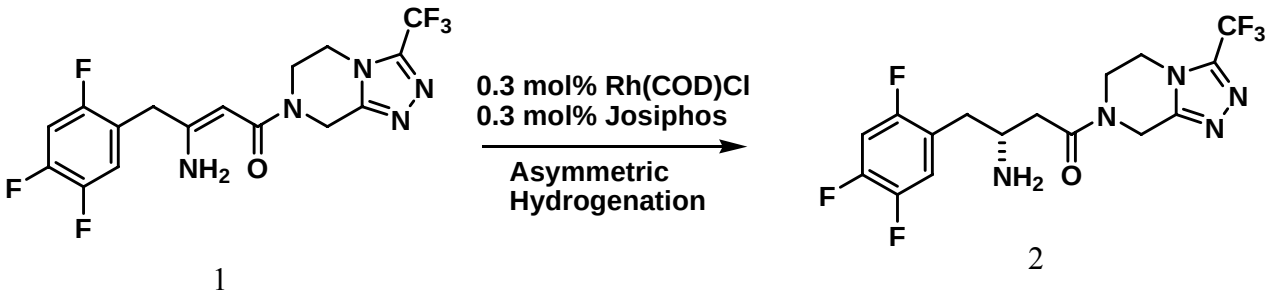

1 2

Reaction 1 Asymmetric Hydrogenation of Enamine Amide

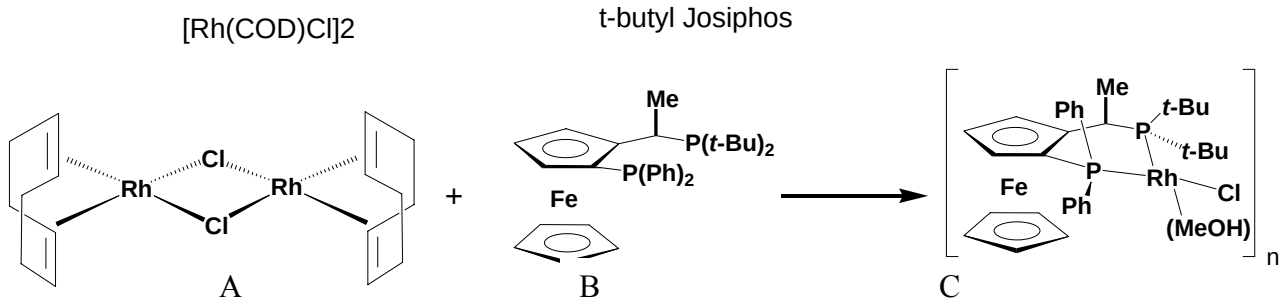

A B C

Reaction 2 In-situ formation of hydrogenation Rh Catalyst

In the reaction, the enamine amide **1** undergoes a rhodium catalyzed asymmetric hydrogenation employing a chiral ligand (t-butyl josiphos **B**) which gives the desired R stereochemistry **2**. $[Rh(COD)Cl]_2$ **A** has been used as Rhodium source and the active catalysts **C** have been generated in situ. The in-situ formatted hydrogenation Catalyst **C**

has proved to be an excellent catalyst for the preparation of this advanced key intermediate. However, reduction of the residual Rh concentration to acceptable levels represented a major challenge for the production of **2** of suitable quality.

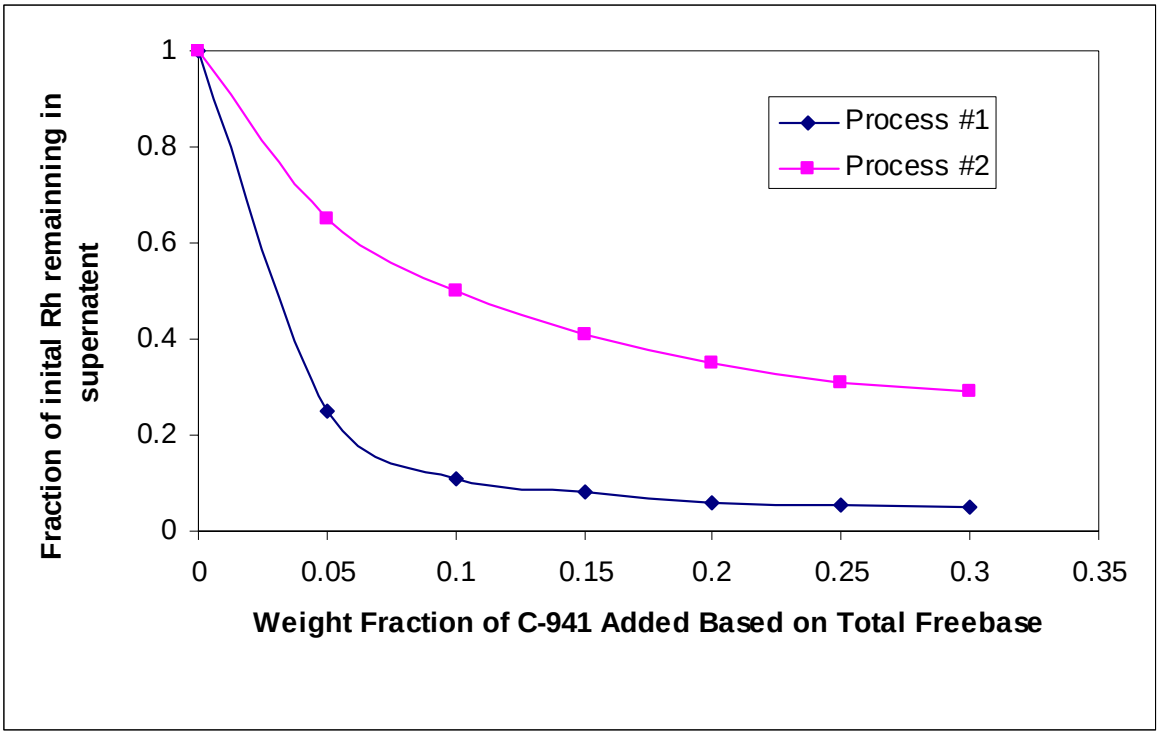

Figure 5.7 Experimental data describing Rhodium removal in two different processes using ecosorb C-941. *(The descriptions of the two metal removal processes are not included since they are irrelevant with the discussion here)*

Figure 5.7 shows the Rh metal removal results using two different processes with ecosorb C-941. By using 30% weight fraction, for process #1, there was only less than 5% Rh left in the supernatant, compared to morn than 30% Rh left in the process #2. Note that the removal characteristics did not change, revealing that chemical changes brought upon by process #2 are irreversible. Only an investigation of each sample steam

from two processes by CE-ICP-MS speciation study can provide insight into the behavior of the catalyst during the reaction and these final removal processes, and reveal the chemical change of the Rh species.

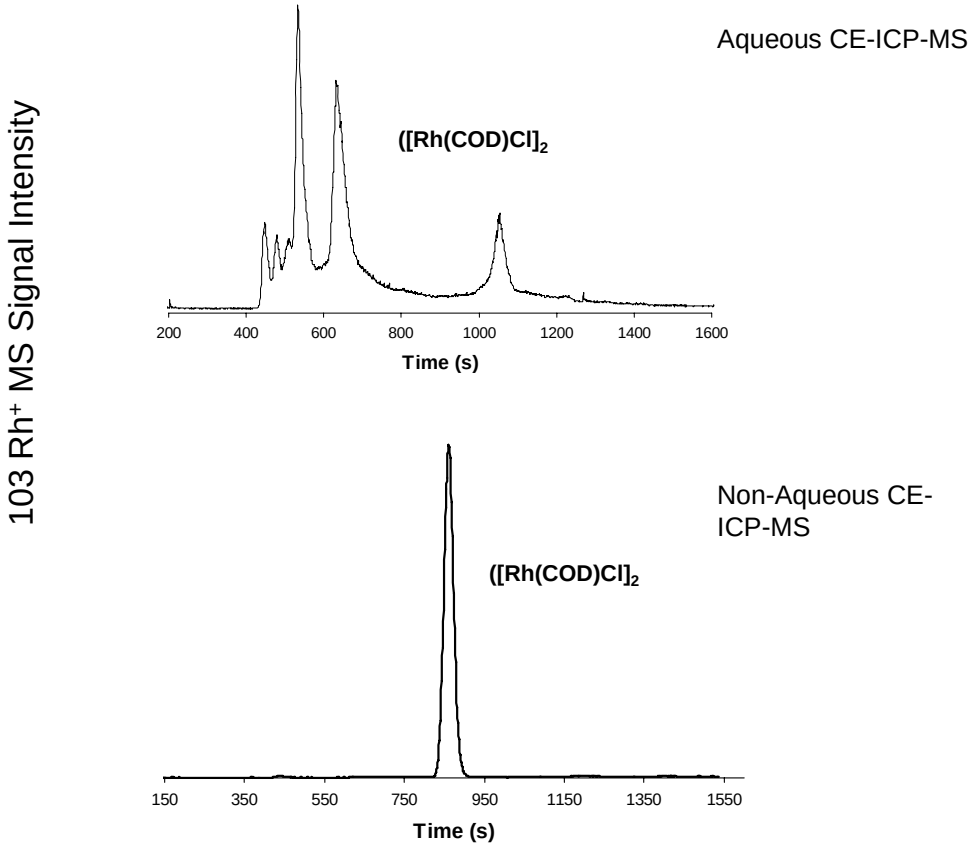

Figure 5.8 CE-HR-ICP-MS Electropherograms Of Chloro (1,5-cyclooctadiene) Rhodium(II) Dimer([Rh(COD)Cl]2) **Upper: result of aqueous CE-ICP-MS analysis,** Electrolyte: 20 mM $NaNO_3$, hydrodynamic injection (5mbar, 4s) injection volume: 47 nL, CE voltage: 30 kV, CE current: 10 μA**. Bottom: result of non-aqueous CE-ICP-MS analysis**, Electrolyte: methanol with 0.5 v% formic acid and 3mM imidazole (apparent pH*=4.3); hydrodynamic injection (5mbar, 4s) injection volume: 47 nL, CE voltage: 30 kV, CE current: ~15 μA

The first experiment conduced was to develop the method for directly analysis reaction steam for detection of Rh species. Both aqueous CE and non aqueous CE experiments were carried out (Figure 5.8). The aqueous CE results shows multiple Rh species peaks, due to that after dissolved $[Rh(COD)Cl]_2$ standard mixed with the aqueous CE buffer, the Rh has undergone hydration/hydrolysis processes as described in previous section. This is demonstrated that the aqueous CE method is not suitable for this application. The bottom electropherogram showed the non-aqueous results, and only one Rh peak was observed. Since COD ligands are effective in stabilizing Rh species, there should be only one Rh species in the dissolved standard. Rh species was preserved under non-aqueous CE conditions. All the experiments in later work are conducted under non-aqueous CE conditions.

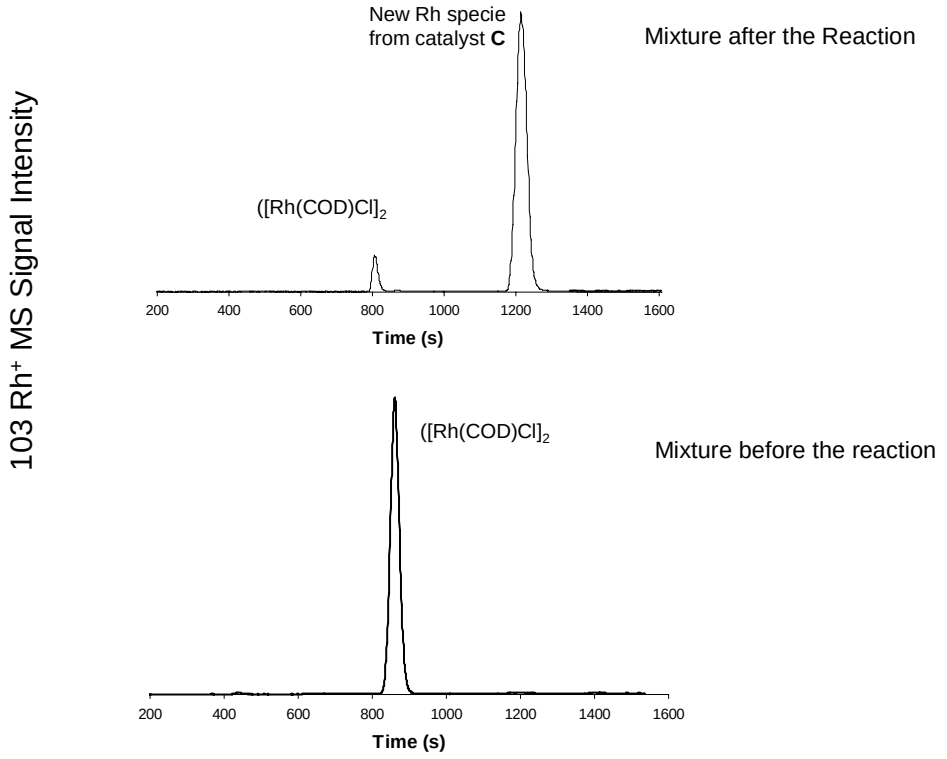

Figure 5.9 Non-Aqueous CE-HR-ICP-MS Electropherograms **Upper: Mixture after the reaction, Bottom: Mixtrue before the reaction**

The figure 5.9 shows the CE-HR-ICP-MS Electropherograms of each mixture from beginning and end reaction steams. At the beginning of the reaction, as illustrated in reaction 2, only one Rh species should be present in the reaction steams-$[RhCODCl]_2$ **A**, just as shown in the bottom electropherograms. At the end of the reaction, Rh catalyst went through formation of **A** to **C**, as demonstrated in the upper electropherogram. The first Rh peak can be identified as [RhCODCl]2 standard by comparing migration time with the bottom electrophergrams. The second Rh peak represents the new species from

Rh complexe **C**. This results illustrate CE-ICP-MS can be used as a tool to monitor transition of Rh catalyst, and detect the Catalytic intermediates during the reaction.

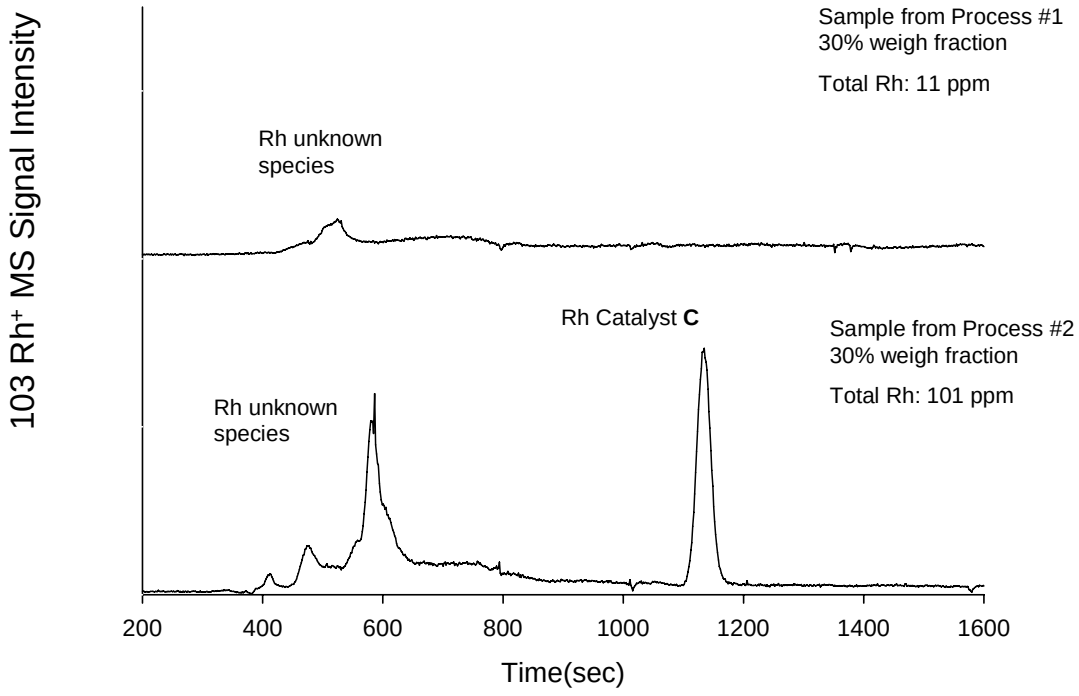

Figure 5.10 Non-Aqueous CE-HR-ICP-MS Electropherograms **Upper: Sample from Process #1, 30% weigh fraction, Bottom: Sample from Process #2, 30% weigh fraction**

Figure 5.10 shows the results of CE-ICP-MS investigation of removal of Rh from asymmetric hydrogenation of Enamine Amide reaction stream containing product **2** using a adsorbents at 30 wt % loading (i.e., 30 mg of adsorbent + 100 mg of product). Process #1 showed good selectivity, as illustrated in upper Figure. In this instance, Majority Rh impurity has been removed (total 11 ppm Rh left in the reaction steam), only one Rh species present. For the process #2, not only the total concentration of Rh is much higher at 101 ppm, there are actually still 4 different Rh species left in the reaction steam. One major species can be identified as Rh catalyst **C** from reaction 2. The other three Rh species, which can not be identified now, are new Rh species converted from Rh catalyst species during the removal process. This result clearly shows that process #2 is not effective to removal Rh impurity due to its inability to remove Rh catalyst C and inducing Rh chemical changing during the process.

5.6 Conclusion

In summary, non-aqueous CE coupled with ICP-MS has been shown to be a powerful tool in separation, identification, and quantitation of various rhodium species during the course of the model reaction leading to the formation of Rh_2(5*S*-MEPY)$_4$. It is especially useful for identifying and quantifying intermediate species with great selectivity and sensitivity, thus providing insight into the fine details of the mechanism and kinetics of the catalyst formation. The combination of non-aqueous CE and HR-ICPMS has proven to be a valuable tool for the investigation of species evolution in catalyst formation process. These technical developments will surely contribute to a

deeper understanding of catalyst synthesis in pharmaceutical process research and other related fields.

The most significant outcome from this work is the development of methodology capable of separation and identification of various catalyst metal species during the course of reaction and during the purification process of the products. A number of other important conclusions can be drawn including (1) Speciation analysis for a series of samples along the reaction pathway and removal process can illustrate the change of individual species over time; (2) using ESI-MS can identify Rh peak to understand chemical change of Rh species; (3) Using peak area can perform quantitative analysis to follow the increasing, decreasing, emerging and disappearing of various catalytic intermediates over the course of the reaction; (4)using the speciation analysis as a tool can provide fundamental understanding of removal metal impurity process and guideline for design metal removal process.

References

1. I. Ojima (Ed.), Catalytic Asymmetric Synthesis,2nd edn., Wiley, New York, 2000;

2. J. M. Hawkins, T. J. N. Watson, Angew. Chem. Int. Ed. 2004, 43, 3224–3228;

3. Qiang Tu, Tiebang Wang, Christopher J. Welch, Peng Wang, Xiujuan Jia, Conrad Raab, Xiadong Bu, and Michael P. Doyle, Anal. Chem., 78 (4), 1282 -1289, 2006

4. Christopher J. Welch, Qiang Tu, Tiebang Wang, Conrad Raab, Peng Wang, Xiujuan Jia, Xiaodong Bu, Darren Bykowski, Benjamin Hohenstaufen, Michael P. Doyle, Adv. Synth. Catal. 2006, 348, 821 – 825

5. Y. Hsiao, N. R. Rivera, T. Rosner, S. W. Krska, E. Njolito, F. Wang, Y. Sun, J. D. Armstrong III, E. J. J. Grabowski, R. D. Tillyer, F. Spindler, C. Malan, J. Am. Chem. Soc. 2004, 126, 9918–9919

6. H. M. De Vries, C. E. Tucker, J. A. Miller, Innov. in Pharm. Tech. 2001, 01, 125–126, 128, 130.

7. Kannamkumarath, S. S.; Wrobel, K.; Wrobel, K.; B'Hymer, C.; Caruso, J. A. J. Chromatogr., A **2002**, 975, 245-266.

8. Michalke, B.; P, S., Fresenius J. Anal. Chem. **1997,** 357, 594-599.

9. Michalke, B.; Lustig, S.; Schramel, P., Eelectrophoresis **1997,** 18, 196-201.

10. Olesik, J. W.; Kinzer, J. A.; Olesik, S. V., Anal. Chem **1995,** 67, 1-12.

11. Kinzer, J. A.; Olesik, J. W.; Olesik, S. V., Anal. Chem. **1996,** 68, 3250-3257.

12. Maria Montes-Bayon, Daniel Pröfrock, Alfredo Sanz-Medel and Andreas Prange Journal of Chromatography A, Volume 1114, Issue 1, 5 May 2006, Pages 138-144

13. Gloria Álvarez-Llamas, María del Rosario Fernández de laCampa and Alfredo Sanz-Medel TrAC Trends in Analytical Chemistry, Volume 24, Issue 1, January 2005, Pages 28-36

14. R. Nageswara Rao and M.V.N. Kumar Talluri Journal of Pharmaceutical and Biomedical Analysis, Volume 43, Issue 1, 4 January 2007, Pages 1-1

15. Al-Ammar, A.; Siripinyanond, A.; Barnes, R. M. Spectrochim. Acta, Part B **2001**, 56, 1951-1962.

16. Caruso, J. A.; Montes-Bayon, M. Ecotoxicol. Environ. Saf. **2003**, 56, 148-163.

17. Waddell, R.; Lewis, C.; Hang, W.; Hassell, C.; Majidi, V. Appl. Spectrosc. Rev. **2005**, 40, 33-69.

18. Schramel, O.; Michalke, B.; Kettrup, A. J. Chromatogr., A **1998**, 819, 231-242.

19. Rosenberg, E. J. Chromatogr., A **2003**, 1000, 841-889.

20. Sharp, B. L.; Sulaiman, A. B.; Taylor, K. A.; Green, B. N. J. Anal. At. Spectrom. **1997**, 12, 603-609.

21. Svelana, S.; Anatoly, P.; Gumenyuk, S.; Lubov, F.; Andrei, R.; Talanta 61 (2003) 195-202

22. C. J. Welch, J. Albaneze-Walker, W. R. Leonard, M. Biba, J. DaSilva, D. Henderson, B. Laing, D. J. Mathre, S. Spencer, X. Bu, Xiadong, T. Wang, Org. Proc. Res. Dev. 2005, 9, 198 – 205;

23. Doyle, M. P.; McKervey, M. A.; Ye, T. Modern Catalytic Methods for Organic Synthesis with Diazo Compounds; John Wiley & Sons: New York, 1998.

24. Doyle, M. P. In Chiral Dirhodium(II) Carboxamidates for Catalytic Asymmetric Synthesis, in New Methodologies in Asymmetric Catalysis; Malhotra, S., Ed.; Oxford University Press: Oxford, England, 2004.

25. Timmons, D.; Doyle, M. P. In Chiral Dirhodium(II) Catalysts and their Applications, in Catalysis by Di- and Polynuclear Metal Clusters, 3rd ed.; Cotton, F. A., Murillo, C. A., Walton, R. A., Eds.; Springer Science: New York, 2005.

26. Doyle, M. P.; Phillips, I. M.; Hu, W. J. Am. Chem. Soc. **2001**, 123, 5366-5367.

27. Doyle, M. P.; Valenzuela, M.; Huang, P. Proc. Natl. Acad. Sci. U.S.A. **2004**, 101, 5391-5395.

28. Doyle, M. P.; Winchester, W. R.; Hoorn, J. A. A.; Lynch, V.; Simonsen, S. H.; Ghosh, R. J. Am. Chem. Soc. **1993**, 115, 9968-9978.

29. Doyle, M. P.; Winchester, W. R.; Protopopova, M. N.; Kazala, A. P.; Westrum, L. J. Org. Synth. **1996**, 73, 13-24.

30. Doyle, M. P.; Raab, C. E.; Roos, G. H. P.; Lynch, V.; Simonsen, S. H. Inorg. Chim. Acta **1997**, 266, 13-18.

Chapter 6

Determination of Halogens in Organic Compounds by High Resolution Inductively Coupled Plasma Mass Spectrometry (HR-ICP-MS)

6.0 Introduction

Traditionally, the halogen elements (F, Cl, Br, and I) are analyzed by ion chromatography (IC)[1] , it is not only very time-consuming but also offers no isotopic information.

It is well known that ICP-MS offers the analyst an almost unrivaled technique for the determination of metallic elements in a variety of complex matrices, but little attention has been paid to the determination of non-metals, such as halogen elements. Since only unit mass resolution is achievable for most commercial ICP-MS instrument equipped with a quadrupole mass analyzer, severe spectral interferences alone made their analysis extremely difficult or impossible. The majority of such interferences are caused by the presence of the plasma gas, water, acids used, and concomitant elements, from which a variety of molecules with overlapping nominal mass to charge ratios (m/z) are formed. The nominal mass to charge ratios (m/z) of these interfering polyatomic ions are mostly less than 80 a.m.u.(atomic mass unit), which can be identical to those of halogen elements [2] as well as to those of many other elements of interest.

In order to extend the multi-element capabilities of a quadrupole ICP-MS (ICP-QMS) system, cool plasma techniques have been developed and applied by manufacturers and ICP mass spectroscopists. The idea of cool plasma is to lower the excitation temperature thus leading to reduced formation of molecular species generated from the combination of Ar with O, N and H [2,3]. Although the cool plasma conditions can dramatically reduce the formation of interfering molecular species for these elements, the much lower ionization temperature would also suppress the ionization of the halogen elements which require significantly higher ionization energies to be ionized than those of K or Fe[5]. Overall this would result in unacceptable sensitivities for the halogen elements.

An effective solution to the spectral interference problems in ICP-MS is to use a high resolution instrument equipped with a double focusing mass analyzer consisting of a magnetic and electrostatic sector instead of a quadrupole filter [3,4]. Since the new generation sector-field ICP mass spectrometers can provide a resolution of as high as 14000 ($m/\Delta m$), it provides the ICP mass spectrometrists new possibilities for interference-free, accurate determination of these elements. Besides high resolving power, another attractive feature of a magnetic sector instrument is its very high sensitivity combined with extremely low background level. High ion transmission in low resolution mode translates into sensitivity specifications of typically 100-200 million counts per second (mcps) per ppm, while background levels resulting from extremely low dark current noise are typically 0.1-0.2 cps. This compares with a typical sensitivity specification of 10-50 mcps per ppm and a typical background level of ~10 counts per second (cps) for a quadrupole instrument[4]. High ion transmission combined with

extremely low background levels results in superior detection limits, typically orders of magnitude better than those achievable by a quadrupole-based instrument. Halogen elements have much higher ionization potentials than most other elements in the periodic table. This explains their relatively lower sensitivities in ICP-MS. The most obvious example is fluorine (with an ionization potential of 17.42 eV), its estimated ionization efficiency (F^+/F) based on the *Saha Equation* is only about $9x10^{-4}$ % at an ionization temperature of 7500 K, whereas under the same conditions sodium (with an ionization potential of 5.14 eV)[5] is estimated to be 100% ionized. That is the major reason why sensitivity of fluorine is about 2 million times lower than that of fully ionized sodium.

The inherent nature of high sensitivity together with high resolving power of the sector-field ICP-MS makes accurate determination of these elements possible.

The goal of this study is to develop reliable, robust and accurate methods for the determination of these four halogen elements from sub ppm to major levels in various organic compounds, which included bulk drug substances in development at Merck. These methods would open the way for rapid determination and confirmation of stoichiometries of many halogenated organic compounds and drug substances as well as the detection of halogen impurities in them. This would help to the ever-increasing demands from organic chemists to efficiently support new drug discovery and development programs.

There have been few reports on the direct determination of these elements by various ICP methods [6-13]. This can be partially attributed to severe spectral interferences, high ionization potentials of these elements, and the memory effects some of these elements have; all of which have been seemingly too serious to be circumvented.

Okamoto [9] reported determination of fluorine in aqueous samples by electrothermal vaporization inductively coupled plasma mass spectrometry (ETV-ICP-MS). Bayón [10] also reported an indirect method, which was based on the formation of aluminum monofluoride complex and the sequential monitoring of the aluminum ions at mass 27. Several studies for the determination of fluorine and other halogen elements in geological samples were also reported[14-18]. However, few comprehensive studies of all four halogen elements and their spectral interferences have been found in the literature.

6.1 Experimental

All the measurements were carried out with a Finnigan Element 2 (Finnigan, Bremen, Germany) high resolution inductively coupled plasma sector-field mass spectrometer. The instrument is equipped with a double focusing mass analyzer using reversed Nier-Johnson geometry. The system allows three pre-defined nominal mass resolutions ($m/\Delta m$) of 300, 4,000, and 10,000 by means of selectable slits. The actual mass resolutions vary between 300-500 for low, 3,500-4,500 for medium, and 8,000-14,000 for high-mass resolution mode depending on the optimization of parameter settings.

Samples were introduced into the plasma through a PFA micro-concentric nebulizer and a PFA spray chamber (Elemental Scientific, Omaha, NE). Passive aspiration was used to improve the stability of the ion beam and eliminate possible memory effects from the PVC tubing of the peristaltic pump.

RF Power	1150-1450 (Watts)
Sample uptake rate	100-150 (□l min^{-1})
Plasma gas flow	17.0 (l min^{-1})
Auxiliary gas flow	0.87 (l min^{-1})
Nebulizer gas flow	0.9-1.1 (l min^{-1})
Additional gas flow	0.05-0.15 (l min^{-1})
Nebulizer	PFA microconcentric nebulizer
Spray chamber	PFA spray chamber (room temperature)
Sampler	Platinum 1.1 mm aperture diameter
Skimmer	Platinum 0.8 mm aperture diameter
Torch position	Optimized daily
Guard electrode	Yes
Acquisition mode	E-scan; electric scanning over small mass ranges
Number of scans	10
Number of acquisition points	20
Acquisition window (%)	100
Search window (%)	100
Integration window (%)	60
Dwell time per sample (ms)	50

Table 6.1 HR-ICP-MS operating conditions and measurement parameters

The typical instrument conditions and measurement parameters used throughout the work are listed in Table 6.1. These conditions are optimized daily by using a 1.0 ng ml^{-1} multi-element standard tuning solution containing Li, B, Na, Al, Sc, Fe, Co, Ga, Y, In, Rh, Ba, Lu, Tl and U. An accurate mass calibration at the beginning of the measurement session was routinely performed for low resolution (LR), medium resolution (MR), and high resolution (HR) modes using the same tuning solution.

Reagents and standards

Deionized water was prepared by passing distilled water through a Milli-Q water system (Millipore Corporation, Bedford, MA) to a resistivity of 18 MΩ cm^{-1} and was used throughout for rinsing and solution preparations. Ultra-pure grade nitric acid (Optima, Fisher Scientific, Fair Lawn, NJ) was used throughout. A 5% (v/v) ammonium hydroxide solution was prepared by diluting 5 ml of concentrated ammonium hydroxide solution (Fisher Scientific, Fair Lawn, NJ) to 100 ml with deionized water.

A stock standard solution of fluorine (10,000 µg ml^{-1}) was prepared by dissolving an appropriate amount of NH_4F (Sigma-Aldrich, St. Louis, MO, USA) in 100 ml deionized water. Calibration standards of fluorine were prepared by serial dilutions of the 10,000 µg mL^{-1} stock standard in deionized water. The calibration standards of Br, Cl, and I were prepared by serial dilutions of 1000 µg mL^{-1} stock standard solutions purchased from Inorganic Venture (Lakewood, NJ) in 5% (v/v) ammonium hydroxide solution.

All the organic compounds used in this study were purchased from Sigma-Aldrich (St. Louis, MO). The drug substances used in the experiments were from Merck Research

Laboratories (Merck and Co. Inc, Rahway, NJ). The structures of the compounds are not relevant to the study and therefore are not revealed.

Samples preparation

Fluorine analysis

Solid samples were prepared by weighing approximately 100 mg of sample into a 10 ml volumetric flask, and bringing to volume with either deionized water, concentrated nitric acid or acetonitrile depending on solubility. Further dilutions were always performed in deionized water as needed to bring the sample concentrations within the linear range of the calibration curve.

Chlorine, bromine, and Iodine analysis

Solid samples were prepared by weighing approximately 100 mg of sample into a 10 ml volumetric flask, and bringing to volume with deionized water, concentrated nitric acid or acetonitrile depending on solubility. Further dilutions were always performed in 5% (v/v) ammonium hydroxide solution to bring the sample concentrations within the linear ranges of the calibration curves.

6.2 Results and discussion

6.2.1 Fluorine detection

Fluorine cannot be directly determined by conventional quadrupole ICP-MS because of intense water-derived spectral interferences and extremely low sensitivity. High resolving powers combined with high sensitivity of the sector-field ICP-MS affords

us another chance to reliably and accurately determine the fluorine contents in organic compounds and drug substances from sub-ppm to percentage levels.

In the experiments, the instrument was operated under hot plasma conditions as shown in Table 6.1 using the CD-1 guard electrode option. A low-flow (~100 µl min^{-1}) self-aspirating PFA capillary nebulizer and a PFA spray chamber were used to introduce the sample into the plasma. Fluorine is measured as F^+ (m/z 18.998) ion. Medium resolution is required to resolve $^{19}F^+$ from interference species such as $^1H_3{}^{16}O^+$, $^1H_2{}^{17}O^+$, $^1H_3{}^{18}O^+$, and $^{38}Ar^{++}$. The medium resolution ($m/\Delta m$ = ~ 4,000) ICP-MS spectrum of fluorine ion resolved from interferences at m/z 19 are given in figure 6.1. It is clearly shown that at a resolution of about 4,000, $^{19}F^+$ can be confidently baseline-resolved from all its interferences.

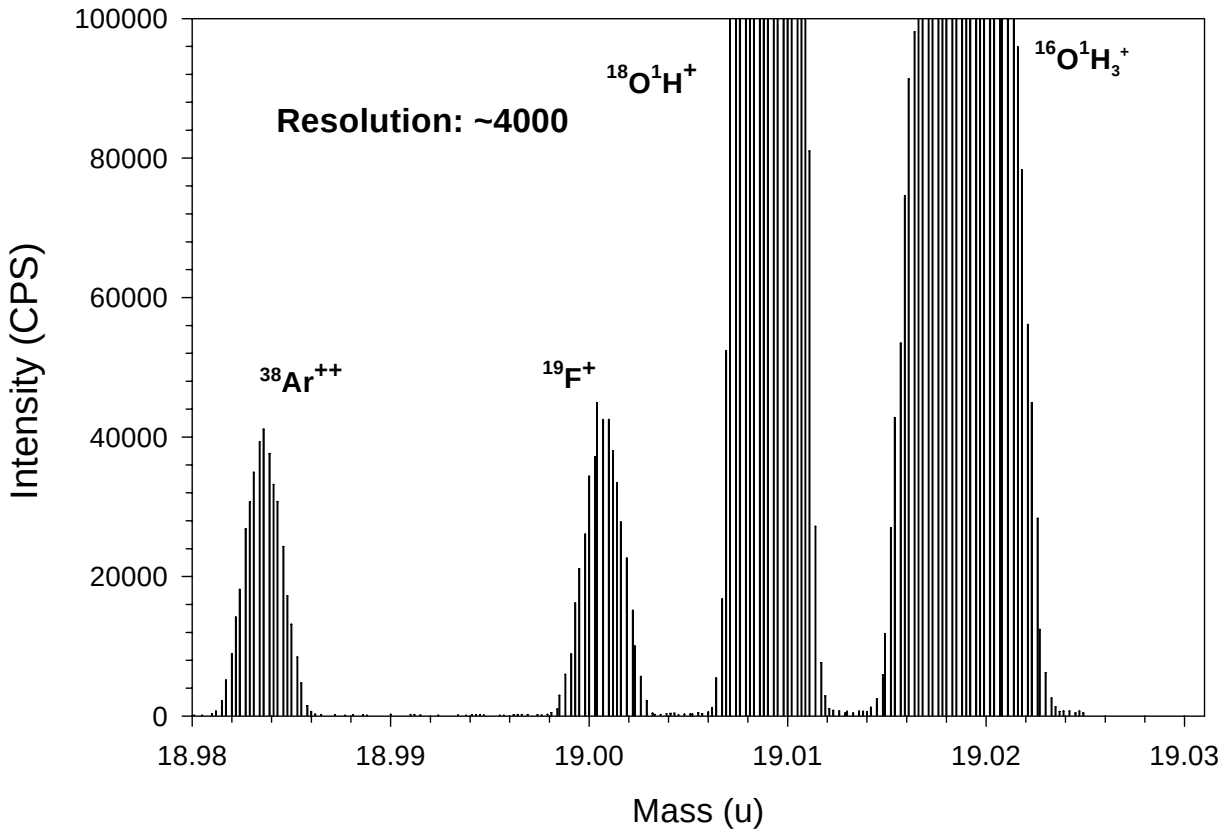

Figure 6.1 HR-ICP-MS spectrum of fluorine ion resolved from interfering species at m/z 19

An external calibration curve of $^{19}F^{+}$ is shown in Figure 6.2. Standards used were 200, 500, and 1,000 μg ml^{-1} prepared by serial dilution of a 10,000 μg ml^{-1} stock standard solution. The measured signal intensity of $^{19}F^{+}$ under the current experiment conditions is approximately 30 cps ppm^{-1} (or 30 cps per μg ml^{-1}), whereas the signal intensity of $^{23}Na^{+}$

under similar conditions (m/z = 23, m/Δm = ~ 4,000, hot plasma conditions) is roughly 6 x 10^7 cps ppm^{-1}, approximately 2 million times higher than that of $^{19}F^+$.

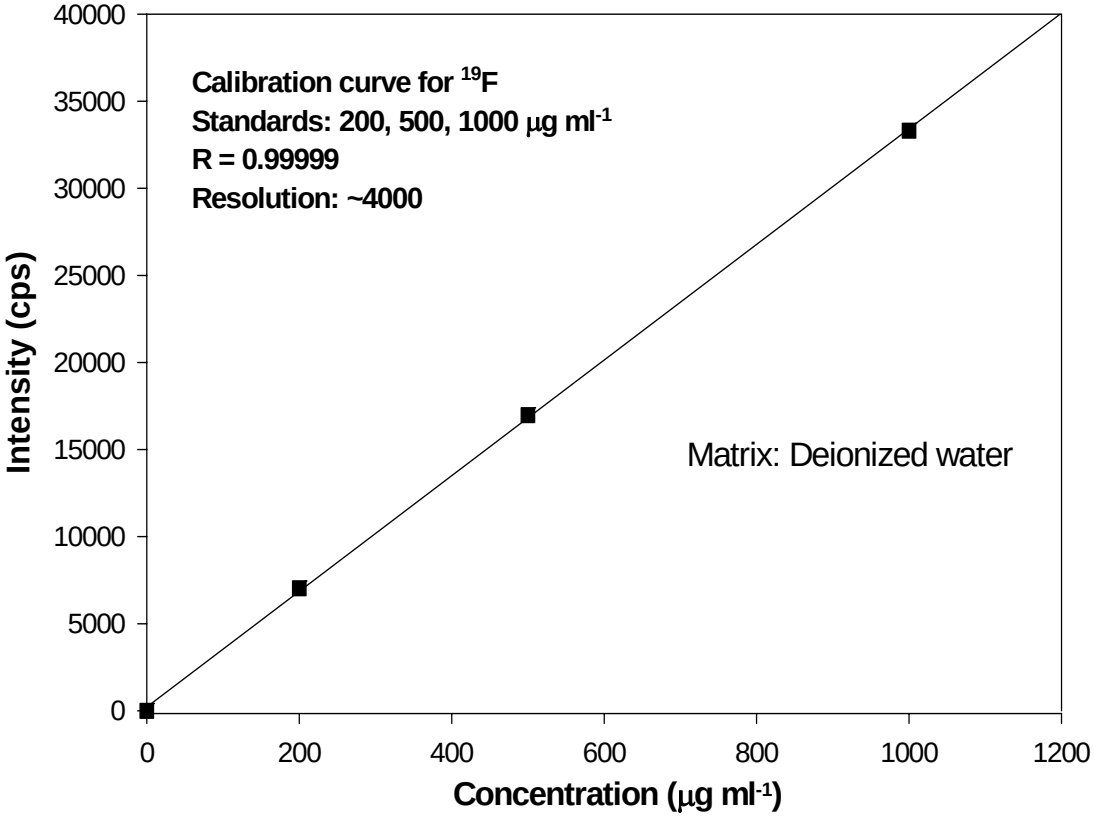

Figure 6.2 Calibration curve of fluorine ion in deionized water

6.2.2 Chlorine, bromine and Iodine detection

Compared to fluorine, sensitivities are less of an issue than spectral interferences for these three elements. Table 6.2 lists all of the major spectral interferences and the resolution required to resolve them for all the isotopes of fluorine, chlorine, and bromine. Iodine was not listed since it does not suffer major interferences from plasma-derived species like the other halogen elements. $^{37}Cl^+$ determination is very important to the

isotope ratio measurement. However, the accurate ICP-MS determination of $^{37}Cl^{+}$ is difficult with quadrupole ICP-MS because of the interference from $^{36}Ar^{1}H^{+}$. Figure 6.3 shows the comparison of $^{37}Cl^{+}$ spectrum at medium resolution and at high resolution. Clearly, at medium resolution $^{37}Cl^{+}$ analyte and $^{36}Ar^{1}H^{+}$ interference cannot be totally baseline separated, while high resolution is adequate to avoid the overlap. However, unless zinc ($^{70}Zn^{++}$) and germanium ($^{70}Ge^{++}$) are present at significant levels, medium resolution is more than adequate to ensure an interference-free determination of $^{35}Cl^{+}$ as shown in Figure 6.4. For comparison, the high resolution spectrum of ^{35}Cl is also given in Figure 6.4. Similarly, high resolution is required to fully resolve $^{81}Br^{+}$ from the interference of $^{40}Ar^{40}Ar^{1}H^{+}$ as shown in Figure 6.5. Theoretically speaking, ^{79}Br suffers interference from $^{40}Ar^{38}Ar^{1}H^{+}$. Upon close examination of the medium and high resolution spectra of ^{79}Br in Figure 6.6 and Figure 6.7, it is clear that the formation of $^{40}Ar^{38}Ar^{1}H^{+}$ under the current experimental conditions is extremely minimal. From the close-ups of the $^{79}Br^{+}$ spectra at both medium and high resolutions, the intensities of $^{40}Ar^{38}Ar^{1}H^{+}$ are only about less than 0.3% of that of the $^{79}Br^{+}$. Since the spectra in Figure 6.6 and Figure 6.7 were obtained from 100 ng ml^{-1} bromine solution, the contribution of $^{40}Ar^{38}Ar^{1}H^{+}$ to $^{79}Br^{+}$ is only about less than 0.3 ng ml^{-1}, which is the detection limit of $^{79}Br^{+}$ at medium resolution, as will be shown later in this paper. Therefore, it is safe to say that the use of medium resolution for the determination of $^{79}Br^{+}$ is acceptable under the current operating conditions. As for $^{127}I^{+}$, it is mono-isotopic and the spectral interferences are not a big concern unless $^{89}Y^{+}$ ($^{89}Y^{38}Ar$), $^{87}Sr^{+}$ ($^{87}Sr^{40}Ar$), $^{87}Rb^{+}$ ($^{87}Rb^{40}Ar$), $^{91}Zr^{+}$ ($^{91}Zr^{36}Ar$), $^{111}Cd^{+}$ ($^{111}Cd^{16}O$), and $^{109}Ag^{+}$ ($^{109}Ag^{18}O$), are present at significant levels in the samples.

Isotope	Mass	Main Interference	Mass	Resolution Required
^{19}F	18.9984	$^{38}Ar^{++}$	18.98137	1116
^{19}F	18.9984	$^{1}H^{18}O$	19.00699	2212
^{19}F	18.9984	$^{1}H_2{}^{16}O^{1}H$	19.0184	950
^{35}Cl	34.96885	$^{18}O^{16}O^{1}H$	35.0019	1058
^{37}Cl	36.9659	$^{1}H^{36}Ar$	36.97538	3899
^{79}Br	78.91834	$^{40}Ar^{38}Ar^{1}H$	78.93294	5405
^{81}Br	80.91629	$^{40}Ar^{40}Ar^{1}H$	80.93259	4964

Table 6.2 Resolution required to separate analyte ions from interfering ions

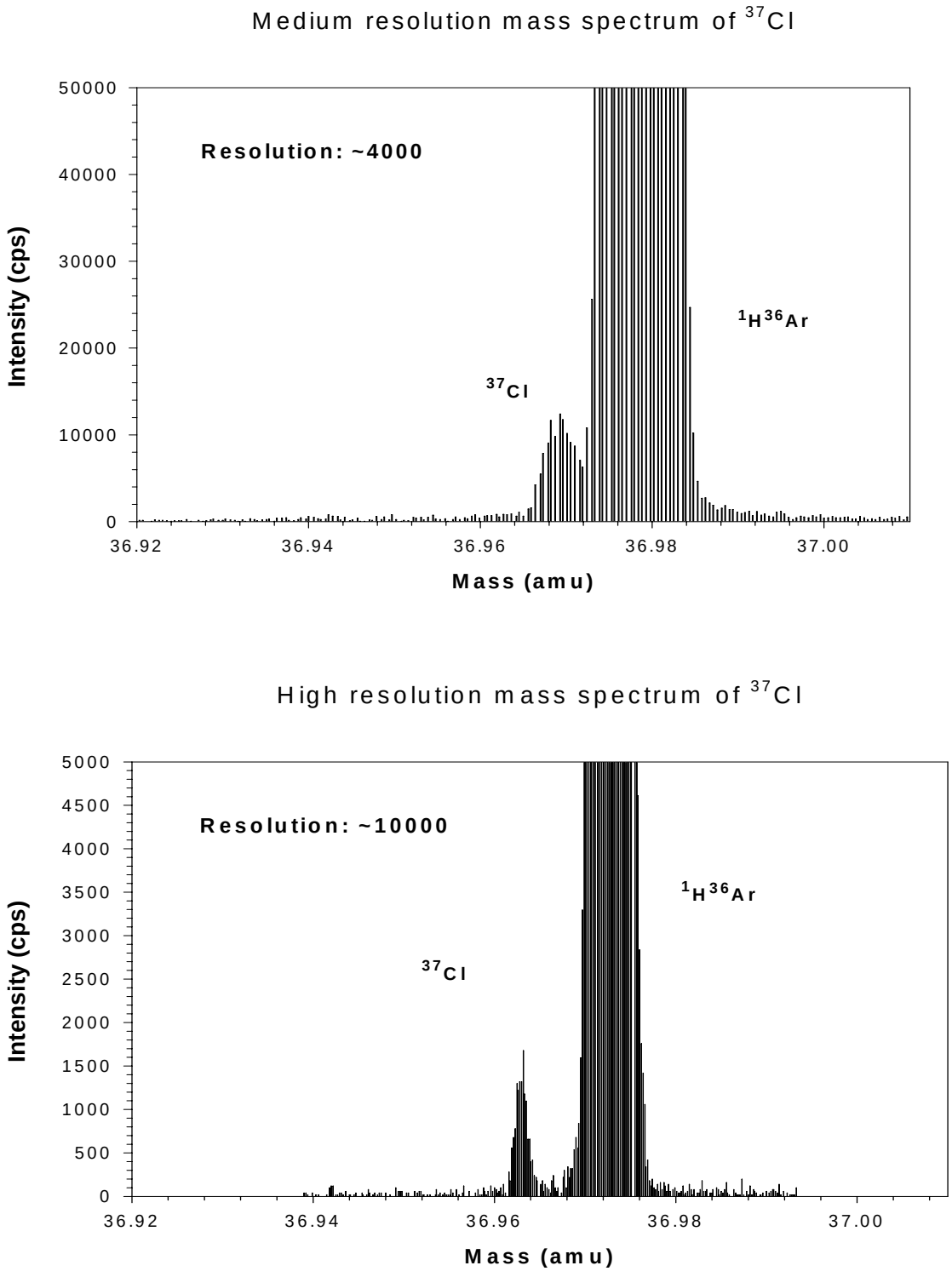

Figure 6.3 HR-ICP-MS spectral comparison of ^{37}Cl at medium and high resolution modes

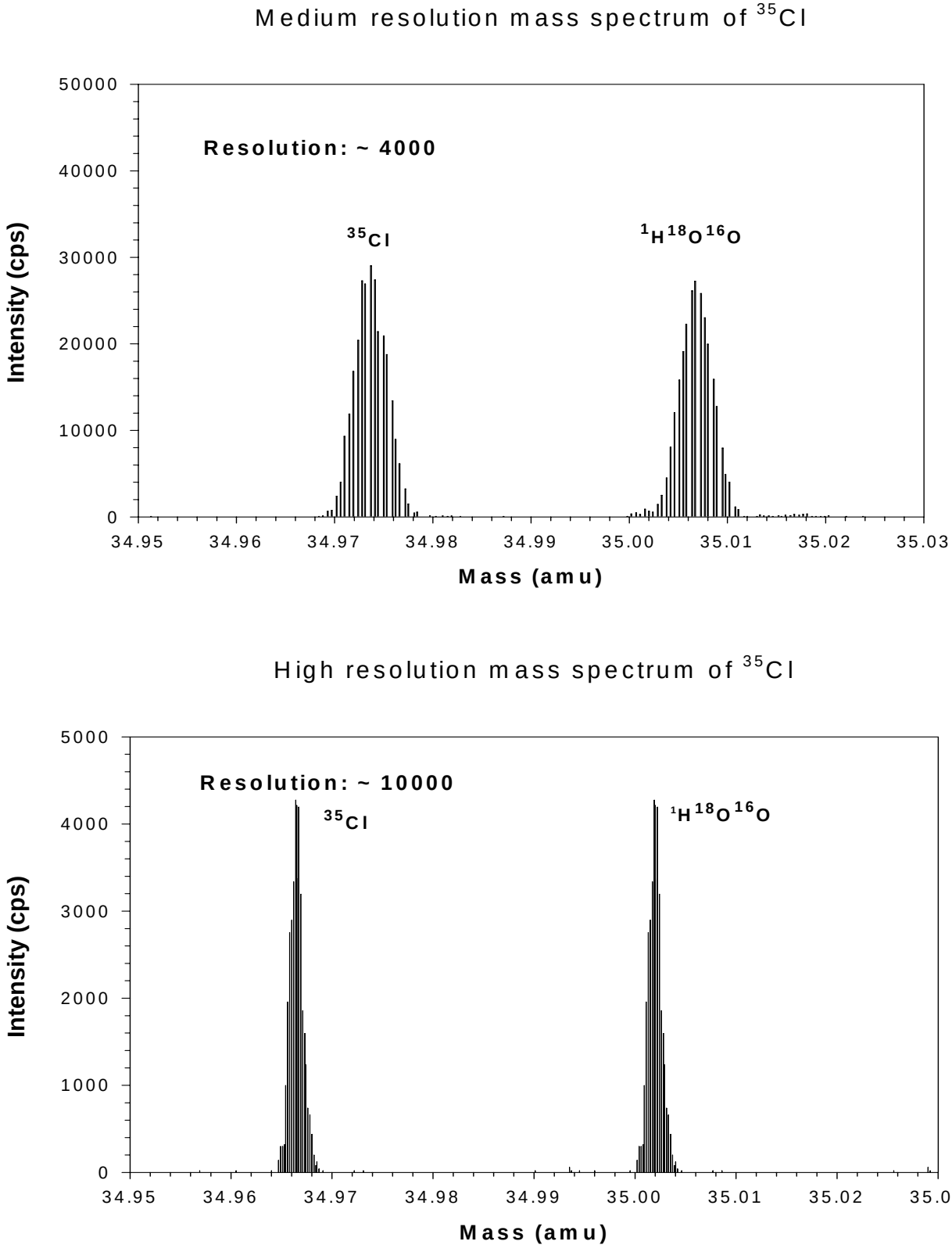

Figure 6.4 HR-ICP-MS spectral comparison of ^{35}Cl at medium and high resolution modes

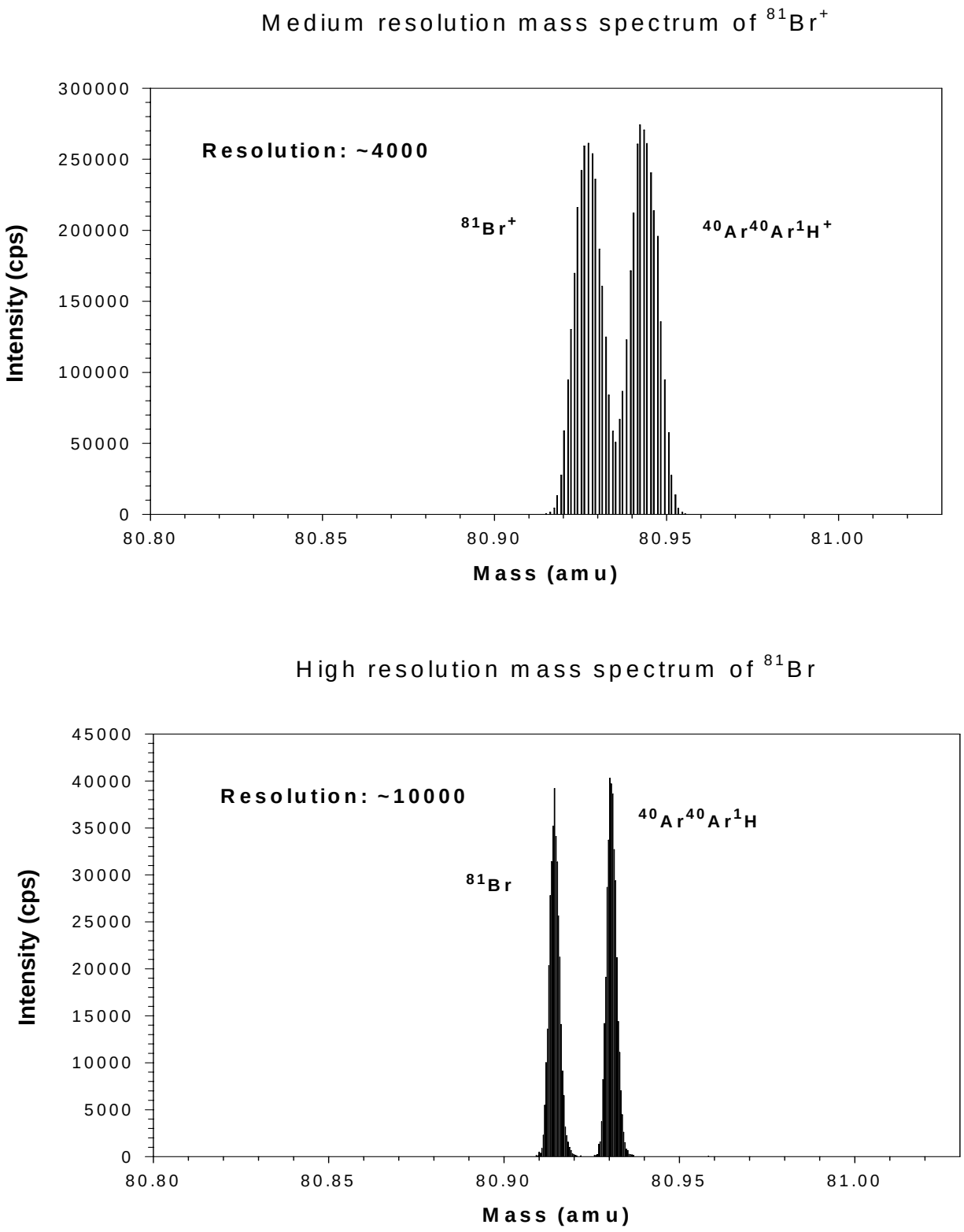

Figure 6.5 HR-ICP-MS spectral comparison of ^{81}Br at medium and high resolution modes

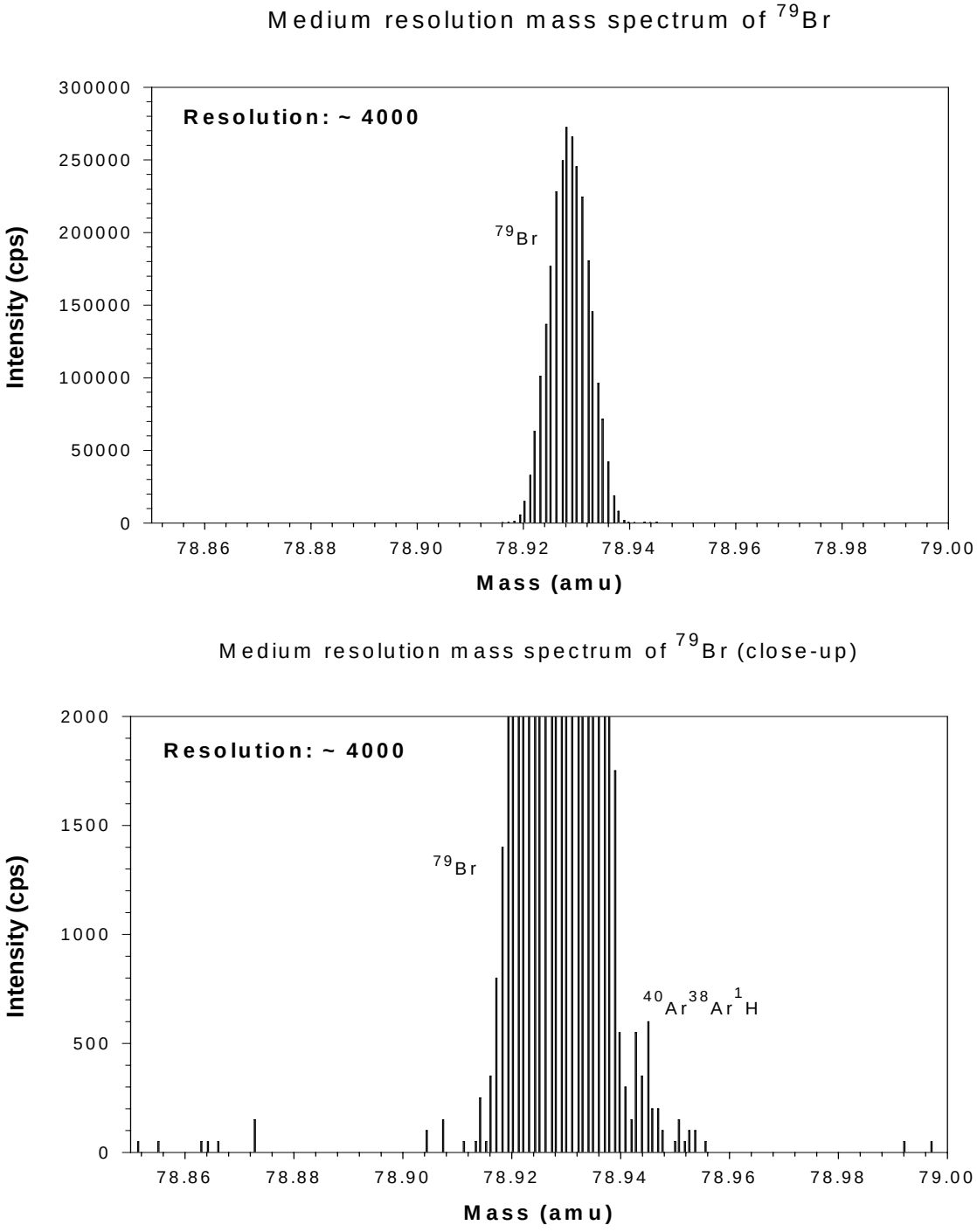

Figure 6.6 HR-ICP-MS spectrum of ^{79}Br at medium resolution

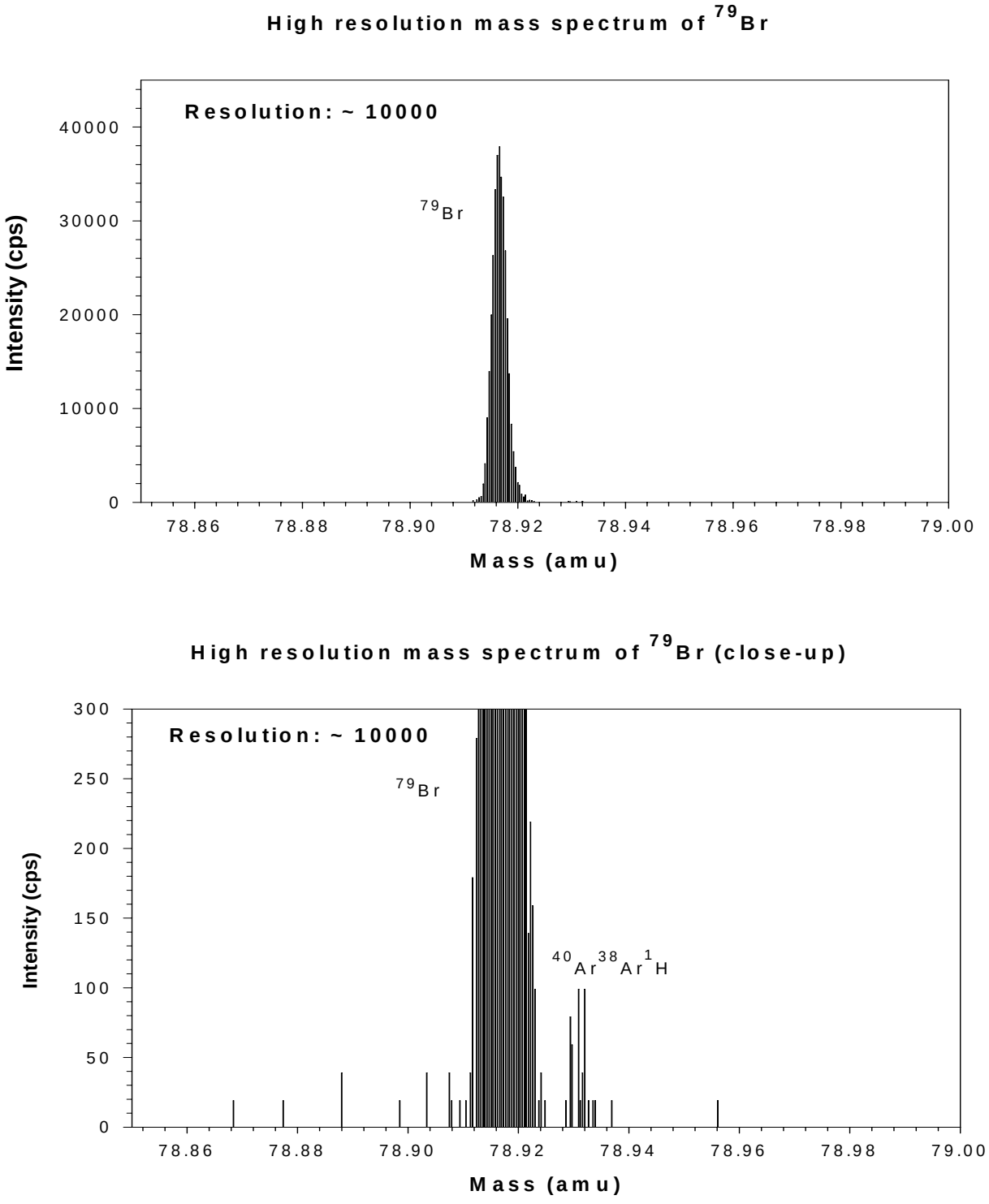

Figure 6.7 HR-ICP-MS spectrum of ^{79}Br at high resolution

The calibration curves for chlorine, bromine, and iodine are given in Figure 6.8, Figure 6.9 and Figure 6.10, respectively.

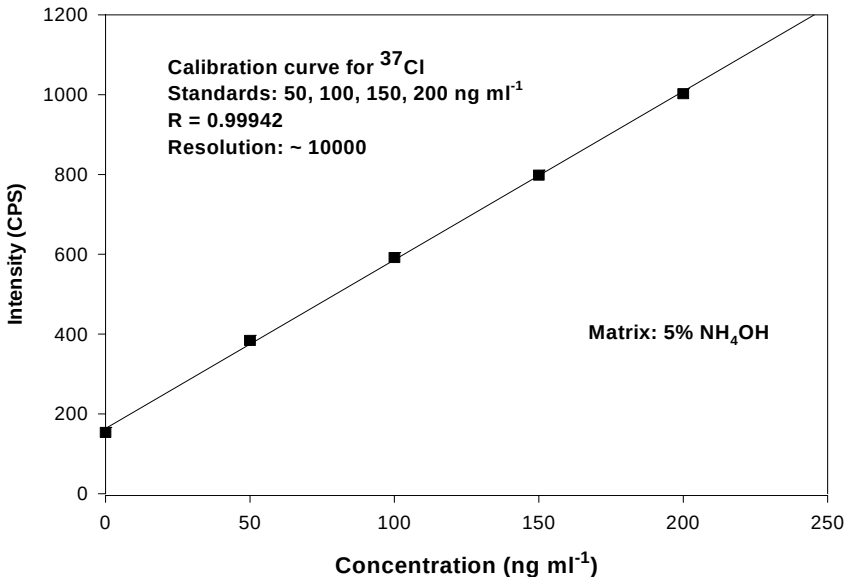

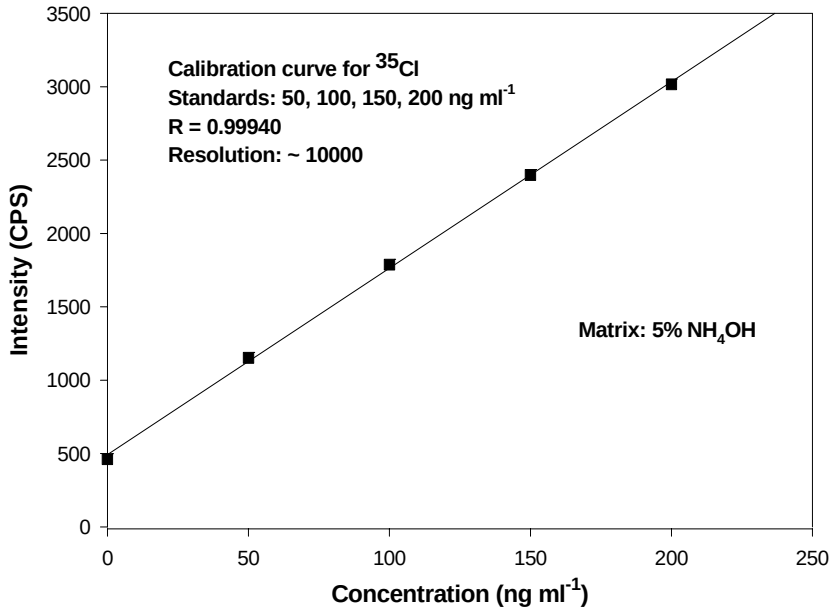

Figure 6.8 Calibration curve of Cl in 5%NH_4OH

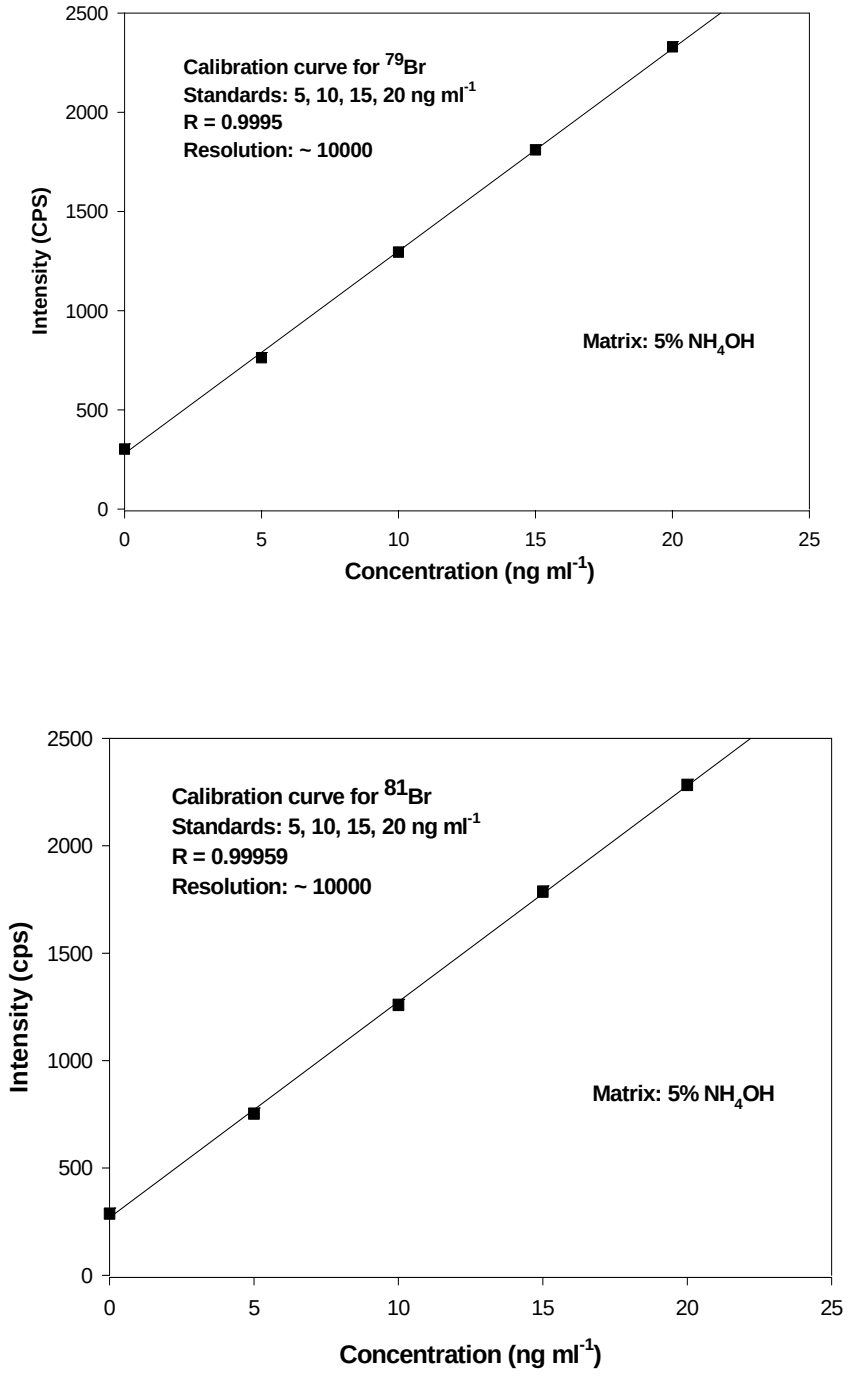

Figure 6.9 Calibration curve of Br in 5%NH_4OH

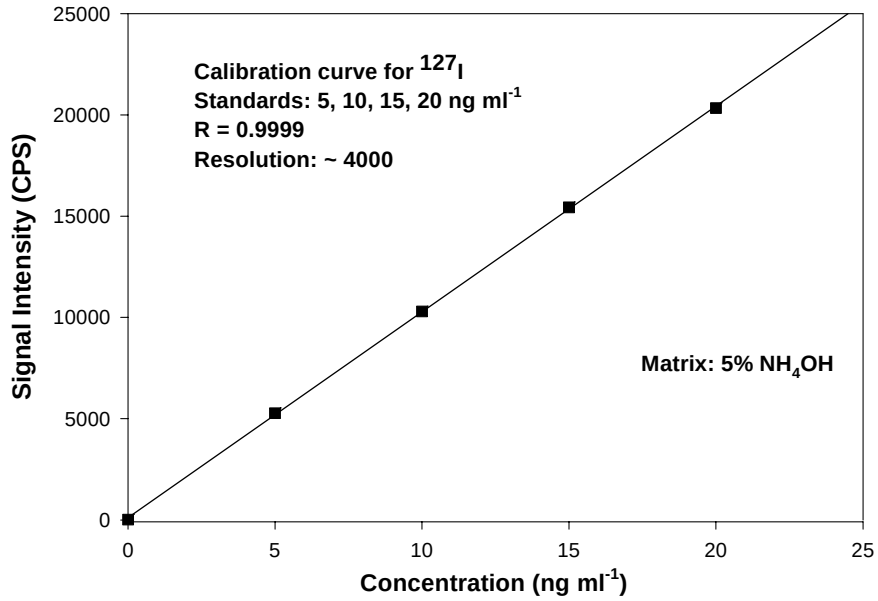

Figure 6.10 Calibration curve of I in 5%NH_4OH

6.2.3 Solvent selection

Since halogen elements are known for their severe memory effects if nebulizer based sample introduction systems are used[19, 20], more attention should be paid to this aspect in the selection of solvents. The memory effects of these four elements in 20% and 5% nitric acid solutions, deionized water, and in 5% ammonium hydroxide solution were evaluated by studying their wash-out behaviors. The wash-out experiments were carried out by continuously measuring and monitoring the signal intensity variations with time for these four halogen ions while aspirating appropriate blank solutions immediately after various halogen element standard solutions were aspirated. The wash-out curves of ^{19}F

(200 μg ml^{-1}), ^{35}Cl (200 ng ml^{-1}), ^{79}Br (50 ng ml^{-1}), and ^{127}I (50 ng ml^{-1}) are given in Figure 6.11, 6.12, Figure 6.13, and Figure 6.14, respectively.

It is demonstrated clearly in the four figures that the memory effects of all four elements can be eliminated effectively by rinsing the system with 5% ammonium hydroxide solution. It only takes about 120 seconds wash time to bring the intensities of the four elements down to as low as 0.1% of their original levels. It is also conclusive that the less acidic the solution is, the more effective the wash-out of the four elements will be. Unlike the other three elements, deionized water is almost as effective as 5% ammonium hydroxide for ^{19}F. This is the reason why if only fluorine was to be determined, deionized water was used in both sample and standard preparations for convenience and simplicity. If one or more of the other three elements are to be determined together with fluorine, the use of 5% ammonium hydroxide makes more sense. From Figure 6.12, it is shown that chlorine presents the most severe memory effect in 20% nitric acid. Even after a 10 minute wash, as much as 30% of the counts of the original 200 ng ml^{-1} ^{35}Cl remains, whereas only about 0.1% of the counts of the original standard solution remains if 5% ammonium hydroxide solution is used as the wash solution in merely about 2 minutes. Although not as effective as for ^{19}F, it takes less than 3 minutes to wash down to about 1% of their original signal intensities of the other 3 elements with deionized water as shown in Figure 6.12, 6.13 and 6.14.

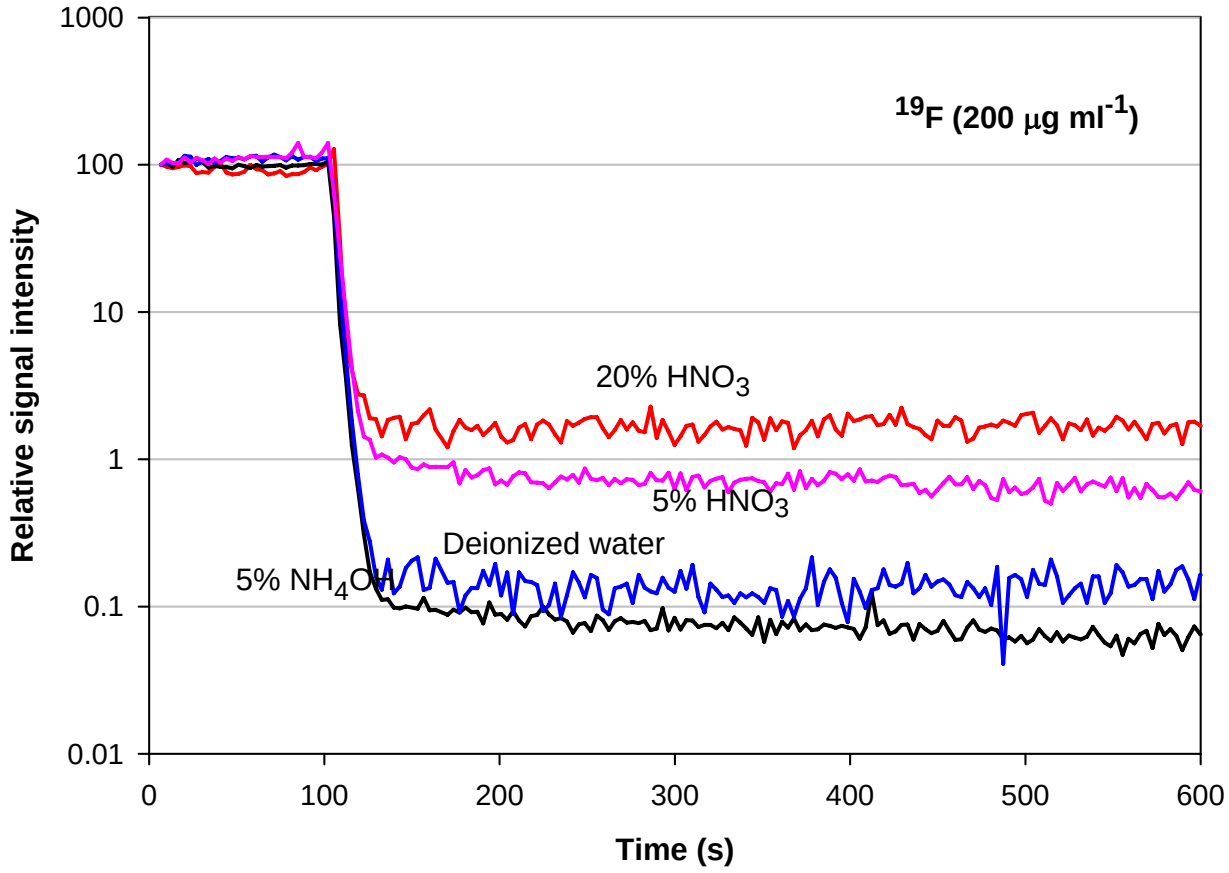

Figure 6.11 Wash-out curve for ^{19}F in various matrices (200 µg ml^{-1})

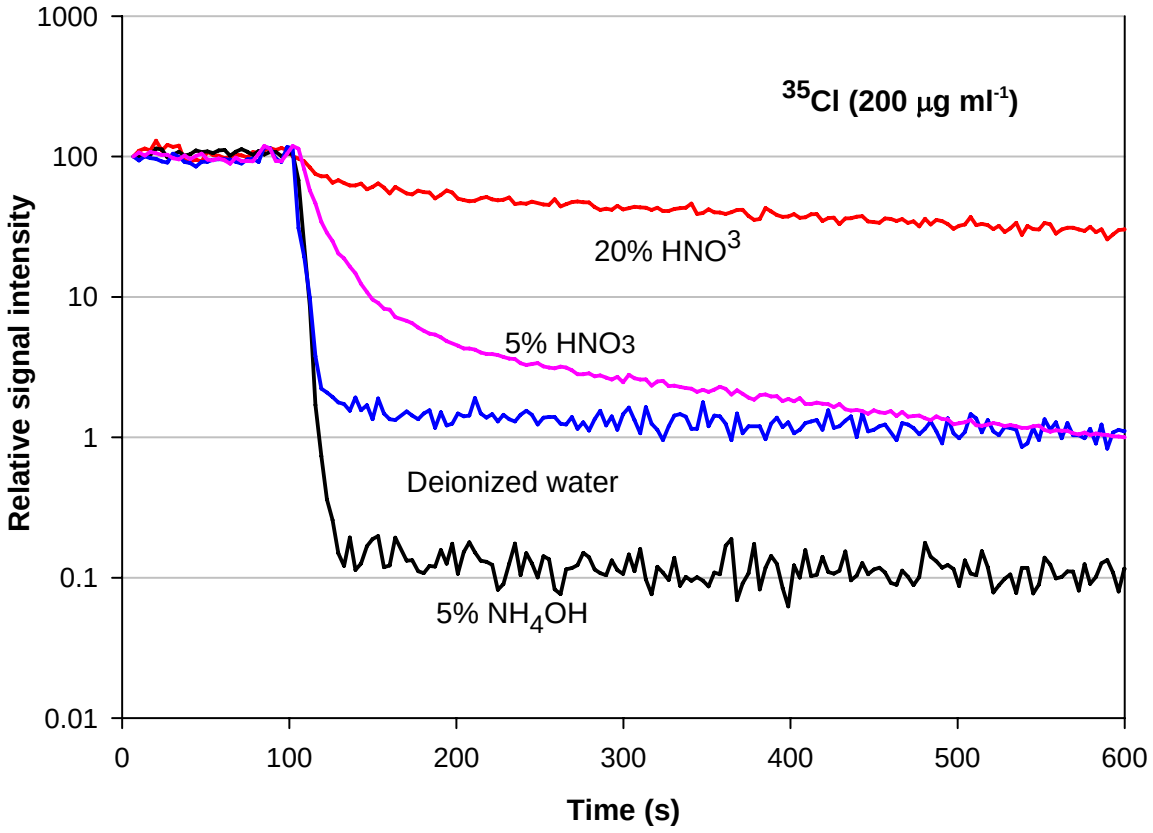

Figure 6.12 Wash-out curve for ^{35}Cl in various matrices (200 ng ml^{-1})

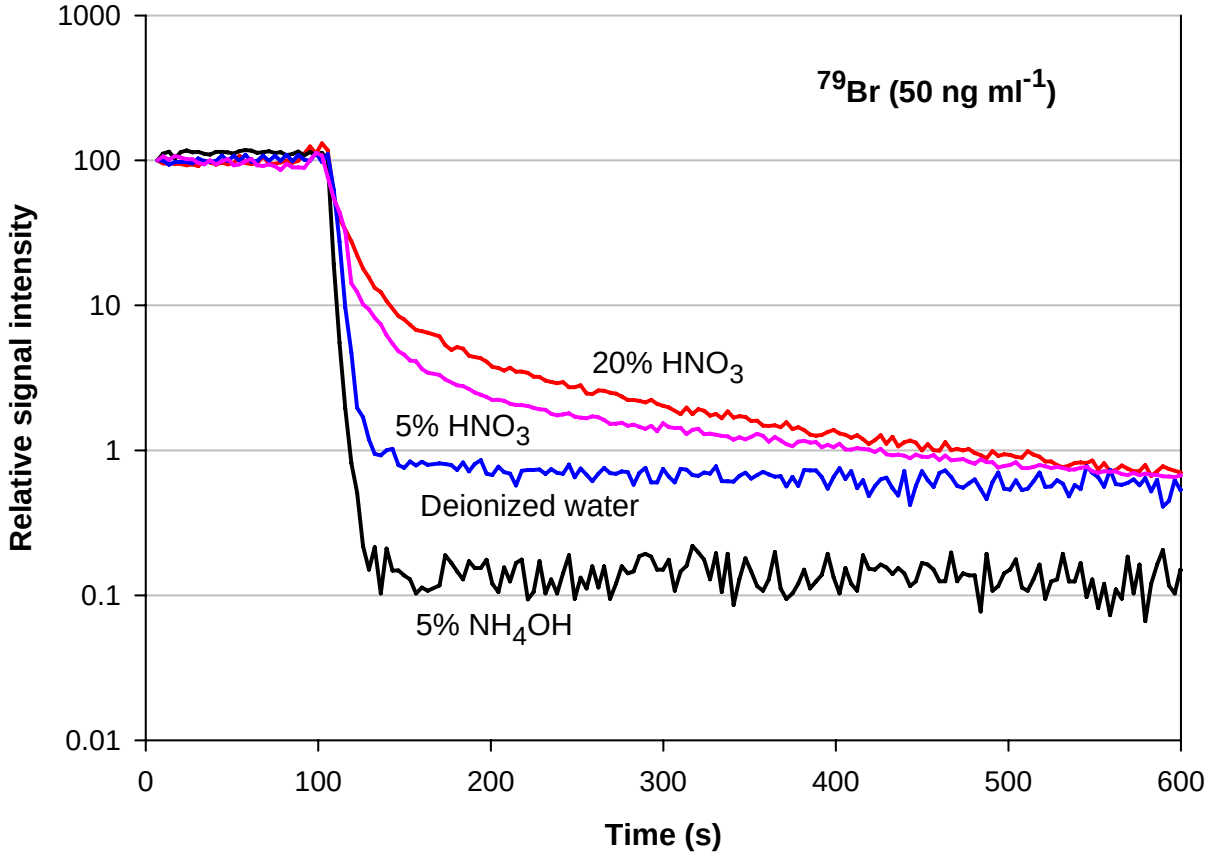

Figure 6.13 Wash-out curve for ^{79}Br in various matrices (50 ng ml^{-1})

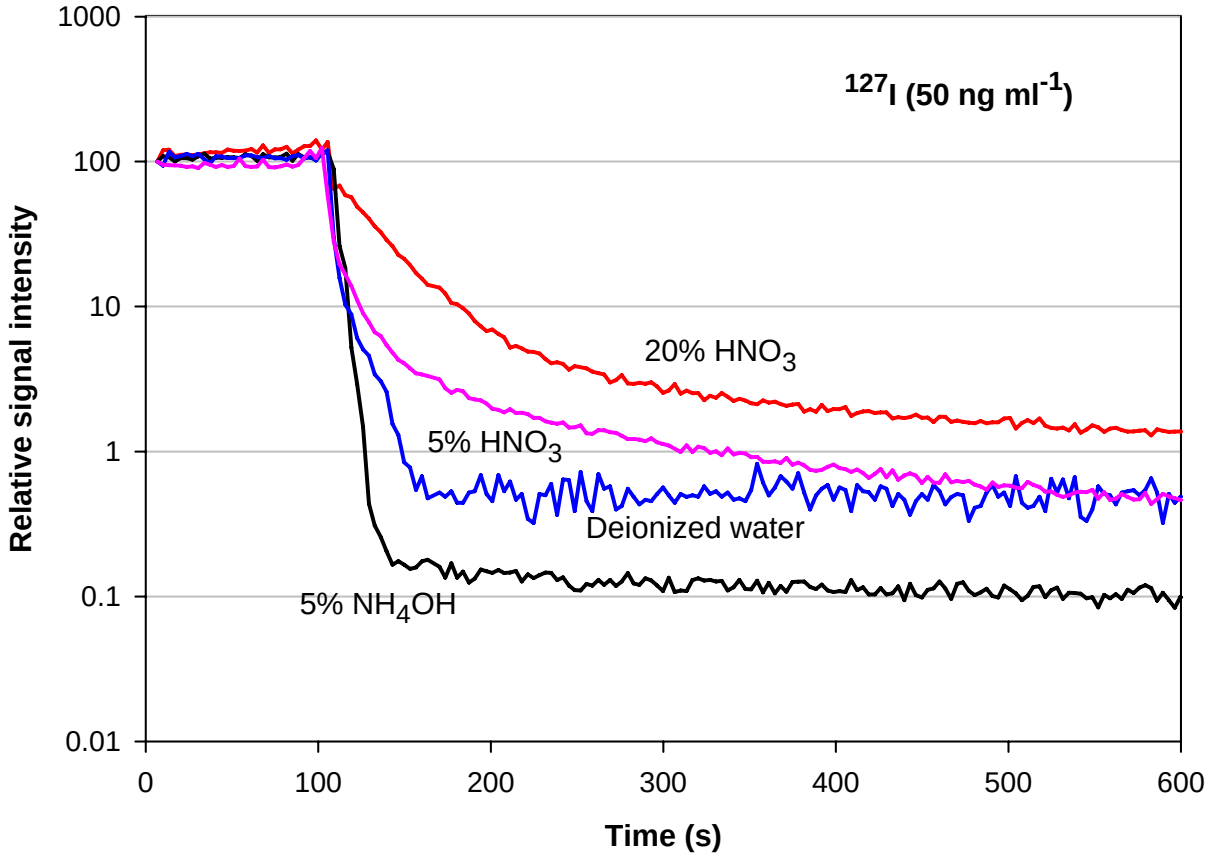

Figure 6.14 Wash-out curve for ^{127}I in various matrices (50 ng ml^{-1})

The effects of the same four solvents on the relative sensitivities of these four ions are shown in Figure 6.15. All the signal intensities in various solvents were obtained under optimized operating conditions, i.e. after each solvent-switching the system was always re-optimized before the next measurement was taken. Since the signal intensities were normalized, the inclusion of ^{37}Cl and ^{81}Br is redundant. It is also obvious that in deionized water all four elements exhibit highest intensities under optimized operating conditions.

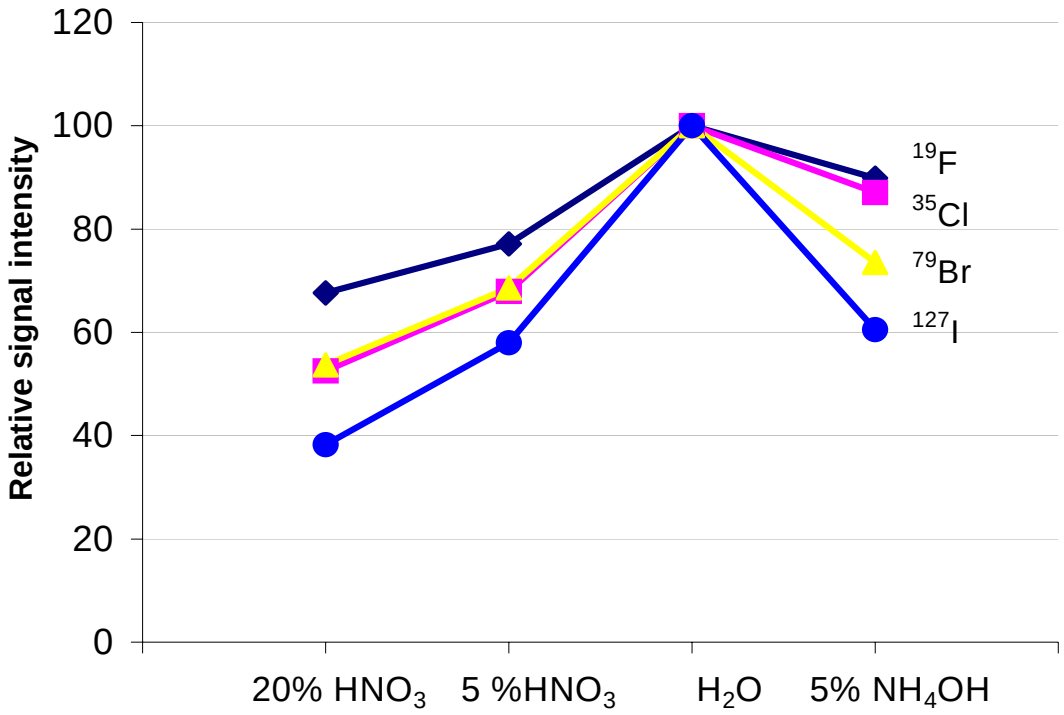

Figure 6.15 The effects of solvents on the sensitivities of the halogen elements (F, Cl, Br, and I).

Taking into account of both sensitivity and memory effects, it is obvious that deionized water is the most appropriate solvent for the determination of F if the solubilities of the compounds permit. However, for the determinations of Cl, Br, and I, 5% ammonium hydroxide solution is a better choice than deionized water due to the superior wash-out behaviors of 5% ammonium hydroxide solution for these three elements, although all three elements have slightly better sensitivities in deionized water. For simplicity and matrix matching, in addition to sample preparations, 5% ammonium hydroxide solution is also used to prepare calibration blanks, working calibration standards, and also serves as the rinsing solution whenever the determination of any or all these three elements is required.

6.2.4 The effects of nebulizer gas flow rate and ICP RF power

Nebulizer gas flow rate is one of the key plasma operating parameters affecting analyte ion signal intensities in ICP-MS. In the present work, the effect of nebulizer gas flow rate on the signal intensities of these elements was evaluated. The results are given in Figure 6.16. For easy viewing and comparison, all ion intensities were normalized in the figure. Nebulizer gas flow rate was varied in steps of 0.025 l min^{-1}, and a 30-second delay was included in the running sequence after each flow rate change in order for the plasma to stabilize. As shown in the figure, at a fixed RF power of 1250 Watts, the optimum nebulizer gas flow rates for F and Cl, were achieved at 0.8 and 0.85 l min^{-1}, and Br and I at 0.875 l min^{-1}, respectively. This correlates well with the ionization potentials of these elements since higher nebulizer gas flow rate leads to “cooler” plasma, and

fluorine possesses the highest ionization potentials of these elements thus needing the "hottest" plasma at relatively low nebulizer gas flow rate.

The effects of RF power on the signal intensities of these elements are shown in Figure 6.16. The power was varied in steps of 25 Watts at a fixed nebulizer gas flow rate of 0.85 l min^{-1}. The highest signal intensities for F and Cl were achieved at about 1300 and 1225 Watts, respectively; while For Br and I the highest signal intensities were obtained at around 1100 to 1125 Watts. This is also consistent with the finding in the nebulizer gas flow rate experiments above. Similar to a lower nebulizer gas flow rate at fixed RF power, higher RF power at a fixed nebulizer flow rate also leads to "hotter" plasma, thus favoring elements in the decreasing order of F (17.14 eV), Cl (13.01 eV), I (10.45 eV), and Br (11.84 eV), almost the exact decreasing ionization potential order for these elements.

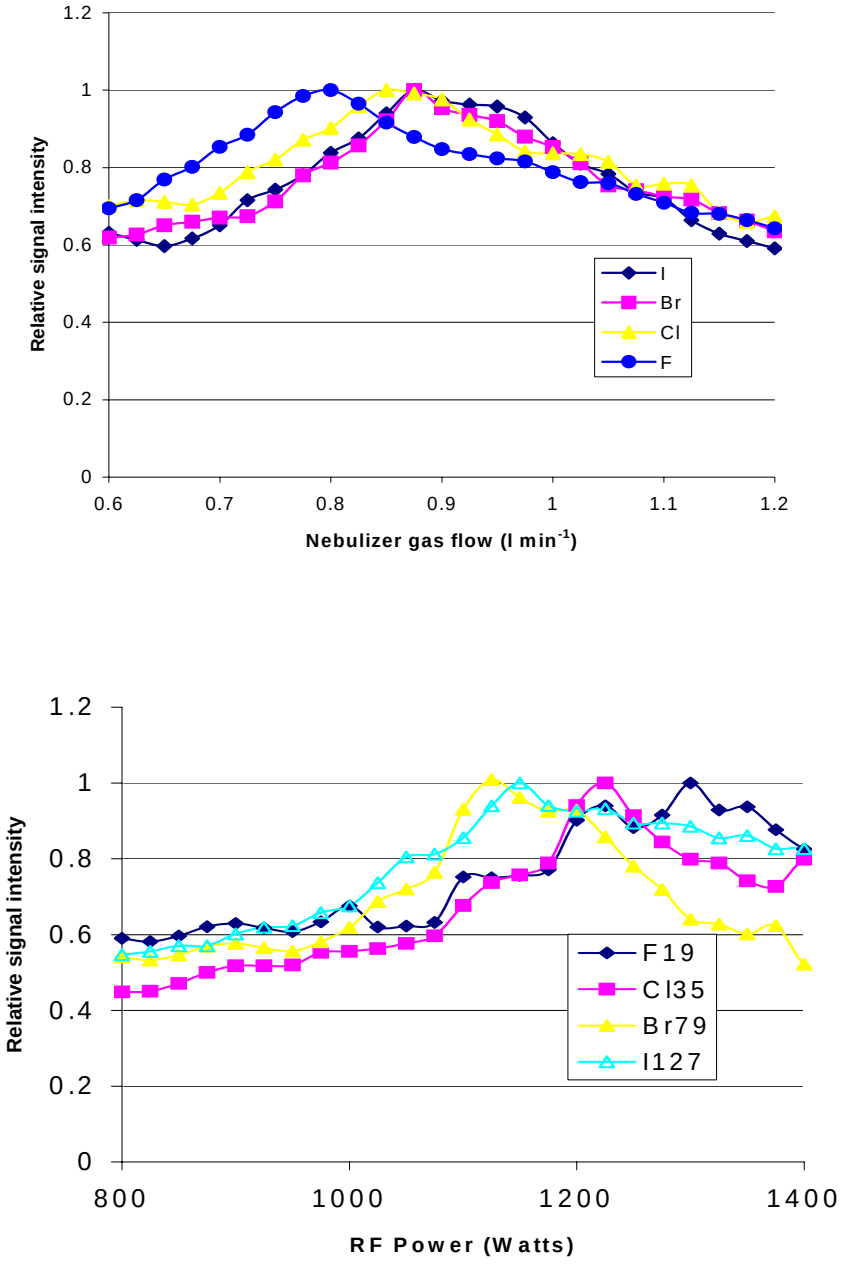

Figure 6.16 Upper: Effect of nebulizer gas flow rate on the intensities of different halogen elements Bottom: Effect of RF generator power on the intensities of different halogen elements

6.2.5 Instrumental limit of detection (LOD) and sensitivities

The instrumental limits of detection (LOD's) and sensitivities (counts per ng ml^{-1}) of all four halogen elements at medium (MR) and high (HR) resolution modes by HR-ICP-MS were evaluated and are listed in Table 3. The instrumental limits of detection (LOD's) for the four elements were estimated by analyzing ten replicate blank solutions as ten samples. The instrumental limit of detection (LOD) is defined as three times the standard deviation of the ten measurements. Sensitivities for the four elements were derived from analyzing 100 μg ml^{-1} F standard solution, 0.10 μg ml^{-1} Cl standard solution, 0.01 μg ml^{-1} Br and I standard solutions, respectively. As shown in Table 3, the best limits of detection (LOD) for F, Cl, Br and I are 5067, 3, 0.08 and 0.03 ng ml^{-1}, respectively. These are part per trillion (ppt) LOD's for Br, and I.

In Table 6.3, it is also interesting to note that although an increase in the mass resolution did lead to lower intensities for all four elements, this did not necessarily translate into high limits of detection. This is because higher resolution not only reduced the ion transmission but also the background transmission as well. For ^{19}F and ^{127}I , higher resolution resulted in slightly deteriorated limits of detection, whereas for ^{35}Cl and ^{79}Br, higher resolution yielded modestly improved limits of detection.

	MR		HR	
Element	Detection Limits (ng ml^{-1})	Sensitivity (counts per ng ml^{-1})	Detection Limits (ng ml^{-1})	Sensitivity (counts per ng ml^{-1})
^{19}F	5070	0.026	8530	0.003
^{35}Cl	7.01	69	3.25	15
^{37}Cl	N/A	N/A	4.18	6
^{79}Br	0.23	6630	0.08	126
^{81}Br	N/A	N/A	0.10	124
^{127}I	0.03	6970	0.05	1020

Table 6.3 Detection Limits and sensitivities in medium resolution(MR) and high resolution (HR) modes

6.2.6 Precision and accuracy

The precision of the methods used for the determination of F, Cl, Br, and I was estimated by analyzing 100 □g ml^{-1} F solution at medium resolution, 100 ng ml^{-1} Cl, Br, and I solutions at high resolution ten times as ten samples with rinsing in between. As described in the methods, the fluorine solution was prepared in deionized water, whereas the Cl, Br, and I solutions were prepared in 5% ammonium hydroxide solution. The

results are listed in Table 6.4. The relative standard deviations (RSD's) of the ten measurements varied from 1.5% to 3.6% for the four halogens.

In order to evaluate the accuracy and the extent of the matrix effect caused by an actual drug substance using these methods, three Merck compounds were chosen for this study. One of these compounds contained a percentage level of F, the second one percentage levels of Cl and Br, and the third one contained iodine in the molecule also at a percentage level. These compounds were dissolved and diluted such that the concentration of each of the four elements was approximately 100 to 200 ng ml^{-1} (F, □g ml^{-1}). These solutions were then spiked with 200 □g ml^{-1} F, 100 ng ml^{-1} Cl, Br, and I, and both spiked and unspiked samples were analyzed at appropriate mass resolutions. The results are given in Table 6.5. The spike recoveries ranged from 94% to 107%, except ^{35}Cl at medium resolution.

Replicate Number	Measured Result					
	^{19}F (MR) . □g ml^{-1})	^{35}Cl (HR) (ng ml^{-1})	^{37}Cl (HR) (ng ml^{-1})	^{79}Br (HR) (ng ml^{-1})	^{81}Br (HR) (ng ml^{-1})	^{127}I (HR) (ng ml^{-1})
1	99.6	101.1	98.3	108.3	99.3	103.1
2	97.6	100.4	95.8	100.2	95.9	101.5
3	98.2	98.5	96.6	98.7	95.6	99.3
4	99.2	97.9	94.7	97.3	98.5	102.2
5	102.5	93.3	92.0	97.5	98.8	99.2
6	101.2	102.6	101.9	105.4	101.8	102.2
7	98.9	98.8	100.2	101.1	97.5	103.3
8	99.1	98.0	99.3	99.7	99.5	103.8
9	100.8	101.6	102.3	104.3	98.3	99.9
10	98.2	97.6	102.2	102.0	98.6	94.5
Mean	99.5	99.0	98.3	101.5	98.4	100.9
SD	1.53	2.7	3.5	3.6	1.8	2.8
RSD(%)	1.54	2.73	3.56	3.55	1.83	2.78

Table 6.4 Precision of the methods for the determination of F, Cl, Br and I

Isotope	Original Sample ($ng\ ml^{-1}$)	Spiked Sample ($ng\ ml^{-1}$)	Recovery (%)
^{19}F (MR)	138 ($\mu g\ ml^{-1}$)	348 ($\mu g\ ml^{-1}$)	105
^{19}F (HR)	141 ($\mu g\ ml^{-1}$)	355 ($\mu g\ ml^{-1}$)	107
^{35}Cl (MR)	94	203	109
^{79}Br (MR)	120	219	99
^{127}I (MR)	119	216	97
^{35}Cl (HR)	92	203	111
^{37}Cl (HR)	91	200	109
^{79}Br (HR)	102	199	97
^{81}Br (HR)	101	203	102
^{127}I (HR)	115	216	101

Table 6.5 Spike recovery studies with actual Merck drug substances at both medium and high resolutions

To further validate the methods, eight commercially available organic compounds and nine Merck drug intermediates or active pharmaceutical ingredients containing one or more of the four elements were tested to determine the accuracy of the procedures. The results are given in Table 6.6 and 6.7. As can be seen from these Tables, most of the results are in excellent to reasonable agreement with the theoretical or known values. It is obvious that most results that are not in perfect agreement with theoretical or known values have lower than 100% recoveries. This can be easily explained by the presence of other impurities in the compounds.

Compound Name	F (%)		Cl (%)		Br (%)		I (%)	
	Theoretical or known	Measured	Theoretical or known	Measured	Theoretical or known	Measured	Theoretical or known	Measured
Pentafluorobenzoic Acid ($C_6F_5CO_2H$)	44.3	41.2 ± 0.52						
Tetrafluorohydroquinone (C_6F_4-1,4-$(OH)_2$)	40.9	40.9 ± 0.22						
2-Florocinnamic Acid ($FC_6H_4CH=CHCCCO_2H$)	11.2	10.98± 0.27						
2-Fluoro-6-iodobenzoic acid ($FC_6H_3(I)CO_2H$)	6.92	6.61± 0.14					46.3	44.2± 0.52
3',4' Dichloroacetophenone ($Cl_2C_6H_3COCH_3$)			37.1	38.2± 0.45				
5-Bromo-2-chlorobenzoic acid ($BrC_6H_3(Cl)CO_2H$)			14.8	14.2± 0.11	33.2	32.5± 0.62		
1,4-Dibromobenzene ($C_6H_4Br_2$)					66.4	64.2± 1.30		
3-Bromo-5iodobenzoic acid ($BrC_6H_3(I)CO_2H$)					24.0	24.6± 0.52	38.4	36.8± 0.75

Table 6.6 Accuracy and precision of determination of F, Cl, Br and I in organic compounds

Compound Name	F (%)		Cl (%)		Br (%)		I (%)	
	Theoretical or known	Measured	Theoretical or known	Measured	Theoretical or known	Measured	Theoretical or known	Measured
Merck compound #1	10.0	9.5± 0.12						
Merck compound #2	23.2	22.1± 0.19						
Merck compound #3	4.36	4.14 ± 0.08	8.13	7.85± 0.12				
Merck compound #4	4.13	3.67± 0.09	7.71	7.22± 0.21				
Merck compound #5			5.81	5.79 ± 0.09				
Merck compound #6	12.9	11.2± 0.017			27.2	26.2± 0.69		
Merck compound #7	17.7	15.4± 0.19						
Merck compound #8					35.7	33.9± 0.58		
Merck compound #9							31.2	33.2± 0.38

Table 6.7 Accuracy and precision of determination of F, Cl, Br and I in Merck drug compounds

6.3 Conclusion

HR-ICP-MS proves to be a powerful and rapid tool for the determinations of sub ppm to percent levels of all four halogen elements in organic compounds and drug substances. The samples can be easily prepared by dissolving them in appropriate solvents and then diluting them in either deionized water or 5% ammonium hydroxide solution. By applying medium to high resolution, major spectral interferences can be

easily isolated from the isotope of interest. In solution, the limits of detection were estimated to be 5 □g ml^{-1} for F, and 3.0, 0.08, and 0.03 ng ml^{-1} for Cl, Br, and I, respectively. Precise and accurate results have been obtained for eight commercially available compounds and nine Merck drug substances containing one or more of these four halogen elements. Undoubtedly, HR-ICP-MS has added one more arsenal to the development and discovery of new pharmaceutical products.

References

1. L.E. Vanatta and D.E. Coleman, Journal of Chromatography A, 1997, **770**, 105-114.
2. N. Jakubowski, L. Moens and F. Vanhaecke, Spectrochimica Acta Part B,1998 **53**, 739-763.
3. D. Stuewer and N. Jakubowski, J. Mass Spectrom. 1998, **33**,579-590.
4. F. Vanhaecke, Spectrochimica Acta Part B, 1998, **53**, 1739-1763.
5. F. Vanhaecke, Anal. Bioanal. Chem., 2002, **372,** 20-21.
6. L.E. Vanatta and D.E. Coleman, Journal of Chromatography A, 1997, **770**, 105-114.
7. K.E. Jarvis, A. L. Gary amd R. S. Houk, Handbook of ICP-MS, Blackie, Glasgow, 1999.
8. P. Evans, C. Wolff-Briche and B. Fairman, J. Anal. At. Spectrom., 2001, **16**, 964-969.
9. T. Prohaska, C. Latkoczy and G. Stigeder, J. Anal. At. Spectrom., 1999, **14**, 1501-1504.
10. M. Tran, Q. Sun, B. W. Smith, and J. D. Winefordner, Applied Spectroscopy, 2001, **55,** 739-744.
11. Y. Okamoto, J. Anal. At. Spectrom., 2001, **16**, 539-541

12. M. M. Bayon, A. R. Garcia, J. I. G. Alonso and A. Sanz-Medel, Analyst, 1998, **124**, 27-32.

13. B. Schnetger, Y. Muramatsu and S. Yoshida, Geostand. Nrwsl., 1998, **22**, 181-187.

14. N. Lihareva, P. Kosturkova and Ts. Vakarelska, Fresenius' J. Anal. Chem, 2000, **367**, 84-92.

15. H. Wildner, J. Anal. At. Spectrom., 1998, **13**, 573-578.

16. E.H. Larsen and M.B. Ludwigsen, J. Anal. At. Spectrom., 1997, **12**, 435-442.

17. R. J. Cox and C. J. Pichford, J. Anal. At. Spectrom., 1992, **7**, 635-641.

18. S. S. A. Buchert, Fresenius' J. Anal. Chem., 1996, **354**, 323-330.

19. H. Baumann, Fresenius' J. Anal. Chem., 1990, **338**, 809-817.

20. A. R. Date and M. E. Stuart, J. Anal. At. Spectrom., 1988, **3**, 659-667.

21. W. Kerl, J. S. Becker and H. Dietze, J. Anal. At. Spectrom, 1996, **11**, 723-726.

22. Y. K. Xiao, R. D. Vocke, Jr., G. H. Swihart, and Y. Xiao, Anal. Chem., 1997, **69**,

Chapter 7

High Precision Analysis of Enriched Stable Isotope Calcium Samples using a High Resolution Inductively Coupled Plasma Mass Spectrometer for metabolic Traces Study

7.0 Introduction

The competition among pharmaceutical companies is becoming fiercer and fiercer as every player wants to be the first to put an innovative and first in class blockbuster in the market. As a result, the pressures to accelerate the pharmaceutical development process have increased, and the process chemists and analytical chemists alike have been forced to come up with new chemical processes, process controls, and appropriate analytical tests on shorter and shorter timeframes. Like any other tests in pharmaceutical industry, metal tests (or elemental analysis) in pharmaceutical raw materials, intermediates, bulk drug substances, and final drug products, are indispensable, as are other impurity tests [1-12].

Metal in pharmaceutical materials may be inadvertently introduced in many ways, such as from raw materials, reagents, solvents; from electrodes, reaction vessels, plumbing and other equipment used in the synthesis; exposure to the air-borne particles; or from container/closure systems, etc. Most importantly, metals may be introduced

through the utilization of catalysts at various steps during the synthesis. Due to the ability of metals to catalyze decomposition and their potential for toxicity, metal content monitoring of process intermediates and final drug substances is widely employed[1-12].

Extreme sensitivity, wide element coverage, and accurate isotopic information provided by ICP-MS, particularly high resolution ICP-MS, can all be taken advantage of in supporting clinical trials in pharmaceutical research[13-14].

The most important and innovative aspect of ICP-MS is the possibility to greatly extend the use of isotopes as tracers in biomedicine, which originates from its ability to determine isotope ratios in biological samples using much simpler and faster procedures than before yet maintaining a precision sufficient enough for most biomedical applications.

Radioisotopes have been used widely as tracers to study bioavailability, fractional absorption, as well as the biological pathways and metabolic fate of experimental drugs. The advantages of using radioisotopes for these purposes include methodological simplicity and easy detection in blood, urine, and feces. Radiation exposure, however, is a potential hazard for patients, and particularly for infants and pregnant women if exposed to this study repeatedly. Enriched stable isotopes used as metabolic tracers have proven to be valuable in studies of the absorption and metabolism of minerals[15-16]. Unlike radioisotopes, they can be used in high-risk population groups such as infants, children, and pregnant or lactating women. The disadvantages of using stable isotopes include the requirement for isotope enrichment and the expenses associated with it, and the complexity of the analysis and the associated cost. With recent advances in instrumentation, both the analytical complexity and the cost have been reduced

dramatically. In the study, absorption of an element can be estimated by determining what fraction of a stable isotope or isotopes given as a tracer is absorbed. Utilization and retention may be investigated using one or more stable isotopes to follow metabolism and to determine pool sizes and turnover with kinetic studies and nutrient modeling.

In above studies, it is very important to accurately determine the isotopes amount of isotope used. ICP-MS has shown great potential to measure stable isotopes[17,18], which can be identified and measured using the molecular weight different from that of the original isotopes. One of the difficulties with using the instrument is numerous interferences that can hider the measurement of specific isotopes.

Among the commonly studied isotopes, Calcium isotopes are used at length in clinical research studies. In adults, calcium deficiency is strongly related to increasing severity of osteoporosis. In children, calcium deficiency is primarily related to the development of rickets. Calcium has six stable isotopes, which include 40Ca, 42Ca, 43Ca, 44Ca, 46Ca and 48Ca. Table 7.1 lists all of the major spectral interferences and the resolution required to resolve them for all the isotopes of Calcium. A regular conditioning quadrupole ICP-MS resolution is often not enough to separate the interferences from measured isotopes. Sturup[4] et al. were able to measure 42Ca/43Ca rations using high resolution magnetic sector ICP-MS to avoid interferences. Patterson[19] et al were able to measure ratios by using a quadrupole ICP-MS in a cool plasma mode, but noted that there are still interferences at 46 Ca and 48 Ca from Titanium. A low power condition along with a configuration to attenuate the secondary discharge has been shown to significantly reduce Ar-based interferences. One limitation using cool plasma is that the formation of matrix induced polyatomic ions is enhanced under cold plasma conditions.

Isotope	Natural abundance (%)	Interferences	Resolution required
^{40}Ca	96.941	40Ar+	192500
^{42}Ca	0.647	40ArH2+	2200
		$^{14}N_3^+$	830
^{43}Ca	0.135	$^{14}N_3H^+$	740
^{44}Ca	2.086	$^{12}C^{16}O_2^+$	1280
		$^{14}N_2{}^{16}O^+$	965
		$^{88}Sr_2^+$	160500
^{46}Ca	0.004	$^{46}Ti^+$	43400
		$^{14}N^{16}O_2^+$	1170
^{48}Ca	0.187	$^{48}Ti^+$	10500
		$^{12}C^{36}Ar^+$	3190

Table 7.1 Resolution required to separate Ca isotopes ions from interfering ions

In this study, a method of using cool plasma combined with high resolution magnetic sector ICP-MS was developed to accurately determine all six Ca isotopes. The interferences from Ar40 isotope at the calcium masses are greatly minimized by operating the ICP-MS in the cool plasma mode. The rest polyatomic ions are overcome by high resolution mode of the ICP-MS.

This study is to support an on going clinic trail, which is to compare changes in calcium absorption following administration of an experiment drug relative to matching placebo. Calcium absorption will be assessed using an enriched stable calcium isotope method. In the experiments, two tracers, one was given orally and the other intravenously, then, fractional calcium absorption will be estimated based on urinary recovery of oral calcium administered as isotopic calcium 43 and an IV calcium 42 isotope.

7.1 Experiment

Chemical reagents and preparation

All the chemical reagents were of analytical grade. A commercial stock calcium standard with natural abundance was used to calibrate the instrument and demonstrate the linearity of the method. Standard stock solutions 10 ppm for Ca were prepared by dissolving the appropriate amount of analytical grade solid reagents in ultra pure water (18MΩ cm-1), which was made in-house with a Milli-Q water purification system (Millipore, Milford, MA, USA). Dilute solutions for analysis were prepared daily. Calcium standards of 0.500, 1.000, 2.000 ug/mL (total calcium concentration – the sum of the concentrations of all calcium isotopes) were prepare by quantitatively diluting the 10.0 μg/mL intermediate calcium standard in 5% nitric acid matrix. This 5% nitric acid solution is also used as the calibration blank. NIST 1640 was diluted 20-time in 5% nitric acid solution before the validation study.

Calcium carbonate samples (Trace Sciences International Inc. 901 Market Street, Suite 460, Wilmington, Delaware) were prepared by accurately weigh

approximately 10 mg of sample into a sample container, add 0.5 mL concentrated nitric acid followed by 9.5 L deionized water. Mix well. Make further dilution as needed.

Instrument

All the measurements were carried out with a Finnigan Element 2 (Finnigan, Bremen, Germany) high resolution inductively coupled plasma sector-field mass spectrometer. The instrument is equipped with a double focusing mass analyzer using reversed Nier-Johnson geometry. The system allows three pre-defined nominal mass resolutions ($m/\Delta m$) of 300, 4,000, and 10,000 by means of selectable slits. The actual mass resolutions vary between 300-500 for low, 3,500-4,500 for medium, and 8,000-14,000 for high-mass resolution mode depending on the optimization of parameter settings.

The ICP-MS operating in regular and cool conditions and data acquisition parameters are given in Table 7.2. Optimization of the ICP-MS operating parameters, including the X-Y position of the plasma torch, ion-optic cylindrical lens, power and nebulizer gas flow rate, was performed daily using a 1 ppm sample solution containing the metal of interest. The optimized nebulizer gas flow rate typically was ~0.90 L/min. The dwell time was 100 ms per peak and the number of replicates was chosen such that the total experiment time was longer than the time required for a given separation. Depending on the number of masses measured, the total analysis time was between 10-30 minutes.

Isotopes:	^{40}Ca, ^{42}Ca, ^{43}Ca, ^{44}Ca, ^{46}Ca, ^{48}Ca,
RF Power:	1000-1200 W (regular plasma);
	600 – 800 W (cold plasma for ^{40}Ca measurement)
Coolant argon flow	17.0 L/min
Auxiliary argon flow:	0.6 - 0.8 L/min
Nebulizer argon flow:	0.9 – 1.2 L/min (regular plasma);
	1.3 - 1.5 L/min (cold plasma ^{40}Ca Measurement)
Additional gas flow	0.05-0.15 L/min
Nebulizer	PFA microconcentric nebulizer
Nebulizer uptake rate	0.050-0.15 mL/min
Spray chamber	PFA spray chamber (room temperature)
Sampler	Platinum 1.1 mm aperture diameter
Skimmer	Platinum 0.8 mm aperture diameter
Torch position	Optimized daily
Guard electrode	Yes
Acquisition mode	E-scan; electric scanning over small mass ranges
Number of runs	6
Number of passes	1
Number of acquisition points	20 - 40
Acquisition window (%)	60 - 80
Search window (%)	60 - 104
Integration window (%)	60 - 80
Dwell *time* per sample (ms)	10 - 50

Table 7.2 HR-ICP-MS operating conditions and measurement parameters

An accurate mass calibration at the beginning of the measurement session was routinely performed for low resolution (LR), medium resolution (MR), and high resolution (HR) modes by using a 1.0 ng ml-1 multi-element standard tuning solution containing Li, B, Na, Al, Sc, Fe, Co, Ga, Y, In, Rh, Ba, Lu, Tl and U.

7.2 RESULTS AND DISCUSSION

7.2.1 Cool Plasma technique for precise and accurate Calcium40 Isotope Measurement

Table 1 lists all of the major spectral interferences and the resolution required to resolve them for all the isotopes of Calcium. Using a hot plasma with 1300 W radio frequency (RF) power, Ca40 cannot be measured because of an irresolvable isobaric interference of 40Ar (39.96238 amu) with 40Ca (39.96259 amu). In order to separate 40Ar from 40Ca, a mass resolution of 190,500 resolution is required, which much higher than the presently available mass resolution of the Element 2 of about 10,000. Even high resolution ICP-MS does not have the power to resolve this interference. Thus, to measure the 40Ar fee 40Ca isotope, the 40Ar signal has to be significantly reduced.

This section describes experiments using the 'Cool Plasma' [20]technique combined with the high resolution of magnetic sector ICP-MS to reduce isobaric overlap for precise and accurate determination of Ca40.

'Cool Plasma' refers to plasma conditions where the RF power is lowered to 650-750 W from 1000-1500 W, resulting in a plasma temperature of 2500-3000 K (Normally 8000-10000K). This significantly reduces the ionization potential of the argon plasma gas. A "Shield Torch", a thin metal cylinder positioned between the work-coil and the plasma torch to reduce the potential difference (and secondary discharge), is also used on

the high resolution ICP-MS to stabilize the plasma at low power conditions. For optimum 'Cool Plasma' results, the plasma sampling depth and gas flows must also be adjusted. The spectrums (Figure 7.1) below demonstrate the effect of cool plasma condition in reducing the atomic interference of ^{40}Ar to ^{40}Ca. The interference background caused by $^{40}Ar^{16}O$ is reduced by a factor of about 100 as seen in the mass spectra, and this way ^{40}Ca can be accurately determined.

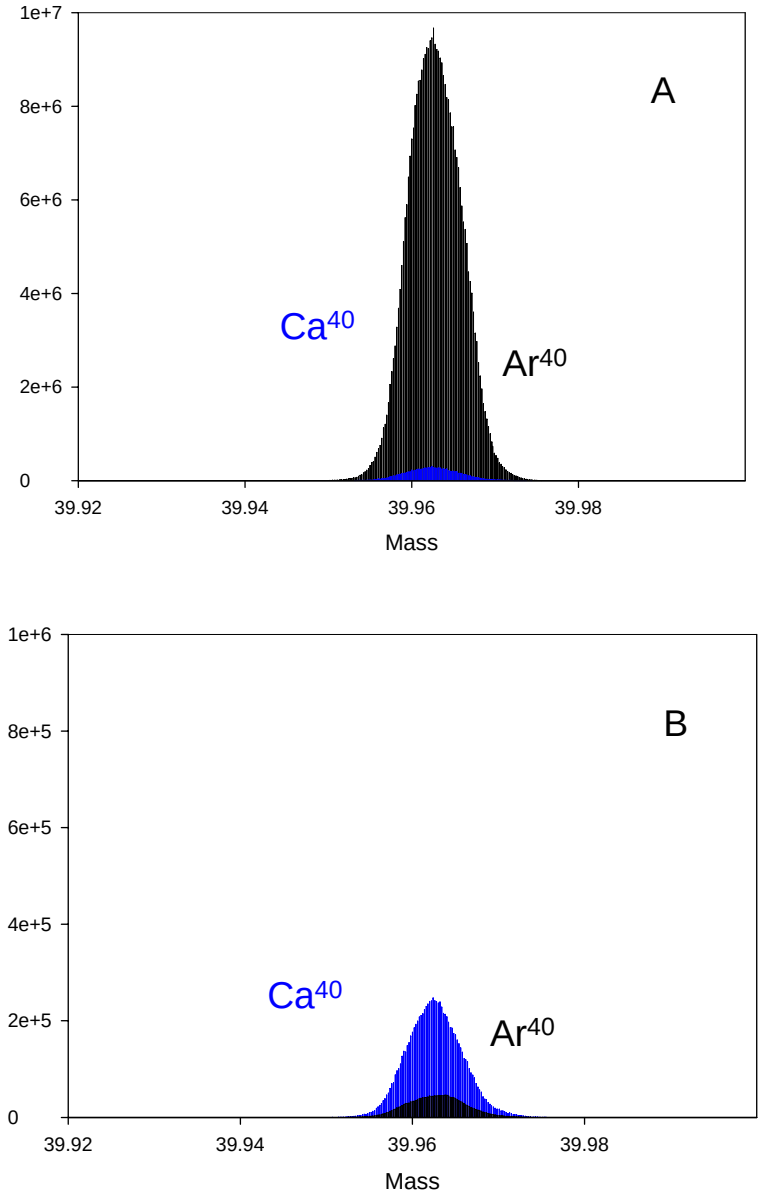

Figure 7.1 Demonstration of Cool plasma technique reduces the Ar40 interfaces A: without cool plasma condition B: with cool plasma condition.

The optimization was carried out to give the maximum signal to noise ratio for Ca40. One of the most sensitive parameters affecting the elemental response is plasma power. As can be seen in Figure 7.2(A), as the power decreases both standard and background signal (from Argon40 ion) decrease, but background signal decreases at faster pace because of the significant reduction in the ionization of Ar40 species. As illustrated in Figure 7.2 (B), best Ca40 signal to noise ratio is obtained at 700 W. This results show that the reduction of the RF energy reduces the 40Ar intensity by a factor about 50 to 100.

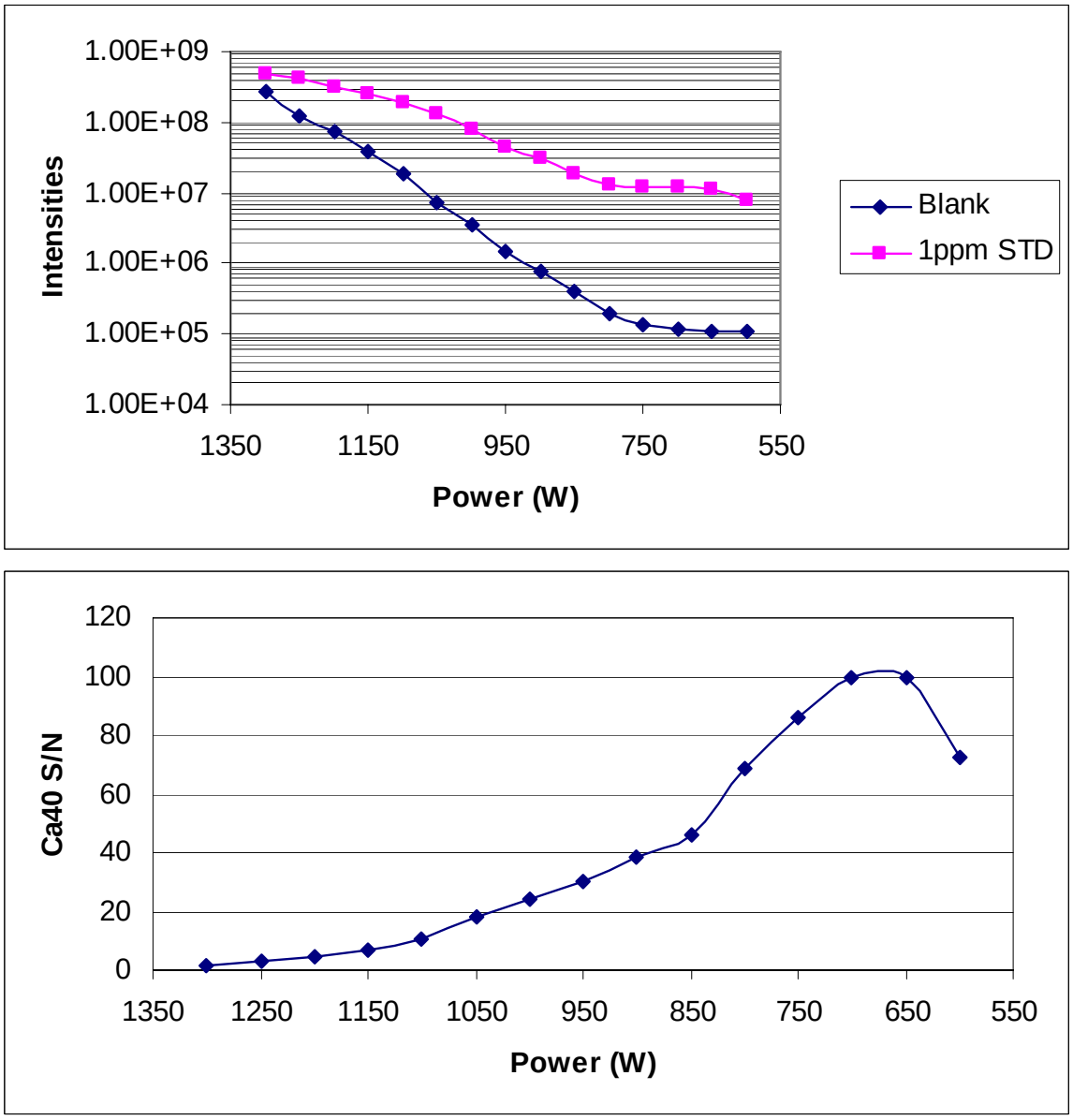

Figure 7.2 Effect of RF generator power on the intensities of Ca40 A: CPS B: S/N

In order to demonstrate that the cool plasma technique produces reliable and reproducible results, Ca40 measurements on NIST 1640 standard have bee performed. Ca40 results from measuring a NIST 1640 standard using the "cool plasma" technique are shown in the following Table 7.3. Both the precision (RSD) and accuracy (measured AVE vs. certified) are excellent.

Run#	**Ca40(MR)**	**Ca40(HR)**
1	7.050	6.919
2	7.061	6.961
3	7.074	7.034
4	7.007	6.960
5	7.088	6.899
6	7.124	7.126
7	7.014	6.948
8	6.902	7.020
9	7.198	7.151
AVE	**7.058**	**7.002**
SD	**0.078**	**0.084**
RSD	**1.098**	**1.193**

Table 7.3 Measurement of 40Ca of NIST 1640 Standard Reference Material-Trace Elements in Natural Water using cold plasma conditions at medium resolution (MR) and high resolution (HR) (mg/Kg) (Ca reference mass fraction values: 7.045±0.089 mg/Kg)

7.2.2 Precise Calcium Isotope Composition Measurement by High resolution ICP-MS

In order to be able to support the ongoing clinic trail, the capability for rapid and reliable determination of Calcium isotopic composition is essential and challenging. Ca42 and Ca43 are particularly difficult to measure, since they have low natural abundance and suffer severe Ar interferences. High resolution ICP-MS with high sensitivity and the ability to resolve interferences is the most suitable technique for performing the analysis.

The most important factor in ICP-MS detection system for isotope measurement is dead time[21, 22]. After an ion generates an electron pulse at the conversion dynode, there is a finite time during which the system is incapable of recording another event. The system is effectively "dead" in this interval, resulting in inaccuracy reading of ion counts. Therefore, the dead time correction should be applied in principle to all ion count rates to compensate for dead time, especially when accurate isotope ratios are required[23, 24].

In this experiment, dead time correction factor was determined by preparing and analyzing Ca at three different concentrations followed by the calculation Ca42/Ca43 isotope ratio at each of the three concentrations. As shown in following Figure 7.3, it is clearly evident that without the dead-time correction the ratio of Ca42/Ca43 decreases with Ca concentration, whereas, with the dead time correction, consistent Ca42/Ca43 ratio is obtained at various concentrations.

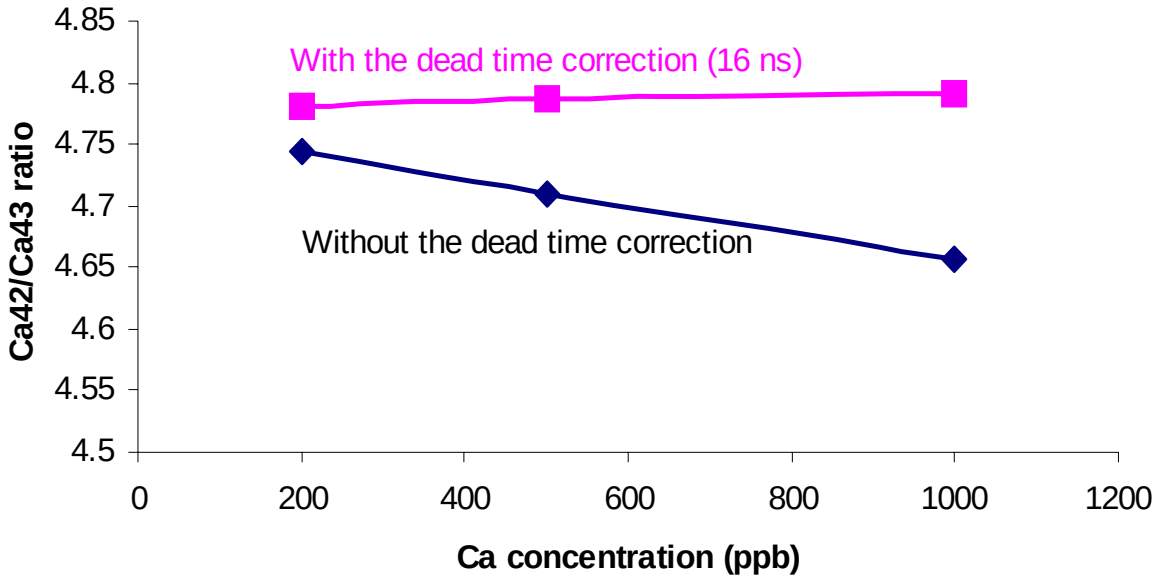

Figure 7.3 The comparison of Ca42/Ca43 ratio with/without the dead-time correction

Ca42/Ca43 ratio results from measuring Calcium standard with natural abundance are shown in the following Table 7.4. Both the precision (RSD) and accuracy (measured AVE vs nature abundance) are excellent considering that both Ca42 and Ca43 are minor isotopes of Ca (0.647% and 0.135%).

Run#	Ca42/Ca43 ratio
1	4.795
2	4.778
3	4.789
4	4.813
5	4.797
6	4.775
7	4.798
8	4.789
9	4.792
AVE	4.792
STD	0.010
RSD	0.215
Natural Abundance	4.793
Accuracy %	-0.0187

Table 7.4 The determination of Ca42/Ca43 ratio

7.2.3 Method linearity, accuracy and precision validation

Due to severe spectral interferences (mainly from ^{40}Ar), ICP at regular operating conditions cannot be used for ^{40}Ca measurement. Cold plasma conditions (reduced power and increased nebulizer gas flow) have been used throughout this study to carry out ^{40}Ca measurements. All other five isotopes were measured under regular operating conditions.

Calcium standards of 0.500, 1.000, 2.000 μg/mL were used to generate calibration curves for each isotope and the correlation coefficients for the isotopes of ^{40}Ca, ^{42}Ca, ^{43}Ca, ^{44}Ca, ^{46}Ca and ^{48}Ca are all greater than 0.999 as shown in Figure 7.4.

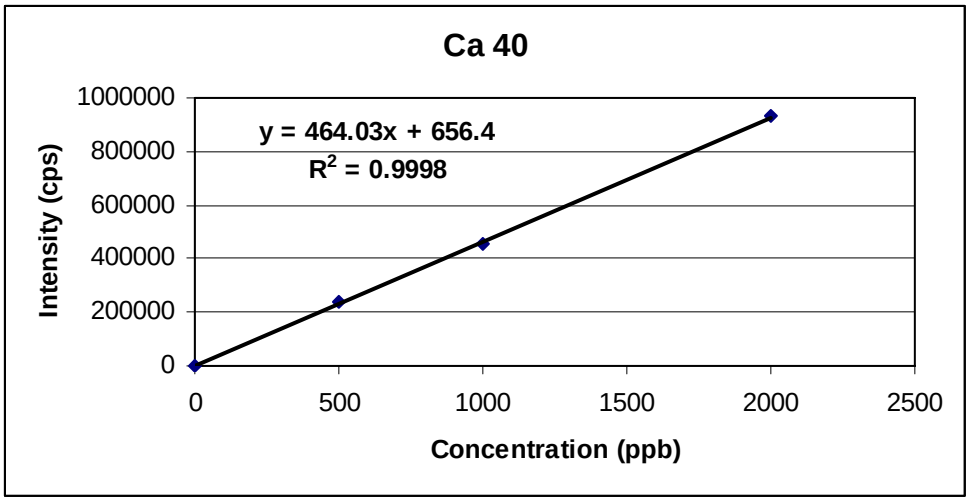
Ca 40
y = 464.03x + 656.4
R2 = 0.9998
Intensity (cps)
1000000
800000
600000
400000
200000
0
0
500
1000
1500
2000
2500
Concentration (ppb)

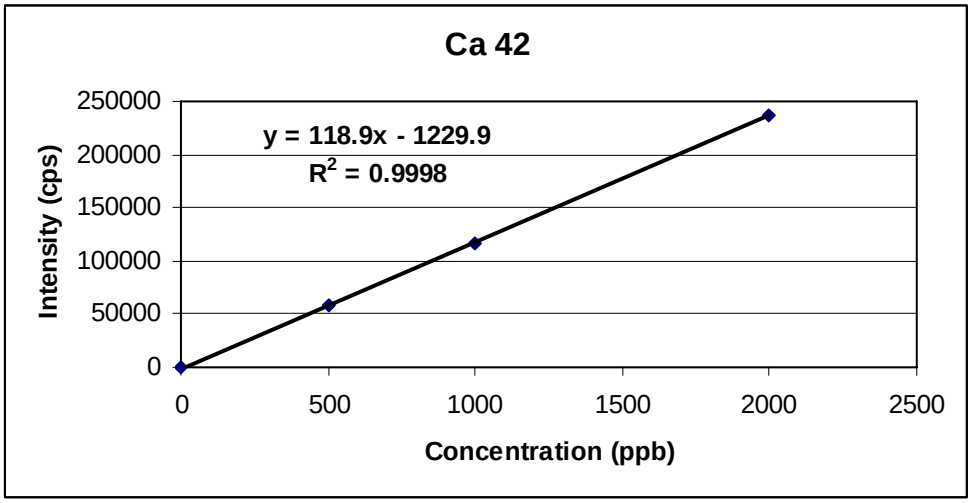
Ca 42
y = 118.9x - 1229.9
R2 = 0.9998
Intensity (cps)
250000
200000
150000
100000
50000
0
0
500
1000
1500
2000
2500
Concentration (ppb)

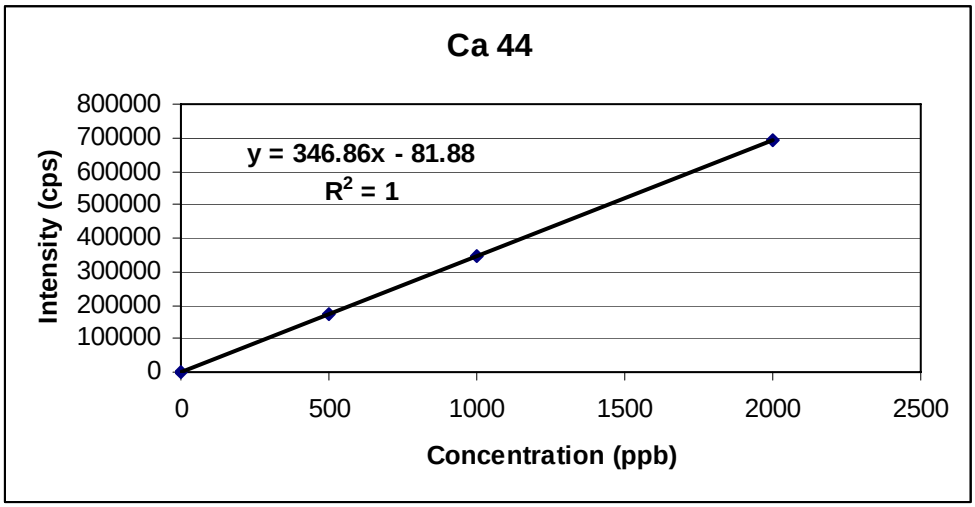
Ca 44
y = 346.86x - 81.88
R2 = 1
Intensity (cps)
800000
700000
600000
500000
400000
300000
200000
100000
0
0
500
1000
1500
2000
2500
Concentration (ppb)

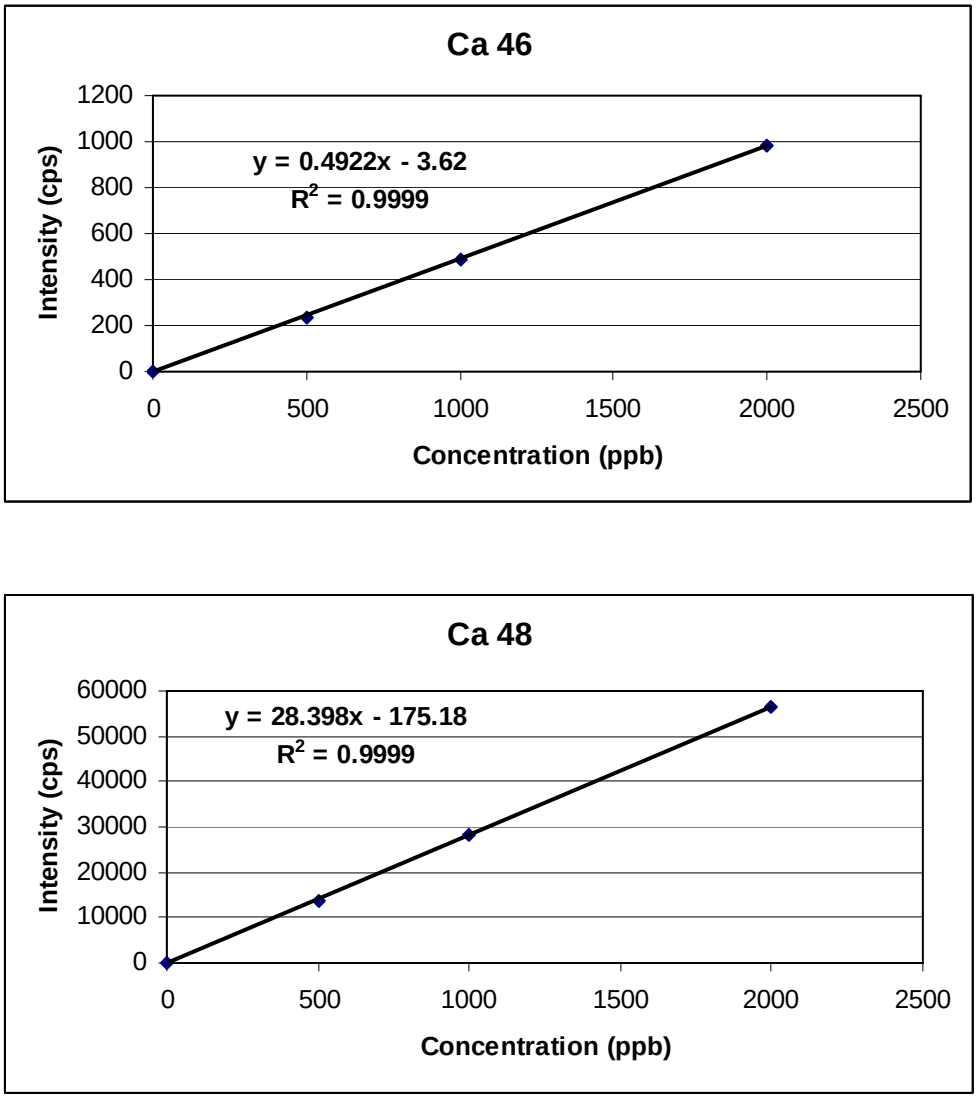

Figure 7.4 Calibration curves of selected Ca isotopes

As seen from Table 7.3, 7.5, 7.6, for NIST 1640, excellent agreement with the reference calcium value (total calcium) was achieved by using all six calcium isotopes, the measurement accuracy of the six calcium isotopes under the current operating conditions has been demonstrated.

Precision of the method was evaluated by the RSD of nine replicate runs of all samples using all calcium isotopes. The results are also listed in Table 7.3, 7.5, 7.6. The RSDs of the nine replicate measurements are mostly under 2% RSD (except ^{46}Ca and ^{48}Ca with low abundance), indicating satisfactory measurement precision of the method.

Both medium ($m/\Delta m = 4000$) and high resolution ($m/\Delta m = 10{,}000$) were used to resolve potential spectral interferences. From Table 3, Table 5 and Table 6, it is obvious that mean calcium mass fraction values from using medium resolution (MR) are very similar to those obtained using high resolution (HR), indicating that medium resolution is adequate for accurate measurements using all calcium isotopes. However, using medium resolution yielded better precision (smaller RSD's), probably due to the high intensity, thus medium resolution was selected for this study. Excellent agreements with the reference value of NIST 1640 were achieved using all calcium isotopes, the specificity of the method for measuring calcium isotopic composition is satisfied.

Run#	Ca42(MR)	Ca43(MR)	Ca44(MR)	Ca46(MR)	Ca48(MR)
1	7.026	7.096	7.189	7.163	6.942
2	7.088	7.055	7.164	7.244	7.063
3	7.179	7.133	7.140	7.439	7.285
4	6.854	6.938	6.982	7.393	6.948
5	6.815	6.947	7.029	7.281	6.912
6	7.128	7.188	7.274	7.261	7.211
7	7.073	7.256	6.977	6.990	7.156
8	6.972	6.893	7.015	6.879	6.894
9	6.921	6.921	6.994	7.114	6.815
AVE	**7.006**	**7.047**	**7.085**	**7.196**	**7.025**
SD	**0.125**	**0.130**	**0.109**	**0.181**	**0.161**
RSD	**1.781**	**1.845**	**1.532**	**2.515**	**2.293**

Table7.5 Measurement of NIST 1640 Standard Reference Material-Trace Elements in Natural Water using regular plasma conditions at medium resolution (MR) (mg/Kg) (Ca reference mass fraction values: 7.045±0.089 mg/Kg)

Run#	Ca42(HR)	Ca43(HR)	Ca44(HR)	Ca46(HR)	Ca48(HR)
1	6.972	6.921	7.090	6.369	6.986
2	7.110	6.960	6.986	6.610	7.032
3	6.620	6.966	6.697	6.462	6.646
4	7.007	6.799	6.877	6.651	6.799
5	7.051	7.194	6.988	6.175	6.865
6	7.213	7.055	7.010	7.012	7.050
7	6.978	6.964	7.004	6.335	6.921
8	7.041	7.027	6.961	6.678	6.831
9	6.957	6.773	6.734	7.041	6.838
AVE	**6.994**	**6.962**	**6.927**	**6.592**	**6.885**
SD	**0.162**	**0.128**	**0.132**	**0.295**	**0.128**
RSD	**2.312**	**1.836**	**1.912**	**4.474**	**1.856**

Table 7.6 Measurement of NIST 1640 Standard Reference Material-Trace Elements in Natural Water using regular plasma conditions at high resolution (HR) (mg/Kg) (Ca reference mass fraction values: 7.045±0.089 mg/Kg)

7.2.4 Instrumental limit of detection (LOD)

The instrumental limits of detection (LOD's) and sensitivities (counts per ng ml^{-1}) of all Ca isotopes elements at medium (MR) and high (HR) resolution modes by HR-ICP-MS were evaluated and are listed in Table 7.7. The instrumental limits of detection (LOD's) for all the isotopes were estimated by analyzing ten replicate blank solutions as ten samples, and defined as three times the standard deviation of the ten measurements. As shown in Table 7, the best limits of detection (LOD) for ^{40}Ca, ^{42}Ca, ^{43}Ca, ^{44}Ca, ^{46}Ca and ^{48}Ca are 0.78, 0.06, 0.32, 0.01, 8.95, 0.25 ng ml^{-1}, respectively.

In Table 7.7, it is also interesting to note that although an increase in the mass resolution did lead to lower intensities for all the isotopes, this did not necessarily

translate into high limits of detection. This is because higher resolution not only reduced the ion transmission but also the background transmission as well. For 43Ca, 44Ca, higher resolution resulted in slightly deteriorated limits of detection, whereas for the rests, higher resolution yielded modestly improved limits of detection.

Isotope	Detection Limits (ng ml^{-1})	
	MR	HR
^{40}Ca	0.91	0.78
^{42}Ca	0.07	0.06
^{43}Ca	0.32	0.35
^{44}Ca	0.02	0.01
^{46}Ca	8.95	9.25
^{48}Ca	0.33	0.25

Table 7.7 Detection Limits and sensitivities in medium resolution(MR) and high resolution (HR) modes

7.2.5 Result of analysis Ca enriched sample

High Resolution Inductively Coupled Plasma Mass Spectrometry (HR-ICP-MS) was used for the release testing of 42Ca-enriched calcium carbonate and 43Ca-enriched calcium carbonate. The spectra (obtained under cold plasma conditions) of ^{42}Ca-enriched calcium carbonate and ^{43}Ca-enriched calcium carbonate) are shown in Figure 7.5 to serve as the positive identification of the two samples. The results confirmed that ^{42}Ca and ^{43}Ca are the most abundant isotopes, respectively.

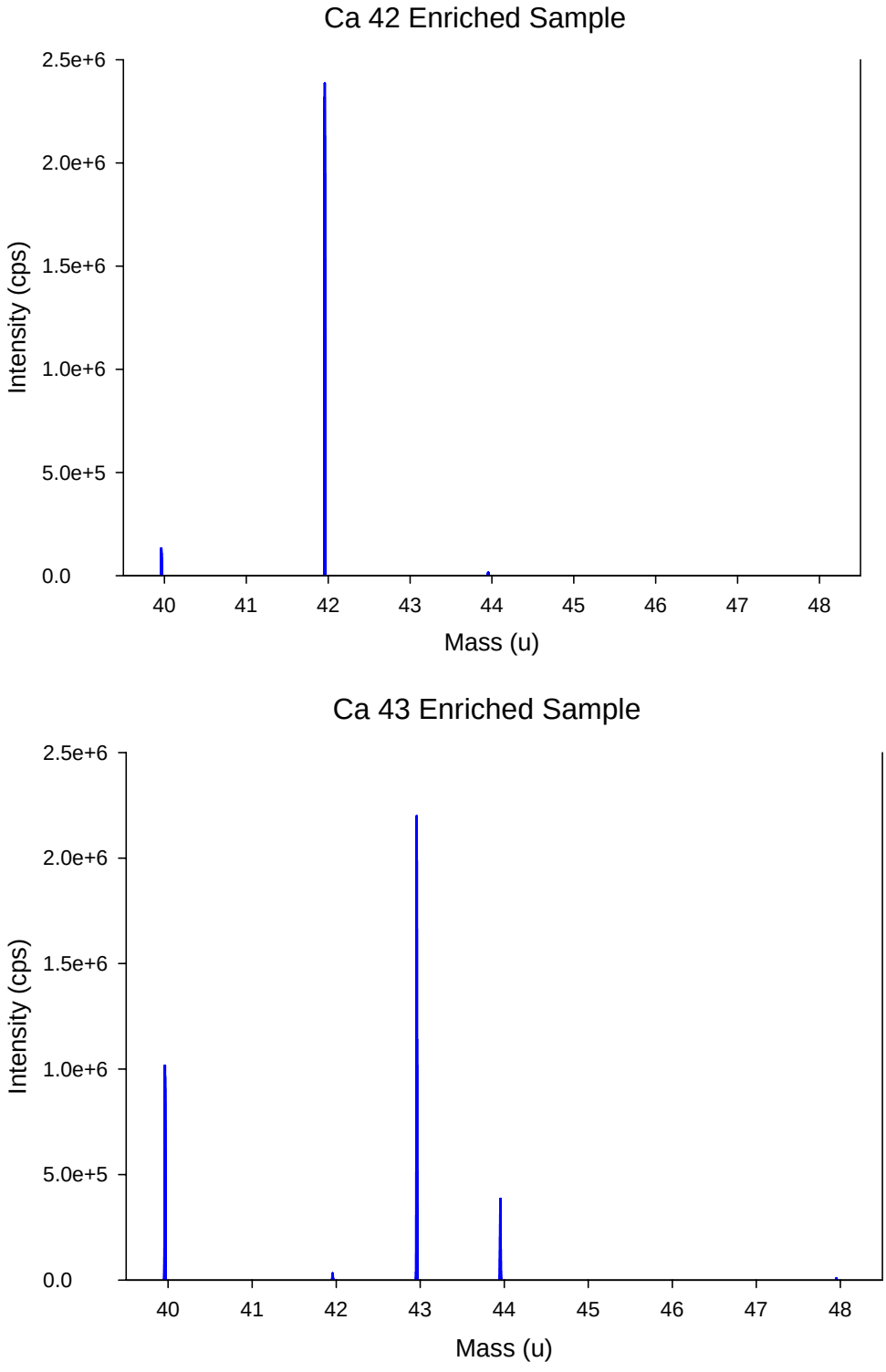

Figure 7.5 (A) Mass spectrum of ^{42}Ca enriched sample. (B) Mass spectrum of ^{43}Ca enriched sample

The enrichment results for each isotope were found to be consistent with those from C of A's provided by Trace. The calcium standards with natural abundance were prepared at 0.500, 1.000 and 2.000 μg/mL to generate calibration curves for the quantitation of each isotope in the samples. For all isotopes, the average results of nine replicate runs +/- standard deviation (SD) are reported. The results in weight percentage, abundance in weight percentage, and abundance in molar percentage for each isotope for ^{42}Ca and ^{43}Ca enriched samples are given in Table 7.8. The results are in satisfactory agreement with C of A's provided by Trace.

Sample	Isotope (Abundance (molar %)	40	**42**	**43**	44	46	48
^{43}Ca enriched	HR-ICP-MS	31.7	0.79	**58.6+/-1.1**	8.72	<0.02	0.13
	C of A	*28.61*	*0.87*	***60.2+/-1.8***	*10.16*	*<0.02*	*0.16*
^{42}Ca enriched	HR-ICP-MS	2.51	**96.9+/-0.08**	0.10	0.46	<0.01	0.013
	C of A	*2.56*	***96.8+/-0.3***	*0.11*	*0.51*	*<0.01*	*0.02*

Table 7.8 Analytical results of ^{42}Ca enriched calcium carbonate and Ca enriched calcium carbonate

7.4 CONCLUSION

High resolution ICP-MS has become an important tool in pharmaceutical research, and will become an essential tool in the near future as the drive to shorten the development time for new pharmaceutical entities is getting stronger and stronger and the detection limit requirements for pharmaceutical impurities and metabolites are getting

lower and lower. The fast, reliable and unambiguous results high resolution ICP-MS provides will be used to meet regulatory requirements, contamination monitoring, process troubleshooting and optimization as well as support of clinical trials.

In this chapter, the application of high resolution inductively coupled plasma mess spectrometer (HR-ICP-MS) for the determination of isotopic composition of enriched stable isotope calcium samples is described. The interferences from ^{40}Ar isotope at the calcium mass 40 are greatly minimized by operating the ICP-MS in the cool plasma mode. The rest polyatomic ions are overcome by high resolution mode of the ICP-Ms. A precision of 0.1-1% for Ca isotope ratio measurement was achieved by deal time determination. The HR-ICP-MS method has been validated in terms of specificity, linearity, accuracy and precision for the determination of calcium isotopic composition by measuring NIST standard reference material 1640. Accuracy of the method was excellent and the precision was mostly under 2% RSD (except ^{46}Ca and ^{48}Ca with low abundance). The limits of detection (LOD) was determined to be 0.78, 0.06, 0.32, 0.01, 8.95, 0.25 ng ml^{-1}, for ^{40}Ca, ^{42}Ca, ^{43}Ca, ^{44}Ca, ^{46}Ca and ^{48}Ca respectively. The method was used for testing of ^{42}Ca-enriched calcium carbonate and ^{43}Ca-enriched calcium carbonate. The enrichment results for each isotope were found to be consistent with those from C of A's provided by vender.

References

1. R. Nageswara Rao, M.V.N. Kumar Talluri, Journal of Pharmaceutical and Biomedical Analysis 43 (2007) 1–13

2. Xiujuan Jia, Tiebang Wang**,** Xiaodong Bu, Qiang Tu and Sandra Spencer Journal of Pharmaceutical and Biomedical Analysis, Volume 41, Issue 1, 11 April 2006, Pages 43-47

3. Xiujuan Jia, Tiebang Wang, Xiaodong Bu and Jane Wu Microchemical Journal, Volume 75, Issue 2, September 2003, Pages 103-107

4. J.G. Hardman, L.E. Limbird, P.B. Molinoff, R.W. Ruddon and A.G. Gilman, Good and Gilman's The pharmaceutical Basics of Therapeutics (9th ed.), McGraw-Hill, New York (1999) p. 3–63.

5. In: S. Gorog, Editor, Identification and determination of Impurities in Drugs, Elsevier Science, Amsterdam (2000), p. 748.

6. S. Ahuja, Impurities Evaluation of Pharmaceuticals, Marcel Dekker Inc., New York (1998) p. 42.

7. S. Husain and R. Nageswara Rao, Monitoring of process impurities in drugs. In: Z. Deyl, I. Miksik, F. Tagliaro and E. Tesarova, Editors, Advanced Chromatographic and Electromigration Methods in Biosciences, Elsevier Science, Amsterdam (1998), pp. 834–888.

8. R. Nageswara Rao and V. Nagaraju, J. Pharm. Biomed. Anal. **33** (2003), pp. 335–377.

9. T. Wang, S. Walden and R. Egan, J. Pharm. Biomed. Anal. **15** (1997), pp. 593–599.

10. E. Sovcikova, M. Ursynyova and L. Wsolova, Toxicol. Lett. **88** (1996), p. 63.

11. M.M. Guzman, A.j. Garcian-Fernandez, M. Gomenz-Zapata, A. Luna, D. Romero and J.A. Sanchez-Garcia, Toxicol. Lett. **88** (1996), p. 60.

12. European Pharmacopoeia Supplement (3rd ed.), Council of Europe, Strasbourg (1999) p. 326.

13. J. Huang, X. Hu, J. Zhang, K. Li, Y. Yan and X. Xu, J. Pharm. Biomed. Anal. **40** (2006), pp. 227–234.

14. Xiaodong Bu, Tiebang Wang, and Gene Hall, Journal of Analytical Atomic Spectrometry, 18 (2003) 1443-1451

15. Patterson KY, Veillon C, Exp Biol Med, 2001, 226, 271-282

16. Judith R. Turnlund, M. C. Michel, William R. Keyes, Janet C. King, Sheldon Margen, The American Journal of Clinical Nutrition, 1982, 1033

17. Yergey Al, Vieira NE, Covell DG, Biomed Environ Mass Spectrom, 1987, 14, 603

18. Strurup S, Hansen M, Molgaard C., J Anal At Spectrom, 1997, 12, 919-923

19. Patterson KY, VeillonC, Hill Ad, Moser-Veillon PB, O'Haver TC, J Anal At Spectrom, 1999, 14, 1673-1677

20. Karen E. Murphy, Stephen E. Long, Michael S. Rearich, Ozlem S. Ertas, J Anal At Spectrom,, 2002, 17, 469

21. Fietzke. J, Eisenhauer. A, Gussone, B, Liebetrau, Chemical Geology, 2004, 11

22. Sergei, F. Boulyga, Irina Segal, Thomas. Platzner, Ludwek Halicz, J, Sabine Beceker, International Journal of Mass Spectrometry, 2002, 218, 245

23. M. Paul Field, Sue Shapses, Mariana Cifuentes, Robert Sherrell, J Anal At Spectrom, 2003, 18, 727

24. Michael E. Wieser, Dieter Bual, Claudia Bouman, Johannes Schwieters, J Anal At Spectrom, 2004, 19, 844

VITA

Xiaodong Bu

September 27, 1972 .....Born -- Fuxin, China

1994 ..... B.S. Material Science, Zhejiang University

1997 .....M.S. Material Science, Tsinghua University

2000 .....M.S. Chemistry, The Ohio State University

Oct. 2007..... P h. D, Chemistry, Rutgers

PUBLICATIONS

"Identification and Characterization of Isomeric Intermediates in a Catalyst Formation Reaction by Means of Speciation Analysis Using HPLC-ICPMS and HPLC-ESI-MS", Tu, Qiang; Wang, Tiebang; Welch, Christopher J.; Wang, Peng; Jia, Xiujuan; Raab, Conrad; **Bu, Xiaodong**; Bykowski, Darren; Hohenstaufen, Benjamin; Doyle, Michael P. Analytical Chemistry (2006), 78(4), 1282-1289.

"Determination of Ruthenium in Pharmaceutical Compounds by Graphite Furnace Atomic Absorption Spectroscopy", Jia, X. Wang, T., **Bu, X**., Tu, Q., Spencer, S., Journal of Pharmaceutical and Biomedical analysis (2006), 41, 43-47

"Study of Hypochlorite-specific Enhancement in ICP-AES and ICP-MS", Jia, X. Wang, T., **Bu, X.,** Tu, Q., Gong, X., Spencer, S.A., Natishan, T. K., Journal of Analytical Atomic Spectrometry (2005), 20(11), 1293-1295

"Adsorbent Screening for Metal Impurity Removal in Pharmaceutical Process Research", Welch, Christopher J.; Albaneze-Walker, Jennifer; Leonard, William R.; Biba, Mirlinda; DaSilva, Jimmy; Henderson, Derek; Laing, Brian; Mathre, David J.; Spencer, Sandra; **Bu, Xiaodong**; Wang, Tiebang. Organic Process Research & Development (2005), 9(2), 198-205.

"Determination of Halogens in Organic Compounds by High Resolution Inductively Coupled Plasma Mass Spectrometry (HR-ICP-MS)", **Xiaodong Bu***, Tiebang Wang, and Gene Hall, Journal of Analytical Atomic Spectrometry, 18 (2003) 1443-1451

"Isolation an analysis of trace level of silicone oil in pharmaceutical bulk drug substance by ICP-AES", Xiujuan Jia, Tiebang Wang, **Xiaodong Bu**, Jane Wu, Microchemical Journal, 75 (2003) 103-107

"An Atomic Spectroscopic Method as an Alternative to Both USP Heavy Metals <231> and USP Residue on Ignition <281>", Tiebang Wang, Jane Wu, Xiujuan Jia, **Xiaodong Bu**, Ivan Santos, and Richard S. Egan, Pharmacopeial Forum, Vol. 29(4), 2003

"Oxidative impairment in scrapie-infected mice is associated with brain metals perturbations and altered antioxidant activities", Wong, Boon-Seng; Brown, David R.; Pan, Tao; Whiteman, Matthew; Liu, Tong; **Bu, Xiaodong**; Li, Ruliang; Gambetti, Pierluigi; Olesik, John; Rubenstein, Richard; Sy, Man-Sun, Journal of Neurochemistry (2001), 79(3), 689-698